University of Strathclyde

Department of Biomedical Engineering

Nanoindentation and Atomic Force Microscopy Surface Characterisation of Human Femoral Head Articular Cartilage

by

Megan Austin

A thesis presented in fulfilment for the requirements of the degree of Doctor of Philosophy

2013

Declaration

This thesis is the result of the author's original research. It has been composed by the author and has not been previously submitted for examination which has led to the award of a degree.

Signed: Date:

Acknowledgements

First and foremost I must thank Dr. Philip Richies who generated the idea for this project and was instrumental in obtaining its funding. More importantly he provided a wealth of knowledge, support and advice as well as keeping a smile on his face despite my prolific questions. Without your constant support and proof reading, I would not have made it this far, thank you. Secondly I would like to thank Dr. Richard Black who was always available to answer questions and provide feedback and guidance. My gratitude also goes to Katie Henderson and Brian Cartilage who advised with histology and microscopy and above all kept me company on the long days in the laboratory.

Thanks are particularly due to Danny for all his phone calls checking up on me, for laying out my clothes and organising food for the next day of testing so I could spend maximum time in bed. Thank you for always listening and calming me down. I will be eternally grateful to my mum and dad for supporting me through every stage of this thesis and for proof reading all my work to help turn it into to a coherent piece of writing. Thank you for encouraging me to follow my dreams despite my difficulties.

Over the last three years I have been lucky enough to make some excellent friends. Andrew Young and Claire Harrison for their IT skills and general all round support and encouragement; you have both gone above and beyond the call of friendship so thank you. To all the coffee girls without those breaks and chats, these past three years would not have been nearly as much fun as they were. Finally I thank God for everything he has done for me, for being in my life every step of the way, never letting me walk alone and always guiding my path.

Contents

List of Figures

List of Tables

Abstract

Articular cartilage (AC) is a remarkable tissue in which a complex composition and hierarchical structure provides an optimized function in load support and joint lubrication. Osteoarthritis (OA) is the degeneration and consequent loss of AC. OA is increasingly becoming more of a problem; an increase in OA leads to a greater number of replacement surgeries creating a financial burden on the population. The mechanical etiology and function of OA is not fully understood.

Nanoindentation and AFM techniques were investigated to measure the nanomechanical properties of AC. Instrumental nanoindentation was employed to characterize the variation of the mechanical properties of OA across the human femoral head and to understand the OA degenerative process further.

Qualitative analysis allowed the visualization and comparison of OA over the femoral head. This demonstrated that the worst affected area of OA was the superior posterior area which corresponds to the area of stiffest cartilage found on healthy cadaveric femoral heads. The qualitative results showed that OA potentially initiates at this location.

A potential biomechanical biomarker of OA has been found medially around the fovea capitis ligament. We hypothesize that when the cartilage surface attaches to a nanoindeter tip this indicates signs of a pannus-like tissue, suggestive of early OA. This is crucial for the development of new early osteoarthritis diagnostic tools. Extensive further work is necessary in the development of more effective diagnostic devices.

Chapter 1

Introduction

The United Nations and World Health Organisation have recognised that musculoskeletal diseases continue to be one of the main causes for severe long-term pain and disability (Woolf and Pfleger, 2003). Osteoarthritis, a clinical syndrome that limits function and reduces quality of life, is the most prevalent of joint diseases. Over the past decade numbers have increased steadily; a world ageing population and increasing obesity may be contributory factors.

The economic costs of OA are difficult to quantify as they can be split into cost of treatments (pharmacological, non-pharmacological, surgery etc.) and associated indirect costs (lost work days, disability benefits etc.). It was predicted £25.65 million would be spent on topical NSAID prescriptions and a further £426 million on total hip replacement surgeries within 2010 (Chen et al., 2012). The Department of Work and Pensions estimated as long ago as 2002 that over £3.2 billion was lost to the economy through OA disability (Arthritis UK http://www.arthritisresearchuk.org). The United States National Arthritis Data Work Group found 27 million Americans suffer from OA costing a staggering $185.5 billion annually (Kotlarz et al., 2009). The precise, present, total cost of OA is unknown but is estimated to be colossal so with increasing admissions and

surgeries, research is needed to prevent OA and to improve diagnosis monitoring and treatments.

It is clear that osteoarthritis is increasingly becoming a financial burden to the NHS; insensitive clinical diagnostic equipment is unable to identify early OA and a greater number of replacement surgeries are performed each year. It would appear that macroscale testing methods are restricted to measuring the bulk material properties of articular cartilage but by reducing the scale of measurment a more sensitive measurement of the structure of cartilage may be possible, with the potential to identify the onset of OA earlier than with traditional techniques. The mechanical aetiology of osteoarthritis is not fully understood nor is the mechanical function of AC in the degenerated condition (Miller and Morgan, 2010). Nanoindentation and AFM hold significant promise for characterising the biomechanical aspects of pathogenesis of osteoarthritis (Franke et al., 2007; Miller and Morgan, 2010; Loparic et al., 2010; Stolz et al., 2009).

The aim of this study is to characterise the variation of the mechanical properties of articular cartilage in non-osteoarthritic and in osteoarthritic human femoral heads. The mechanical properties of AC are regional and depth-dependent (Huang et al., 2005), however a direct comparison of local mechanical properties across degenerated human femoral head cartilage has not been investigated thoroughly. Nanoindentation has the capability to measure mechanical properties at scales at which the curvature of the femoral head is irrelevant.

The growing number of orthopaedic replacement surgeries necessitates further investigation of new and improved techniques and implants as well as increased surgical training opportunities. Fresh frozen human specimens are the optimum tissue for use in research however fresh frozen tissue: is high in cost; increases

infection risk; rapidly deteriorates and is at a premium due to inadequate quantities. For these reasons chemical fixation is inevitable however traditional formalin fixation is known to stiffen the mechanical properties of tissue therefore Thiel fixation is becoming increasingly popular however minimal research investigating the affect this embalming technique has on tissue is available. As the effect of Thiel embalming on articular cartilage has not been published, this thesis examined the mechanical properties of articular cartilage to discover if the Thiel embalming method altered the mechanical properties in comparison to fresh frozen articular cartilage.

1.1 Structure of Thesis

The work presented in this thesis is reported in the following format.

Chapter 2 gives an outline of osteoarthritis after an exhaustive literature search and presents the current diagnostic devices and treatments. It also introduces methods for mechanically testing cartilage, specifically nanoindentation.

Chapter 3 details the nanoindentation and atomic force microscope instrumentation employed in this study to investigate cartilage and the development of appropriate methodologies.

Chapter 4 investigates the effect of loading and unloading rate on bovine articular cartilage to identify the most appropriate experimental parameters.

Chapter 5 reports the nanoindentation experiments on fresh frozen, healthy and osteoarthritic human femoral heads, covering key literature, experimental methodologies, results and discussion specific to these results.

Chapter 6 covers the mechanical testing work on Thiel embalmed articular cartilage including experimental protocol, results and discussion.

Chapter 7 gives overall conclusions, discusses the study's limitations and provides recommendations for future work.

Chapter 2

Literature Review

2.1 Composition of Articular Cartilage

Articular cartilage (AC) is the thin layer of soft connective tissue that overlies the articulating bony ends in diarthrodial joints. It provides a smooth articulating surface for efficient pain free movement (Narhi et al., 2011) and aids load transmission through the joint from high contact stresses. The normal appearance of healthy hyaline cartilage is bluish-white, smooth, glistening and resilient (Outerbridge, 1961).

Articular cartilage consists of cellular material and extracellular matrix (Figure 2.1). The cellular material within the cartilage is known as chondrocytes which produce and maintain the extracellular matrix (Nordin, 2001). The extracellular matrix predominantly consists of: collagen fibres; proteoglycan and interstitial fluid Li et al. (2005).

Proteoglycans have been previously recognised as "protein-polysaccharide or chondromucoprotie". They can be considered as macromolecules with a structure containing: a protein core (consisting of 10-20% of the molecule weight); chondroitin

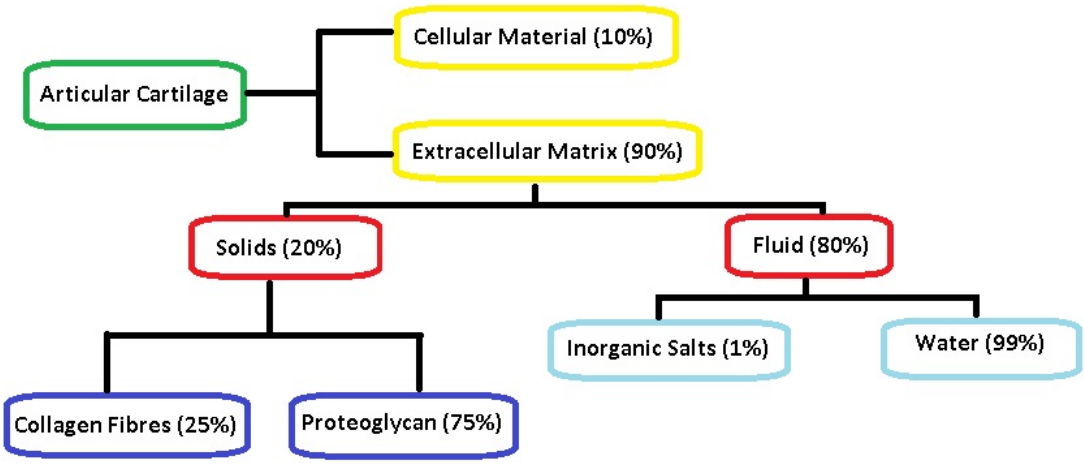

Figure 2.1: The basic structure of cartilage. Note all percentages are approximations of volume and vary between sample.

sulphate (80-90% of weight) and keratin sulphate (a minor but inconsistent proportion of the weight of the molecule) (Mayes et al., 1973; Lee et al., 2010), illustrated in Figure 2.2. Proteoglycans are carbohydrate-protein molecular complexes containing protein and glycosaminoglycan chains (GAG) that mostly exist in an aggregated form (Lu et al., 2007), binding via a link protein on the core to a hyaluronate molecule. The aggregate proteoglycans are present in small quantities, about 10% of the wet weight of the tissue however proteoglycans are responsible for numerous important features of AC.

The flexible hydrophilic quality and high volume of negative charges due to the GAG chains (Stolz et al., 2009) lead to a high osmotic pressure whilst the fine macromolecular mesh certifies a low hydraulic permeability. Each proteoglycan is capable of attracting a volume of water much greater than its own weight. The interstitial fluid is over 99% water and less than 1% inorganic salts. Without the collagen fibres, the proteoglycan and water would produce a highly viscous proteoglycan gel. The interstitial fluid is a major component of AC as it accounts for

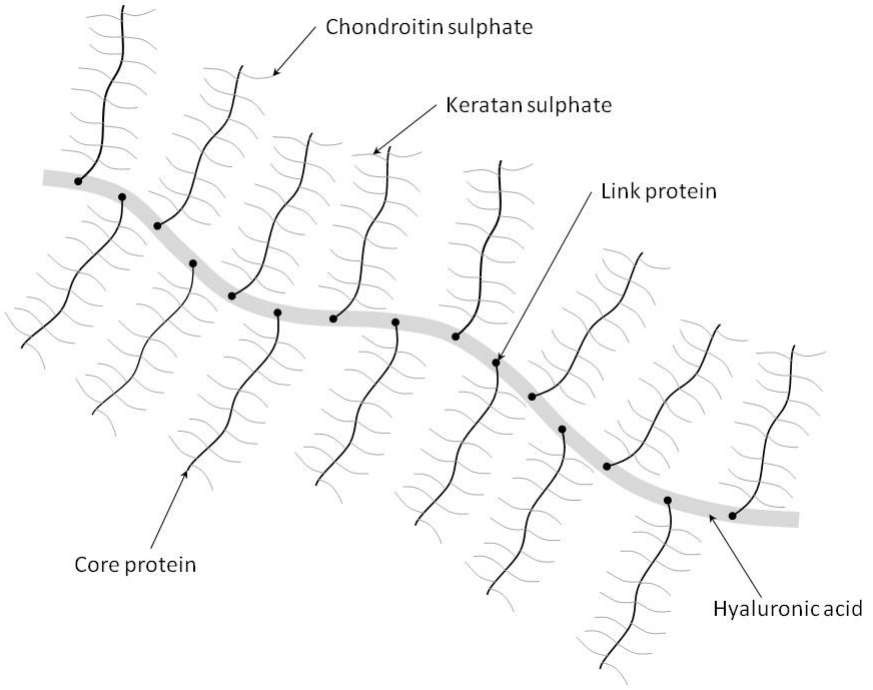

Figure 2.2: Schematic illustration of a proteoglycan macro-molecule aggregate in which GAG chains attach with a link protien.

60% to 80% of the wet weight of the whole tissue. The accurate content of water is decided by the balance involving the swelling pressure of the proteoglycans and the tension of the collagen fibrils.

The collagen fibre meshwork is highly organised in intact mature AC. The fibres are responsible for supplying tensile strength whilst confining the negatively charged proteoglycans. The collagen fibrils range in diameter between 30-80nm with the space between the fibrils in the area of 100nm in magnitude (Clarke, 1974). The collagen fibrils are highly organised as they change orientation through the AC. The fibrils form a **coarse** structure to resist the shear and tensile stresses. The particular orientation of the structured collagen fibrils are closely related to the mechanical function of AC which is described in detail in section 2.2.

The heterogeneous structure of cartilage (Figure 2.3) has four intertwined zones : superficial, transitional, deep and calcified layers, which are key to the mechanical properties of the tissue. The superficial zone is the thinnest, about 10% to 20% of total thickness of the tissue, and consists of two small layers mainly formed from collagen fibres and interstitial fluid. The first layer consists of randomly aligned collagen fibrils with no polysaccharides or cells. In the second layer, there are sparse numbers of proteoglycan and the collagen fibre bundles are orientated parallel to the surface with a minimal number of flat chondrocytes.

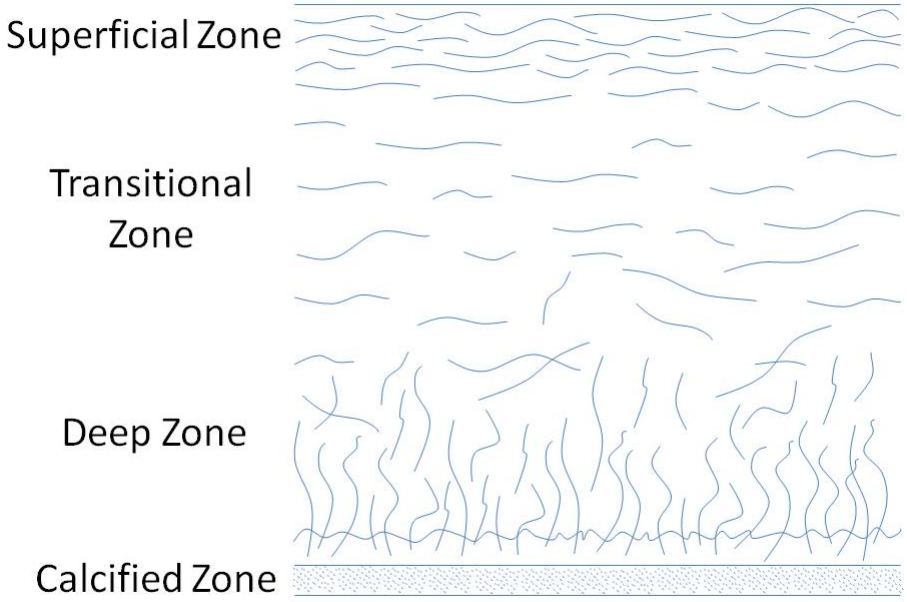

Figure 2.3: Demonstrates the four entwined zones of cartilage.

The collagen content drops through each zone with around 68% in the transitional zone. The transitional zone (also known as mid zone) is about 40% to 60% of total thickness of the tissue, making it the thickest zone with the collagen fibres less parallel than the superficial zone and increasing in diameter. This zone contains proteoglycan and chondrocytes which are spherical in shape and the structure is less strongly bound than the superior layer.

The deep zone is about 30% of the cartilage's thickness. The proteoglycan is at its highest concentration in this layer with large collagen fibril bundles running perpendicular to the surface with low water content. The chondrocytes are spherical in shape and stacked perpendicularly on top of each other. The deep zone is responsible for distributing the load and resisting compression.

The calcified zone contains a tidemark; a basophilic line which bridges the boundary between un-calcified and calcified cartilage. It is a transition zone between soft cartilage tissue and stiff subchondral bone. The calcified zone is mainly composed of collagen type X fibres; these collagen fibres anchor the deep zone cartilage to the subchondral bone.

The swelling and low water permeability of AC under pressure allows this tissue to dissipate the energy from joint loading. Articular cartilage is a resilient, almost frictionless, tissue that helps to protect joints when healthy. The composition and structure of AC is adapted during growth and maturation due to transformation of the AC matrix (Narhi et al., 2011). It has been reported (Hyttinen et al., 2009; Julkunen et al., 2010; Brama et al., 2009) that remodeling can be caused by external loading of the joints. It appears that joint loading induces specific changes in the collagen network architecture by increasing the parallelism of the collagen fibrils and affecting the depth wise fibril orientation, especially in the

superficial collagen network (Narhi et al., 2011). It is clear that AC has a specialised structure which is closely related to its mechanical function, which will be described in the following section.

2.2 Mechanical Characteristics of Articular Cartilage

Healthy AC executes three main functions in the synovial joint: predominantly to reduce the stresses applied to the subchondral bone; to stop abrasion between the articulating bones and to provide a low friction, smooth surface for efficient motion (Schinagl et al., 1997). AC is repeatedly subjected to high impact forces as well as prolonged periods of compression during daily activities. The mechanical function of AC is determined by the organisation and distribution of the collagen fibril network, proteoglycan and interstitial water (Stolz et al., 2009). Animal models have extensively investigated the complex mechanical characteristics of AC using techniques such as confined compression, unconfined compression and indentation (Athanasiou et al., 1994; Chen et al., 2001; Ateshian et al., 1997; Froimson et al., 1997; Korhonen et al., 2002b; Jurvelin et al., 1990; Korhonen et al., 2002a; X L Lu, 2009; Boschetti et al., 2004; Boschetti and Peretti, 2008; Kiviranta et al., 2006; Laasanen et al., 2003b; Hung et al., 2004; T L Willett, 2005; DiSilvestro and Suh, 2001). The mixture of fluid and extracellular matrix provides the biomechanical and low friction properties of articular cartilage.

AC has can be viewed as a biphasic tissue (Kiviranta et al., 2006; Mow et al., 1980; Miller and Morgan, 2009; Lyyra et al., 1999; Setton et al., 1993, 1994; DiSilvestro and Suh, 2001; Ateshian et al., 1997; Taylor et al., 2012; Mak et al., 1987; Mow

et al., 1989) with two major phases: the fluid phase composed of water and the solid phase consisting of collagen fibres, proteoglycans and other minor proteins, Figure 2.1. The solid phase has low permeability due largely to a high frictional resistance with a high drag co-efficient of $\sim$1014 m^4/Ns (Einhorn et al., 2000), this fundamentally prevents the permeability of interstitial fluid. The fluid phase is responsible for the flow-dependent viscoelastic characteristics of AC which arrive from loading conditions that permit the interstitial fluid to move through the extracellular matrix (Stolz et al., 2004). The regulation and permeability of the velocity of fluid exudation through the solid tissue (Mow et al., 1980) is intrinsic to the mechanical behaviour of AC (Boschetti et al., 2004). The low permeability of the solid phase results in high pressurisation in the fluid phase. The relaxation time of AC reduced from 25 s to 15 s when the proteoglycan was depleted (Han et al., 2011) confirming that hydraulic permeability is closely linked to the pressurisation (Burry, 1974). More than 90% of load transmission can be associated with the pressurisation in the fluid phase (Ateshian and Wang, 1997; Soltz and Ateshian, 2000; Macirowski et al., 1994; Soltz and Ateshian, 1998). The high pressure of the fluid phase due to the low permeability of the solid phase establishes both cartilage compressive stiffness and viscoelasticity (Pearle et al., 2005; Felson et al., 2000).

Isolated collagen fibres have been illustrated to have a viscoelastic response to loading with a fast reaction time of 7 s (Shen et al., 2011). It is suggested that the short relaxation time of the collagen fibres are intrinsic in the fast recovery time of cartilage. The viscoelastic shear modulus has been documented to increase with collagen fibre crosslinks (Hayes and Bodine, 1978), further indicating that the collagen fibres are intrinsic to the viscoelasticity of the tissue. The interaction between the proteoglycan molecules and collagen fibrils creates a fiber-reinforced composite solid matrix (Garcia and Cortas, 2007). The proteoglycans are en-

twined and compressed within the collagen interfibrillar space, which helps to preserve a porous-permeable solid matrix and establishes the movement of the fluid phase of the matrix. Confined compression experiments demonstrated, fluid flow and pressurisation to govern the mechanical response (Setton et al., 1993) rather than isolated collagen fibres. Li et al. (2005) suggest that the axial compression is dominated by fluid pressure but collagen fibres have a small influence on the viscoelasticity and are critical to the tensile properties (Kempson et al., 1968).

The most abundant component of AC is interstitial fluid which is predominantly contained by the proteoglycans. The sulphate and carboxyl groups, attached along the GAG chains (Figure 2.2), become negatively charged in a natural biological environment. The density of the negative charge in the proteoglycans is known as the fixed charge density and gives rise to electrostatic swelling pressure in the cartilage. (Maroudas, 1976; Mow and Huiskers, 2005). This pressure is known as the Donnan osmotic pressure at equilibrium (Donnan, 1924). The osmotic swelling pressure depends on the extrafibrillar space between the collagen fibres which trap the proteoglycans and resist swelling. The osmotic pressure can contribute 30%-50% of the apparent stiffness in AC (Wan et al., 2004; Mow et al., 1998; Huang et al., 2001; Guterl et al., 2010).

The fluid phase (osmotic pressure) provides the tissue with its time-dependent properties: reversible deformability and ability to dissipate energy which plays an important role in the load support ability of cartilage (Donnan, 1924). The response of AC to a load of finite duration, such as standing, requires two responses to be taken into account as an amalgamation: the instantaneous response with the initial deformation when the load is applied and then the gradual response when deformation increases or creeps while the load is sustained (Serafini-Fracassini and

Smith, 1974). The expression of the interstitial fluid from the superficial layer is associated with the creep phase. Under dynamic loading, the shear modulus varied from 0.1 - 2.5 MPa but after constant compression (no swelling pressure) the quasistatic compressive modulus ranged from 0.4 - 1.5 MPa (Einhorn et al., 2000) suggesting the mechanical function of AC, during motion is influenced by swelling pressure. Recent studies have revealed a positive relationship between the apparent mechanical properties of cartilage and the fixed charge density (Mow et al., 1980; Williamson et al., 2001; Appleyard et al., 2003). Osmotic pressure provides a considerable component of load support of the cartilage, which protects and shields the solid phase of the matrix from stresses and load absorption.

Cartilage has been described to have: time-dependent; viscoelastic; poroelastic; biphasic and triphasic and other mechanical characteristics. These descriptors of the mechanical behaviour of cartilage are all correct, under differing loading and deformation circumstances. The mechanical response of cartilage is very load dependent and compositional dependent. The organised zonal structure of cartilage (Figure 2.3) affects the functional capabilities of AC as the intertwined layers change composition described in section 2.1. The superficial zone provides a smooth gliding surface to reduce friction, and resists shear loads. The high collagen density in the superficial zone, specifically the parallel fibres at the articular surface, contribute to the resistance against shear load more than any other zone and the tensile stresses are greater as the fibres contain the swelling pressure from the underlying tissue. However the compressive modulus is lowest at the superficial zone which can deform approximately 25 times more than the mid zone (Pearle et al., 2005). The flat chondrocytes in this zone prefer to express proteins that play a lubrication and protecting roll to allow the synovial joint to move smoothly (Wong et al., 1996).

The equilibrium confined compression modulus increases with distance from the articular surface from 0.1 MPa in the layer closest to the surface to 1.94 MPa in the deep zone (Schinagl et al., 1997) demonstrating that as depth increases the tissue more predominantly deals with load distribution because of the high proteoglycan compressive stiffness at this depth. The increase in compressive modulus in transitional zone from the superficial zone can be attributed to relatively low fixed charged density in the superficial zone which increases to maximum in the transitional zone (Burry, 1974) due to the loosely packed collagen fibres and larger numbers of proteoglycans, resulting in increasing swelling pressure. The deep zone is composed of large diameter collagen and high numbers of protoeoglcans with a low volume of interstitial fluid, see section 2.1: this arrangement of structural components are responsible for the deep zone having the highest compressive stiffness (Schinagl et al., 1997) due to the swelling pressure and high intrinsic stiffness of the solid matix (Lu et al., 2004). The deep zone is responsible for distributing the load and resisting compression.

The mechanical characteristics of AC are not only influenced by loading condition, composition and depth but are also position dependent and species dependent. The variation in anatomical position of the cartilage appears to have functional mechanical consequences. Confined compression tests on bovine AC demonstrated an increase in Young's Modulus from 0.34 MPa on the femur to 0.62 MPa on the patella, increasing further to 0.81 MPa on the humerus (Korhonen et al., 2002b). In the canine knee joint cartilage, the shear modulus was found to be greatest at the patellar groove (0.964 MPa) reducing to the lowest shear modulus at the medial plateau of the tibia (0.385 MPa). Table 2.1 demonstrates Athanasiou et al. (1991) results who compared: human; bovine; dog; monkey and

rabbit to show that variability in aggregate modulus and permeability is not only seen in anatomical position but between species.

Table 2.1: Aggregate modulus and permeability variability between species Athanasiou et al. (1991).

Species	H_A (MPa)	$k(m^4/Ns)$
Human	0.53	2.137
Bovine	0.472	1.422
Dog	0.555	0.927
Monkey	0.522	4.737
Rabbit	0.516	3.842

The most essential aspect of AC is to protect the bony ends of the joint from high contact stresses. Rigid surfaces in contact, unless they are an absolute harmonious shape, will produce large contact stresses when loaded. Joints are incongruous in shape, with microscopic structures uneven and the overall outline not a perfect match. Introducing a flexible, malleable sheet such as AC between the rigid structure (bone), facilitates the applied loads to spread more evenly over a wider surface area hence AC lessens or attenuates load and stresses in the joints. The transient response of AC and optimum compliance is a consequence of the fluid flow through the solid matrix. Despite the importance of contact stresses to joint health, disagreement remains regarding the normal magnitudes and distribution of contact stress in healthy hips (Harris et al., 2012). To date there are no experimental methods available to assess hip contact stresses on a subject-specific basis and the integrity and function of AC are seriously jeopardised by the degeneration of AC as detailed in section 2.3.

2.3 Osteoarthritis

Osteoarthritis (OA) is a prevalent, debilitating joint disease that leads to disability and poor quality of life in the elderly. OA is the most common form of arthritis (Felson and Zhang, 1998) and is becoming increasingly more common with a concomitant greater number of replacement surgeries creating a financial burden on society. OA is the degeneration and consequent loss of AC and since AC has no blood supply, it has a poor healing capability when physically damaged (Kleemann et al., 2005). This disease is characterised by the progressive destruction of the cartilage and sclerosis of the underlying subcondral bone within the joint capsule.

Chondrocytes in OA tissue have illustrated an increase in sulphate $^{35}SO_4$ uptake (Collins and McElligott, 1960) as the disease progresses macroscopically. They found that the chondrocytes in OA cartilage were hyperactive, not lifeless. This discovery changed the concept of OA disease from a mechanical condition initiated and progressed solely by "wear and tear", to a disease with a biological reaction also. The latest biological enhancements have enabled classification of OA cartilage pathology characteristics into those of activity and progression, and have facilitated functional correlation of osteoarthritic cartilage morphologically (Brandt et al., 2003). The specific pattern and path of OA development is also influenced by heredity, age, gender, obesity, trauma to the joint and other factors (Manninen et al., 1996). OA provokes a loss in cartilage volume making the tissue more vulnerable to damage during injury or excessive use (Byrd and Jones, 2004). The earliest change visible to the eye is seen when the cartilage becomes dull or even slightly yellowish white. Immunohistochemistry tests have demonstrated a pannus-like tissue to incompletely integrate with underlying cartilage in early OA developing into a fibrocartilagenous tissue (Barley et al., 2010). Traditionally

'pannus' is identified as a soft cloth-like tissue covering AC in rheumatoid arthritis (RA), (Fassbender and Simmling-Annefeld, 1983). Pannus is known to be an invasive vascular granulation tissue however the pannus-like tissue on OA has distinct differences to that found in RA: it has less vascularity and fibrous properties than RA pannus (Yuan et al., 2004). Granulation tissue, reparative fibrocartilage, reparative tissue and pannus are all reported descriptions of soft cloth-like tissue found on OA cartilage. OA pannus-like tissue has been found to have high levels of aggrecan and an altered collagen network compared to healthy AC (Barley et al., 2010). As osteoarthritis progresses irregular deep fissures develop and the affected area becomes a mass of villous like cartilaginous flakes attached to the subchondral bone until the whole bone is affected (Outerbridge, 1961).

Mankin et al. (1971) has illustrated that OA cartilage of the femoral head demonstrated marked variation in histological, histochemical, biochemical and metabolic parameters. There have been grading systems in the past by Collins (1949) and Mankin et al. (1971) based on advanced OA specimens. Basing a grading system on advanced OA specimen resulted in a lack of full understanding of the early stages of OA and created grading systems that were not linear for mild or early OA. The most recent histological standardised grading system was presented by Pritzker et al. (2006) (OsteoArthritis Research Society International grading method), with six grades describing healthy AC to end stage OA: as the grade increased this indicated a greater disease progression.

With the OARSI (OsteoArthritis Research Society International) grading method, grades 1 to 4 involve articular cartilage only and grades 5 and 6 additionally include the subchondral bone. Grade 0 is normal healthy cartilage. The surface is smooth and the extra cellular matrix and chondrocytes are organised into their zones accordingly. No enlargement or deformation of chondrons and no

proliferative transformations of chondrocytes are observed. Grade 1 is the threshold of OA commencement. Within this grade mild abrasion is observed distinguished by microscopic cracks in the superficial layer known as "superficial fibrillation". Superficial fibrillation is recognised to be a direct response of mechanical induction alone (Bartel et al., 1986) which is inadequate for diagnosis of OA as there is no biological reaction therefore histolgically the OARSI working group included focal or widespread cartilage matrix swelling identified as oedema. Prolification of the chondrocytes in the superficial zone: deterioration of the chondrocytes or groups of chondrocytes, may be evident. Cell death may also be observed by the absence of chondrocytes on the inside of the chondron. With Safranin O staining, and similar cationic stains, the lack of matrix colouration can be an important defining feature, this stain can indicate longstanding proteoglycan depletion. The preservation of the superficial area is key to grade 1 OA (Pritzker et al., 2006).

Grade 2 OA is distinguished by the superficial layer principally discontinuing. It is expected that this grade includes the deterioration from shear forces leading to the partial loss of the outermost superficial matrix creating small fragments; materialised as "flakes" or "fibrils" discovered in the synovial fluid. The "flaking" of the surface is more commonly known as spallation, a kind of exfoliation. Deep fibrillation, a few fractures elongated through the complete superficial matrix, is encompassed in this grade. Chondrocytes in the mid zone may now show some or all of the evidence of: bundling, amplification and loss of orientation of the chondrons.

Grade 3 of the OARSI standardised grading system is characterised by the augmentation of the fissures in the matrix of the superficial layer to the mid layer which initially are seen as vertical clefts. This grade also includes the clefts

expanding and forking in different directions. With staining, an increase in proteoglycan depletion is observed and the whole matrix becomes increasingly miscellaneous and incongruous. The use of Picro Sirius red stain, at this stage, can indicate the purification and concentration of the collagen fibres in the mid layer (Junqueira et al., 1979). Chondrocyte death is more prominent at this stage particularly close to the cracks in the matrix.

Grade 4 can be described as the erosion of cartilage as the superficial zone distinctly delaminates. This occurs as there are an increased number of cracks in the matrix that extend from the superficial layer to the mid layer; consequently the extracellular matrix deteriorates at the intersection between these layers. For this to fully transpire the extracellular matrix underneath the deteriorated area must be relatively unbroken and remain together so a difference at the interface of the layers is evident, for example one is soft, the other hard. Fissure proliferation will normally occur first as it develops at another angle away from the initial vertical fissures. When a cleft expands the fragment become unstable and flaking and delamination can occur. The development of cysts in the mid layer is also an indication of grade 4 OA. Cysts are a result of continual oedema which ultimately results in loss of extracellular matrix creating holes in the tissue which can contribute to delamination. To a lesser extent the degeneration of the matrix is called lacunar reabsorption where the collagen fibres do not repair or renew and this tends to take place in thicker cartilages. The delaminating of the superficial zone has been documented histologically as the cartilage surface appearing reasonably smooth, however, the underlying tissue demonstrates organised cartilage of the mid zone composition and alignment (Pritzker et al., 2006).

Grade 4 OA can also illustrate signs of excavation. Chondrocyte death and renewal, along with extracellular degeneration through loss of collagen condensation

or fibre rarefaction, are found in the tissue bordering the clefts. The clefts deepen and combine until the section is highly unstable then dislodges. The collagen fibres more distant from the clefts may demonstrate an increase in number and new fibres may be formed. The new collagen fibres are more likely to be type I collagen fibres produced from chondrocytes that have undergone metaplasia to become fibro-chondrocytes or chondrocytes which have moved from repaired cartilage (Pritzker, 1977). These new fibres are likely to be thicker and more birefringent than the original fibres.

Grade 5 OA is characterised by the exposure of areas of the calcified cartilage or underlying bone. Commonly, the unprotected bone demonstrates a thicker surface compared to the adjoining bone surface that is still protected by cartilage. Although the bone plate may be denser, it is normally less calcified than deeper trabecular bone and is noticeably more metabolically active. Micro-fractures of the articular plate have fibrocartilage repair that expands into the deep zone of the cartilage, with healthier cartilage above. Grade 5 OA can be characterised by fibrocartilage being present on the surface nevertheless under the criteria of OARSI grading system for this stage no deformation of the joint surface is acceptable (Pritzker et al., 2006).

Grade 6, end stage OA is defined by the deformation of the articular surface of the bone. This can happen initially by the growth of reparative fibrocartilage specifically above the earlier degenerated cartilage level and the completely eroded articular surface. As OA progresses, the microfractures escalation into the lateral bone and repair tissue multiply ocurring in adjacent positions and continue to lengthen. Fibrocartilage propagation and the formation of osteophytes is evident from the lateral, and occasionally central, areas of connective tissue at the tideline. Generally grade 6 is characterised by the remodelling and deformation

of the bone surface with an increase in the metabolic activity of the connective tissue at the cartilage bone interface.

The OARSI system for assessing OA is thought to be superior to and more reproducible than other grading systems (Pritzker et al., 2006). The scheme above describes in detail the current physiological knowledge of the breakdown of healthy cartilage to end stage OA. Unlike other methods it is thought to provide more reliable results for all users not only experienced professionals. The OARSI sytem is based on the features of OA found vertically, and reflects the biological degeneration of the disease as the clefts extend. This system, at its most basic, diagnoses 4 stages or 6 grades depending on the method of analysis however if more detail is required analysis can be broken down further to give scores between 0 to 24. In addition this method identifies early stage OA in greater detail than other methods however it involves the removal of tissue so only provides information once the cartilage is no longer in use thus the macroscopic Outerbridge grading system (Outerbridge, 1961) may be more practical. Currently there is no disease specific approach for measuring the overall severity of OA in a clinical setting (Do and McAlindon, 2005) with as much detail as the OASI system. Presently questionnaires on pain and joint stiffness etc are commonly used to assess the severity of OA clinically, however, whilst providing a psychological description of AC degeneration, this has not been matched to a biomechanical description.

2.3.1 Current Diagnosis

Hip pain can be caused by a multitude of disorders ranging from avascular necrosis to labral tears to greater trochanteric pain syndrome to OA and many more. Additionally other disorders commonly lead to early OA and pain including: femoroacetabular impingement; developmental dysplasia and slipped capital femoral epiphysis. The fundamental concern for physicians is to correctly diagnose the pain amongst various diseases.

In the past, MRI high resolution noncontrast has been the standardised diagnosis technique utilised by physicians for hip pain. This procedure is non-invasive which results in reduced risk to the patient (Mintz et al., 2005) and is lower in cost than other methods. Its shortcoming however is that MRI demonstrates 25% sensitivity and 65% specificity (Byrd and Jones, 2004) when detecting articular damage which is a lower level of accuracy compared to MR Arthrography and other techniques. Evidence of early OA is identified by chondral hyperintensity and loss of normal grayscale stratification on the MRI. It is also possible to see surface fibrillation from an MRI image. However Blitzer (1993) concluded MR Arthrography to have superior sensitivty in detecting OA than MRI; Blankenbaker et al. (2011) found MR Arthrography to have a sensitivity of 70% and a specificity of 84%. A study of direct comparison between MRI and MR arthrography (Byrd and Jones, 2004) demonstrated an increase in diagnostic accuracy of 41% sensitivity and 50% specificity for MR arthrography.

A representative protocol for MR arthrography involves a fluoroscope guiding a large needle to the correct intra-articular position in the joint (Sadro, 2000). Once this position is ascertained a maximum amount of a solution comprising of saline, gadolinium and bupivacaine is injected into the joint and an MRI is

performed within an hour (Thomas Byrd, 2002; Byrd and Jones, 2010). The best results employ a 1.5-T or 3-T magnet with the addition of a small field view wrap coil, a shoulder coil or a multiple channel cardiac coil (Stoller, 2007; Erb, 2001; Sadro, 2000). A torso coil significantly improves the signal to noise ratio yet maintains the imaging quality of both hips. Fat suppressed T1-weighted fine spin echo images in the axial, coronal and sagittal views complete the protocol for optimal diagnostic imaging (Blitzer, 1993; Hardya et al., 2000).

MRI noncontrast imaging and MR arthrography techniques, endorsed by numerous studies, are the current standard practice for diagnosing OA. Variations of MR imaging methods specifically T2 mapping and $T1\rho$ investigate the collagen orientation and proteoglycan content in AC to identify early OA, however comparatively only a few studies in literature exist, and T2 mapping and $T1\rho$ are not yet the primary method widely used for diagnostic purposes.

T2 mapping, Figure 2.4(c), generates a colour coded image to enable appraisal of water content and collagen fibre orientation. At various echo times, T2 mapping requires procurement of several images per slice. These images provide different values of T2 decay for the three non calcified AC zones; this allows differentiation and visualisation of the compositional layers of AC. The deviation from the normal zonal structure allows identification of the areas with early OA (Natzli et al., 2002), occasionally with morphologically healthy cartilage (Koff and Potter, 2009; Jazrawi et al., 2011).

Spin lattice relaxation in the rotating frame, commonly known as $T1\rho$, Figure 2.4(d), maps the cartilage by inspecting the proteoglycan content. $T1\rho$ evaluates abnormal proteoglycan content which changes through the cartilage layers. High values of $T1\rho$ are interpreted as proteoglycan depletion which results in

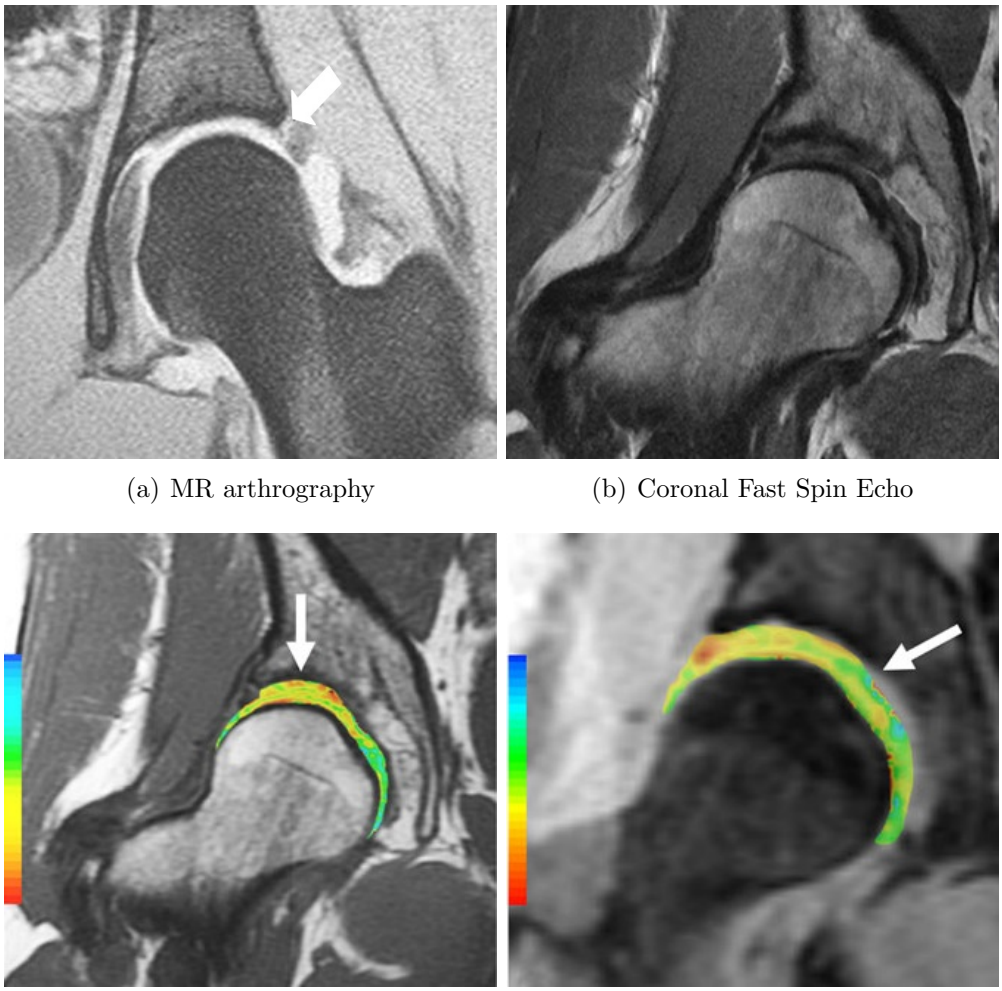

(a) MR arthrography (b) Coronal Fast Spin Echo

(c) T2 map (d) T1ρ map

Figure 2.4: (a) An MR arthrography of a 19 year old with a suspected tear in the lateral labrum. Adapted from Byrd and Jones (2004). (b)-(d) images of a 42 year old with suspected developmental dysplasia, the arrows highlight the amplification of T2 and T1ρ values. Adapted from Gold et al. (2012).

degenerated AC (Koff and Potter, 2009). This procedure provides superior information to current techniques in the clinical field (Carballido-Gamio et al., 2008; Keenan et al., 2011)when attempting to detect early OA using non-invasive methods.

The large and increasing number of joint replacement surgeries provide a unique opportunity to validate diagnostic techniques, since quantitative MRI measures can be undertaken prior to surgery and the removed tissue can subsequently be examined for validation. Quantitative MR techniques can detect early OA by the changes in collagen orientation and proteoglycan content (T2 mapping and $T1\rho$). MR arthroscopy and high resolution noncontrast MRI detect early OA most accurately when the patients have signs of chondral or labral pathology. Further studies are needed to investigate the longitudinal data to improve the diagnostics of early OA and standardize a cartilage scoring system (Gold et al., 2012). Assessment of hip cartilage biochemistry is essential to provide a more sensitive means by which to assess early osteoarthritis that may occur before development of morpholgic changes perceived on standardised MR techniques or before the development of osteoarthritic changes on standardised radiographs. However, these imaging techniques alone are unable to quantify changes in the functional properties of the cartilage, sensitively impaired in early OA (Julkunen et al., 2010). Thus biomechanical testing of the tissue is of great interest in studies that aim for more sensitive diagnostics of OA.

2.3.2 Current Treatment

The general objective for OA treatment by NHS is "to relieve pain, reduce disability and provide support to live an active life as much as possible". The OARSI key recommendation to achieve the NHS objective is optimal management of OA (Figure 2.5) requiring a combination of non-pharmacological and pharmacological modalities (Zhang et al., 2007). The first steps of clinical practice when a patient presents with early OA is to provide education. A fuller understanding of the disease has shown evidence of self-efficiency and the subsequent adoption of preventative techniques reducing cost to the NHS (Mazzuca et al., 1999).

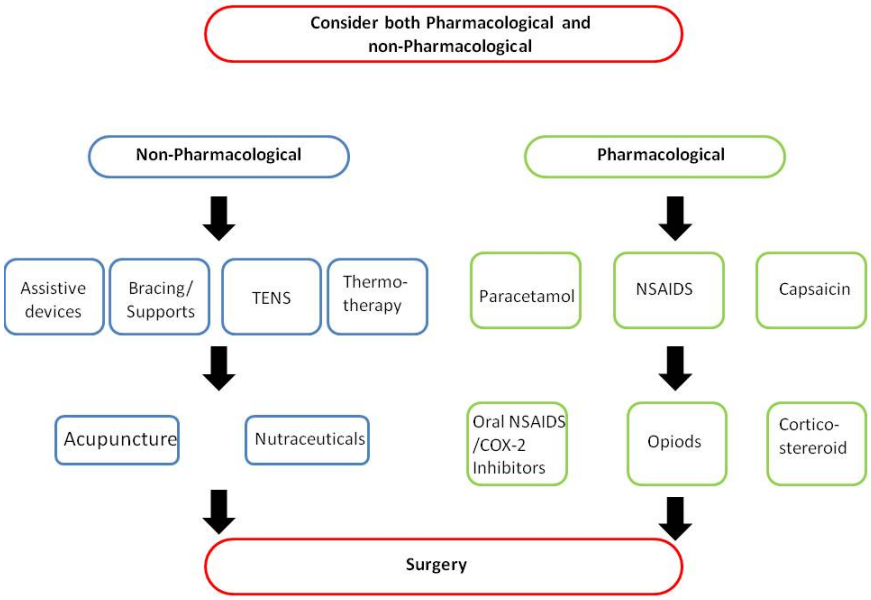

Figure 2.5: A flow chart of the advice for treatment of OA to NHS patients diagnosed with OA (http://healthguides.mapofmedicine.comchoicesmapopen/osteoarthritis2.html accessed 12:16:2013).

Patients are encouraged to start with non-pharmacological modalities. Exercises to strengthen the affected joints, specifically resistance training, have demonstrated improvement at multiple levels: muscle strength; reflex muscle inhibition; proprioception, and disability (Baker and McAlindon, 2000). Aerobic and mus-

cle strengthening exercise has been shown to provide pain relief, improve joint function and strength for a patient with OA. Long term exercise was able to deter the decline of the physical function of the joint that occurs with aging, but has not significantly improved the baseline (Ettinger WH, 1997). Specifically, patients with hip OA are advised to exercise in water (Zhang et al., 2007) to reduce load on the joint.

Obesity is a major risk factor for OA, with weight loss being a recommended treatment for many patients with OA in order to reduce the load on the articular joints. Weight loss appears to reduce the development of knee OA and improves pain relief (Baker and McAlindon, 2000). A combination of weight loss and exercise has been found to be most effective in relieving symptoms of OA (Messier et al., 2004).

To reduce joint pain assistive devices such as canes, crutches or wheeled walkers are recommended along with instructions for optimal use, otherwise bad posture and misalignment may exacerbate OA symptoms. Patients may also benefit from other assistive devices such as: insoles which can reduce pain and improve ambulation (Simon et al., 1972) by reducing damaging load; heel wedges which may reduce lateral thrust (Yasuda, 1987) and lateral wedges have been proven to reduce the intake of anti-inflammatory drugs (Pham, 2004); support sleeves which increase proprioception and may reduce the feeling of insecurity (Perlau et al., 1995). Orthotics provide a cost effective, simple treatment although further research is required to find out the full extent of their benefits.

Thermotherapy involves hot or cold applications to treat OA symptoms. Ice packs may have the effect of reducing inflammation, numbing pain, blocking nerve impulses and muscle spasms to the joint to which the ice pack is applied. Cold

treatment has been demonstrated to be most effective to acute flares of OA with minor swelling present (Brosseau et al., 2003). More studies have found the application of cold to be more productive than heat in effectively reducing pain and helping patients. The application of heat to the affected area may reduce pain and stiffness due to: relaxation encouragement; joint flexibility improvement and increasing blood flow to the joint, although applying heat may also contribute to increased swelling and oedema in the joint (Zhang et al., 2008a).

TENS (Transcutaneous electrical nerve stimulation) is a non-pharmacological pain relief. TENS is recommended for short-term pain control with patients who have knee or hip OA (Zhang et al., 2008a). TENS therapy has demonstrated significant pain relief over a 2-4 week period of treatment (Bjordal et al., 2007; Ainsworth et al., 2006). The level of nonreceptive nerve transmission suppression is dose dependent and greater understanding could provide interpretation of the efficiency of TENS for OA. TENS aids pain relief, with its greatest advantage being no reported serious adverse effects (Bjordal et al., 2007).

Additional adjunctive treatments have been advised for treatment of OA by the NHS but there is a range in quality of supportive data to provide significant evidence of the efficiency of these treatments. Many of the treatments and studies have found that a placebo is equally as effective for treating OA (Zhang et al., 2008b). Acupuncture is a controversial therapy although it has been recommended by Zhang et al. (2007) for symptomatic treatment of OA in the knee or hip, conversely, a study based on exercise and acupuncture executed by physiotherapists found that acupuncture provided no additional improvement to pain relief (Foster et al., 2007).

The efficiency of "Nutriceuticals" is undetermined for treating OA. Glucosamine and chondriotin have been in existence since the 1960s however the results for the use of these may have benefited from publication bias (Do and McAlindon, 2005). Other compounds that have exhibited evidence of reserved improvement are avocado sunsaponidiables, diacerhein, S-adenosylmethionine, ginger extract and collagen hydrolysate (Reginster et al., 2003). The true effectiveness of all nutriceuticals in treating OA is still unkown.

Pharmalogical interventions as well as non-pharmalogical interventions have been considered for treatment throughout the progression of OA. The primary recommended drug is acetaminophen; this oral treatment helps patients with mild to moderate pain. Nonsteroidal anti-inflammatory drugs (normally abbreviated to NSAIDS) are the most commonly prescribed medication for OA (Zhang et al., 2008b) however their predominant efficiency, in comparison to the safer acetaminophen, is limited by the toxic effect of long term use (Bradley et al., 1992; Smalley et al., 1996). Topical NSAIDS and capsaicin (an anti-inflamitory specific to neuropeptide concerned in the pathogenesis of inflammation and pain in OA) are frequently used as alternatives to oral treatment and studies have found that the treatment of capsaicin showed significant improvement in pain relief however, a burning sensation was noted as a side effect (Deal et al., 1991).

As pain increases and the disease progresses, intra-articular injection of corticosteroids to the affected joint are advised. Steroid injected joint displayed improvement in range of motion and pain however there was no significant sign of improvement of the joint structure (Raynauld et al., 2003; Yavuz et al., 2012). If other pain relief is ineffective, only then are weak opioids prescribed. When patients are not able to obtain adequate pain relief and functional movement then total joint replacement is considered. Replacement arthroplasties are effective for pa-

tients with reduced life quality despite pharmacological and non-pharmacological treatments. Techniques and prosthetic joints continue to improve and to provide enhanced post-operative improvement. Earlier diagnosis may prevent OA in many cases or extend the time of pain free movement before a joint replacement is required. Whilst imaging (section 2.3.1) may perform this task to a certain extent, biomechanical measures may be more sensitive to the early stages of OA degeneration.

2.4 Indentation

Nanoindentation is a versatile technique that investigates the mechanical behaviour of materials at the nanoscale. Nanoindentation, also known as depth sensing indentation or instrumented indentation, is becoming increasingly popular as a technique for analysing the mechanical response of materials. In general, conventional hardness tests consist of the application of a single static force and a related dwell time with a particular tip material and shape, resulting in a permanent impression in the surface in the order of millimetres (VanLandingham, 2003). As indentation testing has advanced, indentation instruments have become capable of applying a specific force or displacement that is controlled, measured concurrently and constantly over the whole loading and unloading cycle. Furthermore, exceptionally small loads and displacements are also possible with a resolution of $1\mu N$ or $0.2nm$ or even smaller depending on the system utilised (VanLandingham, 2003). The increased control, sensitivity and data acquisition mean that indentation is a worthy testing method for mechanical behaviour of materials at the micrometer and sub-micrometer scales. Examples of previous areas of studies using indentation to investigate the material properties are: metals (Nix and Gao, 1998; Corcoran et al., 1997); bone (Fan et al., 2002); polymers

(Cheng et al., 2000; Loubet et al., 2000; VanLandingham et al., 2001); thin films (Huber et al., 2002; Saha and Nix, 2002). Currently a number of researchers are investigating finite element modeling and dimensional analysis to relate the material's behaviour to the indentation data and attempt to predict the stress strain behaviour of the material (Wilson et al., 2004). The assessment of mechanical behaviour of materials is expanding as modern materialisation techniques are improving and being employed.

A schematic of a standard nanoindenter system is shown in Figure 2.6. Most commercial instruments use electromagnetic or electrostatic actuation or expansion of a piezoelectric element to control force attenuation while displacement is monitored normally by a capacitance or inductance sensor (Fischer-Cripps, 2004; VanLandingham, 2003). There are a range of commercially available systems, and whilst some systems apply force and measure displacement through alternative means, other systems use the same transducer for applying force and measuring displacement. Irrespective of the operational variation in equipment, the raw displacement and raw force data are always coupled (VanLandingham, 2003), enabling the force to be plotted as a function of displacement. Most indenter systems are force driven devices, such that the force of the indenter tip is controlled easily, with displacement controlled through a feedback signal (VanLandingham, 2003). A displacement controlled system (or a force controlled system using a constant loading rate) is simpler as it requires no feedback signals unlike the force driven devices. Operationally the tip is positioned onto the middle plate of the capacitor and a load is applied to move the tip into the sample (Ebenstein and Pruitt, 2006), with the load and displacement under constant monitoring to produce load-displacement curves. Nanoindentation has three aspects which make it attractive to use (Oyen and Cook, 2009): initially its sensitivity to sub-micron level, and its ability to continuously control the load and displacement; secondly

nanoindentation theoretically requires minimal sample preparation of the test material; finally this method has a large variety of modes of measurement, including an array of loading conditions, a choice of tip shapes and materials; dwell times and indentation depths. Nanoindenters are simply universal test machines that use local contact and automatic triggering resulting in a user friendly machine.

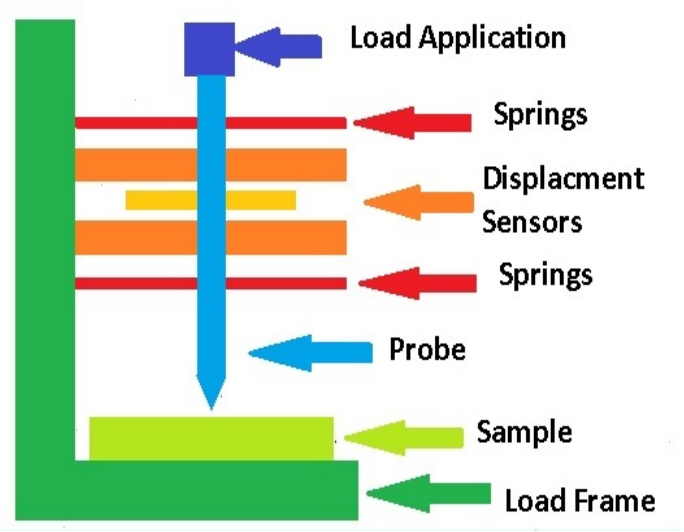

Figure 2.6: Indentation instrument schematic.

2.4.1 Indentation of biological tissue.

Nanoindentation bridges the gap from macroscale mechanical testing (tensile, confined and unconfined compression test) and Atomic Force Microscopy (AFM). Nanoindentation improves spatial force and displacement resolution, compared to traditional indentation techniques, to present a valuable device for the characterisation of biological and soft materials. Due to the small tip sizes, nanoindentation can measure local material properties in small, thin and heterogeneous samples which are unsuitable for traditional mechanical testing techniques. Nanoinden-

tation is an effective technique for biomaterials as it is also able to: detect and determine mechanical properties of microstructural features within larger heterogeneous samples; distinguish individual components within complex or diverse samples, or record material properties across the surface of the sample (Ebenstein and Pruitt, 2006).

Reviews by Kinney et al. (2003) and Haque (2003) have investigated retrospectively the application of nanoindentation in mineralised tissues, dentine and bone. Areas that have been investigated in bone are: localised differences between lamellar versus interlamellar bone (Rho et al., 1999b; Zysset et al., 1999; Hoffler et al., 2000; Donnelly et al., 2006; Rho et al., 2002); diversity between trabecular versus cortical bone (Roy et al., 1999; Turner et al., 1999; Rho et al., 1999a; Hoffler et al., 2000); the dissimilarity in specific layers of osteocondral bone (Rho et al., 1999a); all the variation between healthy bone and diseased bone (Akhter et al., 2004; Chen et al., 2003; Guo and Goldstein, 2000; Jamsa et al., 2002; Silva et al., 2004; Wang et al., 2002) and these studies have provided further understanding of local tissue mechanical properties in bone. Nanoindentation studies on dentine have focused on mapping of the surface and how the material composition and chemicals affect the mechanical properties (Marshall et al., 2001; Fong et al., 2000; Urabe et al., 2000; Tesch et al., 2001; Cuy et al., 2002); as the mineral content decreases, a decrease in modulus and hardness is demonstrated. Softer biomaterials such as diseased and healthy artery tissue (Ebenstein et al., 2001; Lundkvist et al., 1996); deminaralised dentine (Balooch et al., 1998); skin (Yuan and Verma, 2006); aragonite block (Bruet et al., 2005); insect cuticle (Enders et al., 2004; Barbakadze et al., 2006); polymer gels (Liu et al., 2009) and many more have also been investigated using nanoindentation. Nanoindentation has been able to demonstrate that the mechanical properties do not vary across the human meniscal surface (anterior = 1.63 MPa, central = 1.67 MPa, posterior

= 1.47 MPa) (Moyer et al., 2012). Li et al. (2007) similarly found the Young's modulus of mini-pig menisci's to be 1.3 MPa. These nanoscale experiments were an order of magnitude larger those reported in the microscale and above studies (Sweigart et al., 2004; Joshi et al., 1995; Chia and Hull, 2008).

The application of nanoindentation in comparison to traditional bulk testing, is highly recommended for characterising microstructures for their mechanical properties. As the numbers of joint replacements are increasing per year, OA is becoming an increasing health problem, further understanding of the mechanical properties of AC and a more sensitive diagnostic method for OA is required.

2.4.2 Cartilage Indentation

As cartilage is innervated and repair is difficult, many studies have identified that further understanding of the biochemical and mechanical properties of cartilage is important to help generate new biomaterials of similar quality for replacement, or to identify early degeneration to prevent further deterioration of the joint. Indentation techniques on the millimetre scale have been employed for many years to characterise the viscoelastic and biphasic bulk mechanical properties of articular cartilage (Mow et al., 1989; Mow and Huiskers, 2005; Mak et al., 1987; Kempson et al., 1971a; Athanasiou et al., 1991; Setton et al., 1994; Hasler et al., 1999). Clinical indentation devices (handheld, arthroscopic devices) currently used to estimate the mechanical properties of AC use tips with diameters in the millimetre range (Appleyard et al., 2001; Shepherd and Seedhom, 1997; Lyyra et al., 1995). Such large scale device measure the mechanical properties of tissue over a large volume reducing the resolution and sensitivity. Consequently the determination of local heterogeneity is limited with a larger tip diameter. Nanoindentation has

the theoretical ability to measure cartilage *in situ*, and with the smaller probe size it can measure the localised differences of the microstructure of cartilage, and access smaller joints than the larger traditional indentation technique. However the range of methods for applying nanoindentation techniques make comparisons between studies difficult (Table 2.2).

Tip geometry is a key parameter in the analysis and interpretation of nanoindentation data. Bae et al. (2006) demonstrated that for human cartilage, a $1mm$ wide rectangular prism tip generally resulted in higher strain magnitudes than a $1mm$ cylindrical tip for surface, mid, and deep zones of AC. Indenter tips are normally made of hard materials like diamond and sapphire so that the stiffness of the tip is much greater than that of the sample. Tip geometries of three-sided pyramidal tips, such as the Berkovich tip, or cubed corner tips are easy to manufacture and are commonly used for metals, mineralised tissue, polymers and generally stiffer materials. A sharp point is not a concerning factor for these materials however for softer tissue, like cartilage, some researchers are concerned that, compared to a spherical shape, the sharp point will cause plastic deformation and greater stress concentrations to the extent that AC does not return to its original shape (Ebenstein et al., 2004; Li et al., 2006). Spherical geometries however generally have a larger diameter and contact area so finding localised nanoscale mechanical properties is not typically possible. Berkovich tips are used to increase the spatial resolution and allow specific microstructure positions to be measured (Ebenstein and Pruitt, 2006).The Berkovich geometry is corroborated by many studies for its use in soft materials because its opening angle (illustrated in Figure 2.7) confines damage to the tissue (Franke et al., 2007, 2008; Gelse et al., 2008; Franke et al., 2011) and these studies also insist that the edges have a very small involvement in contact area in comparison to the sides. Fischer-Cripps (2004) advocates that due to the self similarity of the tip geometry and the subsequent stress field Berkovich

Table 2.2: Comparison of the litrature protocols and measurements.

Sample	Method	Indenter	Measure	Reference
Human Fixed	Oliver Phar	Berkovich	Modulus (GPa) = 21 - 27	Gupta et al. (2005)
Human	Arthroscope	1 mm Cylindrical	Indenter Force (N) = 2.4 - 5.6	Lyyra et al. (1999)
Human	Scaled measurement	1 mm Hemispherical	Indentation Stiffness Value = 2.4-4.1	Bae et al. (2003)
Bovine	Hayes Model	1 mm Porous	Modulus (MPa) = 0.47 - 1.15	Korhonen et al. (2002b)
Bovine	Linear Isotropic Half Space	5 μm - 4 mm Flat & Conospherical	Modulus (MPa) = 0.62 - 3.43	Simha et al. (2007)
Bovine	FE Biphasic Model	50 μm Conospherical	Modulus (MPa) = 0.53 -0.738	Miller and Morgan (2009)
Bovine	FE Biphasic Model	50 μm Conospherical	Modulus (MPa) = 0.53 - 0.95	Miller and Morgan (2010)
Bovine	Biphasic Poroviscoelastic Model	1 mm Porous & Nonporous	Modulus (MPa) = 0.63	DiSilvestro and Suh (2001)
Bovine	Fibre Reinforces Poroelastic Model	100 μm Conospherical	Modulus (MPa) = 1 - 2.4	Gupta et al. (2009)
Bovine	Dynamic	Cylindrical	Dynamic Modulus (MPa) = 1.5 - 9.5	Kiviranta et al. (2007)
Porcine	Step Loading Oliver Pharr	Berkovich	Stiffness (N/m) Fresh = 200 - 3500 Fixed = 400 - 1600 Reduced Modulus (MPa) Fresh = 0.2 - 8 Fixed = 10.7 - 14.1	Franke et al. (2007)
Porcine	Dynamic	Berkovich	Storage Modulus (MPa) = 2.5 - 7 Loss Modulus = 1.5 - 5	Franke et al. (2011)
Rabbit	Compliance Theory	100 μm Conospherical	Stiffness (N/m) = 12.8 - 237	Li et al. (2006)
Rabbit	Elastic Theory	100 μm Conospherical	Stiffness ($\mu N/nm$) Healthy = 0.170 Repair = 0.03-0.100	Ebenstein et al. (2004)
Horse	Compliance Theory	5 μm Spherical	Modulus (GPa) = 12.44 - 13.65	Doube et al. (2010)
Beagle Dog	Biphasic Poroelastic Model	0.4 mm Cylindrical	Shear Modulus (GPa) Instant = 0.737 Equilibrium =0.0385 - 0.1002	Korhonen et al. (2002a)

tip is beneficial compared to other tip geometries. Flat punches have been used previously for viscoelastic materials (Cheng et al., 2000; Balooch et al., 1998; Larsson and Carlsson, 1998) as they have the advantage of a known, constant contact area without a sharp penetrating point. A study has investigated the effects of different sizes of flat ended punches, ranging from 5 μm to 4mm diameters, on the Young's modulus of cartilage and found clear evidence of increasing tip size results in decreased equilibrium Young's modulus for bovine articular cartilage (Simha et al., 2007) (Figure 2.8). The most significant change in results was demonstrated between 90 μm and 1000 μm. Tip selection will have and does have a great influence on the outcome of nanoindentations results.

Short duration indentation is not affected by a freeze thaw cycle (Kempson et al., 1971a,b; Swann and Seedhom, 1993; Black et al., 1979). However, Franke et al. (2011) investigated the effect of dynamic nanoindentation on porcine AC with a displacement depth of approximately $3\mu m$, and found a significantly lower storage and loss modulus from frozen tissue when compared to fresh tissue. Smaller displacements measure the superficial zone rather than the bulk sample in the earlier study suggesting the superficial layer may be damaged by the crystallization of the water in the cartilage but macroscale mechanical properties are not affected. Again, this suggests that nanoindentation is more sensitive than traditional techniques when analysing AC.

Indentation studies on animals have investigated how the mechanical properties of AC are affected by morphological features. Korhonen et al. (2002a) showed that the thickness of the superficial layer characterised by the tangentially orientation of the collagen fibres strongly affected the isotropic indentation modulus. They also demonstrated that, in canines, as density and orientation of collagen fibrils changed with the depth of AC, the indentation stiffness increased. Signif-

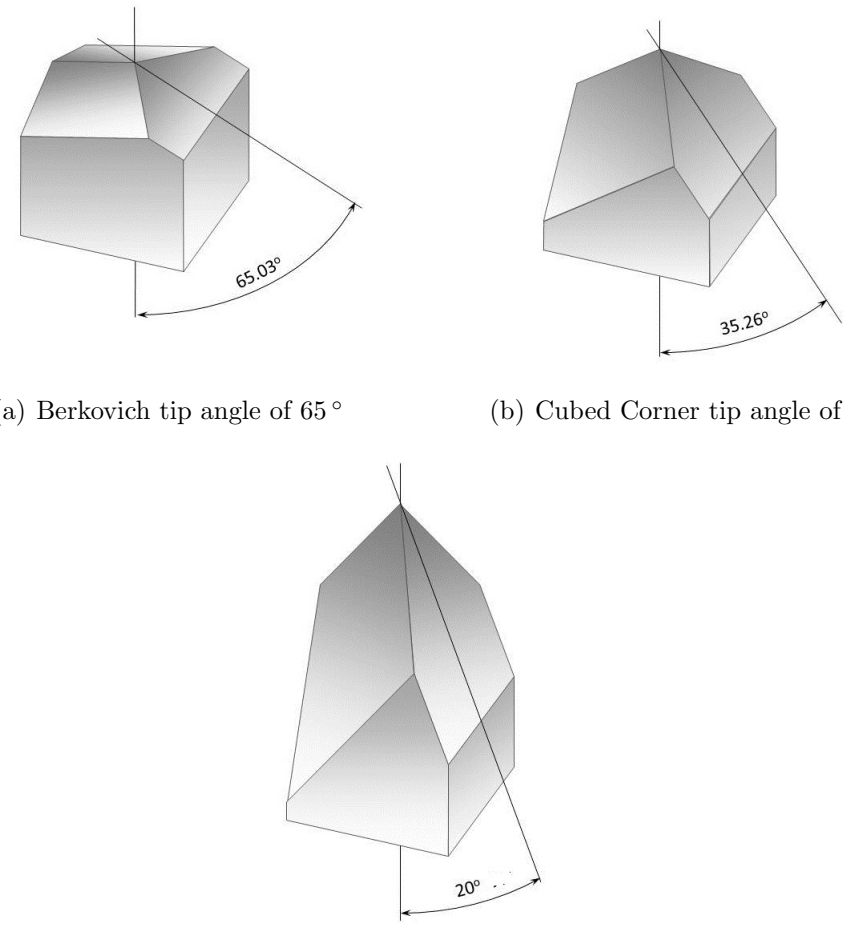

(a) Berkovich tip angle of 65 °

(b) Cubed Corner tip angle of 35 °

(c) Custom tip angles range from 20 ° to 80 °

Figure 2.7: Demonstrates the angle of nanoindenter tips and highlights that the Berkovich tip has an open angle compared with others.

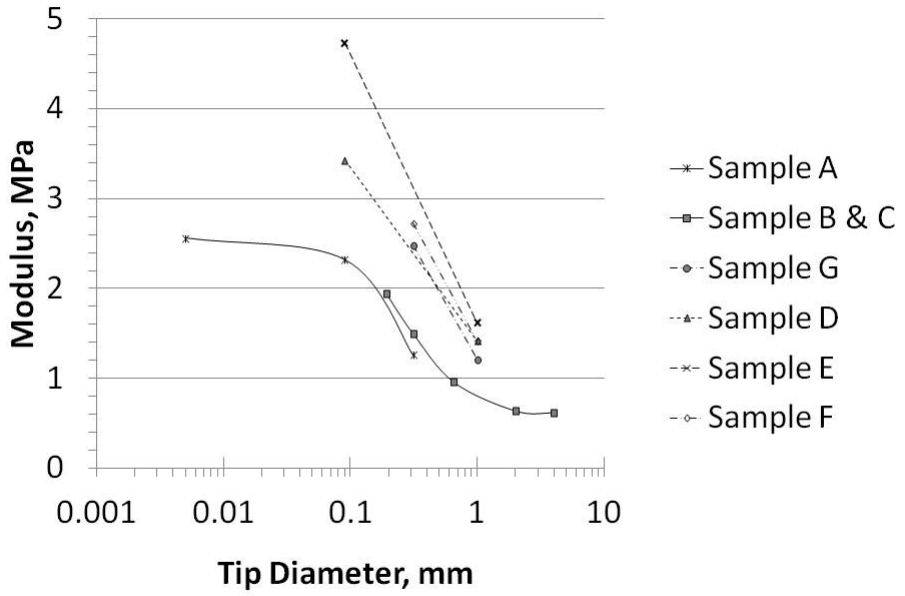

Figure 2.8: An illustration of Simha et al. (2007) results demonstrating a decrease of Young's modulus with increased tip diameter.

icant correlations between the thickness of the superficial zone and the tissues' stiffness and resistance to penetration were identified in rabbit AC (Li et al., 2006). Tomkoria et al. (2004) found a significant gradient increase in Young's moduli from the superficial zone ($0.52MPa$) to the calcifying zone ($1.69\ MPa$) illustrating that the mechanical properties of AC are depth dependent.

Nanoindentation has been used to investigate difference in mechanical properties across several locations in joints. Li et al. (2006) found that on skeletally mature, female, rabbits' left forelimbs, with a more distal position of cartilage, a reduced stiffness of $36.5N/m$ was recorded compared to the proximal locations with a reported stiffness of $146.9N/m$. Tomkoria et al. (2004) also studied rabbits and found the Young's modulus of the medial condyle was $1.46\ MPa$, the lateral condyle was $1.18\ MPa$ and the groove measured the least at $0.96MPa$.

In beagle dogs site-dependent differences were demonstrated, with humeral head shear modulus reported to be $1.002MPa$ compared to $0.385MPa$ recorded at the medial tibial plateau (Korhonen et al., 2002a). Laasanen et al. (2003a) also found regional differences in the mechanical properties of AC in bovine knee joints, demonstrating a significant decrease of dynamic modulus from the lateral facet of the patello-femoral groove (10.1 MPa) to the femoral medial condyle (4.6 MPa) and to the medial tibial plateau (2.9 MPa). Previous work on the topographical variation in the mechanical properties of the human knee has been investigated using a variety of techniques. Indentation methods have demonstrated that the softest cartilage was located at the tibial plateau, the patellar surface of the femur was also soft but the femoral condyles were much stiffer (Swann and Seedhom, 1993; Yao and Seedhom, 1993). Lyyra et al. (1999) used an arthroscopic *in vivo* technique that found the lateral condyle to be softer in the femur and medial plateau in the tibia, Swann and Seedhom (1993) measurements agreed. Biphasic and arthroscopic indentation established that the stiffest measurements were recorded at the lateral femoral condyle and softest located in the patellar groove. However a study on the patellar measured the lateral facet to be stiffer than the medial facet (Froimson et al., 1989) which is conflicting to Mow and Huiskers (2005) and the arthoscopic results (Lyyra et al., 1999) who found the AC on the lateral plateau to be stiffer. These studies do not use techniques that have the sensitivity provided by nanoindentation which may explain the disagreement in results. The studies do highlight the significant differences in mechanical properties in the human knee joint.

To date, the human hip joint has not been characterised, despite it having the highest prevalence of OA of all joints.

2.4.3 Factors affecting AC indentation

Creep is the most commonly observed visco-elastic response of cartilage in indentation tests (Briscoe et al., 1998). In soft materials creep can dominate the unloading curves giving a 'nose' effect, Figure 2.9(a). The 'nose', a result of the material's memory of the loading movement prior to unloading, is apparent in experiments when maximum force is reached yet unloading has begun and the indentation depth continues to increase (Cheng and Cheng, 2005b). It has been noted that with slow loading and unloading the nose is more evident but with increased unloading rate (Cheng and Cheng, 2005a) or when the load is held before unloading, the 'nose' disappears, Figure 2.9(c). The 'nose' effect is only apparent in load controlled indents so is not evident when the indent is displacement controlled.

Thermal drift can also affect end results especially with testing over a longer period. Feng and Ngan (2002) however, proposed that if the modulus is proportional to the contact stiffness and inversely proportional to contact depth and in addition the effects of thermal drift on contact stiffness is equal to the effect on contact depth therefore the effect on thermal drift on modulus can be eliminated due to the realisation of Equation 2.1; the effect of thermal drift on contact stiffness negates its effect on contact depth.

$$t_h \approx \frac{S}{\left|\dot{P}\right|} h_c \tag{2.1}$$

Where t_h is the time of unloading, $\dot{P}$ is the unloading rate at the onset of unloading, S is the contact stiffness and h_c is the contact depth. This study believes

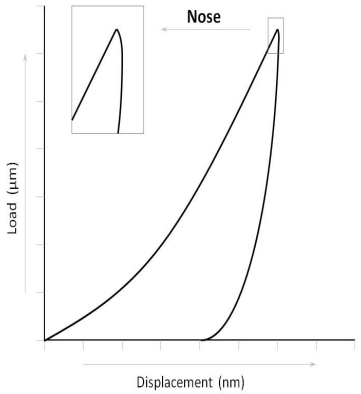

(a) Nose

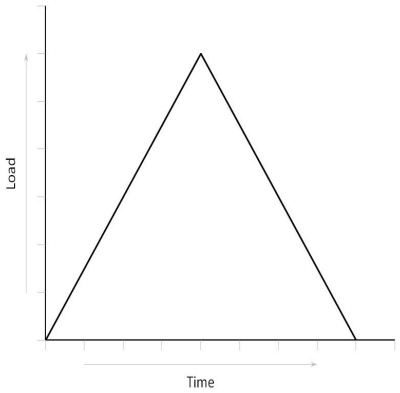

(b) Triangular load associated with the Nose effect.

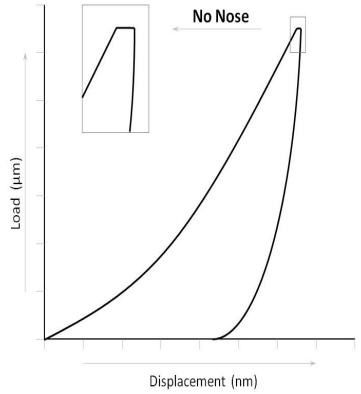

(c) No Nose

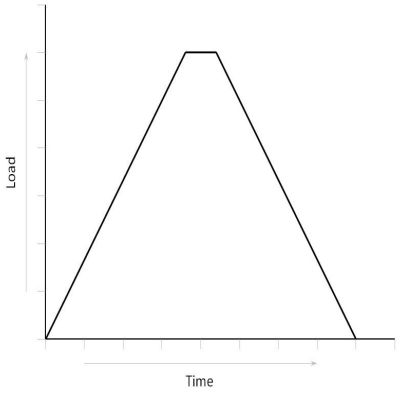

(d) Trapeziodal load associated with removing the Nose effect.

Figure 2.9: (a) Demonstration of the 'nose' effect from viscoelastic material with a triangular load. (c) Demonstration of a trapezoidal load, which results in no 'nose' effect. Adapted from Ebenstein and Pruitt (2006).

that the effect of thermal drift is nullified when measuring modulus so no requirement for correction ensues.

Nanoindentation was initially designed to investigate stiff materials like ceramics or metals, and although theoretically nanoindentation automatically detects the surface of the testing material, surface location for soft biological materials is very difficult (Kaufman and Klapperich, 2009) as biological tissues are 4 - 6 orders of magnitude softer with rougher surfaces (Stolz et al., 2004). This can result in load displacement curves that demonstrate no distinct increase in load to illustrate surface contact. The adhesion behaviour of soft hydrated materials adds to the complexity of surface detection in the direction of the indent (Ebenstein and Wahl, 2006; Wahl et al., 2006) and experiments triggering in the sample surface will result in over estimation of the moduli (Kaufman and Klapperich, 2009). In order to enhance the accuracy of surface location, indentation in displacement control is advised (Cao et al., 2005) and with the use of optics manual location of the surface is possible. Using this method thermal drift during hold segments is reduced and a more consistent depth of indentation is achievable. The explicit determination of surface position is crucial to the correct measurement of mechanical properties.

2.4.4 Analysis Techniques

Nanoindentation has been repeatedly reported to be a powerful tool in measuring mechanical properties and has the potential capability to be used as a diagnostic tool to identify early OA (Franke et al., 2007; Ebenstein and Pruitt, 2006; Bae et al., 2006; Korhonen et al., 2002a). However this technique is not currently in commercial use for diagnosis, perhaps as the literature is inconsistent. In general,

there is a lack of agreement as to the correct material properties to measure and report, plus an absence of agreement on the most appropriate method to analyse and interpret the raw data. This section will describe the variety in analysis methods and highlight the arguments in the literature.

Theoretically, material properties measured using indentation can be split into four modes of deformation: elastic, plastic, viscous, and fracture. Plastic and fracture deformation are categorised by threshold values however elastic deformation is time and rate independent with no threshold and viscous deformation is time-dependent. In reality many materials demonstrate a varying degree of the described deformation. Materials can be elastic-plastic, viscoelastic, poroelastic, visco-elastic-plastic, brittle, biphasic plus further combinations. Oyen and Cooks' guide to nanoindentation (Oyen and Cook, 2009) suggest that identifying the correct indentation protocol and analysis is simple if researchers follow a flow chart similar to Figure 2.10. Literature specific to AC does not agree because of the hierarchical complex structure which results in a highly load and hold history dependent mechanical reaction. Stolz et al. (2004) justify a dynamic indentation method with no hold as they argue that the frequency of unloading and loading of normal ambulation (walking and running) means the cartilage illustrates no fluid movement through the structure in this short time so an instantaneous Young's modulus is an appropriate measure however, as people tend to spend twice as much time standing rather than walking per day (Najafi et al., 2010) the creep response of AC is also an appropriate measure. Many studies insist that the time-dependent factor, mainly due to the 80% interstitial fluid in cartilage, is vital to the material properties with many studies investigating different analysis techniques to include this factor.

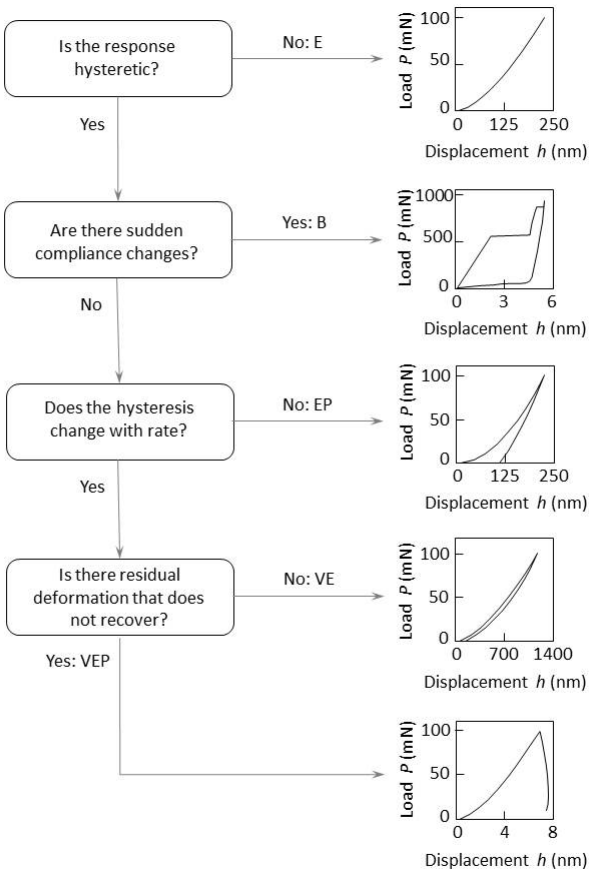

Figure 2.10: A chart for distinguishing dominant modes of deformation in instrumented indentation from force-displacement curves. The five reaction natures are demonstrated as: E, elastic; B, brittle; P, plastic; V, viscous. Adapted from (Oyen and Cook, 2009)

Analysis models traditionally were based on Hertz's contact theory (Hertz et al., 1896), but Doerner and Nix (1986) were the first to produce complete indentation data analysis and assumed a linear relationship between load and displacement for the unloading curve. Most commercial instruments are fitted with the Oliver-Pharr model (Oliver and Pharr, 1992) for analysis; they improved on the Hertz's contact theory by linking Sneddon's relationship (Sneddon, 1965) to simple tip geometries. Sneddon derived a function that described the general relationship among load, displacement and contact area of a punch. The results demonstrated that load-displacement relationships for many punch geometries can be described by

$$P = \alpha h^m \tag{2.2}$$

where P is the indenter load, h is the elastic displacement and α and m are constants. Equation 2.2 calculated the contact area at maximum load and Oliver and Pharr (1992) derived the following relationship (Equation 2.3) from Sneddon's equation to account for the changes in contact area as the tip is unloaded.

$$h_c = h_{max} - \epsilon \frac{P_{max}}{S} \tag{2.3}$$

Where $\epsilon = 0.72$, 0.75 and 1 respectively for conical, paraboloid and flat tip shapes. The correction factor for tip shape imperfections (Oliver and Pharr, 1992) has shown significant enhancement in data analysis.

The Oliver-Pharr method (Oliver and Pharr, 1992) is applied to the unloading curve as it assumes it is characterised by the elastic recovery only. This method continuously measures the force as a function of displacement and records the force-displacement curves; Figure 2.11 illustrates the parameters measured for this method. The Oliver-Pharr model calculates contact stiffness, S, and instantaneous Young's modulus evaluated at maximum displacement. This method also

assumes that the testing material is smooth, homogenous and an isotropic elastic half space. These assumptions do not describe AC well.

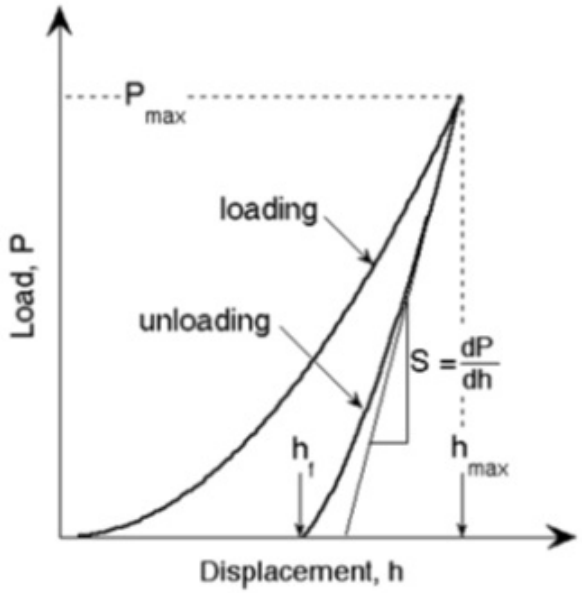

(a) Schematic illustration of force displacement data.

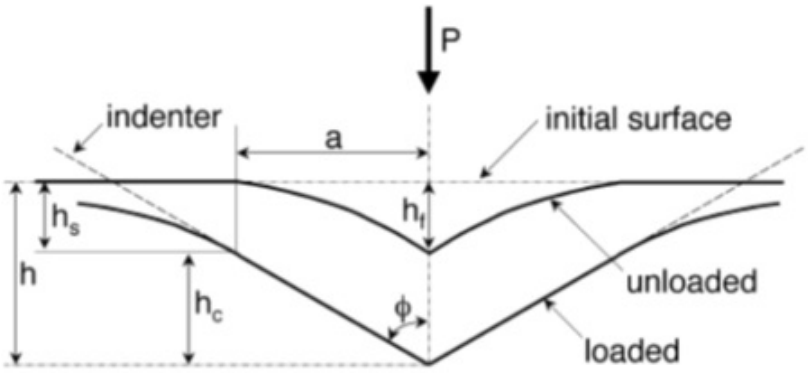

(b) Schematic illustration of indentation.

Figure 2.11: A schematic illustration of the various quantities used in the Oliver-Pharr method (Oliver and Pharr, 1992).

The Oliver-Pharr method has significant errors for application to AC. Firstly cartilage does not confirm to the model's assumptions as it is hetroegnous and not an isotropic elastic half space. The area function that improves this model over others is calibrated on a hard material; as soft materials react differently this correction factor maybe false. With small indentations, tip imperfections have greater effect on the final result (Oliver and Pharr, 1992).

Some studies have investigated adaptions of the compliance method for time-dependent and viscoelastic materials and, as discussed in section 2.4.3, creep is a significant problem for indentation protocol and analysis. Faster unloading of viscoelastic tissue enables the application of the Oliver-Pharr method to produce instantaneous modulus, without creep giving a false negative result (Ebenstein and Pruitt, 2006). In addition a hold section between loading and unloading is also advised for these materials (Briscoe et al., 1998; Ngan et al., 2005) to allow the creep rate to dissipate before unloading (Figure 2.9(c)). Ngan et al. (2005) developed a relationship to measure the instantaneous modulus from the initial unloading slope from an indentation with a hold period.

$$\frac{1}{S_e} = \frac{1}{S} - \frac{\dot{h}_h}{\dot{P}_u} \tag{2.4}$$

In viscoelastic materials S_e is the correct elastic stiffness, S the apparent contact stiffness, $\dot{h}_h$ the tip displacement prior to unloading and $\dot{P}_u$ the unloading rate. This relationship can work in conjunction with the Oliver-Pharr method improving capability by including a viscoelastic situation.

Nonphysical, negative Young's moduli measured using equations involved in the compliance method have resulted in studies suggesting that this method is not applicable for the indentation of viscoelastic materials (Lu et al., 2003; Kumar and Narasimhan, 2004). Cheng and Cheng (2005a) investigated this theory: they determined that with the correct loading and unloading parameters the instantaneous modulus from the initial unloading curve holds true but suggest further investigation is needed into the unloading rate as this is the main source of disagreement between studies.

Dynamic indentation is suggested to be beneficial for viscoelastic materials. Dynamic indentation involves an oscillation superimposed on the normal load signal which supplies a constant recording of modulus throughout the test (also referred to as the continuous stiffness (Oliver and Pharr, 1992)). Dynamic indentation of cartilage displays a phase shift, as long as resonance is not achieved, between applied and measured responses (Franke et al., 2011). The mechanical response can be split into the storage modulus E' and loss modulus E" or together as a the dynamic modulus E*. Cao et al. (2009) performed a comprehensive computational investigation across dynamic indentation protocols and found that dynamic indentation linked with relaxation hold procedures could determine high levels of accuracy (according to numerical simulations): a variety of protocols to measure the viscoelastic mechanical response of cartilage exist in the literature (Wen et al., 2012; Loparic et al., 2010; Li et al., 2006; Stolz et al., 2004; Ebenstein et al., 2004).

As cartilage can illustrate a time-dependent response, dynamic indentation studies have also used a range of protocols and data analysis models for example, Franke et al. (2011) studied the dynamic response of porcine cartilage implementing the Kelvin Solid model (a parallel alignment of dashpots and springs that describe a delayed mechanical response) and presented the results in terms

of storage and loss modulus. Stolz et al. (2004) described their results using the dynamic modulus E* and assumed that E*=E (indentation modulus, equation 2.5) which was calculated from the final unloading curve according to the Oliver-Pharr method.

$$E = \frac{\sqrt{\pi}}{2}(1-\nu^2)\frac{S}{\sqrt{A}} \tag{2.5}$$

In 1982, the biphasic nature of cartilage was addressed by Mow and Huiskes who extended the analysis method to include the effects of fluid flow by including the linear KLM model for cartilage. They suggest that equilibrium modulus, Poisson's ratio (ν) and permeability (K) are sufficient material parameters to describe the instantaneous, equilibrium and time-dependent behaviour of AC (Mow and Huiskes, 1982; Mak et al., 1987). The initial studies focused on numerical algorithms and curve fitting strategies to identify the biphasic indentation behaviour of cartilage (Mow et al., 1980, 1989). Recently attention has focused on computational models using finite element (FE) modelling or discrete computational models. These models have included: biphasic (Miller and Morgan, 2010, 2009); biphasic poroviscoelastic (DiSilvestro and Suh, 2001); fibre reinforced poroelastic (Gupta et al., 2009); and poroviscoelastic fibril reinforced (Wilson et al., 2004; Julkunen et al., 2008) models.

The biphasic-modelled studies used the best matched biphasic material properties between FE computed simulation of the nanoindentation of cartilage and experimental data calculated E, ν and K (Miller and Morgan, 2010, 2009). Cartilage was modelled as a homogenous, isotropic linear material but also as porous material with a void ratio representing the 80% fluid (Miller and Morgan, 2010). DiSilvestro and Suh (2001) developed an FE model based on the mathematical model by Mak (1986), the biphasic poroviscoelastic model. The study (DiSilve-

stro and Suh, 2001) insists this model has an extraordinary capability to account for experimental data from more than one testing method to describe the mechanical response of cartilage. Other studies however have also included the behaviour of collagen fibres as well as the fluid flow. Garcia et al. (1998) state their biphasic viscohyperelastic fibril reinforced finite element model is able to simultaneously consider the non-linear tension-compression response and the fundamental effects of the solid phase (Garcia and Cortas, 2007). Originally the stress, strains and deformation of the collagen fibrils are calculated using an FE poroviscoelastic fibril reinforced (Wilson et al., 2004) model which could be very useful for evaluating cartilage degeneration as the fibril network changes.

With further investigation these models illustrate the complexity of analysing cartilage indentation tests. Furthermore Julkunen et al. (2008) have highlighted that the zonal composition of cartilage, the poro-visco-elastic behaviour combined with the diversity of thickness of cartilage, has not been completely considered by the different models. The literature is inconsistent; all insist their method is superior. Tissue heterogeneity together with model complexity gives rise to an abundance of parameters that can be incorporated into AC analysis. Given this large number of available parameters, it is no surprise that good data fits are achievable however, in unambiguously identifying and characterising OA, it may be best to focus on one or two key parameters in the first instance. Whilst many parameters are available to study, it seems sensible to start with stiffness and Young's modulus, as defined in the Oliver-Pharr model (Oliver and Pharr, 1992), as these have previously been identified as the most important material measurements. Dynamic analysis seems an appropriate secondary step in an understanding of human AC mechanics.

2.5 AFM

Conventionally electron microscopy (EM) was utilised for imagining biological samples (Buckwalter et al., 1984) but sample preparation included: extensive fixation, dehydration; staining and coating. In 1986 Binnig et al. developed Atomic Force Microscopy (AFM); an alternative approach to EM that provides visualisation at an angstrom level. AFM is a technique that produces high resolution images and minimally interferes with the sample in preparation and during imaging. This technique has investigated: DNA proteins, tissues, biomaterials and others.

The principle of AFM depends upon the scanning of a small mechanical probe over the material's surface which establishes the surface topography. AFM relies on the measurement of interatomic forces between the sharp mechanical probe tip (typically $10nm$) and those of the sample (Morris et al., 1999). There are two main AFM modes: contact mode and AC mode (also known as tapping). In contact mode the tip touches the surface and as it moves across the sample the deflection of the cantilever is observed as a feedback mechanism. A height topography image is produced by plotting the data from the feedback correction and the X and Y signal.

A stiffer oscillating cantilever is used in AC mode and the tip stays a defined distance above the surface throughout the scan. As the oscillating cantilever approaches the surface the amplitude changes, the deflection feedback and adjusts the height back to the original distance with respect to the samples surface. Basically the adjustment in the height of the cantilever creates an image of the surface topography without contact of the sample.

2.5.1 Imaging

Understanding the mechanics of tissues continues to be a major scientific challenge and an essential aspect of this is understanding the nanoscopic interplay between the basic compositional elements of the tissue (Gao et al., 2003; Roschger et al., 2003). High resolution of AFM has identified in bone a dense arrangement of interconnected collagen fibres surrounding the tabecular with linked polymers between and on the fibrils (Hassenkam et al., 2004) when dehydrated. This technique has also quantified that that the spacing between the collagen fibres in bone is $15 - 30nm$. With greater understanding of the building blocks of materials, more advanced applications and understanding is possible.

Images of articular cartilage have been acquired with AFM. Sample preparation is key for clear images and a variety of techniques have been used to achieve this. The best resolution occurred when the cartilage samples were cut to $20\mu m$ slices, dehydrated and imaged in contact mode (Stolz et al., 2004; Loparic et al., 2010), Figure 2.12. Imaging fully hydrated AC samples reduces the resolution as illustrated in Figure 2.12(c). The images are still blurred even when initially digested in Chondroitnase AC to extract the extracellular matrix proteoglycans Figure 2.12(c) (Jurvelin et al., 1996). Stolz et al. (2004) only published images acquired in air, presumably as the quality was superior to those in fluid. AFM images improved the superficial fibril clarity and revealed the fibrils to be in a predominantly parallel direction with a mean diameter of $35nm$ and periodic crimping of $60\pm5nm$ (Jurvelin et al., 1996). Often a variety of surface profiles have been revealed with AFM but the most frequently found is described above. Cartilage has been reported to have a surface roughness of $462nm$ (Park et al., 2004).

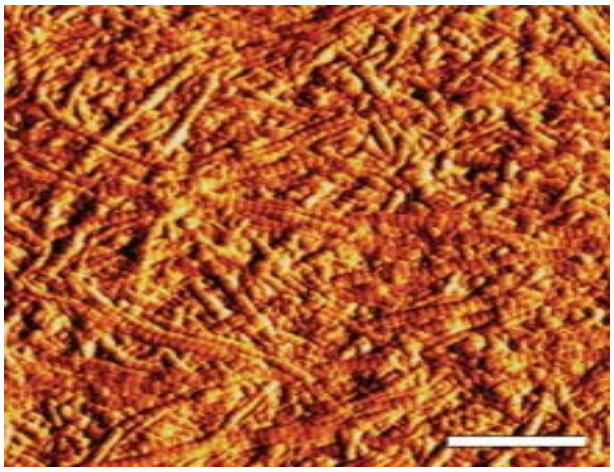

(a) Dehydrated AFM image of Articular Cartilage (Stolz et al., 2004).

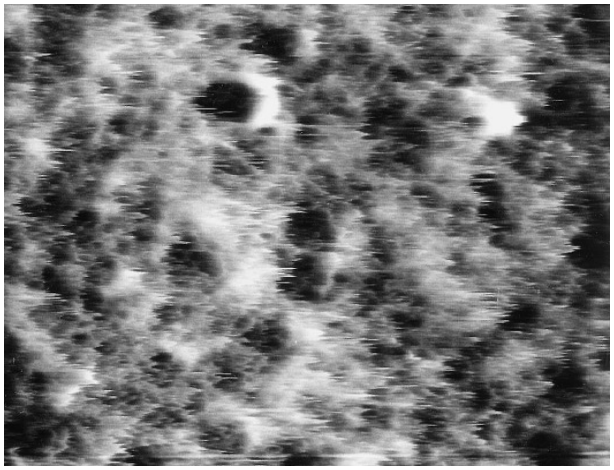

(b) AFM image of Articular Cartilage under buffer solution (Jurvelin et al., 1996).

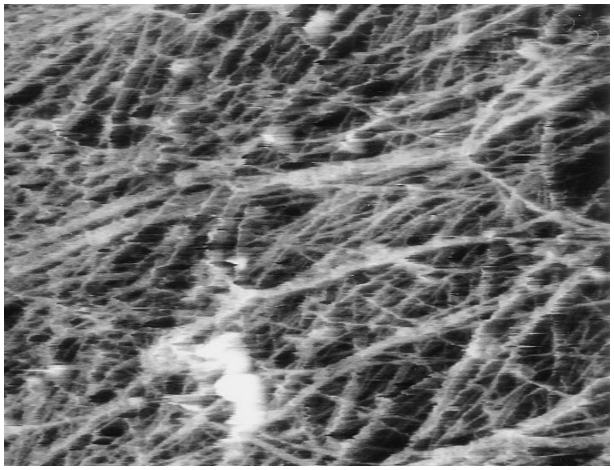

(c) AFM image of Articular Cartilage under buffer solution after digestion with Chondoitnase (Jurvelin et al., 1996).

Figure 2.12: Published AFM images of AC.

For high resolution images a slow scanning velocity with a scanning frequency below $2.5Hz$ is advised as faster velocities skip important features (Jurvelin et al., 1996). An AFM sharp pyramidal tip with a nominal radius of 20 nm is able to clearly image the surface of AC demonstrating the collagen fibre network in detail. In contrast, a microspherical tip with a 2.5 μm radius can image the surface but is not capable of depicting the resolution of individual fibrils, resulting in the surface appearing comparatively homogenous (Stolz et al., 2004).

An age-dependent thickening of collagen fibres has been observed with AFM imaging, a detail not seen in SEM images (Stolz et al., 2009). The apparent diameters of mouse collagen fibrils increased from $52nm$ at 1 month to $812nm$ at 19 months (Stolz et al., 2009). Human studies have observed that the structure of intact AC is characterised by densely packed collagen fibrils while osteoarthritic AC is composed of a disorganised collagen network, but Wen et al. (2012) showed no difference in the D-perodic banding of the fibrils of intact and osteoarthritic AC.

AC is covered by an amorphous, non fibrous lubricant known as synovial fluid. Through AFM analysis Crockett et al. (2005) demonstrated that washing the samples in PBS for 5h removed this gel-like layer, whilst others suggested wiping the surface (Ghadially, 1983), which was not completely effective. The swelling effect when washing the AC in PBS has not been investigated but it has been shown to remove the synovial fluid without damaging the collagen fibres (Crockett et al., 2005). This further demonstrates the importance of sample preparation for quality imaging of AC with AFM.

2.5.2 AFM Indentation

AFM technology permits simultaneous imaging and stiffness measurements of a micrometre and nanometre scale in a natural environment for samples. Nanoindentation AFM was established in the early 1980s to investigate coatings with an enhanced sensitivity to traditional techniques (Newey et al., 1982). It took over a decade for the first work to be published on bone (Thurner, 2009) which has now transpired to be an exceptionally successful assessment tool for the elastic modulus of bone. However strong adhesive forces have been reported when mapping AC in fluid, to the point that the force curves could not be used to calculate the mechanical properties due to the adhesion and surface swelling (Crockett et al., 2005). Cartilage indentation testing has shown greater difficulty when compared to harder materials.

Cartilage studies have compared force maps with microscale spherical tip to nanoscale pyramidal tips. Microscale indentions for porcine AC have been reported to have a narrow Gaussian distribution unloading curve histogram with an average modulus of 1.3 MPa (Loparic et al., 2010). Nanoscale indentation identified a bimodal distribution in the unloading curve histogram, Loparic et al. (2010) suggests this distribution is identifying the proteoglycan gel with an average of 22.3 kPa and collagen fibril modulus with an average of 384 kPa. Stolz et al. (2004) agreed that nanoscale tips measure a smaller modulus reporting an average of 21 kPa compared to 2.6 MPa with a microscale tip.

Force-relaxation experiments with AFM have reported a relaxation instantaneous modulus from 0.11 MPa to 0.06 MPa after a 60 s hold section suggesting the time-dependent behaviour of AC is predominantly characterised by the viscoelastic nature of the extracellur matrix (Han et al., 2011). Time-dependent relax-

ation is also highlighted by dynamic oscillating AFM indentation tests; the loss modulus and dynamic modulus significantly decreased and the storage modulus increased with increasing dynamic deformation amplitude for healthy porcine AC (Han et al., 2011). AFM can be executed with different indentation patterns to observe the different mechanical responses of AC.

Microscale AFM measurements have not identified change in stiffness with age however nanoscale indents have an age-dependent increase in stiffness (Stolz et al., 2009; Wen et al., 2012): specifically Stolz et al. (2009) found that in humans over the age of 71 this alteration was evident with an increase from 15 kPa (between the ages of 38 to 50) to 142 kPa (between the ages of 71 to 96). However osteoarthritic cartilage illustrated a softening when measured with AFM (Stolz et al., 2009) and this dominated the age-dependent stiffening effect. Healthy cartilage has been reported to have a modulus of 83 kPa but diseased AC has progressively softened to a modulus of 5.6 kPa for grade 3 OA in the Outerbridge scale (Stolz et al., 2009). Stolz et al. (2009) suggest this is due to the depletion of proteoglycan as it has been reported that with the digestion of proteoglycans a decrease in modulus is evident (Han et al., 2011). Wen et al. (2012) found that the individual collagen fibrils with OA have an increased stiffness similar to the ageing increase in stiffness of AC, corroborating that proteoglycan depletion is potentially the reason for the reduction in cartilage stiffness in OA specimens.

Indentation with an AFM cantilever is attractive due to the impressive force resolution. However cantilevers have several degrees of freedom in displacement at the tip location, which results in unintended displacements and rotation during indentation, unlike equipment designed only for nanoindentation (Figure 2.13). Given that typical length of contact areas is of the same order of magnitude or smaller than the unintended displacements, nanoindentation experiments with

AFM cantilevers are not able to produce quantitative results, only qualitative comparisons among samples.

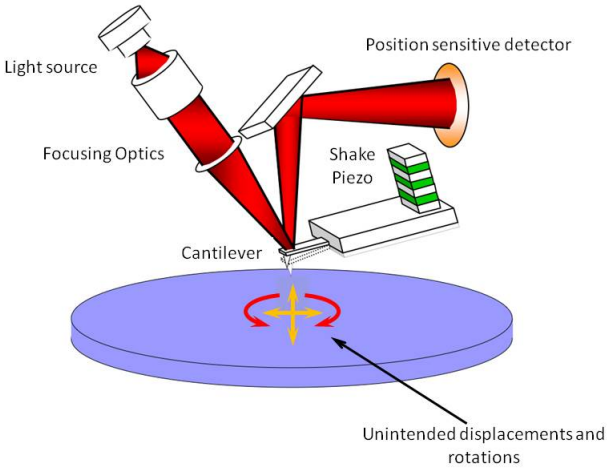

(a) AFM Schematic

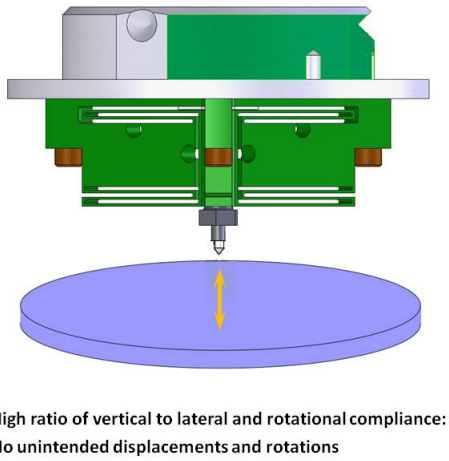

(b) Nanoindeter Schematic

Figure 2.13: Illustrates the inadvertent rotational movement in the AFM compared to the controlled displacement in the Nanoindenter.

2.6 Effect of fixation on tissue mechanics

As medical procedures improve and change, physicians (from interns to specialist surgeons) require training to improve their skills without the pressures of theatre (Supe et al., 2005). Many studies have shown that training on human cadavers rather than on animals is of greater benefit for improving techniques as the anatomical identification is simpler (McCarthy et al., 2002) and it is easier to identify the effectiveness of different approaches (Milsom et al., 1994; Said et al., 1999). Fresh frozen human specimens are the best choice for training as they initially display natural colour, softness and pliability (Macchi et al.), however there is a risk of high biological contamination, rapid putrefaction once thawing occurs and the large cost associated with fresh frozen human tissue make its use problematic. The alternative is chemically embalmed specimens.

Formalin fixation is the most conventional embalming method. Formalin is an aqueous solution of formaldehyde which disinfects and reduces contamination. Formalin preserves tissue while maintaining the tissue composition. The disadvantage of formalin fixation is that the aldehydes react with the amine groups of the collagen chains, resulting in increased cross-links altering the mechanical properties of the tissue. With long term preservation (over 8 weeks) in formalin Ohman et al. (2008) found fixed samples to have a 20% higher yield stress and a 53% higher ultimate strain than fresh frozen bone. Formalin also makes soft tissue more brittle; Viidik and Lewin (1966) found that embalmed tendons had a failure load of 23.9 $kpmm$ compared to fresh frozen tissue with a failure load of 53.3 $kpmm$. A cartilage specific study found formalin to drastically change the mechanical response as the fixed samples could be characterised by an almost linear relation between load and displacement, creating a homogenous tissue unlike fresh frozen cartilage which is heterogeneous (Franke et al., 2007). The reduced

modulus of the fixed cartilage samples was double that of the fresh frozen cartilage (14.5 MPa and 7.2 MPa respectively).

An alternative is Thiel fixation which is becoming ever more commonly used for cadaver workshops as: it maintains natural colour; it causes no hardening of the tissue and is less odoriferous than formalin fixation. Additionally, the compositional structure is preserved and no swelling or contractions of the tissue are evident (Thiel, 1992). Studies disagree whether Thiel fixation affects the mechanical properties of tissue. Boryor et al. (2010) found Thiel-fixed cadaver skulls to follow the same linear material behaviour as fresh skulls. On the other hand (Stefan et al., 2010) compared the properties of fresh and Thiel-fixed human cortical bone and discovered that the Thiel-fixed bone had significantly higher ultimate strain and plastic energy absorption compared to fresh bone however no difference between Young's modulus was observed until 6 months of fixation. The tangential elastic modulus in tendons was measured to be 448 MPa when Thiel-fixed which was significantly lower compared to fresh frozen tendons 654 MPa. Despite the reported altered properties, the general consensus is that Thiel fixation would be an excellent model for training surgeons and could be useful for preliminary experiments on new implants. As the number of joint replacement surgeries is increasing and a growing need for high-quality cadaver workshops and improved implants is required, the effect of Thiel fixation on the mechanical properties of cartilage needs to be investigated as an alternative to fresh tissue.

2.7 Summary of Literature Review

The mechanical characteristics of cartilage are complex, as they alter with activity (standing or walking) and with the depth of the tissue. AC is composed of 4 zones with differing quantities and configurations of: collagen fibres; proteoglycans; interstitial fluid and chondrocytes (section 2.1). The composition is directly linked to the functional capability of cartilage. The collagen fibres in the superficial zone are oriented parallel to the surface providing strength and stiffness as well as resisting shear stress and tensile stress. The chondrocytes in this layer produce proteins that contribute to maintaining a smooth surface for efficient motion. The drop in collagen content, in the transitional zone, allows the negative charges of the proteoglycan to attract more interstitial fluid which increases the osmotic pressure that plays a key part in the load support ability of AC. The distribution of load is the deep zone's most predominant responsibility due to the high level of proteoglycans. Healthy articular cartilage provides a low-friction, wear-resistant surface in joints and disperses stresses to underlying bone, however osteoarthritis is a degenerative joint disease that affects AC and results in disability (section 2.3).

Whilst a histological physiological description of the degenerative process of OA on cartilage is available (multiple different grading systems), there is a distinct lack of understanding of the alterations of the AC biomechanical properties through degeneration, with currently no biomechanical grading system to complement those of the physiological grading systems. To date there are no effective treatments to repair AC or cease deterioration once OA is visible, until the degeneration is so severe and painful that a joint replacement surgery is required, therefore it is essential to detect OA in the early stages at a time when it remains reversible (Pollard et al., 2008). The current diagnostic techniques do not have

the sensitivity to identify OA at this stage and in addition the pathophysiology of OA initiation remains uncertain (Pollard et al., 2008). As nanotechnology has enhanced, it provides the potential to identify OA before permanent microarchitectural damage develops in AC.

Atomic Force Microscopy has demonstrated an ability to produce high resolution images of a variety of biomaterials in an ambient environment. AFM has the theoretical capability to characterise OA degeneration in an ambient environment at nano-scale, unlike the current grading systems which only describe the OA degeneration process once tissue is chemically altered and dehydrated, or do not provide details of early OA degeneration. However current AFM studies (Wen et al., 2012; Stolz et al., 2004; Loparic et al., 2010; Jurvelin et al., 1996; Stolz et al., 2009; Crockett et al., 2005) have only achieved clear images when the AC samples are dehydrated and cut into thin slices. Further work needs to investigate AFM's potential as a useful tool to image cartilage in a physiological natural environment to aid the understanding and early detection of OA.

Nanoindentation has become a common technique for the analysis of biomechanical properties of biological tissue, bridging the gap between AFM and macro-scale mechanical testing (Ebenstein and Pruitt, 2006). Most existing indentation research has focused on hard tissue such as bone, enamel or dentine (Lewis et al., 2008). Load and displacement are observed during indentation and the mechanical properties may be extracted using a variety of analysis methods. There is a growing body of evidence indicating that nanoindentation could provide the fine force sensitivity to identify, in detail, the change in mechanical properties of osteoarthritic cartilage and where osteoarthritis initiates. Recently, micro-scale and nano-scale indentation research has investigated the effect of indenter properties on the measured mechanical properties of AC: with increasing tip diameter there

is a significant decrease in equilibrium elastic modulus (Simha et al., 2007) and the tip geometry affects the elastic modulus depending on the depth of the indent into the cartilage (Bae et al., 2006). The time-dependent mechanical behaviour of AC introduces complexity into the extraction of its mechanical properties, and multiple moduli have been quantified. Moreover, many nanoindentation protocols for calculating these moduli have also been explored: dynamic nanoindentation (Franke et al., 2011); stepwise stress-relaxation indents (Korhonen et al., 2002b); *in vivo* arthroscopic indents (Bae et al., 2003); biphasic-hold indents (Miller and Morgan, 2010, 2009) and computer modeling (Biot, 1956; Mow et al., 1980; Frank and Grodzinsky, 1987; Mak, 1986). Most studies have focused on animal models rather than human models as animal tissue is easier and cheaper to acquire and requires less strict ethical guidelines. Macro-scale mechanical experiments have identified significant differences between the mechanical properties of human cartilage and those of animal cartilage demonstrating that for most relevant and superior understanding of OA human cartilage, human tissue should be investigated.

Fresh human cadaveric specimens are the gold standard for investigating new concepts and implants for treatments of a variety of medical conditions, however for testing over a long duration or surgical training, the limited supply, rapid decay and risk of infection can mean fresh tissue is not always appropriate. Chemical fixation is the alternative method for storing tissue to freezing. Formalin fixation is the most common chemical to preserve tissue, however it is known to harden the tissue (Viidik and Lewin, 1966). Fixation according to Thiel (Thiel, 1992) is another option to conserve human tissue and presents an almost natural mobilisation of a range of body parts, with several surgeons describing it as lifelike. Minimal studies have investigated the mechanical properties of Thiel-fixed tissue (Benkhadra et al., 2008; Holzle et al., 2012; Peuker et al., 2001) and further work

is required to find out how this method affects the mechanical properties compared to fresh frozen tissue as it is becoming an increasingly popular technique. Studies confirmed that formalin fixation increases the Young's modulus of AC (Franke et al., 2007) however currently no studies have demonstrated the effect of Thiel fixation on AC despite the growing need to improve surgical skills and to improve implants needed for joint replacement surgery.

2.8 Aims & Objectives

This chapter has demonstrated that OA is a financial burden on society as there is no cure except complete replacement surgery and there is a lack of knowledge of where and why OA initiates. A total of 80,314 hip replacements in England and Wales were preformed 2011 (National Joint Registry Annual **?**) the majority of these were due to OA. AFM and nanoindentation are techniques with the theoretical potential to provide more informed details about cartilage's specialised mechanical characteristics and how OA affects AC. As these techniques are more sensitive than current osteoarthritic clinical diagnosis devices, they may have the capability to identify earlier biomechanical modification. Previous studies demonstrate high resolution images of dehydrated AC using AFM but there is a lack of published quality images of fully hydrated or full thickness AC samples which is what is required to improve knowledge. The first objective of this project was to investigate and develop methods to analyse articular cartilage in as environmentally natural conditions as possible (hydrated and full thickness) with AFM and nanoindentation and to provide a method to improve the current knowledge of OA.

Nanoindentation has already been demonstrated to be a useful tool to characterise AC in animals, however whilst the effect of some extrinsic factors such as tip size on the various tissue moduli have been investigated, other important experimental factors have not been explored. Although a range of loading and unloading displacement rates ranging from 0.1 $\mu m/s$ to 130 $\mu m/s$ have been implemented in studies (Han et al., 2011; Gupta et al., 2005), their effect has not been quantified. A subsidiary objective was to demonstrate the effects of loading and unloading velocity on contact stiffness and Young's modulus with and without a hold phase, to identify an appropriate protocol for future characterisation of AC.

Animal AC has been investigated with a wide range of protocols and material properties (Table 2.2). Few papers have discussed OA but even less have actually investigated the mechanical properties of human AC which demonstrate different mechanical properties compared to other species (Athanasiou et al., 1994) highlighting the relevance of testing human samples instead of animal. The mechanical properties of AC are regional and depth dependent (Korhonen et al., 2002a; Li et al., 2006; Tomkoria et al., 2004), however a direct comparison of local mechanical properties across healthy or degenerated human femoral head cartilage has not been investigated thoroughly despite the prevalence of OA in this joint. Similar numbers of hip replacement surgeries and knee replacement surgeries take place every year but currently work has concentrated on understanding the mechanical properties of the knee joint (Swann and Seedhom, 1993; Yao and Seedhom, 1993; Lyyra et al., 1999; Froimson et al., 1989). The main aim of this thesis was to map the topographical variation in mechanical properties of cartilage over healthy and osteoarthritic human femoral heads in order: (i) to identify the change in mechanical properties with position on the femoral head which is currently unknown; (ii) to attempt to link this with numerical studies

of gait analysis with the intent to understand why there may be a change with position; (iii) to determine a biomechanical description of OA degeneration from healthy to end stage; and (iv) to potentially identify where OA initiates on the femoral head so it can be diagnosed earlier and treated. In addition tip shape and loading pattern are to be compared (as in everyday life a rage of loading conditions apply) to provide further understanding of human AC and to aid in the comparison of existing literature.

Chapter 3

Instrumentation & Protocol Development

3.1 Instrumentation

This section includes a basic description and explanation of the MFP-3D Stand Alone system (Asylum Research, Santa Barbara, CA) used in this study Figure 3.1. The main components of this system include: MFP-3D AFM; MFP-3D Nanoindenter; MFP-3D XY Scanner; base unit; ARC-2 controller; computer; BCH-45 integrated acoustic enclosure; TS-150 vibration isolation table and IGOR Pro software.

3.1.1 MFP-3D Heads

The system available at the University of Strathclyde has two interchangeable MFP-3D heads, AFM (Figure 3.2(a)) and a Nanoindenter (Figure 3.2(b)). The AFM head, incorporating the optical lever detection system and the vertical motion actuator and sensor, holds the cantilever chip. Within this head (Figure 3.3)

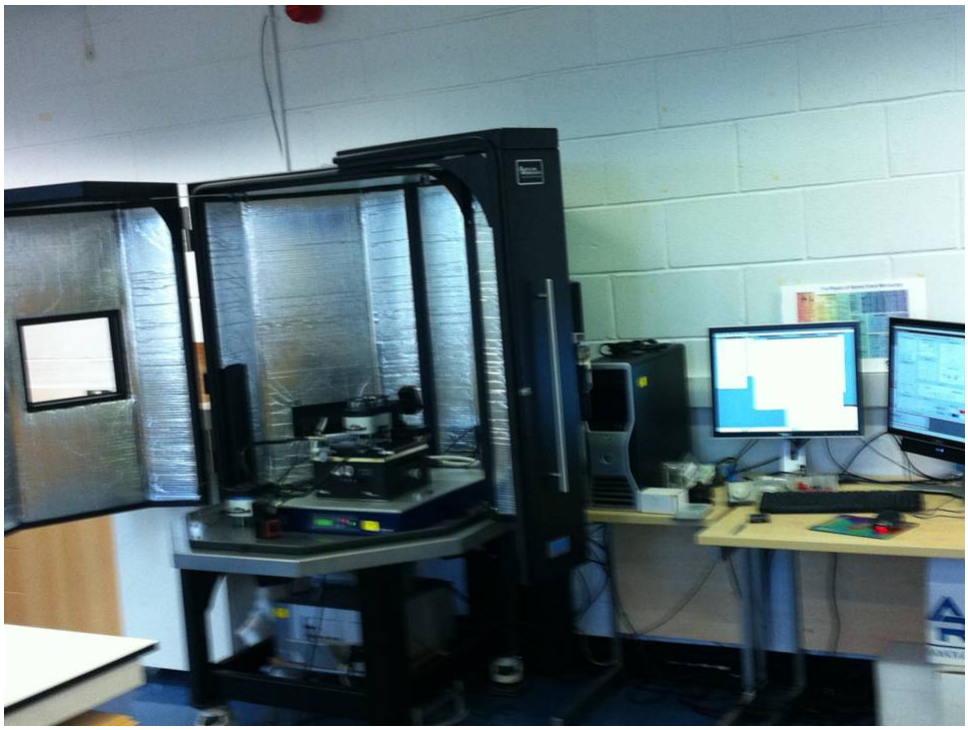

Figure 3.1: Photograph of the whole system with the MFP-3D Nanoindenter head in place.

a super luminescent diode beams onto the rear of the cantilever, mounted at 11 ° in respect to the sample plane. The angle of the deflected cantilever governs the location of the reflected beam on the photodiode. The AFM head has a Z scan range (vertical) of 40 μm and has two cantilever holders; a standard holder for AC and contact mode and an iDrive magnetic actuated holder. More detail on these holders is described later.

(a) MFP-3d AFM

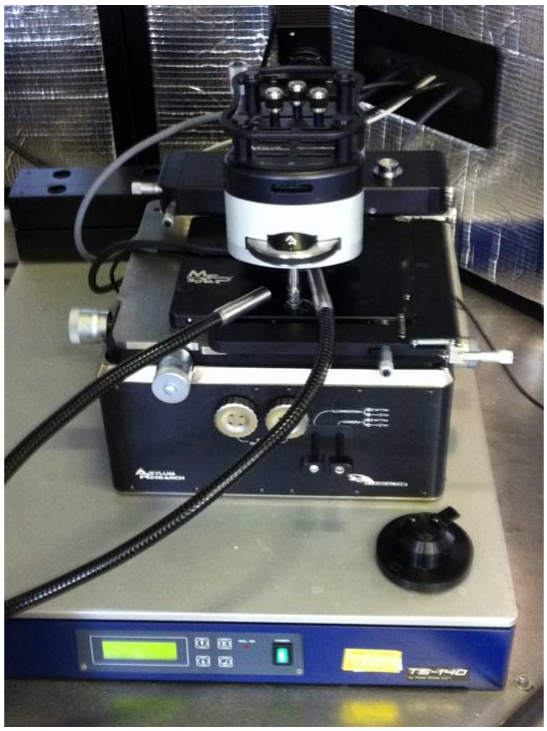

(b) MFP-3d Nanoindenter

Figure 3.2: Photograph of the interchangeable MFP-3D AFM and Nanoindenter heads set up.

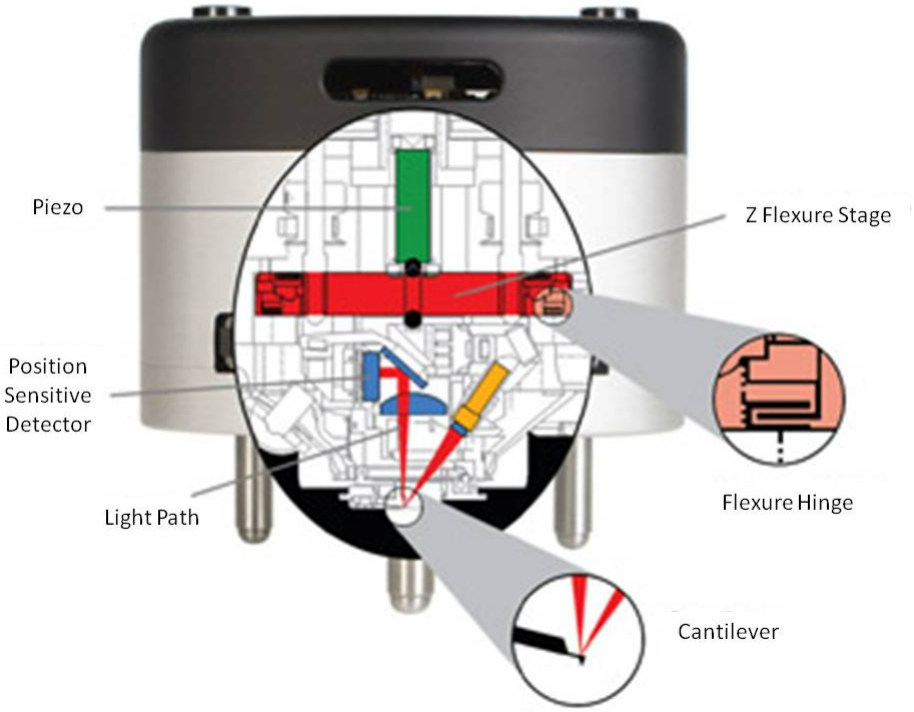

Figure 3.3: Schematic MFP-3D AFM of optical lever technique: a laser beam is reflected by the optical lever transducer into a position sensitive detector(adapted from Asylum Research Manual).

The MFP-3D Nanoindenter is the first AFM based indenter that does not employ cantilevers as part of the indenting mechanism. It is a true instrumented nanoindenter measuring quantitative data with the sensitivity, precision and accuracy of AFM sensing technology. The indenter tip, in contrast to cantilever-based systems, moves perpendicular to the surface (Figure 3.4). The vertical movement prevents the lateral movement and errors that are implicit in cantilever based indenters.

Displacement of the indenting flexure is controlled with a piezo actuator and measured with the Z axis, patented, low-noise NPS sensors. The monolithic design of the flexure and Z axis sensors, illustrated in Figure 3.4 (described in section 2.4),

eliminates drift errors seen in conventional nanoindenters which have electrical actuations causing a rise in temperature of components resulting in drift, therefore measurement inaccuracies. The pre-calibration (at factory), the range of nanoindenting tips and the integrated software provide user friendly equipment with a wide variety of experimental controls. The nanoindenter tips and experimental controls applied in this study are described in subsection 3.2.1.

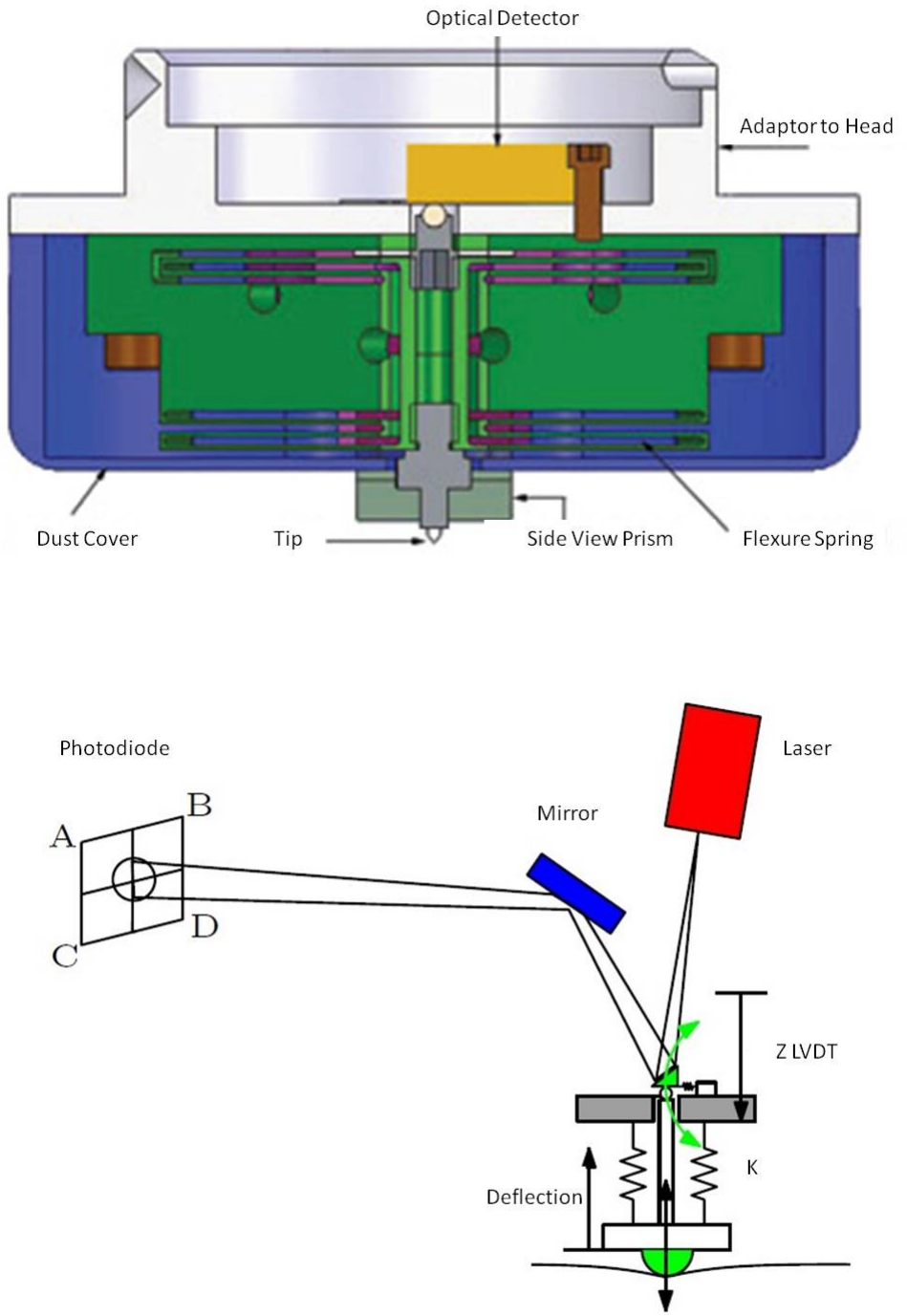

Figure 3.4: Schematic MFP-3D Nanoindenter of optical lever technique: a laser beam is reflected by the optical lever transducer into a position sensitive detector (adapted from Asylum Research Manual).

3.1.2 MFP-3D XY Scanner

The position of the sample in the X and Y direction is controlled by the MFP-3D XY scanner (Figure 3.5). The micrometer driven stage has an X and Y scan axis of $90\mu m$ travel at full range. Within the scanner a petri dish heater is located (Figure 3.1.2 and Figure 3.6). This enables the sample environment to stay at physiological relevant temperatures, 37 °C. The petri dish is held onto the scanner with magnets, minimising unwanted movement.

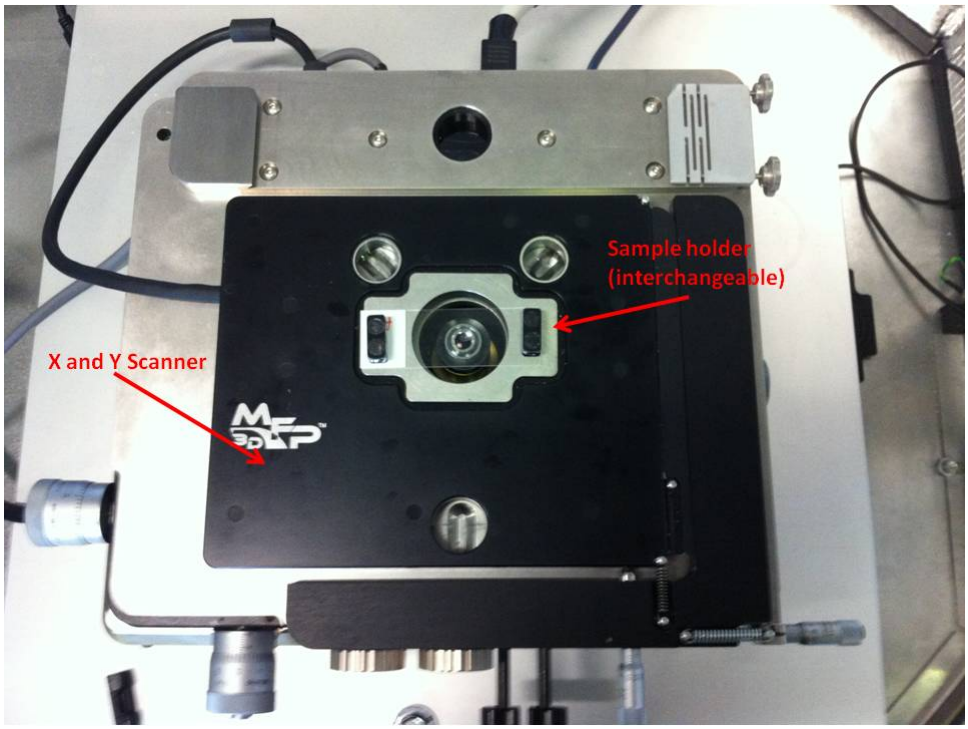

Figure 3.5: MFP-3D XY Scanner.

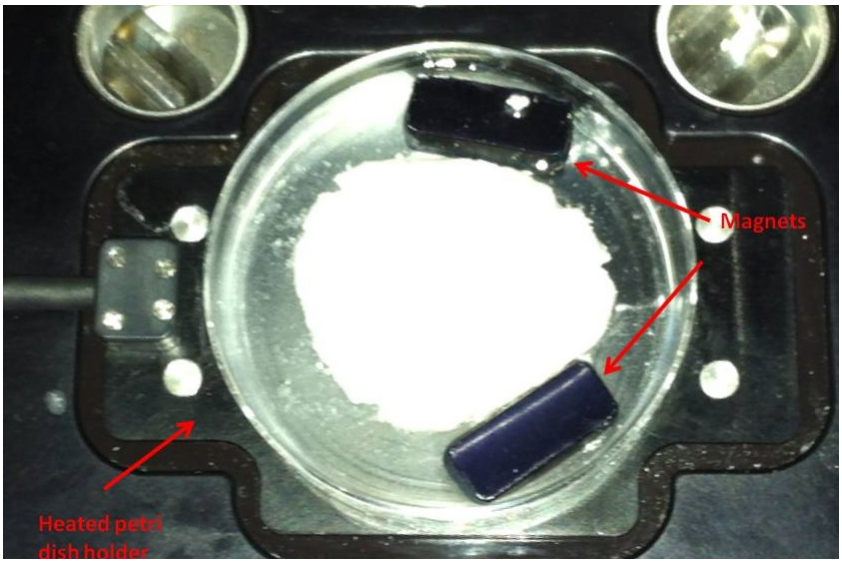

Figure 3.6: Shows the petri dish heater with a sample held securely on top with magnets.

3.1.3 Stand Alone Base Unit & Controller

The MFP-3D Stand Alone uses a square bottom base to provide a platform and to house the optics configuration. The top surface plate of the base is a multipurpose model on which the head and scanner sit. When using the MFP-3D Nanoindenter head, the high resolution camera also sits on the top surface plate. The base has dual view optics for the AFM, illustrated in Figure 3.7, implementing a top down view and a bottom up view depending on the transparency of the sample. The base unit provides an adjustable aperture and field diaphragm for enhancing and altering contrast and light intensity for better images in the built-in charge-coupled device camera (CCD). It also contains the electronic hub for linking the controller to the scanner and head, and routes the camera to the computer. The ARC2 SPM controller contains power supplies and the essential electronics for controlling the scan motion and acquiring raw data from the MFP-3D head (either AFM or Nanoindenter).

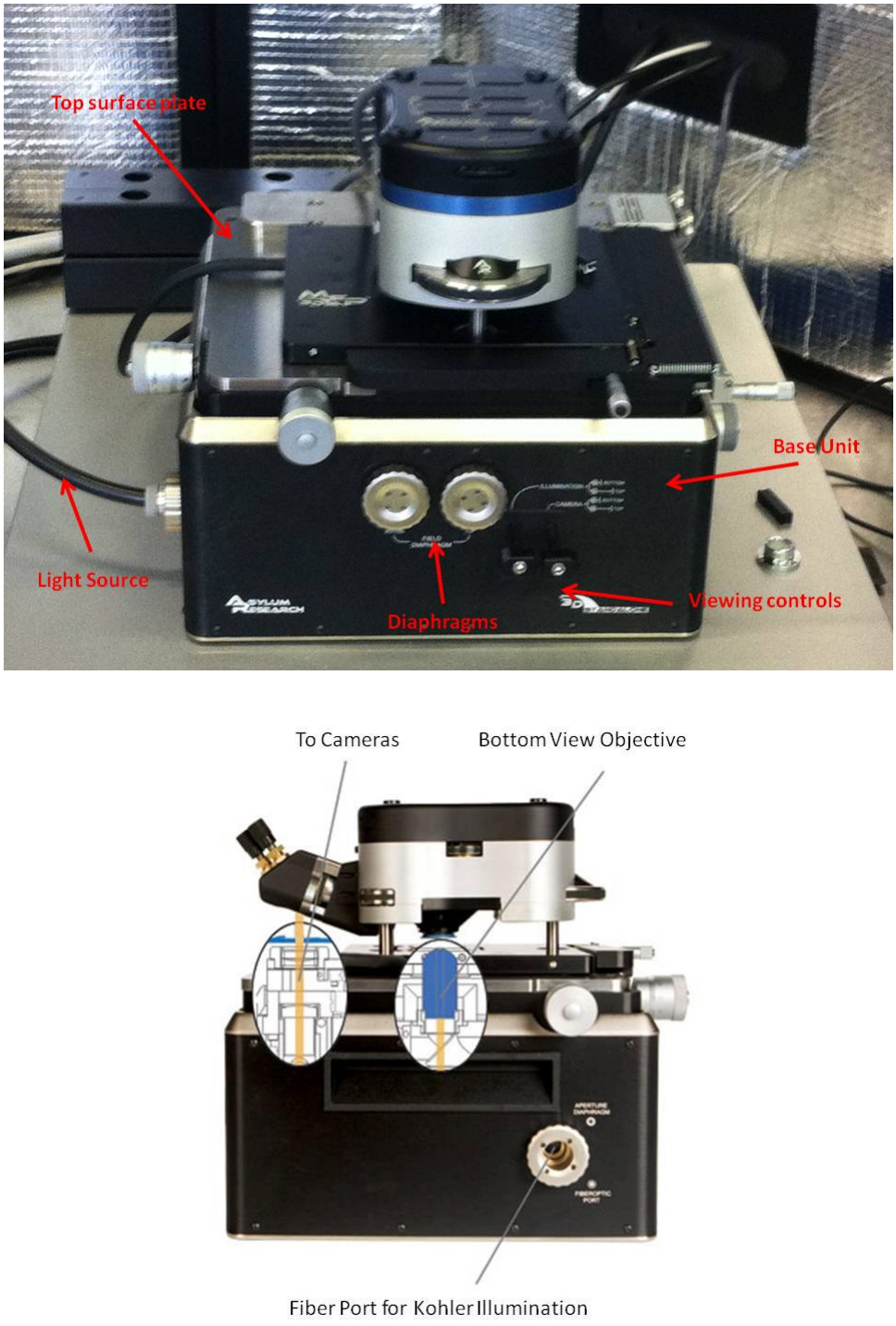

Figure 3.7: MFP-3D Base unit.

3.1.4 Vibration Isolation

Vibration isolation is a key factor which influences the quality of AFM images and indentation measurements. Although the MFP-3D system has one of the lowest noise specifications in the industry, vibrations from the laboratory must also be removed and therefore the MFP-3D system is seated on a vibration isolation table and placed in an acoustic isolation enclosure (Figure 3.1).

A TS-150 vibration isolation table (Figure 3.8) automatically adjusts and stabilises the optical alignment. Isolation activates at $0.7Hz$ and increases to $40dB$. The BCH-45 acoustic enclosure (hood) provides a shield from low frequency passive vibration isolation stopping external noise and vibration affecting experiments. Additionally, it provides protection from air currents that may affect the image stability. The frame and chamber exterior is built of powder-coated steel (Figure 3.9(a)). The sound insulation over such a wide frequency range is mainly due to the proprietary layered interior of the chamber (Figure 3.9(b)). The hood doors open to 180° (Figure 3.9(b)) to give maneuverable room, for example to switch heads or add illumination pillars for the nanoindenter. Another feature of the hood is the dual windows for quick access, small adjustments and viewing.

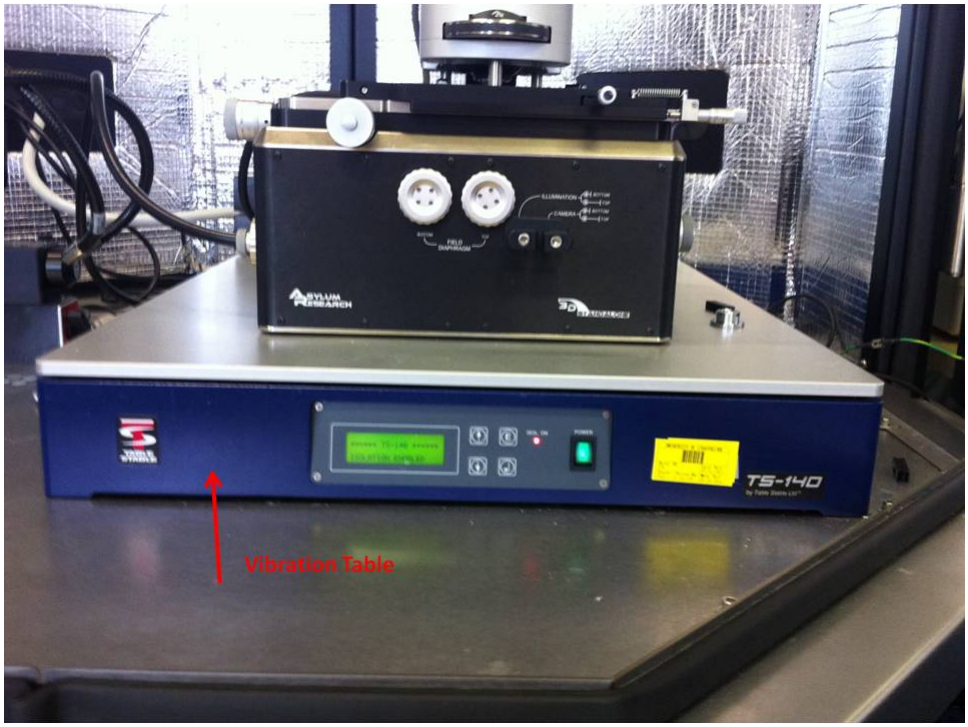

Figure 3.8: Demonstrates the TS-150 vibration isolation table.

Figure 3.9: Photographs of the vibration isolation system which shows the black exterior and silver interior.

3.1.5 MFP-3D AFM

The MFP-3D AFM has two cantilever holders: a standard holder (Figure 3.10(a)) for contact mode and tapping mode imaging and an iDrive cantilever holder (Figure 3.10(b)) for enhanced tapping mode imaging of soft samples in fluid. This section explains the different modes, output images and the AFM probes used in this study.

In contact mode a cantilever is scanned over the sample and the optical lever deflection system produces a defection signal that corresponds to the angle of the cantilever. With no feedback the cantilever would simply bend and move over the surface features and the deflection signal would vary (creating an image). A feedback mechanism allows the cantilever to move in height with the sample as with no feedback the Z range is very small. The Z piezo adjusts the height of the cantilever. With contact mode feedback the height of the cantilever moves when required to maintain a predefined deflection constant (set point). To keep this constant angle the Z piezo must regulate the cantilever, so it traces out the contour of the sample surface while maintaining a constant separation between the back end of the lever and the point of the sample in contact with the tip. The Z piezo position is recorded as the height data. The Z piezo is controlled by the Z voltage feedback system. As the deflection signal increases, greater than the set point, the Z voltage decreases moving the tip away from the surface. As the deflection signal decreases less than the set point, the Z voltage increases moving the tip closer to the surface.

Contact mode has three output image channels: Height, Deflection and Z sensor. The height image is the height data from the Z piezo position. The deflection image is the signal from the photodetector (deflection signal) is subtracted from

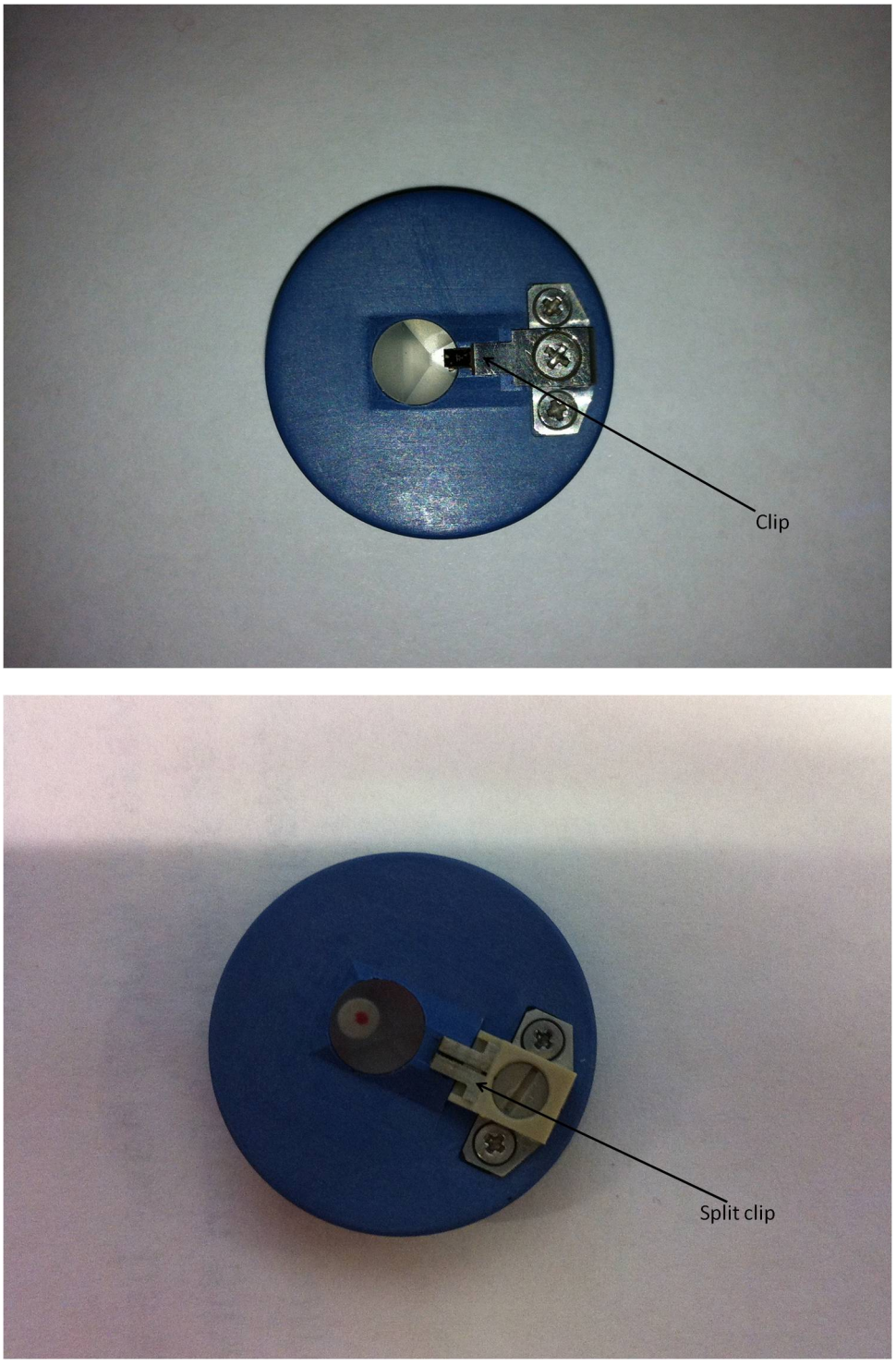

Figure 3.10: Illustrates the two optional cantilever probes (the clip is the noticeable difference between the holders).

the set point. The Z sensor image is the output of the Z voltage movement in the feedback system that monitors the movement of the optical lever detection system.

AFM tapping mode has a cantilever attached to a 'shake' piezo which converts an input voltage into an oscillatory action that drives the base of the cantilever, causing it to oscillate. Normally, the cantilever is excited at a predetermined frequency (set point) close to or below its fundamental oscillation. Similar to contact mode, as the tip moves closer to the sample surface, the amplitude will decrease and the feedback loop tries to maintain the vibration amplitude by adjusting the Z piezo away from the surface. As the amplitude increases above the set point (tip is moving away from the surface) the Z voltage feedback system alters the Z piezo, moving the tip closer to the surface. The cantilever is moved up and down as the interactions of forces from surface features modify the vibration amplitudes.

Tapping mode has four output channels: Height; Amplitude; Phase and Z sensor. The height image is created from the Z voltage data applied to the Z piezo to maintain the set point. The Amplitude image is the error signal of the feedback loop. The Phase image is the phase shift which can be considered to be the 'delay' in oscillation of the probe as it moves up and down interacting with the sample. As the oscillating tip interacts with the sample, the tip can experience repulsive or attractive forces, which subsequently produce a lead or lag in the phase signal in the photodiode. The phase signal has been reported to be sensitive to viscoelastic properties and adhesive forces in soft tissue (Tamayo and Garcia, 1998). The Z sensor image is produced from the movement of the detected distance of the optical lever.

3.1.6 iDrive cantilever holder

With a standard cantilever holder, tapping mode imaging in fluid can be difficult: the piezo shaker not only drives the cantilever but the fluid as well which can also shake the holder. This makes tuning the cantilever difficult because there are many resonance peaks and it can be difficult to choose the correct one. IDrive cantilever holder simplifies fluid imaging by removing the large number of peaks, seen with a standard holder in fluid, due to mechanical coupling that in turn allows auto tuning of the cantilevers in fluid. The patented iDrive holder (Figure 3.10(b)) has a special clip which has been split in two (unlike the standard holder) and contains a magnet creating a magnetic field. Both halves of the clip are part of an electrical current which can implement separate voltages to each side. The iDrive passes a small current through a cantilever (Figure 3.11 illustrates the special iDrive cantilever) in the presence of the magnetic field which turns the current into a force that is exerted on the cantilever, Lorentz force. As the current alters the force vector changes direction oscillating the cantilever. By eliminating the piezo shaker and subsequent resonance peaks the iDrive can automatically tune the cantilever in fluid simplifying AFM imaging in fluid.

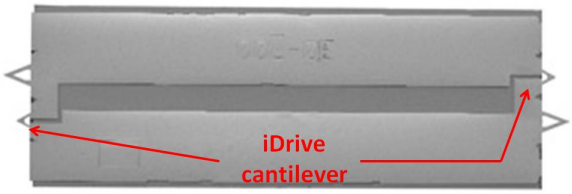

Figure 3.11: Demonstrates the BL-TR400PB iDrive Probe.

3.1.7 AFM Probes

The MFP-3D cantilever holder is compatible with most commercially available probes however Asylum Research work with Olympus probes and suggest the TR400PB probes and AC160TS probes should be applied to biological soft samples (like cartilage) as they have low spring constants that should move easily over soft samples. The TR400PB probe has two triangular silicon nitride cantilevers with: spring constants of $0.09N/m$ and $0.02N/m$; lengths of $100\mu m$ and $200\mu m$; widths of $15\mu m$ and $30\mu m$ and a thickness of $0.4\mu m$. The four sided pyramidal tip on each cantilever is also made of silicon nitride and has a radius of $42nm$ and a height of $3\mu m$. These cantilevers were also used by Jurvelin et al. (1996) and the properties were within range 0.02-$2N/m$, that had be reported by other AFM studies on cartilage (Stolz et al., 2004, 2009; Han et al., 2011; Crockett et al., 2005; Loparic et al., 2010; Ng et al., 2003; Park et al., 2004). The TR400PB probe was recommended by the manufacturer for contact mode and tapping mode in fluid and Olympus recommended the AC160TS probe for tapping mode in air. The AC160TS probe has a rectangular silicon cantilever with an aluminium coating: it is $160\mu m$ in length with a width of $50\mu m$ and a thickness of $4.6\mu m$. This cantilever has a spring constant of $42N/m$ and a frequency of $300kHz$. The silicon three sided pyramid tip has a radius of $3nm$ and a height of $11nm$. This cantilever was stiffer than that reported in previous studies so a SNL probe from Bruker was also employed mirroring Stolz et al. (2009) and Crockett et al. (2005).

The Sharp Nitride Lever (SNL) probe included four cantilevers with varying degrees of force constants and resonants. The four cantilevers range from 120-$205\mu m$ in length and 20- $40\mu m$ in width and $0.6\mu m$ in thickness. The SNL probes had a much lower spring constant range than the AC160TS probe, between 0.06 and $0.35N/m$. The manufacter (Bruker) recommends the SNL probes for tapping

mode in fluid, however Stolz et al. (2009) and Crockett et al. (2005) used the tips for contact mode imaging in fluid.

There are two compatible iDrive probes, the BL-TR400PB probe and the BL-TR800PB probe from Asylum Research. Unlike other magnetically actuated techniques the iDrive does not require magnetically coated cantilevers which can introduce detrimental cantilever bending, possibly damaging metal ions which can jeopardise the sample and solution. The BL-TR400PB iDrive probe is gold coated which is one of the few metals that is acceptable in bio-applications because it is non-toxic and living organisms can survive contact with gold this is why the BL-TR400PB probe is advised to be used with biological samples. It also has a lower spring constant of $0.09N/m$ compared to the BL-TR800PB probe ($0.61N/m$). The BL-TR400PB probe has two triangular cantilevers (Figure 3.11) but only the $100\mu m$ cantilever can be actuated by the iDrive holder.

3.2 MFP-3D Nanoindenter

The nanoindenter uses different optics to the AFM, illustrated in Figure 3.12. The Nanoindenter optics and camera assembly, with light from the illumination pillars, provides viewing of the indenter tip and sample at an angle of 20° from horizontal. Asylum Research has two commercially available flexures, a standard force module and a low force module. This project started implementing the low force module as it had a low spring constant of $800N/m$ and a high force resolution but after encountering problems explained in section 3.3.1 an alternative module was then acquired from the manufacturer that still had a significantly lower spring constant (2469.4 N/m) than the standard module.

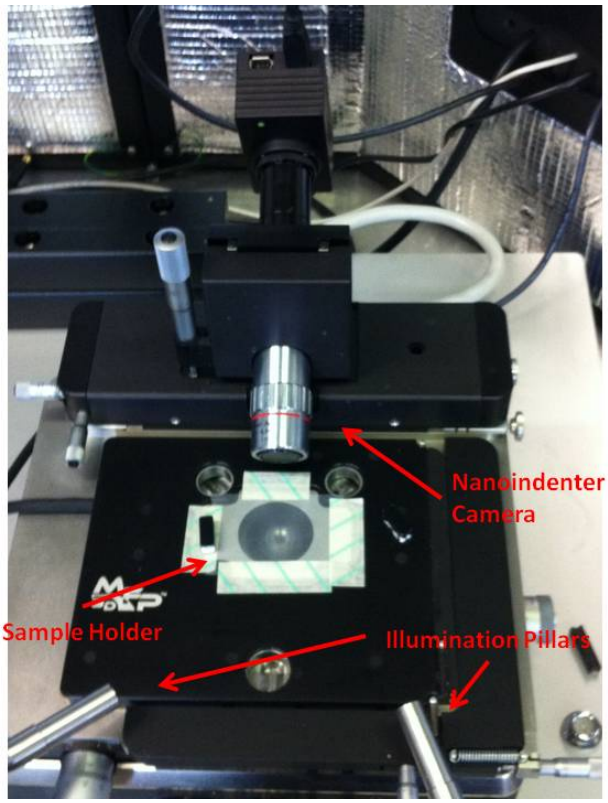

Figure 3.12: Shows the nanoindeter optics and camera system with the illumination pillars located ready for a sample and the head to be positioned.

The user interface linked with the MFP-3D Nanoindenter system means there are a variety of functions that can be changed depending on the experimental protocol. The adaptable experimental parameters are all connected to the input channels from the head (Z sensor, force, deflection and deflection volts). The Z sensor is the movement of the Z piezo and the force is a measure of the force applied to the tip. The deflection is the measurement of movement on the photodiode sensor and the deflection volts is the voltage measurement in the photodiode sensor. By altering the settings it is possible to define whether an indent is load controlled (force feedback), indentation controlled (depth feedback) or displacement controlled (direct movement of Z piezo). It is also possible to define the loading pattern by creating an individual loading function to the required needs by establishing the loading and unloading rate, hold, no hold and other variables if required. Depending on the sample, automatic triggering is available so that the loading function initiates when it reaches the trigger, or alternatively it is possible to complete the loading function from where the tip originates. The software outputs a list of data sets that can then be analysed to understand the material properties of the sample. These data sets outputs include: Z sensor; defection; deflection volts; force; indentation; raw voltage (voltage of the Z stage) and time. The software scripting ability pertinent to the MFP-3D system makes it ideal for characterising materials due to its flexibility.

3.2.1 Nanoindenter Tips

Many tip geometries and sizes are available from Asylum Research and other similar companies; this study used a Spherical tip, a Berkovich tip, a Cubed Corner tip and a unique custom made Flat Ended tip (punch). Figure 3.13 views the nanoindenter tips through the systems optics. Each tip is composed of an

industrial diamond (black coloured) or sapphire, brazed to a screw-threaded hex tooled metallic chuck (Figure 3.14). Each tip is stored individually in a Lexan hex nut driver set screw and protected with a black cap and a vial container. All four tips are contained in a padded box. The Berkovich, Cubed Corner and Spherical tip geometries comply with the International Standard ISO 14577-22 and ISO 17025.1 which defines the internationally accepted nanoindenter dimensions, angles and calibrations. The Flat Ended tip was manufactured as a known contact area can help reduce the analytical errors when calculating Young's Modulus. Figure 3.15 illustrates the Flat Ended tip to have a width of $0.66\mu m$ which means this tip has the potential to measure the mechanics of individual components of cartilage rather than the tissue as a whole as in current clinical devices (section 2.3.1). The Berkovich tip has a more open angle (Figure 3.16 and Figure 2.7) which may damage the tissue less, however may have a lower resolution to individual components of the tissue.

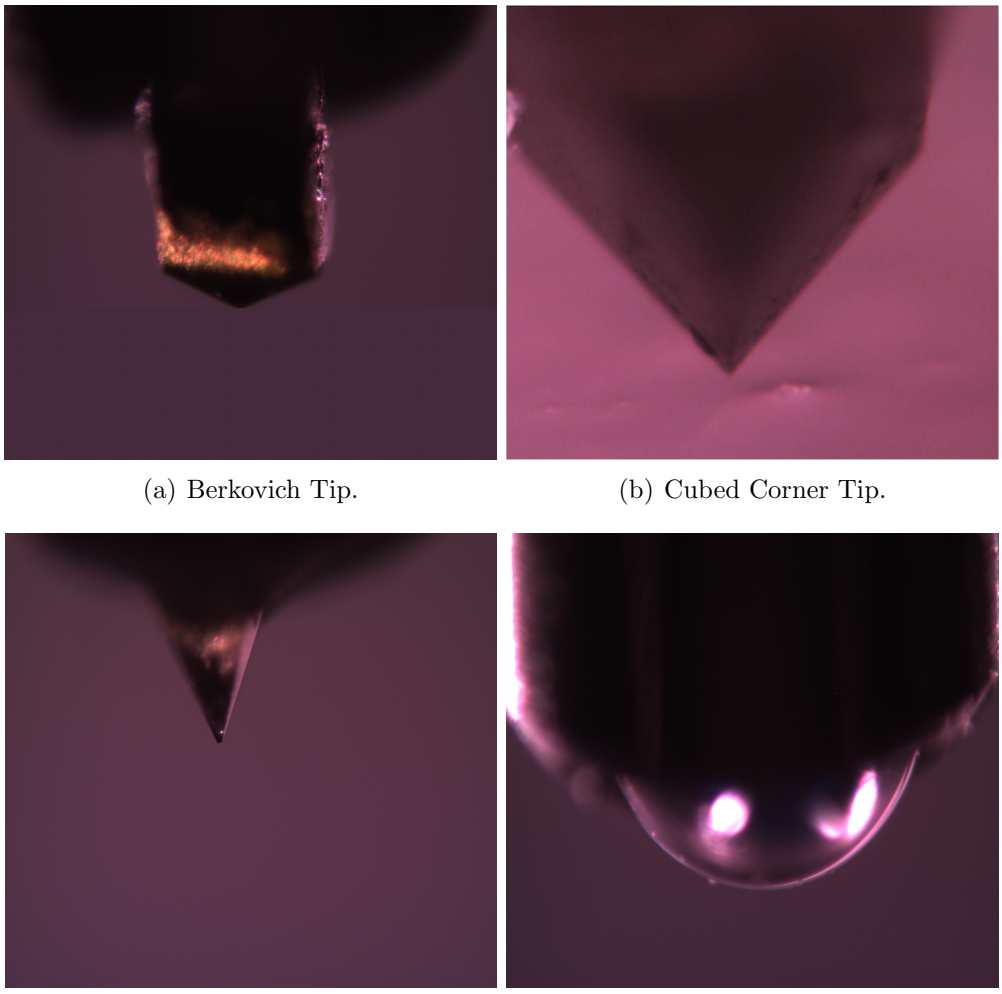

(a) Berkovich Tip.

(b) Cubed Corner Tip.

(c) Custom Made Flat Ended Punch.

(d) Spherical tip.

Figure 3.13: Images through the nanoindeter camera of the four tip geometries used for this study.

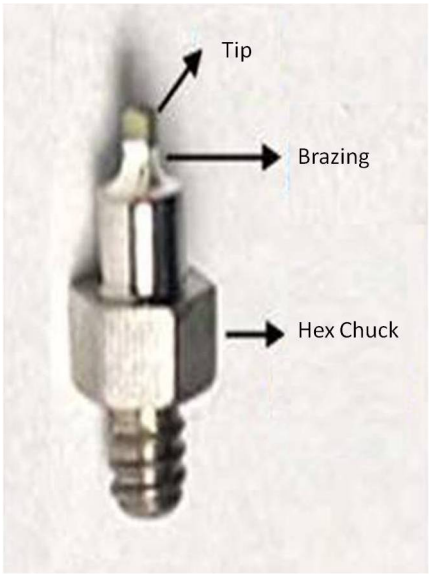

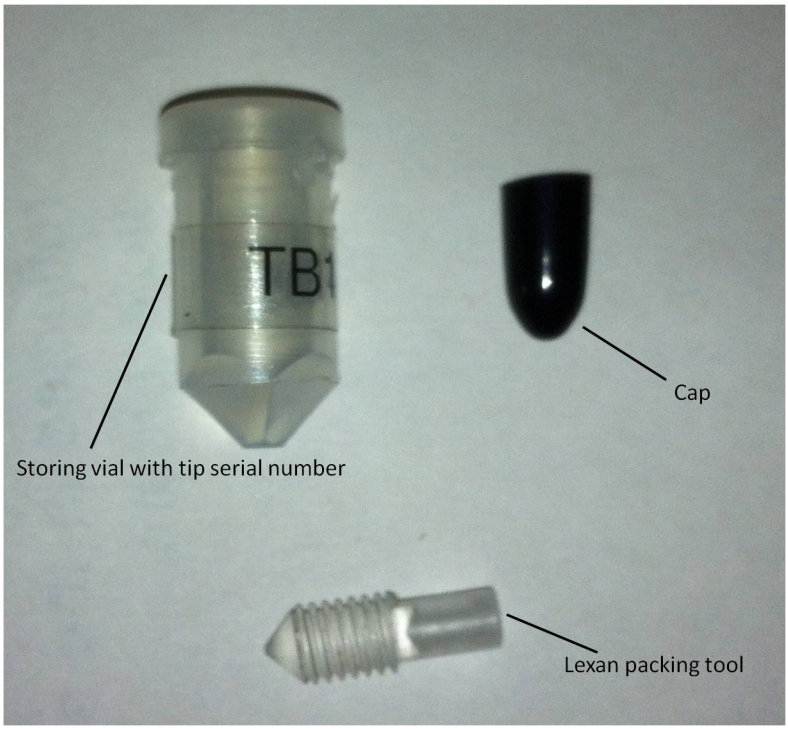

Figure 3.14: An example of a typical nanoindenter tip identifying the different components and the appropriate packaging required for safe storage.

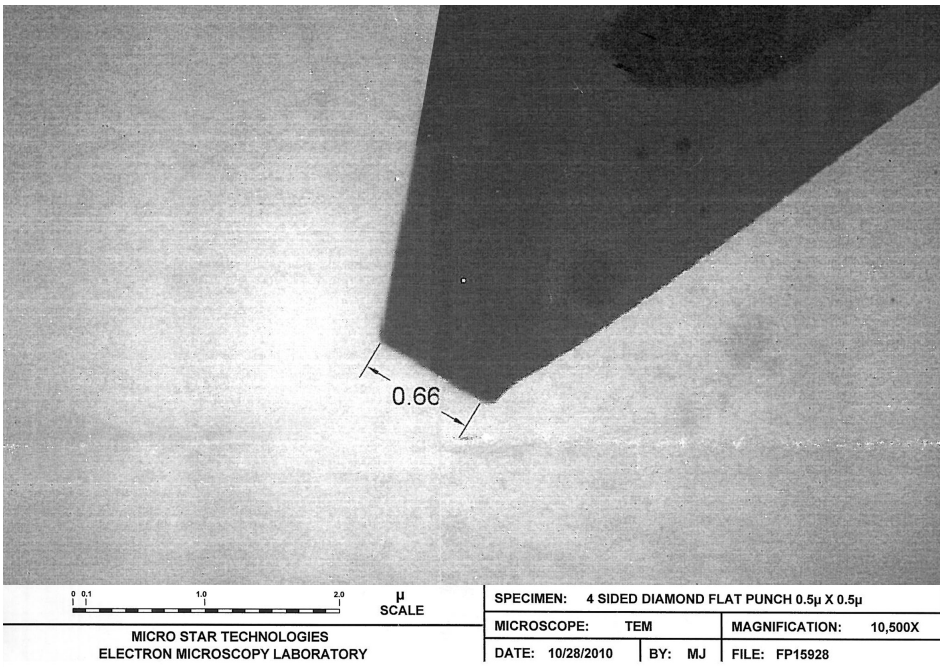

Figure 3.15: SEM Image of the flat ended punch.

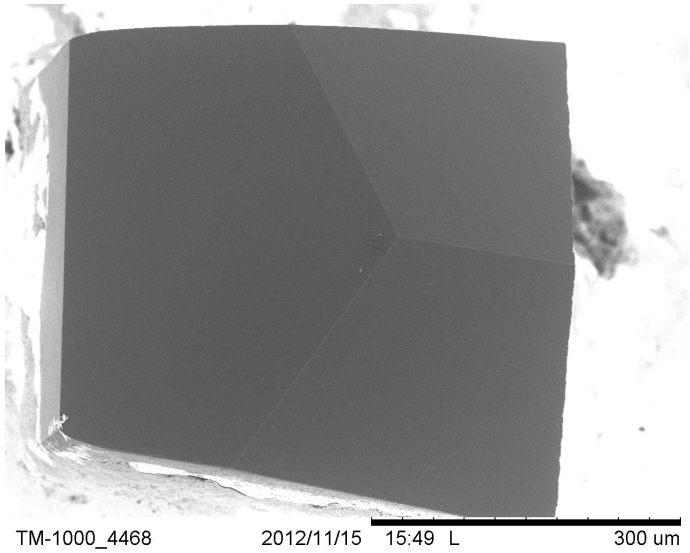

Figure 3.16: SEM Image of the Berkovich tip.

3.3 Nanoindentation Protocol Development

As previously discussed in section 2.4 a broad variety of protocols and material properties exists (Table 2.2). No study was found that utilised an MFP-3D Nanoindenter (Asylum Research, Santa Barbara, CA); only similar equipment by rival companies have been used by published studies.

3.3.1 Instrumentation Failure

Originally a low force MFP Nanoindenter (Asylum Research, Santa Barbara, CA) with a spring constant of $800 N/m$ was employed for mechanical testing. However, the low force module repeatedly broke with frequent use as the epoxied joint failed. This failure had never been reported despite Asylum Research having 15 other low force modules in use by various organisations, but none experimented in the medium of PBS. It was suggested that experiments in fluid may have caused the epoxy joint to fail over time. Despite the use of a fluid guard, multiple protocol changes and considerable investigations to overcome this issue, the 'low' force module continued to fail. Asylum Research normally produces a 'standard' force module flexure with a spring constant of 4000 N/m and a 'low' force module flexure with a spring constant of 800N/m however due to production variation, modules with a spring constant of 2469 N/m were produced. Reviewing the data previously collected using the 'low' force module it was deduced that the module with the spring constant of 2469 N/m would be suitable for this application as it was sufficiently sensitive and resilient to conclude the experiments in fluid. This module flexure optimised the spring constant for both durability and force resolution for AC.

3.3.2 MFP Nanoindenter Calibration

Initially the laser is aligned to the centre of the indenter tip, resulting in a sum of over 9 V. Once the laser is aligned correctly this position is fixed as any adjustment off centre will result in errors. If the sum is less than 9 V realignment is required.

The spring constant is calibrated at the Asylum Research Factory and printed on the nanoindenter module for reference. The photodiode measures a voltage required to be converted into a distance (also known as deflection). This conversion factor, Inverse Optical Lever Sensitivity (InvOLS), needs careful, precise calibration for accurate results.

The spherical sapphire tip (tip must be clean) and sapphire calibration sample (Figure 3.17) are required for InvOLS calibration which assumes that the contact between the sapphire tip and sapphire sample has high rigidity Hertzian contact. The deflection and sum should not be at the maximum as this would indicate incorrect alignment of that laser.

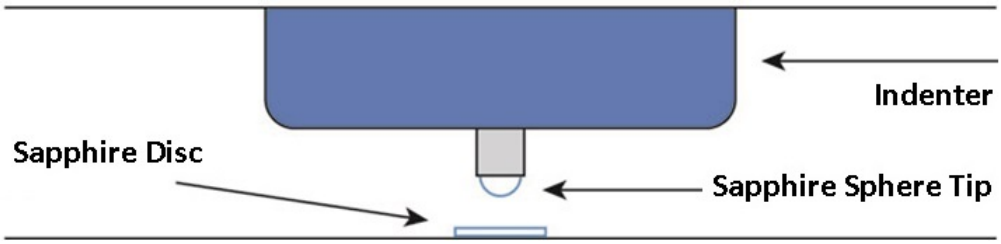

Figure 3.17: Schematic of apparatus setup for calibration.

Virtual deflection calibration calculation was first executed by performing a force curve in air distant from the surface with a preferred force distance of 6 μm. The force curve was checked to ensure no trigger or indentation had occurred. The

software (IgorPro) then calculated the virtual deflection from this curve with a typical value for this parameter of a few $mV/\mu m$. The value was checked by repeating the process; on repetition the force curve should be much flatter than previous, implying a good value was recorded.

Once the Virtual deflection was calculated the deflection was offset to -2 V and the tip was engaged and lowered into the surface until the sum (z voltage) reached 70, then withdrawn. The trigger for the indent was set at deflection volts, with a positive relative point, with a value of 4 V and a scan rate of 0.2 Hz. With all vibration isolation equipment in place, an indent was then performed into the sapphire sample. The trace and retrace were exactly overlying, indicating a good calibration force curve was achieved. From this curve, the software was able to calibrate the InvOLS; this was repeated 60 times and the average was then used for all experiments.

3.3.3 Material

Pilot experiments were performed on porcine and bovine joints collected from local butchers. The author observed a large variation in porcine AC thickness therefore focused on bovine AC which was more easily obtained. When removing AC samples from a bovine joint an autopsy saw was required as the bone was too hard to cut with a simple coring device (unlike porcine and human). The medial and lateral condyles were excluded from further experiments; cutting required touching the cartilage surface and the curved shape reduced the number of suitable samples removable by an autopsy saw. The bovine patella was chosen since: it provided large numbers of suitable samples; the AC surface was not toughed

during cutting; it was easily obtainable; it had no cost and sample location was easily repeatable.

3.3.4 Synovial Fluid

A gel-like layer was evident on the surface of the cartilage presumed to be synovial fluid. It has been suggested that wiping the surface is not completely effective (Ghadially, 1983) in the removal of synovial fluid, additionally touching the surface of the cartilage may result in permanent deformation or damage, influencing final results therefore this synovial fluid removal technique was disregarded. Washing the sample in PBS was deemed more appropriate to remove the synovial fluid despite the potential increase in swelling of the tissue as this method would not damage the AC surface to the same extent as wiping (Crockett et al., 2005).

To ascertain the optimum length of cartilage washing time for removing the synovial fluid from the cartilage surface, the bovine patellae were cut into a number of subchondral plugs and washed in PBS for 5 hr with a sample being removed every 30 min for testing. To inspect the removal of synovial fluid a cubed corner nanoindenter tip was monitored by the nanoindenter optics as it was lowered to the AC surface. Photographs and videos were taken to qualitatively assess the sample-tip interactions.

This washing experiment revealed that the removal of synovial fluid from the surface of articular cartilage occurred unpredictably when washed in PBS; after 30 min of washing of one sample there was no evidence of synovial fluid however another sample after being washed for 2hr still had synovial fluid evident (Figure 3.18). After 3 hours the synovial fluid was removed from all samples in this

experiment (Figure 3.18). Due to the inconsistent removal of synovial fluid by washing in PBS, for future experiments, washing for a minimum of 4 hr would be advisable and if synovial fluid is still apparent further washing would be required.

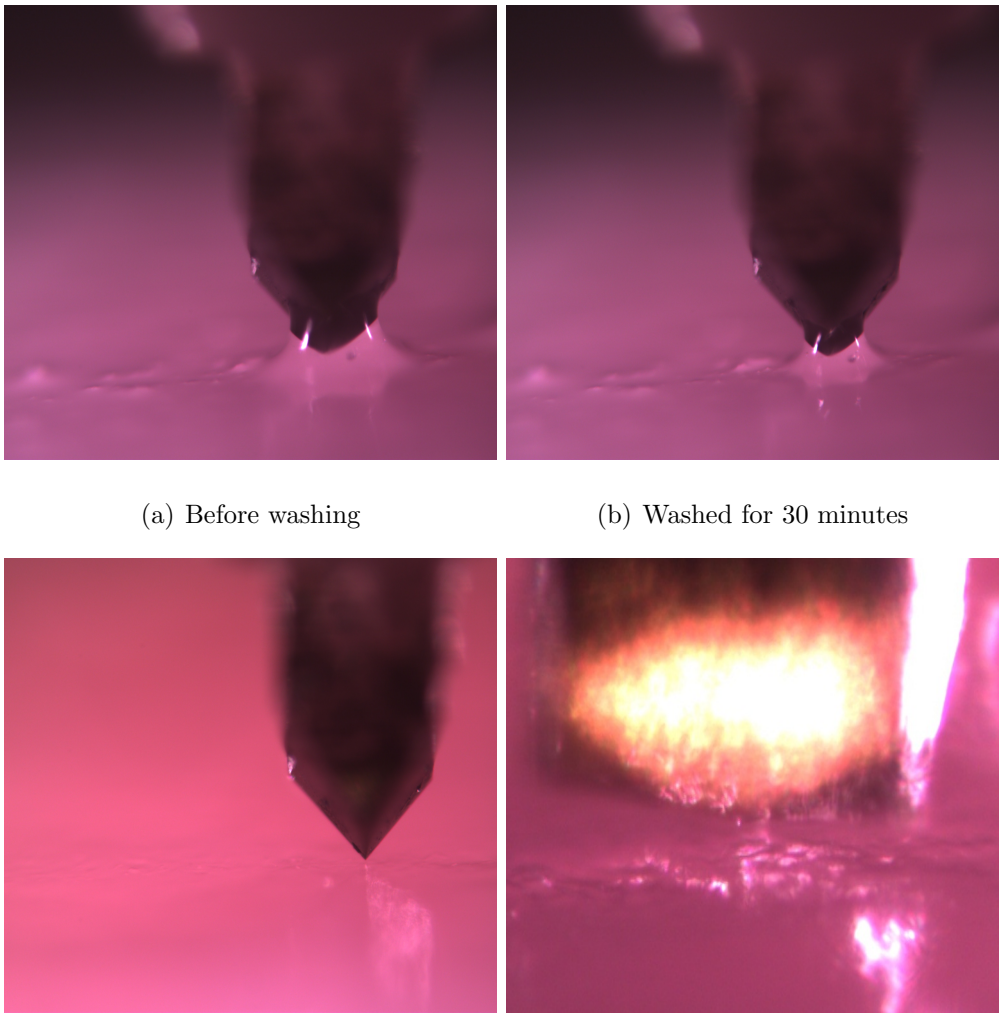

(a) Before washing

(b) Washed for 30 minutes

(c) Synovial fluid completely washed off

(d) Berkovich tip

Figure 3.18: Illustrates the removal of the synovial fluid over the course of 4hrs, (d) Illustrates that the Berkovich tip is less clear than the Cubed Corner tip.

3.3.5 Surface Location

After removing the synovial fluid, the samples were embedded in Tissue-Tek and rapidly frozen to -65 °C to solidify the Tissue-Tek. The samples were then kept at -20 °C whilst being sectioned using a shandon cryotome Figure 3.19. The articular surface was the first 20 μm slice removed before further sections were cut and placed on superfrost plus glass slides. The sample sections ranged from superficial to intermediate layers of articular cartilage.

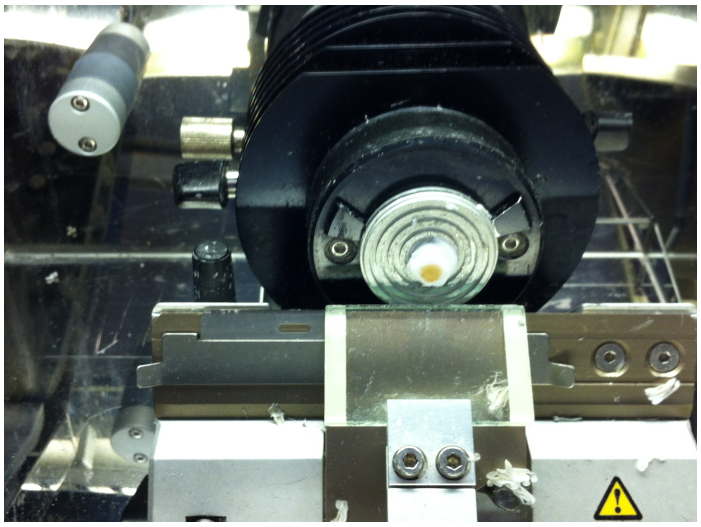

Figure 3.19: An example of an AC sample embedded in Tissue-Tek being sectioned.

The sample sections were placed under the nanoindenter head ready for mechanical testing. While developing the most appropriate experimental protocol it was noted that the nanoindenter was not triggering at first contact with the cartilage surface; it only triggered when the tip was deeper into the cartilage, or when it had split the sample and was reacting to the glass slide. One of the promoted benefits of the MFP-3D nanoindenter is its automatic triggering capabilities allowing the user to adjust the trigger parameters by setting a specific value of force, or displacement, or deflection as a measure of volts or nanometers with the

ability to define whether to set the trigger on an increasing or decreasing value and whether this should be set as an absolute or relative value which will alter the point of automatic triggering. The range of trigger parameters should improve surface location which has been identified to be difficult in AC (Ebenstein and Wahl, 2006; Wahl et al., 2006). For precise measurement of soft hydrated cartilage, it is crucial to locate the surface accurately. Typically nanoindenters use load set points of 1-2 μN to detect the sample; this load is negligible in harder materials however, in soft tissue such as cartilage this load can cause significant deformation (Gupta et al., 2009). A variety of trigger points were subsequently investigated on the full thickness of cartilage to discover the best option for accurate surface location. However, no consistent automatic nanoindentation trigger point was found. Across a range of trigger values, at times with the same value it triggered once the cartilage tissue was penetrated and other times it triggered before the AC surface i.e. if the trigger point was too low, vibration or inertial forces resulted in premature triggering. Some of the unsuccessful force curves investigating the trigger points are illustrated in Figure 3.20. For further experiments, thinly sectioned samples and automatic triggering was rejected. The trigger was disabled and manual identification of the surface, on full thickness cartilage samples, was employed, similar to other studies (Miller and Morgan, 2010, 2009; Franke et al., 2007).

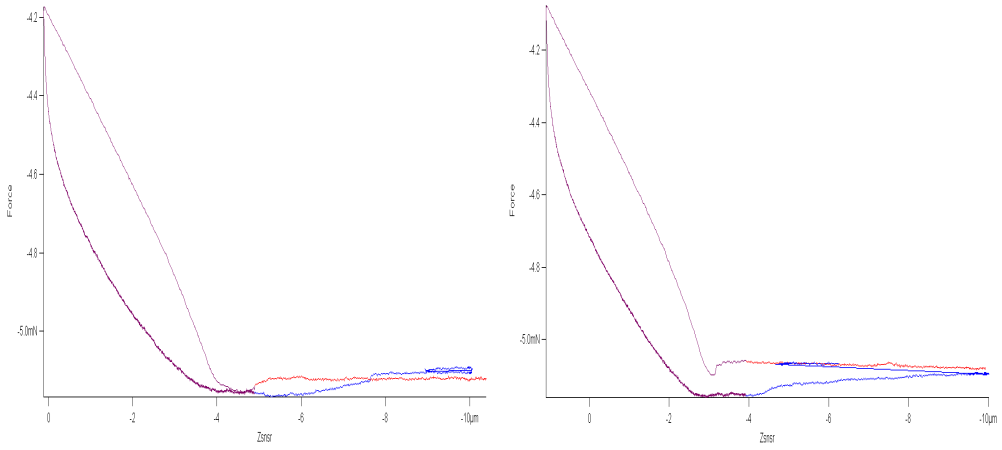

(a) Triggering Early.

(b) Triggering Early.

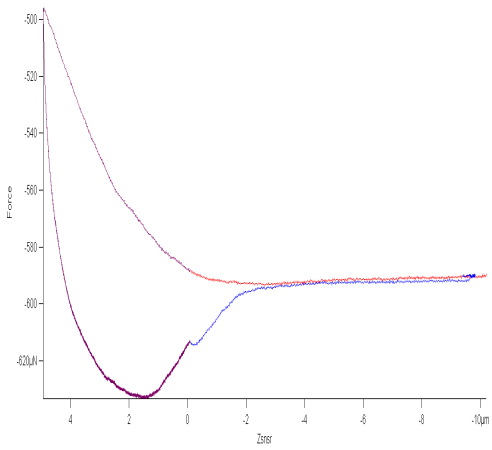

(c) Triggering Late.

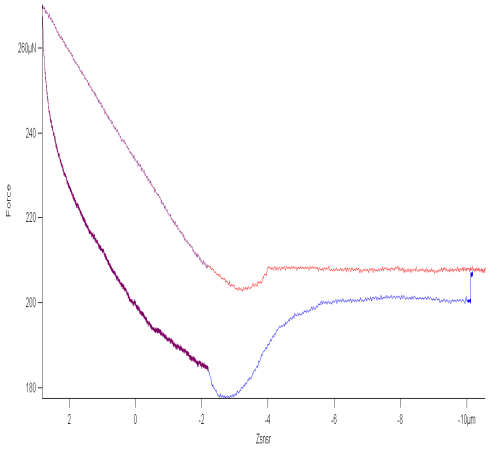

(d) Triggering Late.

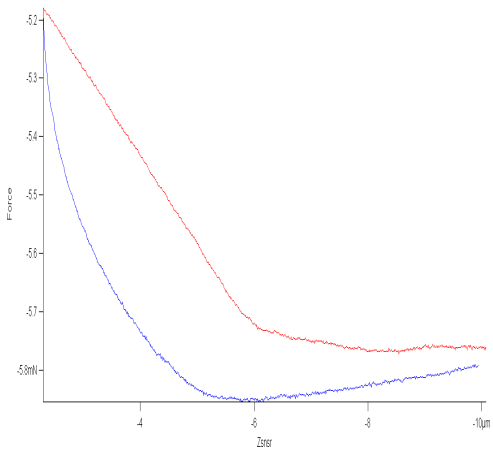

(e) Not Triggering.

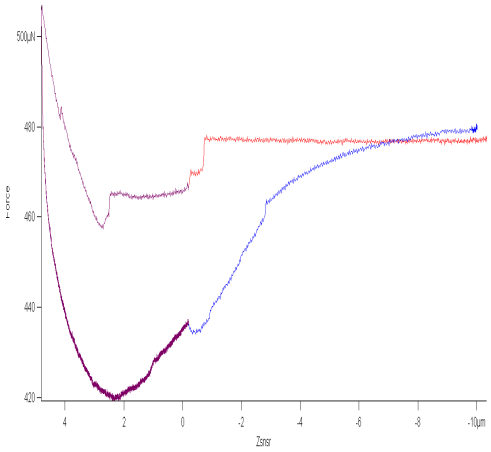

(f) Difficult identifying true surface.

Figure 3.20: Highlights the difficulty using an automatic trigger to achieve consistent results.

3.3.6 Hydration

Hydration was maintained using Phosphate Buffered Solution (PBS) however the quantity was questioned. Fully submerging the sample resulted in swelling of unhealthy tissue and in noisy force-displacement curves which further complicated surface detection issues. Due to the length of time required for indentation tests, hydrating the samples was necessary or tissue would gradually dehydrate resulting in increased adhesion and an alteration in mechanical properties as fluid is an integral component of tissue composition. Optimum hydration and indentation conditions were achieved by maintaining the level of PBS equal to that of the surface but not overflowing.

3.4 AFM Protocol Development

Atomic Force Microscopy (AFM) is able to image at micro and nano-metre scale to clarify structure. AFM allows for simultaneous imaging and stiffness measurements within a natural environment (Loparic et al., 2010), unlike other imaging methods that require the sample preparation by, for example, staining or fixation. Tissue fixation significantly increases the stiffness and reduces the modulus and hardness of the material (Franke et al., 2007) and staining has an unknown effect. Nanometre scale analysis resolves fine structural details exceeding micrometre scale in both imaging and indentation (Stolz et al., 2004). Hence, in comparison to other methods, it is believed that AFM has superior capability to monitor the changes in articular cartilage (Stolz et al., 2009). Nano-inspection of articular cartilage is still in its infancy, and so considerable methodological development was undertaken to achieve the results presented in section 3.4.2, although one would hope that better results well eventually be achieved.

3.4.1 Samples

For initial protocol development, porcine and bovine AC samples were obtained from the local abattoir as these had been used in other studies and were low cost and easily accessible. For further development and fluid imaging attempts, human articular cartilage samples were obtained from fresh-frozen cadaveric and Thiel-embalmed femoral heads, conforming to the ethical approval for this project. 5 mm osteochondral plugs were removed from all joints with a coring device or a band saw. All samples were fully submersed in PBS and washed overnight to remove the effects of synovial fluid from the cartilage surface, section 3.3.4.

The osteochondral plugs were embedded in Tissue-Tek and rapidly frozen to -65 °C and then kept at -20 °C whilst being sectioned using a cryotome, (Figure 3.19). A variety of slice thicknesses were cut parallel with the AC surface from 3 μm to 60 μm, consequently 10-20 μm slices were deemed most appropriate for best results. The slices were placed on superfrost plus slides which were designed to attach cryotomed samples to the slide without the use of glue. A number of samples were fixed using formalin and then rinsed with PBS, others were dehydrated and the remainder of the samples maintained hydration in PBS.

3.4.2 Experimental protocols

All AFM images were collected with a MFP-3D (Asylum Research, Santa Barbara, CA). In the first instance images of 20 μm dehydrated slices of freshly frozen or fixed articular cartilage were obtained in contact mode at a scanning rate of $\tilde{0}.2\ Hz$ in air. These parameters and sample preparation techniques were originally chosen as they corresponded to those of previous studies that had demonstrated images of AC (Crockett et al., 2005; Stolz et al., 2009; Park et al., 2004).

Square-based pyramidal silicon nitride (TR400PB) AFM probes (Olympus, United Kingdom) with a nominal spring constant of 0.16 N/m were employed for imaging as the cantliever properties (described in section 3.1.7) were soft and within the reported range used in other studies. For similarly prepared samples, imaging was then repeated for tapping mode, using rectangular-based silicon (AC160TS) AFM probes (Olympus, United Kingdom) with a spring constant of 42 N/m and resonant frequency of 300 Hz.

Tests then progressed to imaging in PBS to keep the cartilage fully hydrated. An iDrive cantilever holder (Asylum Research, Santa Barbara, CA) was chosen for fluid imaging due to the benefits detailed in section 3.1.6. Square-based pyramidal silicon nitride (BL-TR400PB) AFM probes (Olympus, United Kingdom) with a nominal spring constant of 0.02 N/m were used with i-Drive for imaging in fluid, as from the two probes suitable for the iDrive technology, this probe had the softest cantilever and was compatible with biological samples (section 3.1.7). The samples were submerged in PBS and imaged at a scan rated of $\tilde{0}.1$ Hz with 1024 lines for high resolution. Also images were obtained using contact mode under fluid with the same methodology as previously discussed for air, with an amended scanning rate of 0.1 Hz to follow the surface easier.

In an attempt to improve image clarity, iDrive images of the Thiel-embalmed samples were acquired under 1-nanonol, rather than PBS. The theory was that 1-nanonol would maintain sample hydration without the surface swelling (as PBS may have) potentially making true surface identification easier. 1-nanonol consists of a straight chain alcohol with nine carbon atoms. Its colourless nature allows the cartilage to be identified by the optics and its low viscosity (a density

of 0.827 g/mL) made it a desirable solution to utilise and investigate, as the tip could oscillate at the required frequency.

A range of scan sizes from 50 μm to 2 μm using a variety of experimental parameters were explored for all sample materials and AFM modes in an attempt to produce a repetitive imaging technique for articular cartilage using AFM.

3.4.3 Results

Figure 3.21 and Figure 3.22 illustrate typical examples of contact mode AFM images collected of a 20 μm slice of bovine AC dehydrated in air. The dense net work of collagen fibres are evident in the 10 μm image with the collagen fibre banding clear in the 5 μm image. The 1.4 μm scan is less focussed and detail is lost in the height images in Figure 3.21 but the deflection images emphasize the bands in the collagen fibrils (Figure 3.22). The structure of the collagen network again is evident in Figure 3.23 which demonstrates contact mode AFM images of Theil embalmed human AC.

Few, if any, scans using tapping mode with a AC160TS cantilevers produced meaningful images however the SNL probes produced by Veeco were more successful. Figure 3.24 demonstrate tapping mode AFM images of dehydrated bovine AC and Figure 3.25 is a magnified section of Figure 3.24. The phase image particularly identifies the contrast between collagen fibres.

Figure 3.26 illustrates a 10 μm tapping mode scan of bovine cartilage under PBS. This scan represent the clearest image obtained when applying AFM tapping mode under fluid. The quality is similar to those seen in other studies (Stolz et al., 2004; Jurvelin et al., 1996). In this study, the majority of images obtained

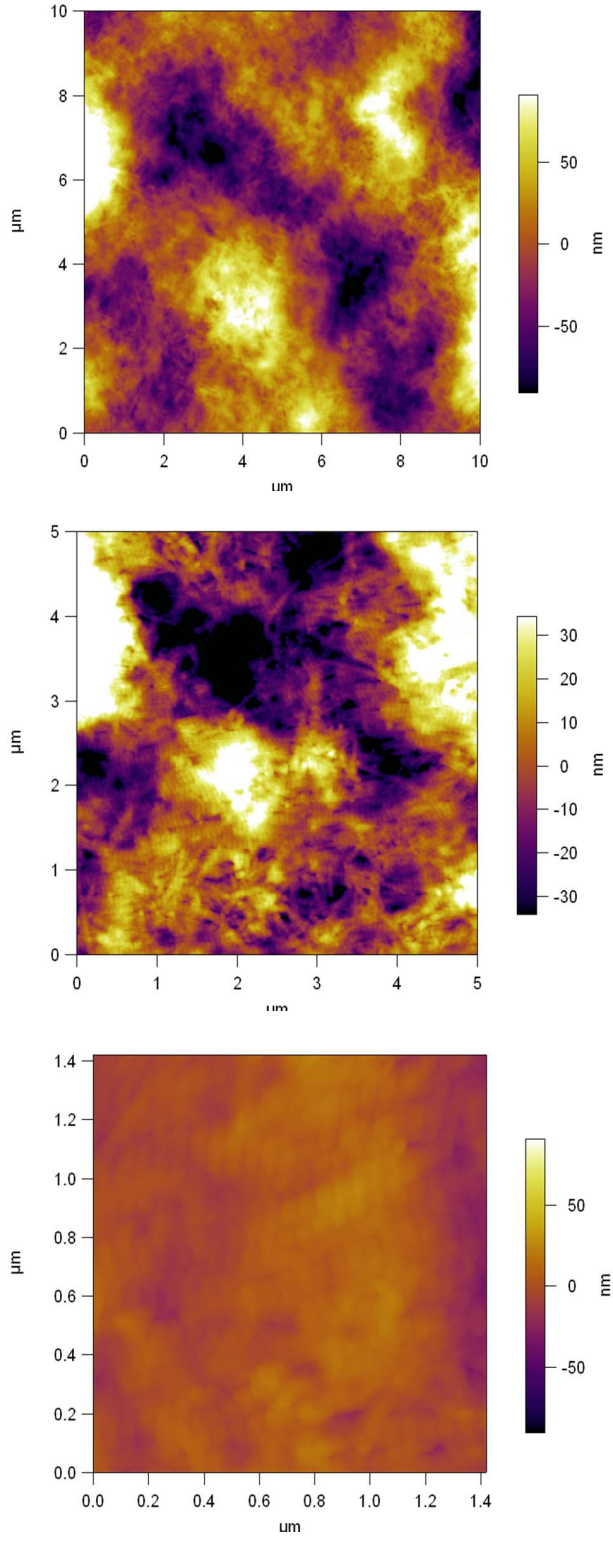

Figure 3.21: AFM contact mode Height images of bovine AC. Scan size reducing from 10 μm to 1.4 μm.

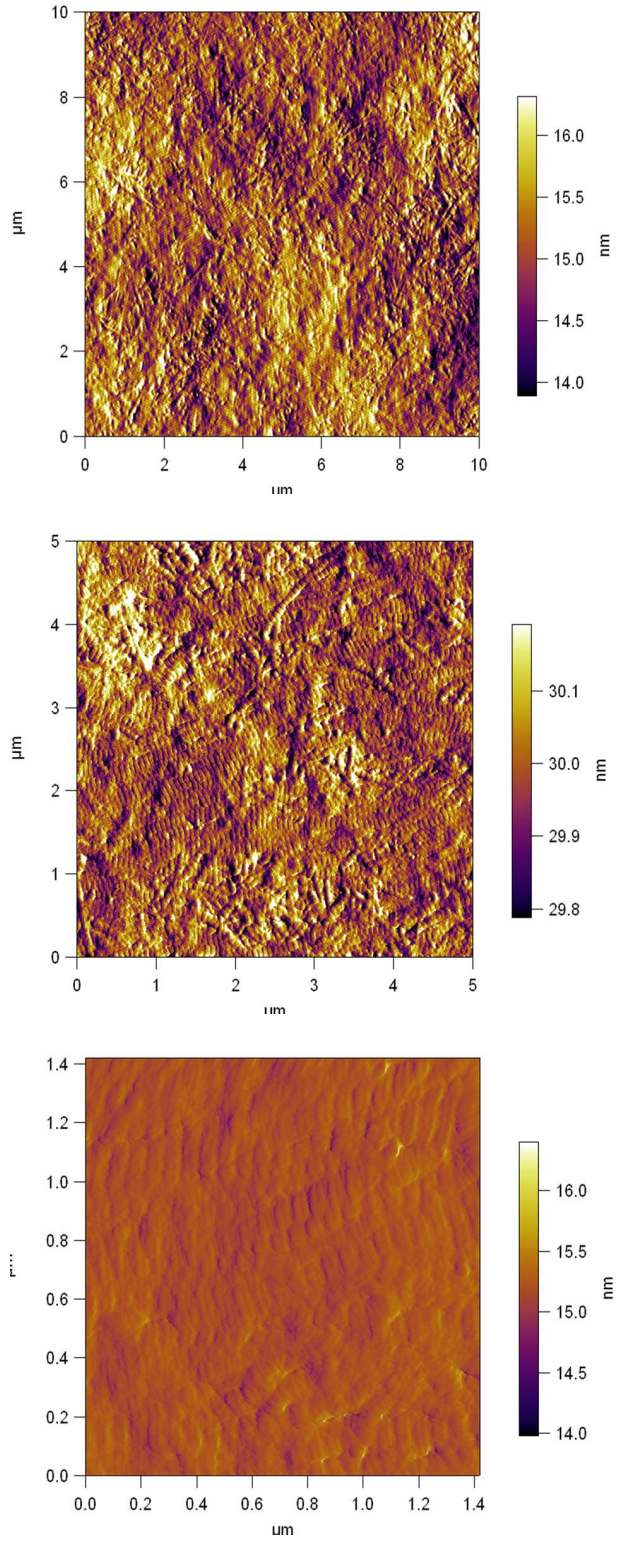

Figure 3.22: AFM contact mode Deflection images of bovine AC. Scan size reducing from 10 μm to 1.4 μm.

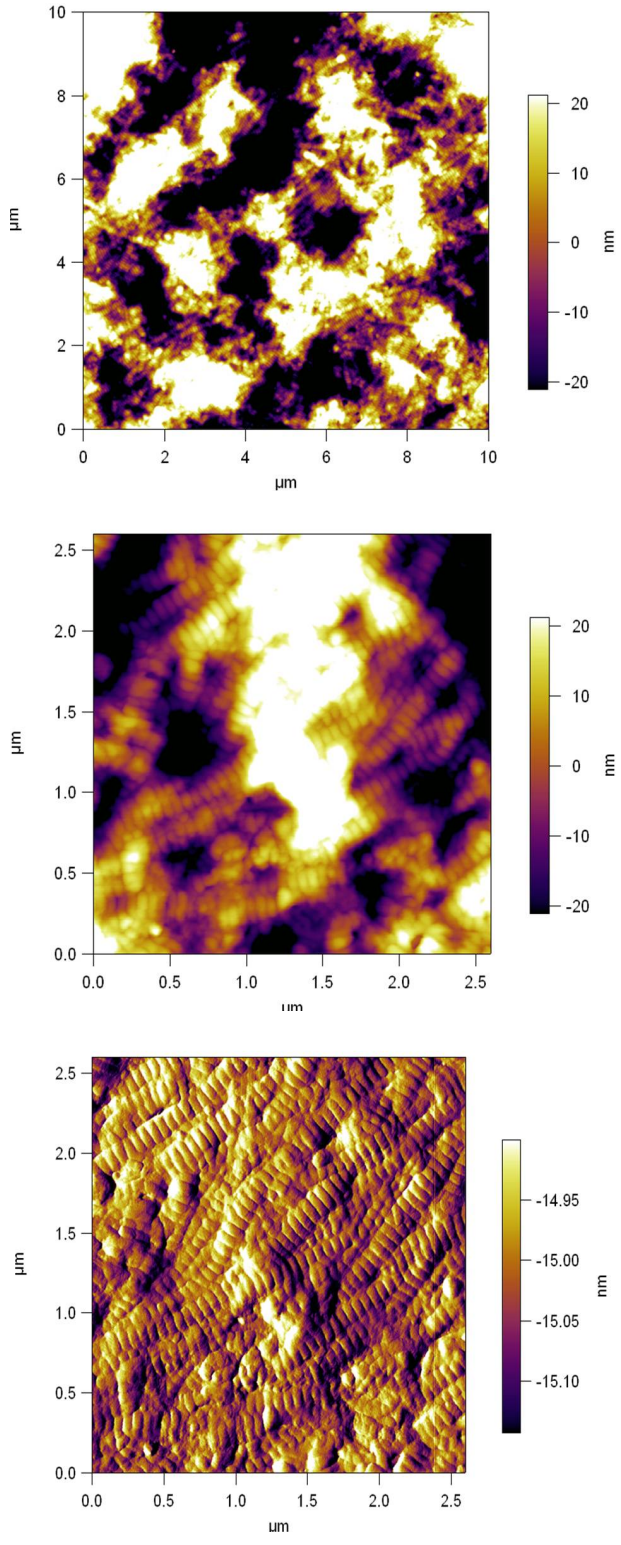

Figure 3.23: AFM contact mode images of human Thiel embalmed AC. Scan size and 10 μm and 2.6 μm.

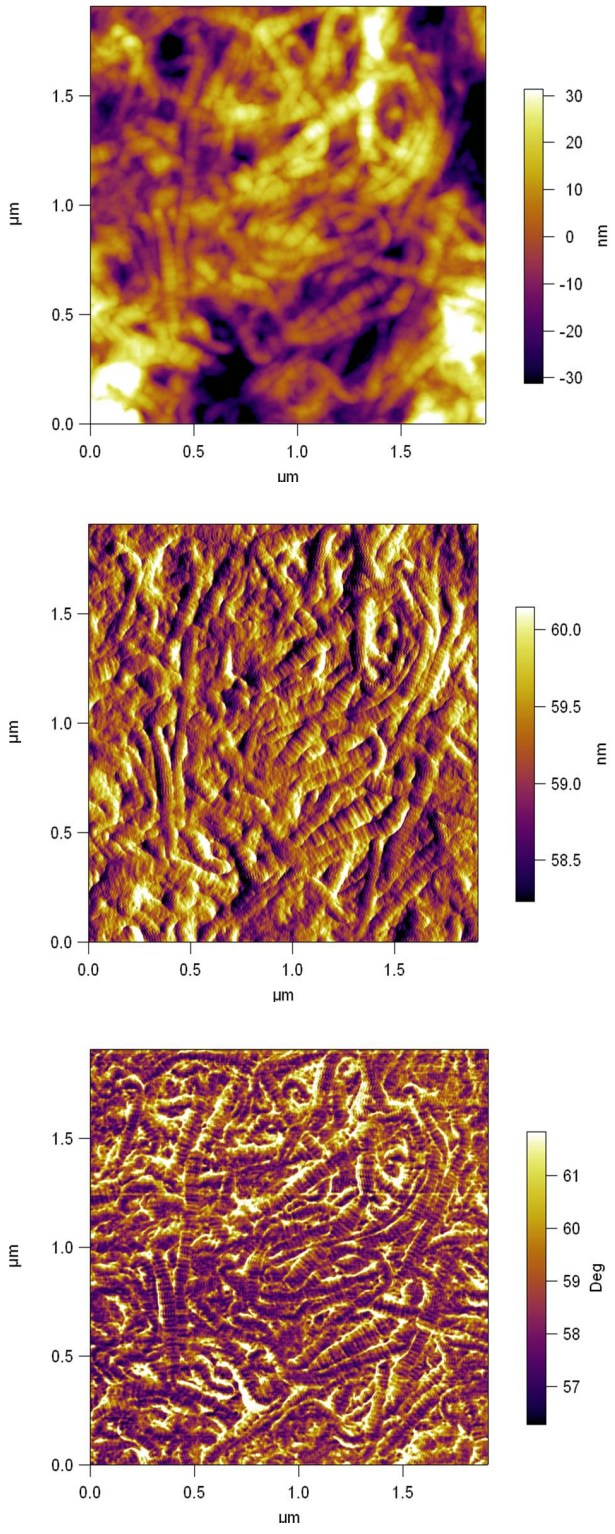

Figure 3.24: Images of bovine AC in tapping mode with SNL AFM Probes; Height image, Amplitude image and Phase image of a 2 μm scan area.

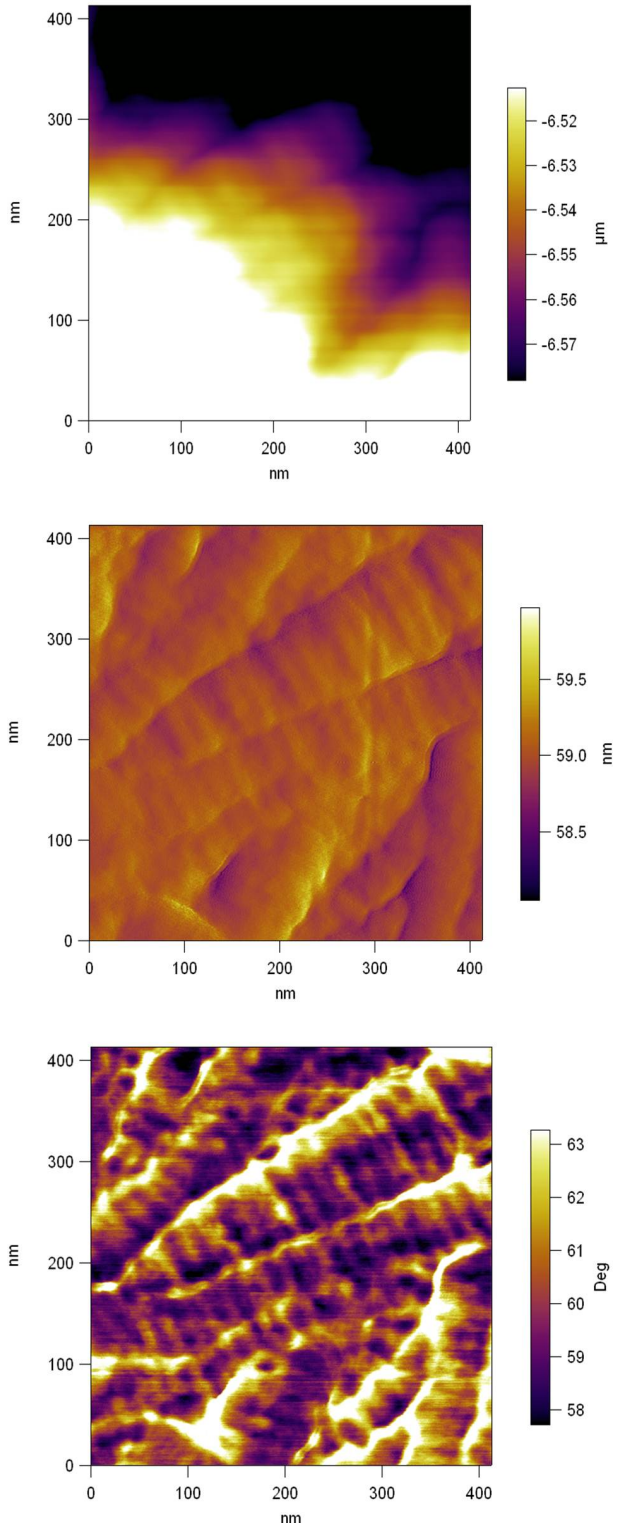

Figure 3.25: Images of bovine AC in tapping mode with SNL AFM Probes; Height image, Amplitude image and Phase image of a scan area less than 500 nm.

are similar to Figure 3.27 which did not show information about the sample composition or surface topography.

Theoretically the iDrive technology should have improved the quality of images in fluid. After several attempts changing experimental parameters, images similar to Figure 3.28(a) were obtained. This gave a surface topography that had not been reported in the literature before. On three separate occasions, it was possible to repeat the image shown in Figure 3.28(b) which is a 10 μm scan with similar topography to Figure 3.28(a). The majority of images produced with iDrive were comparable to Figure 3.28(c). Images in 1-nanonol did not improve image quality under fluid.

3.4.4 Discussion and Conclusion

Good quality images of dehydrated AC samples, human or bovine, were produced with AFM contact mode and tapping mode in air. This technique produced clear images of the collagen network similar in quality to that reported by Stolz et al. (2004). As this project aimed to investigate native articular cartilage fully hydrated, dehydrated imaging was discontinued.

No AFM studies were found that applied the iDrive technology to enhance imaging of articular cartilage under PBS. Images similar to Figure 3.28(a) and Figure 3.28(b) are exciting and intriguing as this topography has not been observed before. However, the lack of repeatability in obtaining these images is disappointing. With no other evidence to support this topography it may be an error artefact of imaging, yet the trace and retrace images had the same topography suggesting it is not an error artefact. It is thought that AFM images in fluid were

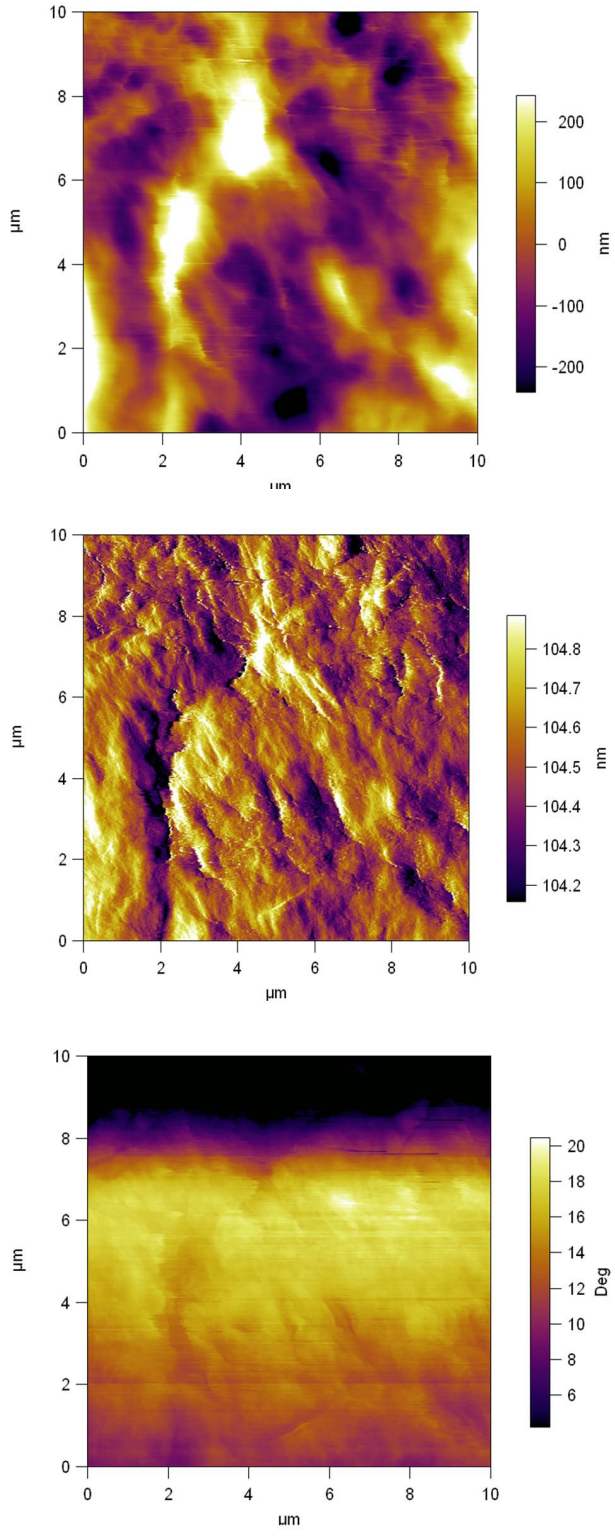

Figure 3.26: Images of bovine AC in PBS using tapping mode with SNL AFM Probes; Height image, Amplitude image and Phase image of a 10 μm scan area.

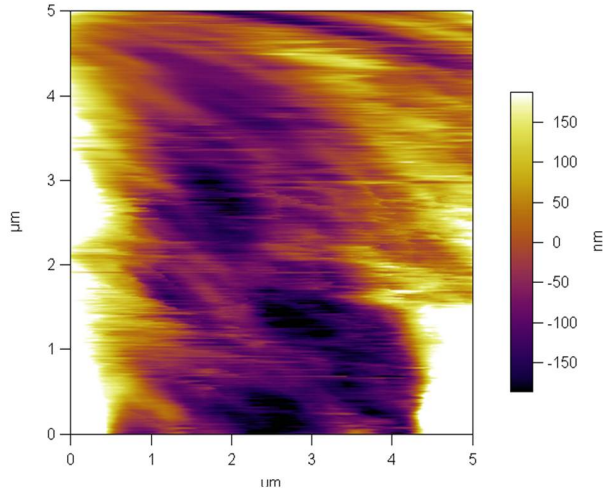

Figure 3.27: A typical bovine AC image under fluid in tapping mode with SNL AFM probes or AC160TS cantilevers.

difficult to obtain as the tissue may have swollen in the PBS resulting in softer tissue making it difficult for the tip to identify what was medium surrounding the sample (PBS) and what was the sample itself. For this reason 1-nanonol was employed in an attempt to prevent excessive swelling. IDrive AFM imaging of AC under 1-nanonol produced meaningless results with no clarity of structure and despite the low viscosity of 1-nanonol it may have reduced the sensitivity of the cantilever making these tests futile. In the absence of consistent reproducible iDrive AFM images in fluid the tests with this technique were also terminated. Consistent AFM imaging of AC under fluid with an SNL cantilever, demonstrated in Figure 3.26, gave similar results to others (Stolz et al., 2004; Jurvelin et al., 1996). However using the extreme sample preparation associated with this technique would change the mechanical properties of AC (i.e. sectioning the sample into 20 μm slices) as the mechanical properties had already been found to be depth dependant (section 2.2).

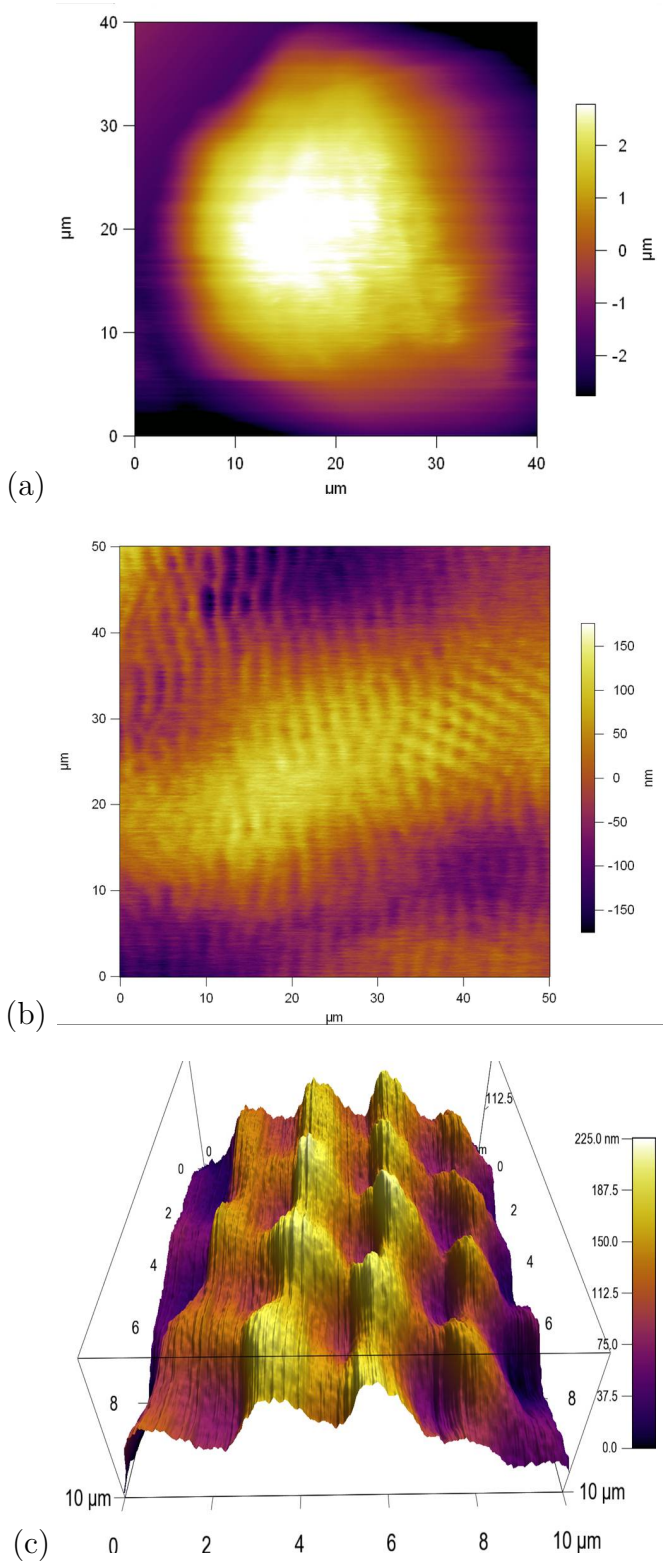

Figure 3.28: iDrive AFM scanning of hydrated bovine cartilage; Height images 2D and 3D.

It was decided that AFM tests would not benefit this study (no further AFM imaging or force mapping) so work focused on nanoindentation for a more appropriate technique to investigate the mechanical properties of healthy AC and the osteoarthritic degeneration process. AFM imaging of AC in a natural environment is required to improve understanding of the compositional structure corresponding to the mechanical properties of AC. IDrive AFM has the potential for quality imaging of AC under fluid however further work is required to determine an appropriate imaging medium that maintains the hydration of the AC sample and the sensitivity of the cantilever. Additionally the development of an iDrive compatible cantilever with a spring constant of 0.06 N/m and a length of 205 μm, similar to the SNL probe, may provide enhanced imaging quality of AC in fluid.

Chapter 4

Experimental determination of the influence of unloading and loading velocity on the mechanical properties AC

Nanoindentation has become a common technique for the analysis of biomechanical properties of biological tissue, bridging the gap between AFM and macroscale mechanical testing (Ebenstein and Pruitt, 2006). Most existing indentation research has focused on hard tissue such as bone, enamel or dentin (Lewis et al., 2008). Load and displacement are observed during indentation, and the mechanical properties may be extracted using a variety of analysis methods. Recently, micro-scale and nano-scale indentation research has investigated the effect of indenter properties on the mechanical properties of AC: with increasing tip diameter there is a significant decrease in equilibrium elastic modulus (Simha et al., 2007) and tip geometry affects the elastic modulus depending on the depth of the indent into the cartilage (Bae et al., 2006). The time-dependent mechanical behaviour of AC introduces complexity into the extraction of its mechanical properties,

and multiple moduli have been quantified. Moreover, many nanoindentation protocols for calculating these moduli have also been explored: dynamic nanoindentation (Franke et al., 2011; Frank and Grodzinsky, 1987); stepwise stress-relaxation indents (Korhonen et al., 2002b); *in vivo* arthroscopic indents (Bae et al., 2003); biphasic (Mow et al., 1980; Mak, 1986); computer modeling (Wilson et al., 2004; Lu et al., 2010) and biphasic-hold indents (Miller and Morgan, 2010, 2009). Whilst the effect of some extrinsic factors such as tip size on the various tissue moduli has been investigated, other important experimental factors have not been explored. In particular, whilst a range of loading and unloading displacement rates ranging from 0.1 $\mu m/s$ to 130 $\mu m/s$ are evident in the literature (Han et al., 2011; Gupta et al., 2005), their effect has not been quantified.

Two of the simplest and commonest parameters that have been used to characterise AC are the indentation stiffness S, the intial gradient of the unloading curve, and traditional Young's modulus E, as calculated by the Oliver-Pharr method (Oliver and Pharr, 2004). An obvious and necessary experiment to perform is the effect of the loading and unloading rate on these parameters. This will enable cross-paper comparisons.

4.0.5 Aims and hypothesis

This study investigates the effects of loading and unloading velocity on S and E, with and without a hold phase, with the aim of identifying an appropriate experimental protocol for future AC characterisation and to aid in the comparison of existing literature.

As the indenter tip redistributes the load through connective transport to the cartilage surface during slow velocities it is expected that the interstitial fluid will have time to permeate resulting in a softer, relaxed tissue compared to a faster indentation velocity which is expected to exhibit larger stiffness as there is insufficient time for the interstitial fluid to permeate through the matrix. Hence the hypotheses are that the AC will become stiffer with increased loading velocity and increased unloading velocity. A third hypothesis is that a 30 s hold at maximum displacement will result in lower S and E due to time dependent relaxation of cartilage. The final hypothesis is that S and E will reduce with repeated indentation at the same location: due to interstitial fluid moving through the extracellular matrix and with each indent the interstitial fluid may not have time to recover.

4.1 Methods

4.1.1 Sample Preparation

The patella was removed from each right hind leg of sixteen cows shortly after sacrifice in an abattoir and kept on ice until utilised.Bovine AC was chosen due to its ease of acquisition but also because previous studies in this field most predominantly utilised bovine tissue (Table 2.2). Visual inspection of the cartilage showed no signs of degeneration or swelling: it was white in colour, hydrated with a smooth looking surface. On the same day, three 5mm square osteochondral samples were excised from the central region of each patella in approximately the same position retaining 2mm of subchondral bone and subsequently frozen at $-20\,^{\circ}\mathrm{C}$ for storage. Hydration of the cartilage was maintained throughout preparation with PBS.

After thawing, samples were fully submersed in PBS and washed overnight to remove the synovial fluid from the cartilage surface (section 3.3.4), thus removing the mechanical effects of synovial fluid on the indentation experiments. After washing, a thin layer of subchondral bone was placed into gypsum plaster with the full thickness of cartilage protruding. Using gypsum plaster allowed the setting of the cartilage surface perpendicular to the indenter tip even with a variable subchondral bone surface. Other adhesives and securing materials were investigated but gypsum plaster was deemed to be best; it did not soak into the tissue potentially changing the mechanical properties and it secured the sample successfully. The sample and the mould were securely attached to the bottom of a petri dish which was then filled to the AC surface with PBS, Figure 4.1. It is key to secure the sample properly as movement enhances the noise in the data.

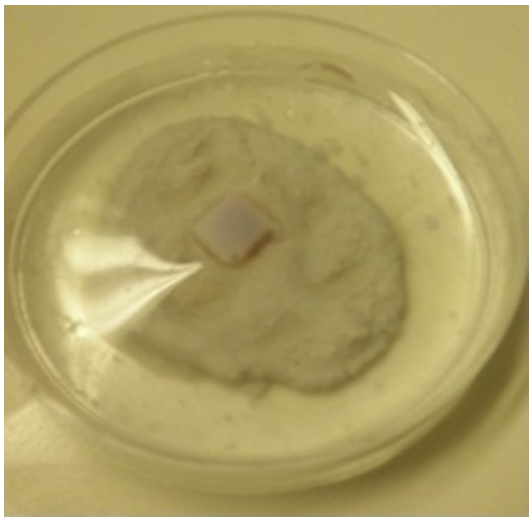

Figure 4.1: A cartilage plug fixed in the gypsum plaster to secure it to the petri dish and maintain a horizontal surface perpendicular to the tip.

4.1.2 Experimental Protocol

The petri dish was magnetically mounted on an MFP Nanoindenter (Asylum Research, Santa Barbara, CA) fitted with a diamond berkovich tip. The AC surface was manually located as described in section 3.3.5. A displacement depth of 5 μm was choosen. The tip height was adjusted so that the start of the open loop displacement-control indentation was located approximately 5 μm above the surface. The peak displacement of the indenter trajectory was defined as 10 μm giving an indentation depth of 5 μm.

Nine triangular loading patterns corresponding to loading and unloading velocities with varying of permutations to 0.5 $\mu m/s$, 5 $\mu m/s$, and 50 $\mu m/s$, and one trapezoidal loading pattern of 5 $\mu m/s$ loading velocity and unloading velocity with a 30 s hold period, repeatedly indented the cartilage (Table 4.1). All indents were positioned at least 1 mm from the sample edge. Ten repeat indentations were made in each tip position. A three minute recovery period separated every group of three indents, with each indent approximately 10 s apart, and the tenth was an individual indent. A total of 5520 indents on sixteen bovine patellae were performed for this experiment.

4.1.3 Data Analysis

Two parameters were determined as measures of tissue mechanical properties in accordance with and for comparison with literature (Miller and Morgan, 2010; Franke et al., 2007; Korhonen et al., 2002b; Lyyra et al., 1999): the contact stiffness (S) and Young's modulus (E). The nanoindention experiment recorded the force displacement curve by continually measuring the load as a function of the tip displacement as the tip extended into the AC tissue. For data analysis, both

Table 4.1: Count of number of indentations per loading profile. * corresponds to the trapezoidal loading pattern.

		Loading velocity $\mu m/s$		
		0.5	**5**	**50**
Unloading velocity $\mu m/s$	**0.5**	720	480	480
	5	480	720/480*	480
	50	480	480	720

loading and unloading curves were saved and exported to Matlab for processing using custom written software.

To determine E, this study implemented the Oliver-Pharr technique (Oliver and Pharr, 1992), a widely accepted approach (Franke et al., 2007; Gupta et al., 2005; Cheng and Cheng, 2005b), to obtain material properties from the unloading curve. A curve was always evident with the manual indentation method employed implying the indentor was in constant contact with the surface in the loading phase. The initial analysis step was to identify the tissue unloading curve from the total manual indent. The retract data was isolated and data from maximum displacement to minimum load was extracted, representing the unloading curve. This resulted in an unloading curve similar to Figure 4.2. This data was used for all further analysis.

$$P = \alpha h^m \tag{4.1}$$

S was determined by fitting a least squares regression in Matlab, Equation 4.1, to the unloading data (where P is the indenter load, h is the elastic displacement and α and m are constants)and finding the gradient at the maximum contact depth Equation 4.2.

$$S = \frac{dP}{dh} \tag{4.2}$$

The reduced modulus, E_r , was determined from:

$$E_r = \frac{S\sqrt{\pi}}{2\sqrt{A}} \tag{4.3}$$

where A is the theoretical predicted contact area at the contact depth:

$$A = 24.5h_c^2 \tag{4.4}$$

where h_c is the vertical distance along which contact is made. Finally, E_r is related to the Young's modulus by:

$$\frac{1}{E_r} = \frac{(1-\nu^2)}{E} + \frac{(1-\nu_i^2)}{E_i} \tag{4.5}$$

where ν was assumed to be 0.5 (Korhonen et al., 2002a). Indenter values calculated by Asylum Research were taken as $\nu_i = 0.2$ and $E_i = 1050$ GPa.

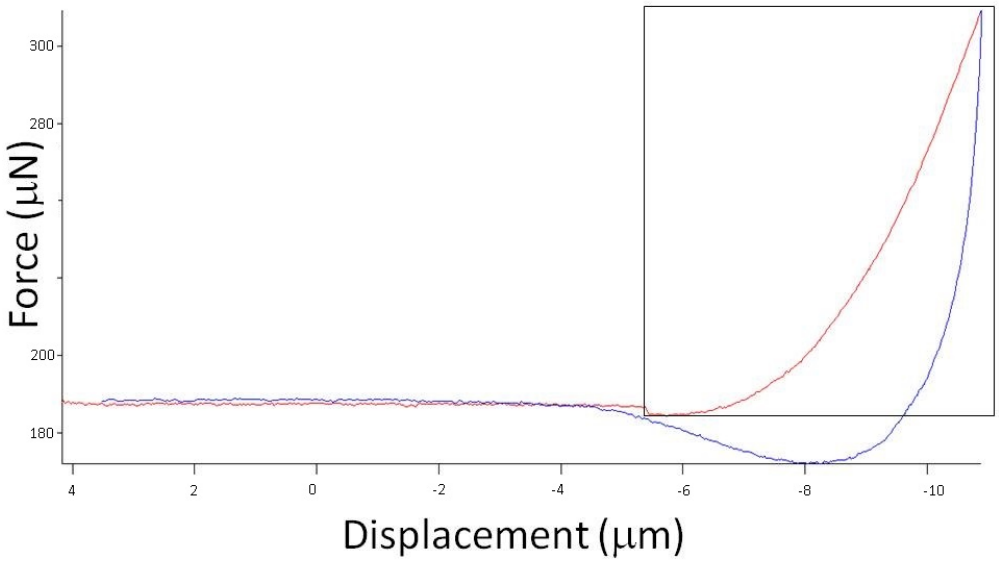

(a) Force-displacement curve.

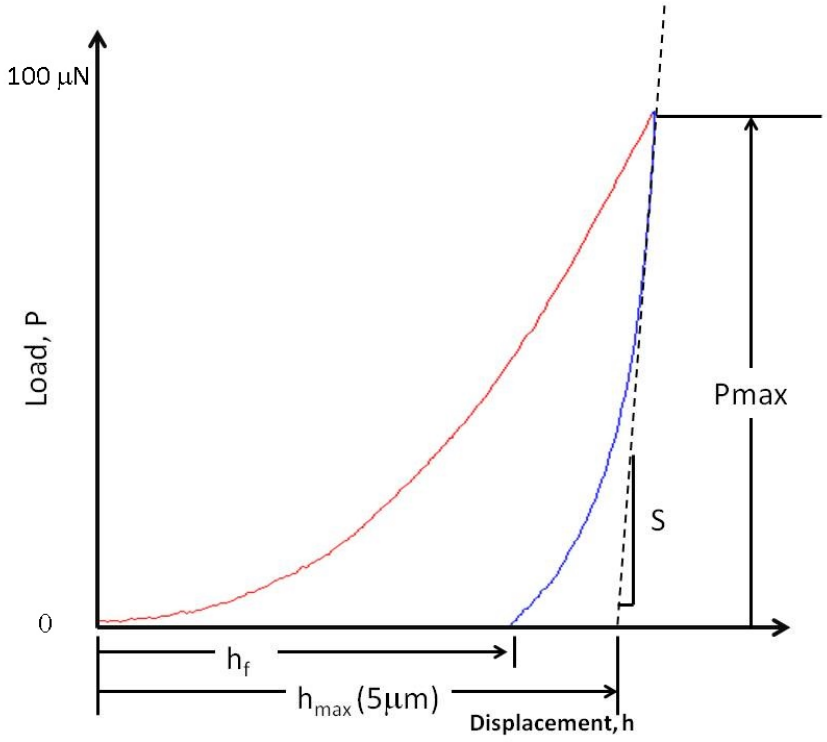

(b) Demonstration of quantities measured.

Figure 4.2: A typical force-displacement curve **for all bovine samples** (red is loading, blue is unloading).

All statistical analyses in Chapter 4 were carried out using statistical software (SPSS version 20.0). Statistical variances of S and E due to repeated indentation (repetition number 1 to 10) and between loading velocity (0.5, 5, 50 um/s), unloading velocity (0.5, 5, 50 um/s) and hold (yes/no) were determined by repeated measures analysis of variance (ANOVA). Significance was taken at $p < 0.05$. Data are reported mean ± S.E.M.

4.2 Results

Repeated indentation had no effect on S or E (Figure 4.3). Notably, one sample showed a dramatic loss of stiffness after the first indent but this trend was not apparent for other samples.

Indentations with a 30 s hold resulted in significantly less stiff AC than when determined without a hold ($p < 0.05$). Additionally, Young's modulus with a hold was 4.2 MPa, approximately half that of indents without a hold, 8.1 MPa ($p < 0.05$, Figure 4.4).

Loading velocity significantly affected S and E ($p < 0.05$). As the loading velocity increased, an increase in S and E was evident. Unloading velocity also had a significant impact on S ($p < 0.05$) and E ($p = 0.05$): as unloading velocity increased, S and E increased (Figure 4.5 and Figure 4.6). Increasing the loading rate by a factor of 100 approximately doubled S and E, whilst increasing the unloading rate by the same factor only increased the S and E by approximately 25%. Figure 4.7 demonstrates a representative histogram of the variation of E with loading and unloading velocity.

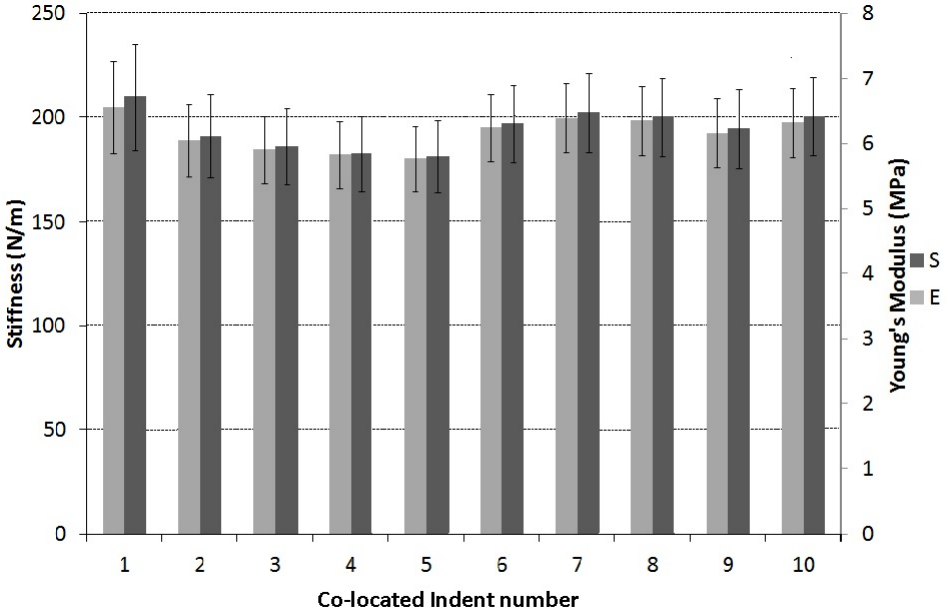

Figure 4.3: Mean stiffness and Young's modulus without a hold for all 16 animals for each co-located indent.

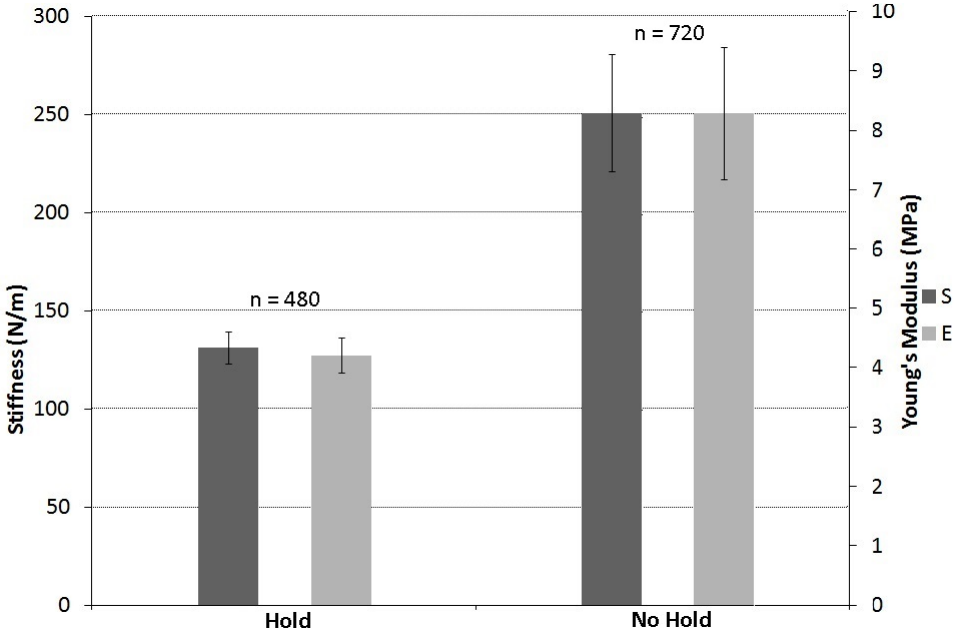

Figure 4.4: The mean S and E for all indents with a loading and unloading velocity of 5 $\mu m/s$ with a hold of 30s and without a hold.

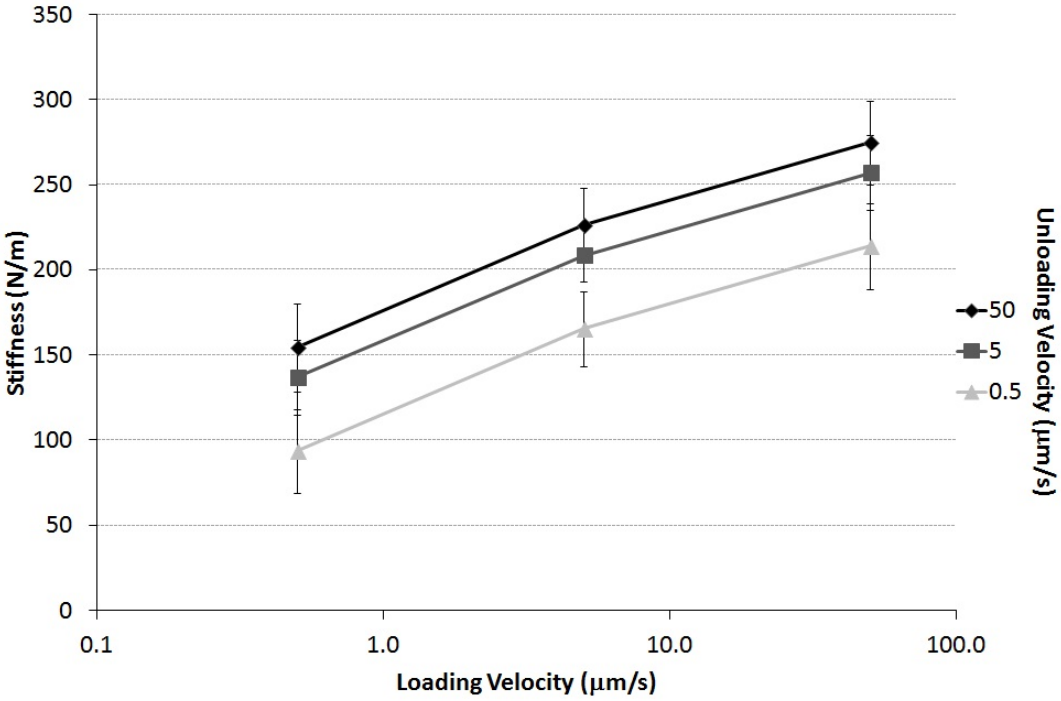

Figure 4.5: Stiffness variation with loading and unloading velocity.

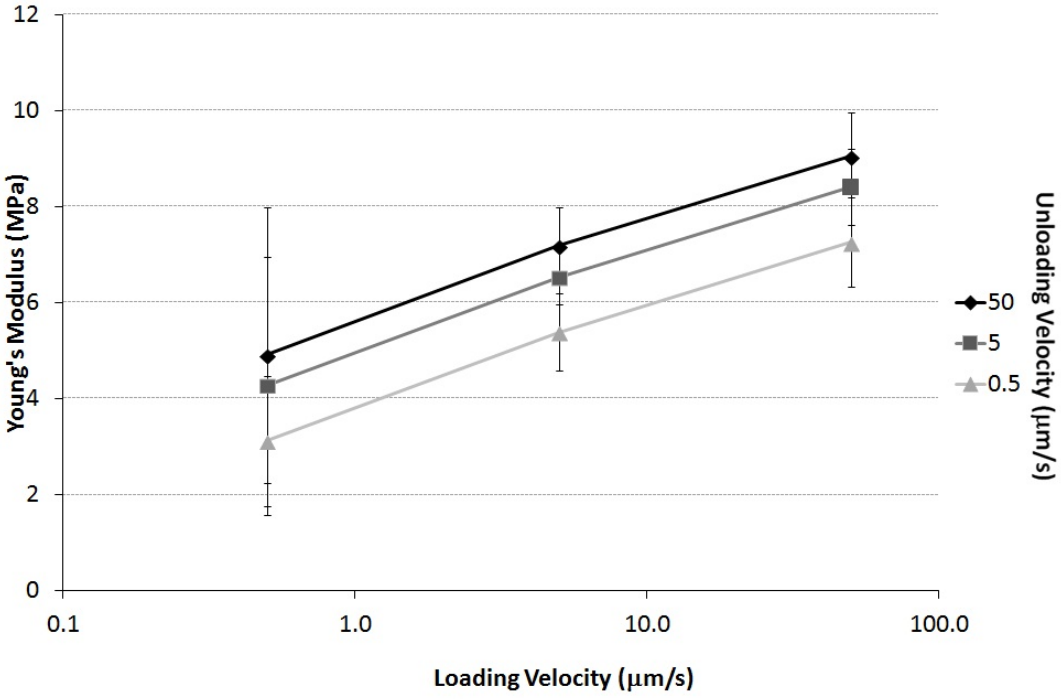

Figure 4.6: Young's modulus varaition with unloading and loading velocity.

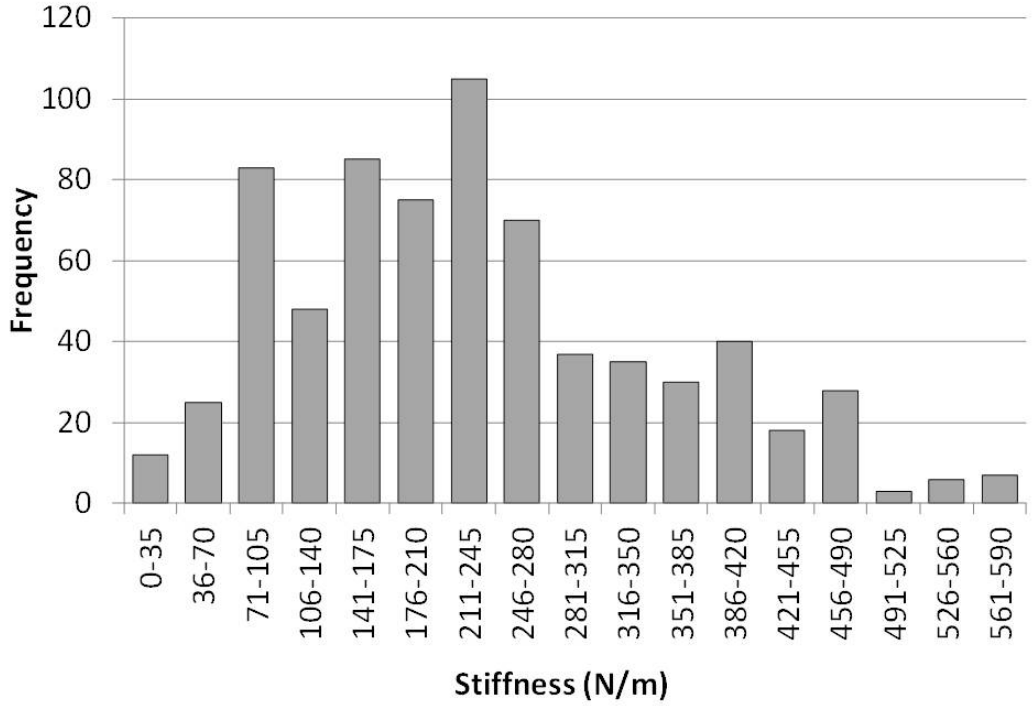

Figure 4.7: Young's modulus variation with unloading and loading velocity.

4.3 Discussion

The mechanical properties of bovine AC reported in this study are comparable (see Table 2.2 on page 36) to existing literature (Franke et al., 2007; Simha et al., 2007; Franke et al., 2011; Kiviranta et al., 2007; Li et al., 2006; Gupta et al., 2009). It is clear from this table that when indenting fixed tissue, values of E are of the order of GPa (Gupta et al., 2005; Doube et al., 2010), much greater than that of fresh-frozen tissue. In addition, this experiment exhibited greater moduli than those found by Korhonen et al. (2002b); Miller and Morgan (2009); DiSilvestro and Suh (2001), possibly due to the known indenter size effect (Simha et al., 2007).

Our results indicated a high variation in cartilage S and E between animal, reflected in previous studies (Lyyra et al., 1999). The mean S is 241.3 N/m ($\pm$5.4) and E has a mean of 7.97MPa ($\pm$0.19). This range may be explained by inherent biological variation. Figure 4.7 demonstrates a typical histogram that indicated no evidence of bimodality (Loparic et al., 2010), implying a homogeneous surface (combined measurement of collagen fibres and proteoglycans) rather than a hetrogenous surface (with individual measurement of collagen fibres and proteoglycan). Bimodality was found through AFM nanostiffness indentations on porcine AC (Loparic et al., 2010). The Berkovich tip is less sharp than the AFM nanoscale tip therefore produces less resolution thus no bimodality, agreeing with Loparic et al. (2010) who found no bimodality with AFM at the microscale. A significant difference between sample position on the patellar was also noted, as the sample positions move superiorly there was increase in S and E. Whilst the patellar is not a load bearing bone, it was possible the regional variation across the patellar surface could reflect the adaption of the cartilage to distinct wear from the movement of the joint.

Since E and S did not vary with repeated indentation, this confirmed that our protocol did not damage our healthy sample surfaces (Bae et al., 2006) and suggested that it was not necessary to precondition AC if approximately 10 s lapses between indentations of depth 5 μm, contrary to Miller and Morgan (2010) and our fourth hypothesis.

As hypothesised stress relaxation during loading, hold, and unloading phases may explain the observed changes in apparent stiffness of the matrix. This stress relaxation can be attributed to both fluid flow within the matrix and flow-independent collagen fibre viscoelasticity. An increase in the loading rate by a factor of 100, roughly doubled E and S but an increase in unloading rate of a factor of 100

only showed an increase of around 25%, indicating that the loading history had a greater effect on stiffness than the unloading regimen. The velocity of loading is key to fluid pressurisation beneath the indenter. A loading velocity of 50 $\mu m/s$ resulted in high stiffness and Young's modulus suggesting the tissue acts more like an incompressible material because of an increase of fluid pressure in the matrix (Korhonen et al., 2002b). A loading velocity of 0.5 $\mu m/s$ resulted in a low stiffness and Young's modulus suggesting reliance primarily on the compressive stiffness of the solid matrix (Lu et al., 2004), as the interstitial fluid has permeated through the extracellular matrix reducing the osmotic swelling pressure, a time dependant reaction (Han et al., 2011). Since poro(visco)elastic mechanisms, detailed above, could explain our variations in stiffness, this suggests that fast velocities determine the apparent properties of cartilage, whilst slower velocities are more likely to capture the intrinsic characteristics of the solid matrix only.

4.3.1 Limitations

Our analysis of E is based on the Oliver-Pharr method and assumed the tissue was a smooth, homogenous, isotropic, elastic half space. This does not describe AC well. Inverse numerical methods provide an alternative to parameterise the tissue, however a variety of models have been utilised making comparisons difficult between studies. Since the aim of this study was to enhance cross-study comparisons, it was felt that the limitations of the Oliver-Pharr method were acceptable in this case. We assumed $\nu = 0.5$, however, if ν was taken to be $= 0$, E would have scaled accordingly (a difference of 25 %), remaining within the range of the literature values. However, stiffness calculations did not involve such assumptions and they demonstrated equivalent variance.

4.4 Conclusion

This study has quantified the effect of loading and unloading displacement rates on AC stiffness with the intention that this data can ease cross-study comparisons involving different nanoindentation protocols.

The main conclusions of this study were:

1. Loading rate has greater effect on S and E than the unloading rate.
2. Time-dependent relaxation is evident after 30 s hold
3. Preconditioning (ie multiple indention prior to measurement indent) of healthy bovine articular cartilage is not necessary as this repeated indentation protocol had no detrimental effect on mechanical properties of AC.

Chapter 5

Nanoindentation of human femoral heads

5.1 Introduction

Cartilage contact stresses are highly diverse as they change depending on activity (Harris et al., 2012; Horak et al., 2011) i.e.how the joints are loaded. The mechanical characteristics of cartilage are complicated as cartilage is required to adapt and transfer load under many different conditions. Structurally, healthy AC can be separated into superficial, transitional, deep and calcified layers with varying arrangements of: collagen fibres; proteoglycans; interstitial fluid and chondrocytes (section 2.1). The mechanical behaviour of AC is closely related to its composition. Healthy AC plays an important role in providing effective load transmission and efficient movements of diarthrodial joints; osteoarthritis is a deteriorating disease that causes disability and pain (section 2.3) that affects 80% of the population over the age of 75 years (Simon et al., 1972; Taylor et al., 2012). Once OA is identified with current diagnostic techniques, no treatments are able to repair AC or stop the degeneration. Total joint replacements are a standard treatment for patients with OA: this procedure involves serious surgery

and extensive removal of bone, thus limiting revision options. In 2012 in England and Wales, 89,633 total hip replacements were performed. Osteoarthritis causes great financial burden to the National Health Services and to society and creates a significant social burden on the patient, reducing their quality of life (Horak et al., 2011). It was shown in section 2.3.1 that the current clinical diagnostic methods for OA do not possess the sensitivity to detect the early stages of OA or quantify the changes in the functional properties of OA. This has encouraged further investigation into early detection of OA to identify the onset of the disease while it remains reversible (Pollard et al., 2008) and to expand understanding of the OA degeneration process.

The degenerative process of OA on cartilage has been mapped with histological methods providing physiological grading systems. Histological techniques require extreme sample preparation that changes the biomechanical properties of the cartilage and in addition histology does not include the effect of interstitial fluid (vital in cartilage composition) because dehydration is required. AFM force mapping using a 5 μm glass spherical tip found a decrease of E in both chondrocyte pericellular matrix and extracellular matrix as OA degeneration worsened on the human medial condyle (Wilusz et al., 2013). Due to sample preparation AFM force mapping does not record the alteration of full thickness natural AC mechanical properties when degenerated by OA. The biomechanical alteration of osteoarthritic AC is not fully understood and currently no biomechanical grading system is available to complement those of the histological grading systems. The current diagnostic methods do not identify early OA and the pathophysiology of OA initiation remains uncertain (Pritzker et al., 2006). Changes due to ageing and osteoarthritis have been visibly depicted earlier at the nanometre scale than the morphological changes have been observed using present diagnostic methods

(Stolz et al., 2009). With greater understanding of the OA degeneration, preventative measures and improved OA treatments may be available in future.

Nanoindentation has repeatedly been reported to be a powerful tool in measuring mechanical properties and has further potential as a diagnostic tool to identify early OA, possibly before permanent microarchitectural damage develops (Franke et al., 2007; Ebenstein and Pruitt, 2006; Bae et al., 2006; Korhonen et al., 2002a). Section 2.4.2 discussed the current literature investigating nanoindentation of cartilage and most studies used animal tissue rather than human tissue. Mechanical testing of human tissue has demonstrated human tissue to have different mechanical properties to that of other species (Stolz et al., 2009). AC mechanical properties showed not only dissimilarities between species but also anatomical position. Indentation experiments in the human knee joint indicated that the femoral condyles have stiffer cartilage than the tibial plateau and the patellar surface of the femur (Swann and Seedhom, 1993; Yao and Seedhom, 1993). To the best of the author's knowledge, despite the prevalence of hip replacement surgery, no study has determined and compared the mechanical properties of the AC surface in healthy or OA human femoral heads. This knowledge could be key to the understanding of OA degeneration, specifically where OA may initiate predominantly, to help focus early diagnosis. Additionally, it may contribute to further understanding of the contact stresses and loads within the hip joint and how the cartilage adapts to them, as disagreement persists regarding the locations of predominant loading during normal daily activities (Abraham et al., 2013; Harris et al., 2012; Horak et al., 2011).

As the cartilage has a range of mechanical responses, dependent on the activity i.e. loading pattern, a variety of methods and different loading arrangements have been investigated as detailed in section 2.4.2: dynamic nanoindentation

(Franke et al., 2011; Frank and Grodzinsky, 1987); stepwise stress-relaxation indents (Korhonen et al., 2002b); *in vivo* arthroscopic indents (Bae et al., 2003); biphasic-hold indents (Miller and Morgan, 2010, 2009) and biphasic (Mow et al., 1980; Mak, 1986). Bae et al. (2006) reported a change in mechanical properties of human cartilage with increasing tip size demonstrating experimental factors alter the measured mechanical properties of AC. Two tip geometries were investigated in this study for better comparison of our results with current literature. The Berkovich tip (Figure 3.16) was employed as this traditional tip has been used in various nanoindentation studies; it is less sharp than similar tips such as the cubed corner tip and is more sensitive to individual material properties than a spherical tip. A unique flat ended punch with a width of 0.69 μm was the second tip utilised for testing (Figure 3.15) and was selected because of its known contact area which would reduce assumptions for data analysis; submicron indentations were capable with this tip, potentially enabling improved indentation sensitivity. This study implemented two loading patterns in an attempt to gain better understanding of the AC response and to enable comparisons with other studies.

5.1.1 Aims & Hypotheses

The aims of the study in this chapter were:

1. to map the topographical variation in mechanical properties of cartilage over healthy and osteoarthritic femoral heads and to compare the experimental results with numerical studies of the natural gait. It was hoped to obtain fundamental knowledge of healthy cartilage properties that could be used as control data for comparison with the OA cartilage. Furthermore, it was hoped this would show how OA affects the mechanical properties of AC over the femoral head and identify where OA degeneration initiates. Linking experimental results with previous numerical studies of the natural gait may further understanding of the change in contact stresses during daily activities.

2. to identify the biomechanical signature of degeneration through OA. This will provide criterion for future clinical arthroscopic nanoindentation device users to guide them in identifying early OA and assessing the health of the tissue.

3. to determine whether S and E correlate to the recognised Outerbridge grades (Outerbridge, 1961) of osteoarthritic human cartilage. This will further the understanding of how OA degeneration affects the mechanical properties of AC and link biomechanical changes to observable structural changes.

4. to compare the effects of triangular loading and trapezoidal loading on healthy and OA human AC (hold of 30 s) because cartilage is known to have a time-dependent mechanical reaction to load. Comparing healthy cartilage with OA cartilage will further the understanding of how OA affects the mechanical properties of AC.

5. to compare a traditional Berkovich tip with a unique flat ended tip in order to discover if a small and constant tip area is more sensitive to changes in mechanical properties, reducing experimental error and to aid comparisons with other studies.

The first and second hypotheses are that nanoindentation tests will identify stiffer AC in the superior posterior location of the femoral head due to the presumed larger contact stresses at this location in normal gait (Abraham et al., 2013; Harris et al., 2012). thirdly it is hypothesised that S and E will decrease with increasing severity of osteoarthritis due to the degeneration of collagen fibres. The fourth hypothesis is that a trapezoidal loading pattern will display a lower S and E than those of the triangular loading pattern. The fifth hypothesis is that S and E will differ when the tip geometries are altered as nanoindentation is a sensitive device; a slight change to the contact area will affect the measured outcome.

5.2 Methods

5.2.1 Ethics

All tissue collected and tested in this experiment conformed to the ethical permission granted by the NHS West of Scotland Research Service (application reference: 11/AL/0343). Written consent for the tissue had already been acquired by either the NHSGGC Bio-repository or the Anatomy Gifts Registry (Maryland, U.S.). It was stipulated that the tissue from the NHSGGC Bio-repository must be returned to the original source of collection for disposal and incineration. The exclusion criterion insisted that the femoral heads remained in one piece to retain orientation after removal.

5.2.2 Sample Collection

Following ethical permission, twelve human femoral heads were harvested following total hip replacement surgeries and collected via the NHSGGC Bio-repository. On the day of surgery the femoral heads were wrapped in tissue soaked saline and frozen at $-20\,^{\circ}\mathrm{C}$ until testing. Six fresh frozen hemi-pelvis to toe cadaveric legs were obtained from Anatomy Gifts Registry. These specimens had no medical history of OA and had been previously thawed once for knee arthroplasty surgical training and refrozen. The six cadaveric femoral heads were removed following a typical surgical protocol as described in the next section.

5.2.3 Typical Surgical Protocol

A brief description of the surgical protocol in removing the femoral head follows. The skin incision extended proximally and distally to the tip of the greater trochanter (Figure 5.1(a)). A charnley was positioned beneath the fascia lata equal to the level of the trochanter. With the scalpel, the trochanteric bursa was divided and moved posteriorly, uncovering the gluteus medius. At their connection on the femur bone, the short external rotators were separated including no less than the proximal half of the quadrates femoris. The interval between the gluteus minimus and superior capsule was bluntly dissected. A blunt cobra was placed superiorly and inferiorly to obtain exposure of the superior, posterior and inferior portions of the capsule. The soft tissue was then completely dissected as illustrated in Figure 5.1(b) and the femoral head was dislocated by flexing, adducting and internally rotating the hip (Figure 5.2(a), Figure 5.2(b)). A bone hook was placed under the femoral neck to help lift the head out of the acetabulum; occasionally the ligamentum teres needed to be cut to allow the femoral head to be fully exposed. The femoral neck was then divided for removal of the femoral

head. It was presumed that the femoral heads from hip replacement surgery were removed with a similar surgical protocol and care was taken to protect the nerves in order to conserve function for rehabilitation.

5.2.4 Sample Preparation

All the femoral heads followed the same sample preparation protocol for nanoindentation experiments. Each femoral head was labeled with a specific identification number which corresponded to a data sheet that detailed, when available, the gender and age of patient and any medication taken. All information remained anonymous.

On the day of testing, the femoral heads were thawed and tissue hydration was maintained with PBS. The nanoindentation tests were completed within 72 hours of the thawing. Five photos were taken of the whole femoral head before any further dissection occurred, similar to those in Figure 5.3, enabling a complete reference to be archived for the future. These are available in the attached electronic appendix. Twenty-two cylindrical osteochondral plugs ($5mm$ diameter) were removed from identical areas on each femoral head (Figure 5.4). These positions covered all regions of the femoral head allowing a good range of locations for detailed comparison later. The osteochondral plugs were removed with a tissue punch (Figure 5.5) permitting a clean cut, unlike a band saw or an autopsy saw. The plugs included the full cartilage depth and approximately 2 mm of subchondral bone and initially each was visually graded for OA using the Outerbridge grading system (Outerbridge, 1961).

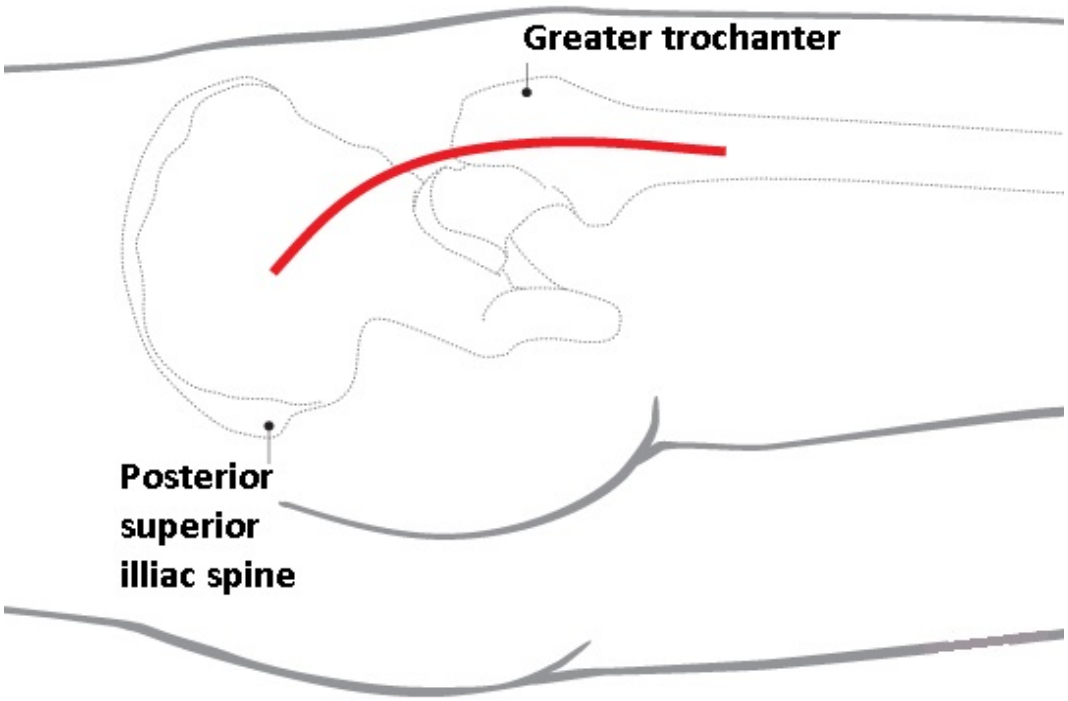

(a) Skin incision for posterolateral appoach to hip

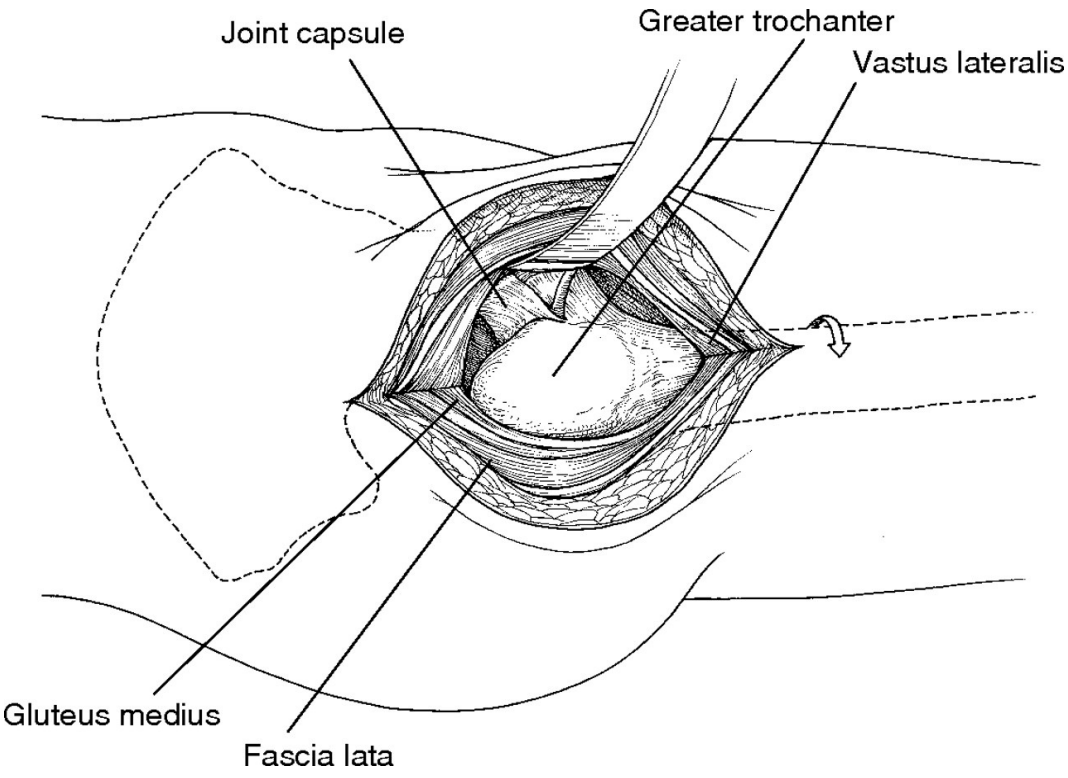

(b) Completed soft tissue dissection

Figure 5.1: Diagrams of the initial stages of total hip replacment protocol.

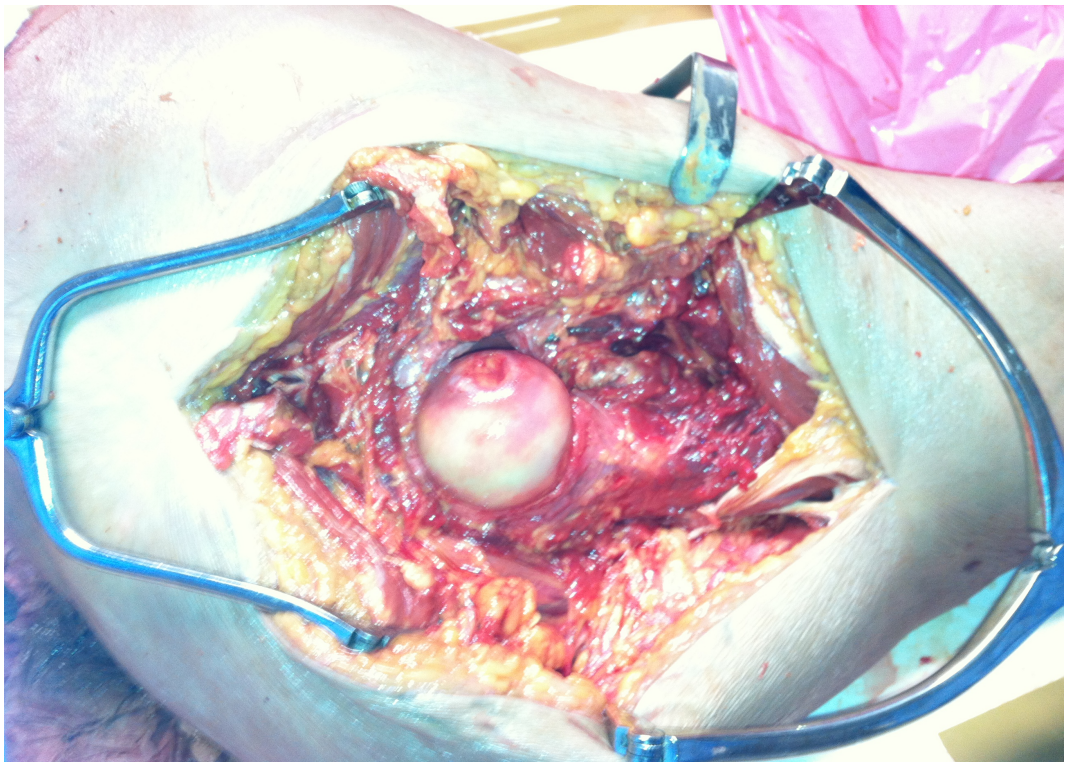

(a) Dislocated femoral head ready for removal

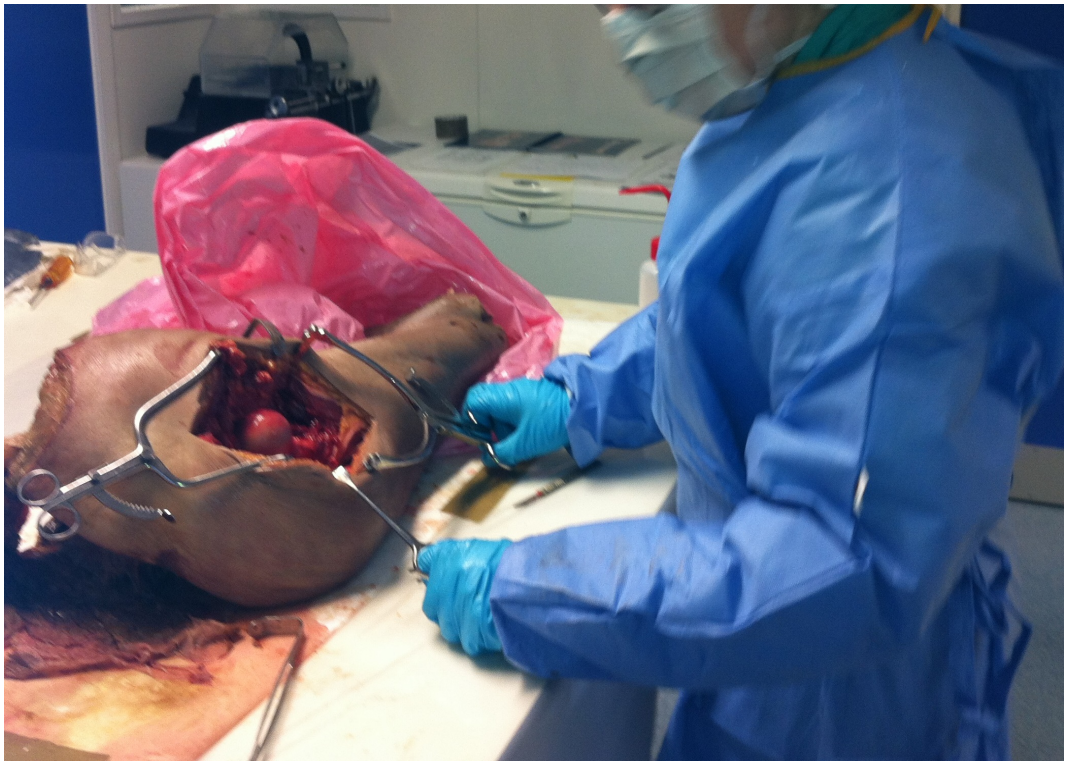

(b) Dislocated femoral head ready for removal.

Figure 5.2: Images of a cadaveric leg after hip dislocation and before femoral head removal.

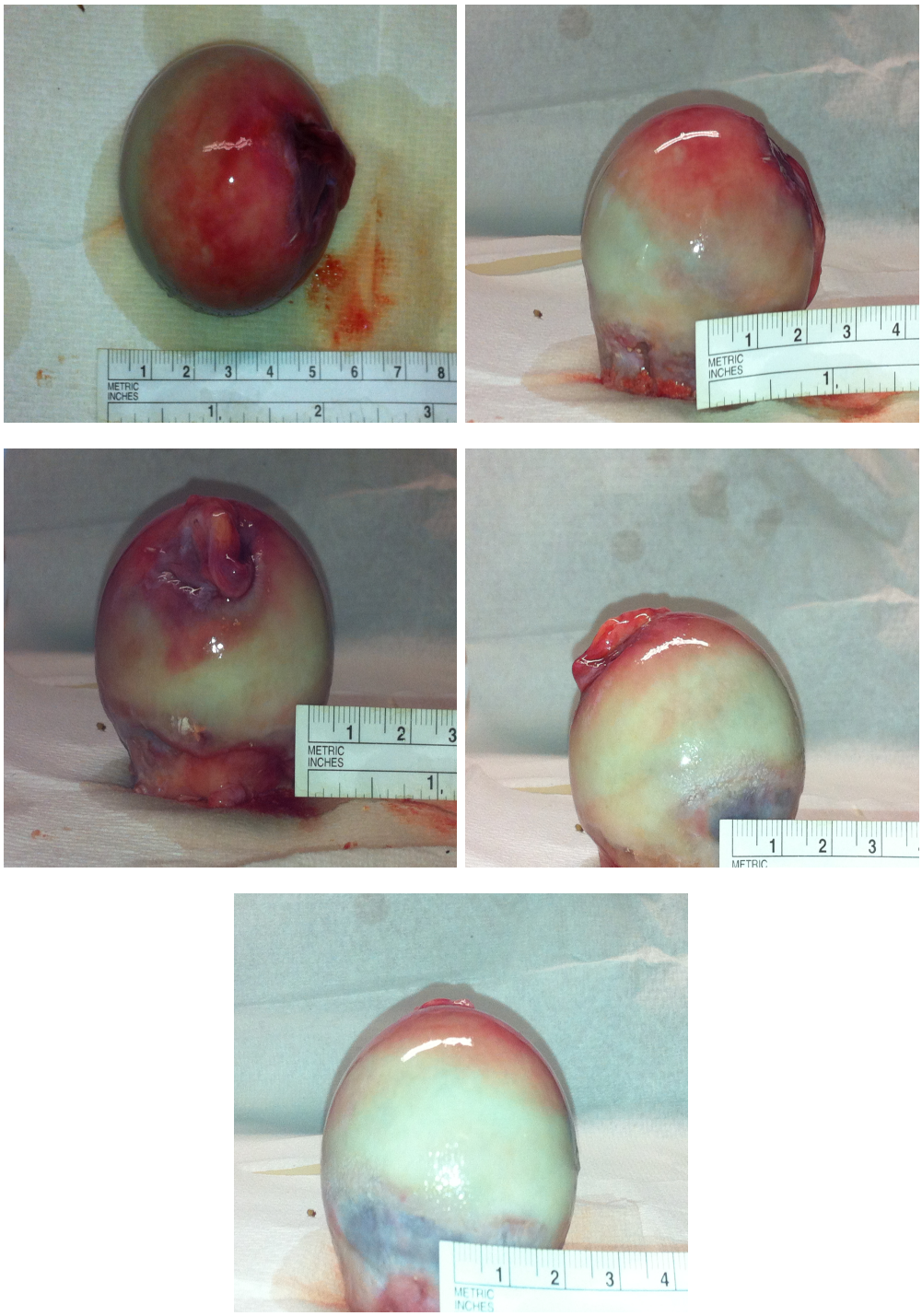

Figure 5.3: Five typical photos of a femoral head, showing all angles, before dissection.

The Outerbridge system (Outerbridge, 1961) classifies AC degeneration into grades identifying increasing severity of osteoarthritis beginning with grade 0 which denotes healthy cartilage. Grade 1 represents AC with softening and superficial lesions, grade 2 describes partial thickness defects with fissure length never exceeding 50% of cartilage thickness, grade 3 refers to severely damaged AC with fissures extending to subchondral bone, and grade 4 describes end stage OA with areas of cartilage erosion to the bone. This scale is based on macroscopic changes.

The orientation for each plug was identified by gluing a small piece of coloured thread to the superior (green thread) and posterior (red thread) edges of the bottom of the bone (Figure 5.6(a)). As previously discussed, the osteochondral plugs were washed in PBS to remove surface synovial fluid and after washing the subchondral bone was secured in a petri dish using gypsum plaster with the full thickness of cartilage protruding (Figure 5.6(b)). Red and green dots were placed on the base of the petri dish and the threads were aligned accordingly to clarify orientation (Figure 5.6(b)). To maintain hydration the petri dish was then filled with PBS, level with the cartilage surface.

Figure 5.4: A represention of the 22 locations of the osteochondral plugs on a femoral head.

Figure 5.5: 22 plugs were taken from across each femoral head using a tissue punch.

(a) Red and green threads attached to the cartilage sample to maintain and clarify orientation.

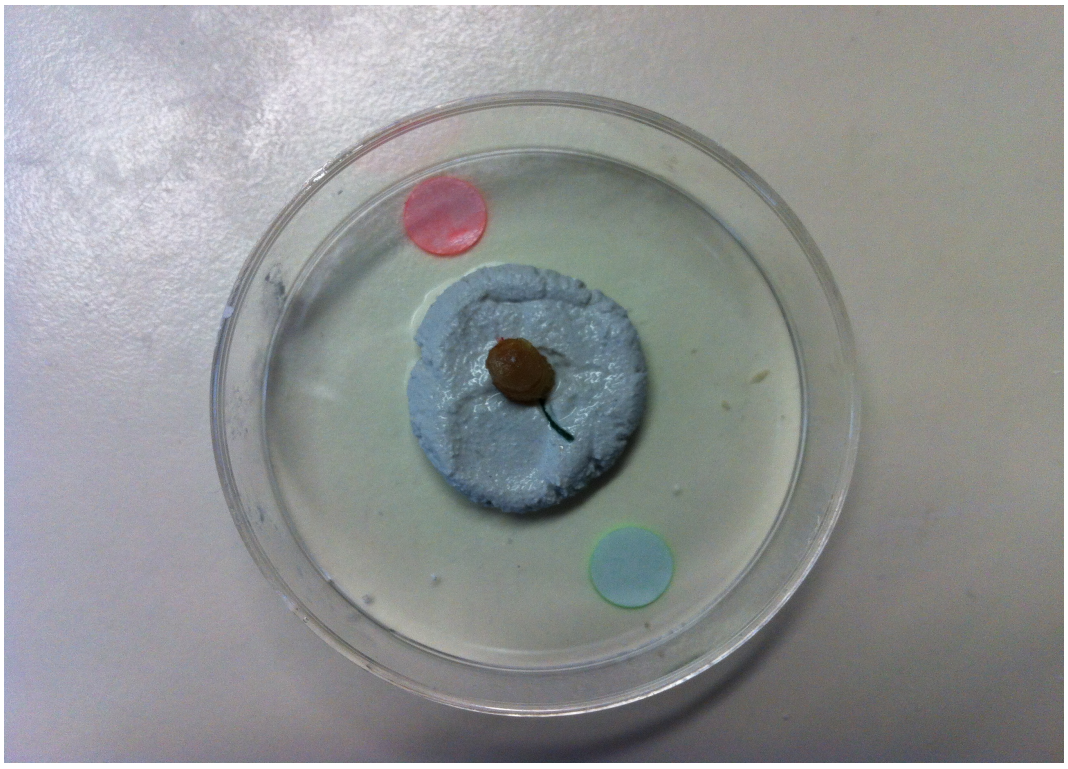

(b) Photograph of the sample setup ready for mechanical tests.

Figure 5.6: Photographs of sample oreientation and setup.

5.2.5 Experimental Design

The nanoindenter InvOLS calibration and laser alignment were verified before the tests began as described in section 3.3.2. The petri dish, containing the osteochondral plug, was then placed on the heated platform to maintain the sample's temperature at 37 °C; the sample was orientated so the superior edge (green thread or dot) was closest to the optics. The petri dish was secured by magnets (Figure 5.7) and the vibration isolation equipment was operated (Figure 3.9) in preparation for testing, in order to minimise all vibration.

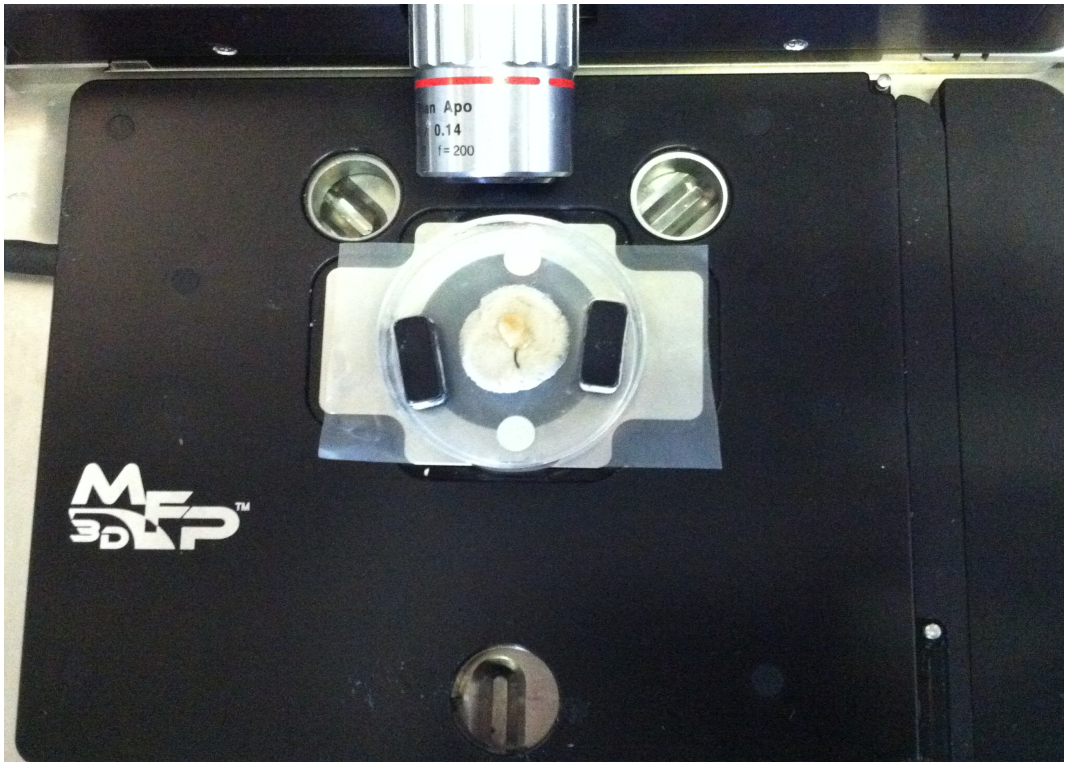

Figure 5.7: Sample in correct orientation.

Four experimental parameters were investigated, two tip geometries and two loading patterns, to compare their affects on the mechanical properties of AC. For all indentations manual surface detection was used to ensure a precise measurement of indentation depth, as described previously in section 3.3.5. For each tip

geometry a 50 μm x 50 μm area, similar to Figure 5.8 was identified for indentation. 16 indent locations (4 x 4 grid) were identified as illustrated in Figures 5.8. For each tip geometry two indents were taken per location: one trapezoidal and one triangular, with the initial indent per location alternated. A central location, a minimum of 1mm from the edge of the sample, was identified as the 50 μm x 50 μm indentation area. Occasionally the OA affected sample had minimal cartilage remaining on the 5 mm plug (grade 4 Outerbridge) so in this situation the author chose the largest area of cartilage available to indent.

Triangular and trapezoidal indentation functions were applied with displacement and retraction rates of 5 $\mu m/s$ and the trapezoidal indentation function included a 30 s hold at maximum displacement (Figure 5.9). The previous study (Chapter 3) found slower indentation velocities characterised the solid matrix whilst faster velocities characterised the apparent properties. A rate of 50 $\mu m/s$ was deemed to retract too quickly for the cartilage reaction therefore 5 $\mu m/s$ was chosen as the optimum loading and unloading rate for this experiment. If the sample's surface remained attached to the indenter tip quantative data analysis on the unloading curve could not be completed so video evidence was recorded for qualitative analysis. A total of 25,344 open loop indents were intended for this study (Figure 5.10).

5.2.6 Data Analysis

For mechanically viable AC samples, force-displacement curves were analysed and the contact stiffness S and Young's modulus E were calculated from the initial gradient of the force-retraction data at maximum contact depth in accordance with the Oliver-Pharr method (Oliver and Pharr, 2004) as described in

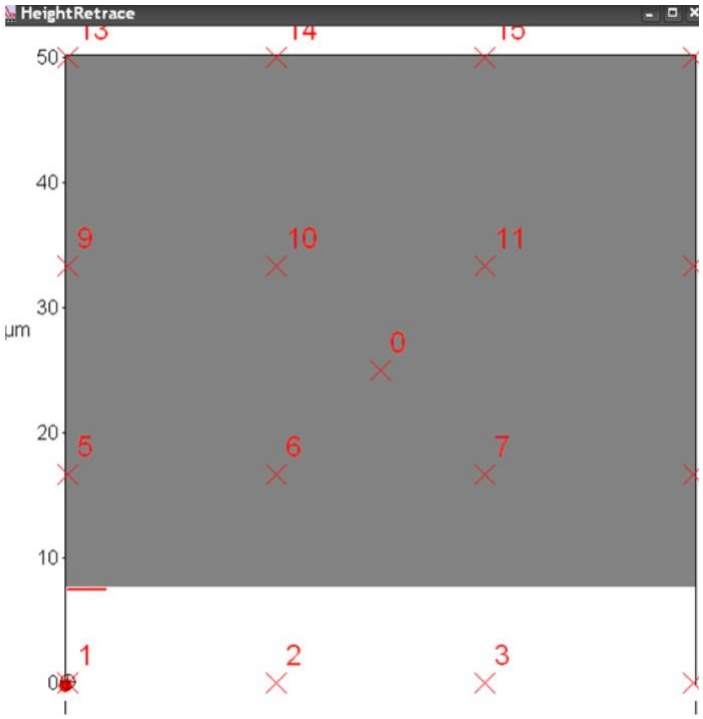

Figure 5.8: an example of the 16 indent locations over a 50 by 50 μm area.

section 4.1.3. Furthermore the calculation of displacement was enhanced from the previously described method. For this experiment, the h_{max} parameter was calculated from the loading curve: the point of sudden increase in force to maximum displacement (Figure 5.11). Extracting h_{max} from the loading curve instead of the unloading curve, improved accuracy of the analysis of raw data.

In addition to the S and E, the hold section of trapezoidal indents was analysed to evaluate the relaxation of the tissue. A five parameter viscoelastic model (Equation 5.1) was fitted to the 30 s hold portion of the force vs time data. The force was zeroed at the final raw data point of the hold phase and then scaled accordingly. Figure 5.12 demonstrates the fit according to the data. The five parameter viscoelastic model determined the three parameters a, b, and c and two time constants τ_1 and τ_2. The parameters a and b and the time constants were extracted for comparison between the experimental factors. If the time

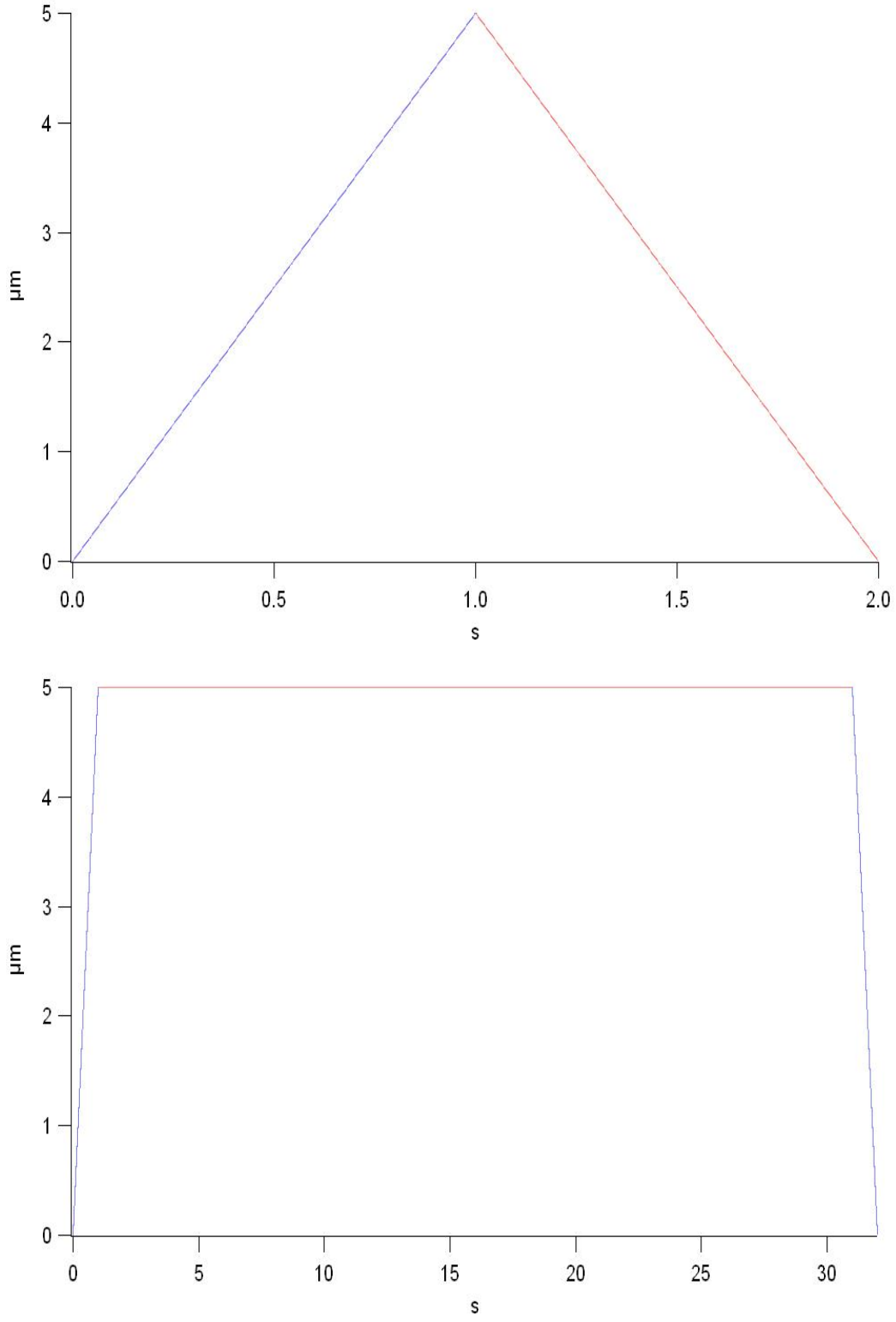

Figure 5.9: The triangular loading pattern and the trapezoidal loading pattern.

Explant	12
Cadaveric	6
Position	22
Tip Geometries	2
Loading Conditions	2
Positions per Sample	16
Total Indents = (12 + 6) x 22 x 2 x 2 x 16	
Total Indents =	**25344**

Figure 5.10: Total number of indents indented for this study.

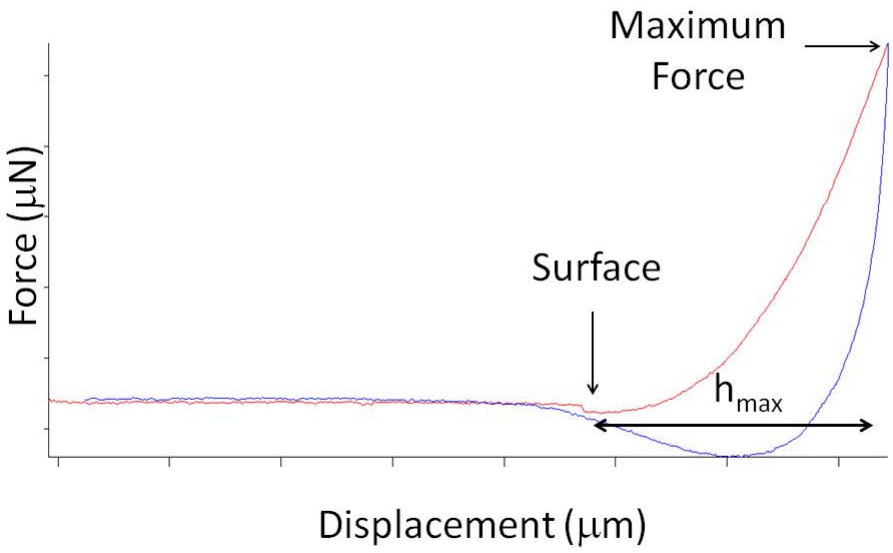

Figure 5.11: Schematic illustration of the extraction of h_{max} from the loading curve for data analysis.

constant τ_1 was greater than τ_2 this suggested that the slow mechanics of AC had greater influence on the stress-relaxation of AC whereas if the time constant τ_2 was greater this suggested that the fast mechanics of AC had greater influence on the stress-relaxation of AC. For a relatively small number of indents the five parameter viscoelastic model did not fit the curve so these indents were excluded from the analysis.

$$P = a \times \exp^{(-\frac{t}{\tau_1})} + b \times \exp^{(-\frac{t}{\tau_2})} + c \tag{5.1}$$

Samples were qualitatively grouped into 3 classifications according to biomechanical performance: samples with missing AC were denoted by "3", whilst mechanically viable AC was classified "1". Frequently, a surface response was elicited whereby the surface stayed attached to the tip during full retraction resulting in permanent deformation (Figure 5.13 and Figure 5.14). In this case a value of "2" was noted for the sample (video in electronic appendix). This information was then displayed on a basic sample location model of a femoral head, with red indicating bone and light blue indicating mechanically viable AC.

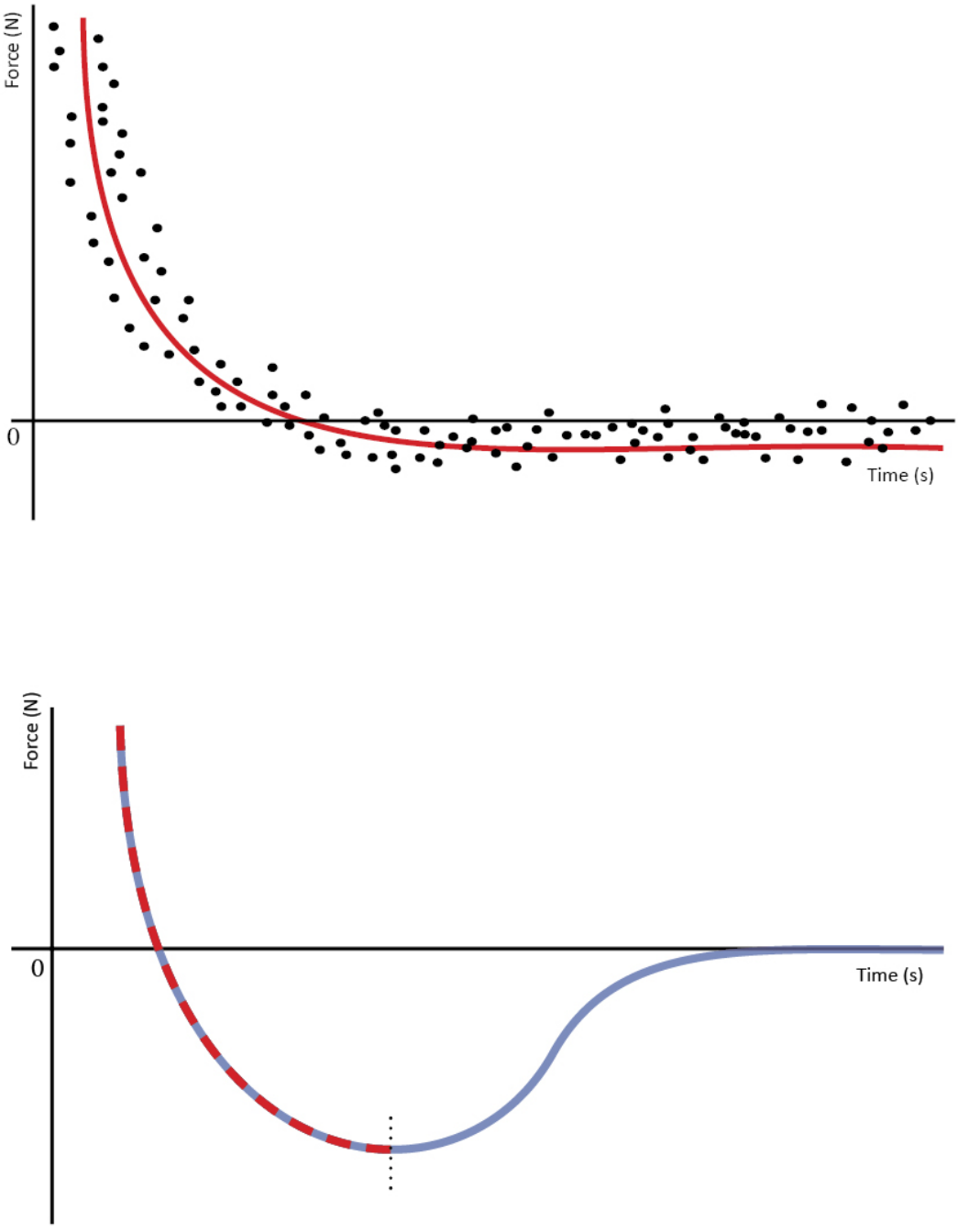

Figure 5.12: Schematic examples of the how the five parameter viscoelastic model fitted the raw data, (a red colour represents the fitted line).

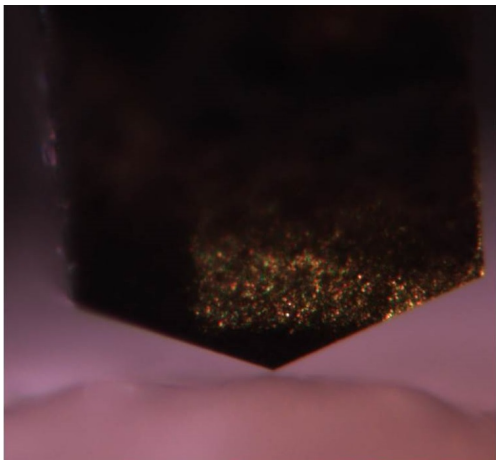

(a) Tip above the surface.

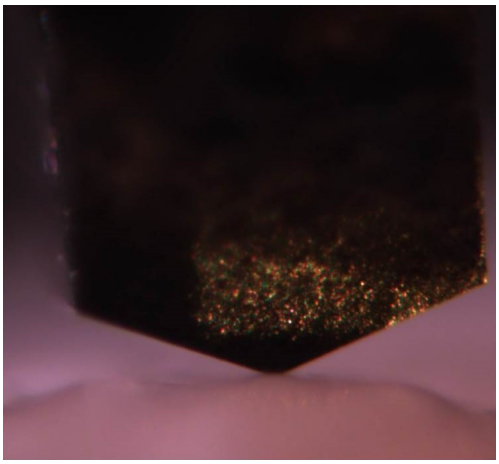

(b) Tip 5 μm into the surface.

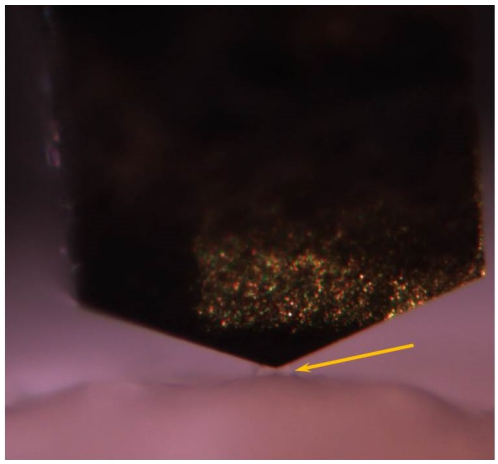

(c) Tip fully retracted but sample still attached.

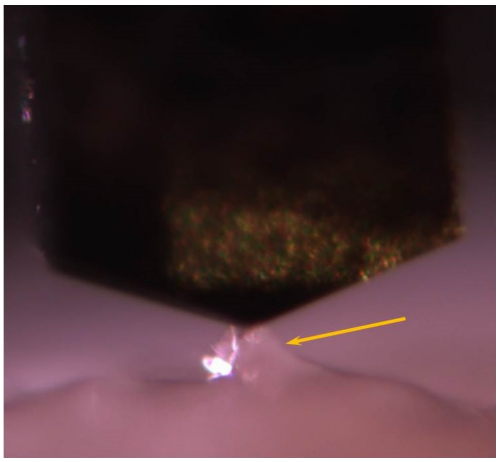

(d) Tip manually lifted away from the sample.

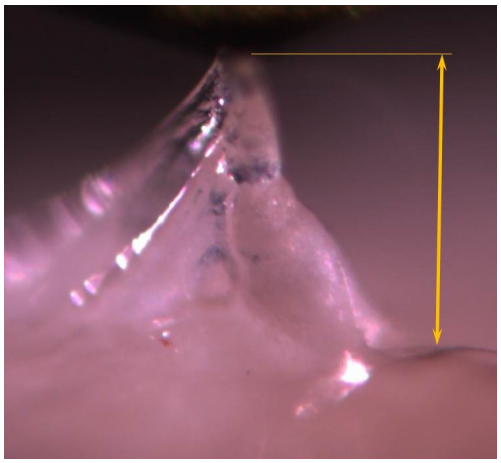

(e) Arrow indicates distance tip has been manually lifted from initial original surface location.

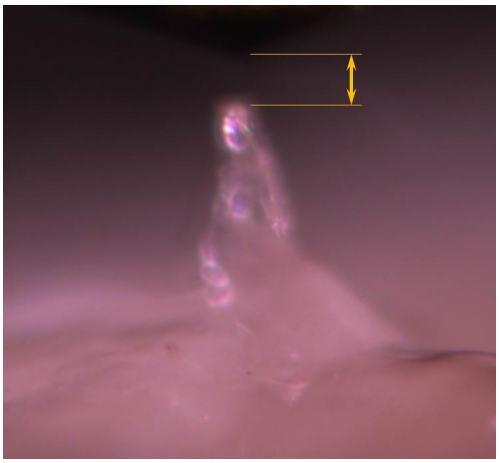

(f) Sample no longer attached to tip highlighted by arrow.

Figure 5.13: A typical example of a grade "2" mechanical classification of cartilage.

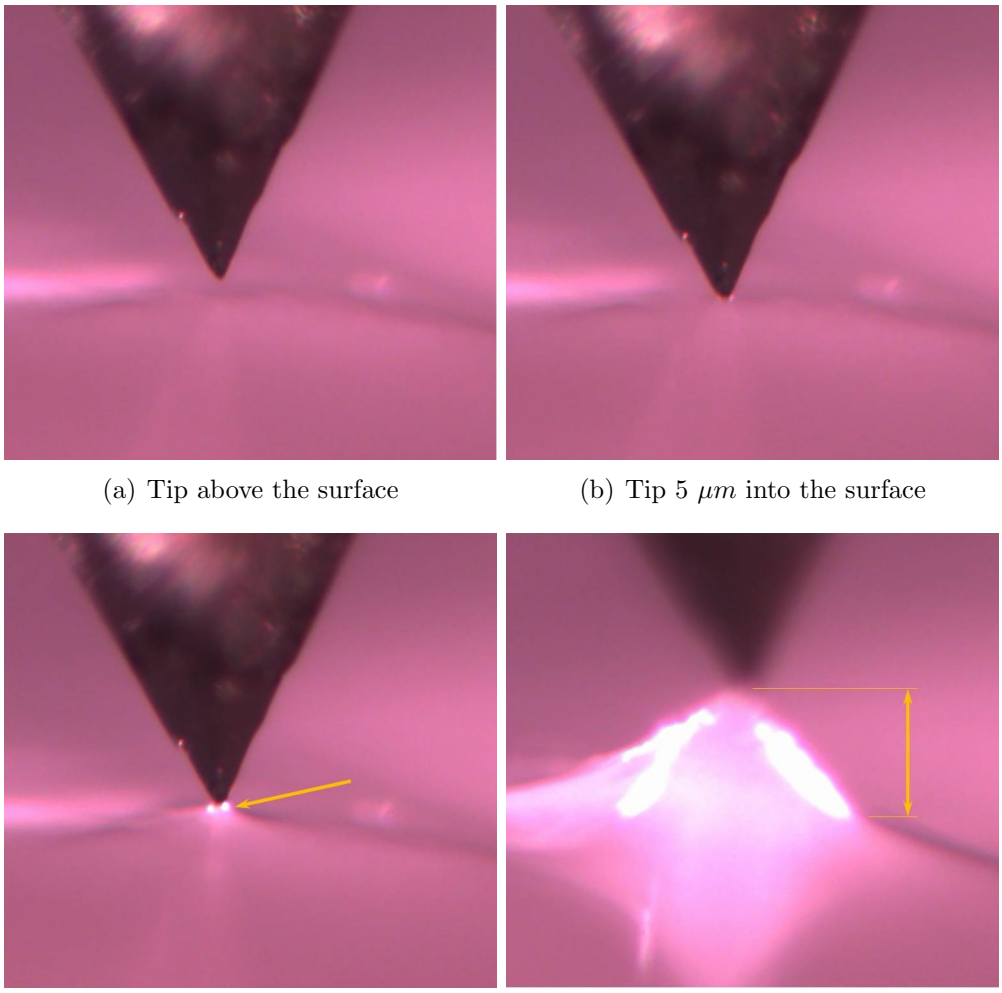

(a) Tip above the surface

(b) Tip 5 μm into the surface

(c) Tip fully retracted but sample still attached

(d) Arrow indicates distance tip has been manually lifted from initial original surface location.

(e) Sample no longer attached to tip, highlighted by arrow.

(f) Cartilage surface relaxing further with time but permanent deformation has occured.

Figure 5.14: A typical example of a grade "2" mechanical classification of cartilage.

5.2.7 Statistics

All statistics were performed using SPSS version 20.0. Univariate statistics were performed since the dependent variables are mathematically connected. Therefore due to this covariance, multivariate ANOVA was inappropriate, rather multiple univariate analysis were performed. Multiple univariate ANOVAs were used to test the effect of sample position, cartilage degeneration, loading parameters and tip geometry on S and E. Significance was set at $p \geq 0.05$. Multiple univariate ANOVAs were also performed to test the effect of sample position, cartilage origin and tip geometry on the parameters a and b and on the time constants. Data was presented as mean $\pm$ standard error.

5.2.8 Histology

Fifteen samples over a range of Outerbridge degeneration grades and mechanical classifications were histologically analysed in an attempt to further the understanding of the alteration in mechanical properties of osteoarthritic AC. The histological process is explained below.

To fix the samples, they were first removed from the gypsum plaster and placed in test tubes of 10% buffered formalin and refrigerated at 4 °C for 7 days. Every other day the solution was changed with fresh 10% buffered formalin. The specimens were then rinsed in PBS and placed in test tubes of 10% EDTA in 0.1M phosphate buffer (pH 7) to decalcify for 14 days at 4 °C. This solution was changed every day. After decalcification was complete, the specimens were rinsed in distilled water and stored in 70% ethanol for transporting to the Institute of Infection, Immunity and Inflammation at the University of Glasgow, as they had the required equipment and skill to section and stain the samples. The samples

were embedded in paraffin and thin sections were cut perpendicular to the cartilage surface. Serial $5\mu m$ sections were acquired and placed on glass slides to be stained. Two staining methods were used on different sections of the same specimens: Hematoxylin and Eosin (H & E) staining and Safarnin-O staining. All histological slices were imaged using a Zeiss AxioImager Z1 upright microscope (Carl Zeiss Ltd., UK) and to obtain the best possible image various magnification levels were used.

5.3 Results

Donor information regarding gender and age was available but it was not possible to subdivide the results according to these parameters due to sample size. It was assumed that the age range (45 - 83) of donors would make little difference to the mechanical properties (Benkhadra et al., 2008) so all eighteen femoral heads were analysed as a single group. Other factors that may have affected tissue properties, such as cause of death, diet and activity levels, were not available so could not be accounted for. Any variation due to these parameters would reside in the experimental error.

5.3.1 Mapping of the mechanical properties

Qualitative analysis allowed visualisation of and comparison of the different anatomical locations. Figure 5.15 displays the average qualitative analysis for the explant femoral heads and Figure 5.16 displays the average qualitative analysis for the cadaveric femoral heads. A light blue colour (representing a value of "1") symbolises the cartilage was mechanically viable, i.e. it was possible to obtain satisfactory force-displacement curves. A yellow/orange colour (representing a value of "2")

describes cartilage present at this location but not mechanically viable; the cartilage stayed attached to the indenter tip during full retraction and manual raising was required. A red colour (representing a value of "3") signifies that the cartilage had fully degenerated and only subchondral bone was present.

Figure 5.15 suggests, on average, the worst affected area of OA in the explanted femoral heads was in the superior-posterior region which was consistent for both tip geometries. Grading the severity of OA with the Outerbridge scale supports this finding (Figure 5.17(a)). Figure 5.16 demonstrates that on average the cadaveric femoral heads were much healthier, showing no signs of end-stage OA, than the explant femoral heads (cadaveric mean = 1.15 compared to explant mean = 1.9 $p < 0.05$). This is consistent with the Outerbridge grading of the tissue (Figure 5.17 and Figure 5.24) as this specifies no grade 4 for the cadaveric tissue (Figure 5.17(b)) and no grade 0 for the explant tissue (Figure 5.17(a)). Figure 5.16 also indicates that medial positions close to the fovea capitis femoris and the anterior area of the cadaveric femoral heads demonstrated a number of samples attached to the indenter tip and permanently deformed the surface, highlighted by the green colour in Figure 5.16 which is consistent with Figure 5.17(b) that indicates signs of degeneration at this location. A Spearman's rank correlation identified a significantly strong correlation between the mechanical grading scale and the Outerbridge grading scale as $\rho = 0.585$ for the Berkovich tip and $\rho = 0.571$ for the flat ended punch.

From the 22 locations of sample removal Figure 5.18 and Figure 5.19 display the mean contact stiffness for each of the 22 locations. Comparisons were made between each location for cadaveric and explanted femoral heads using both the Berkovich tip (Figure 5.18) and the flat punch (Figure 5.19). Univariate statistical analysis found a significant difference ($p < 0.05$) between the range of

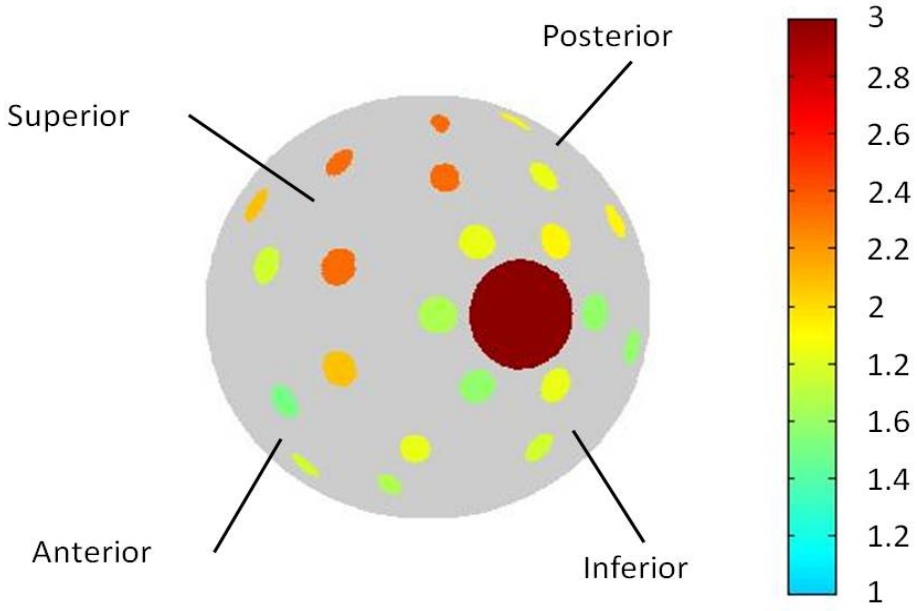

(a) Berkovich

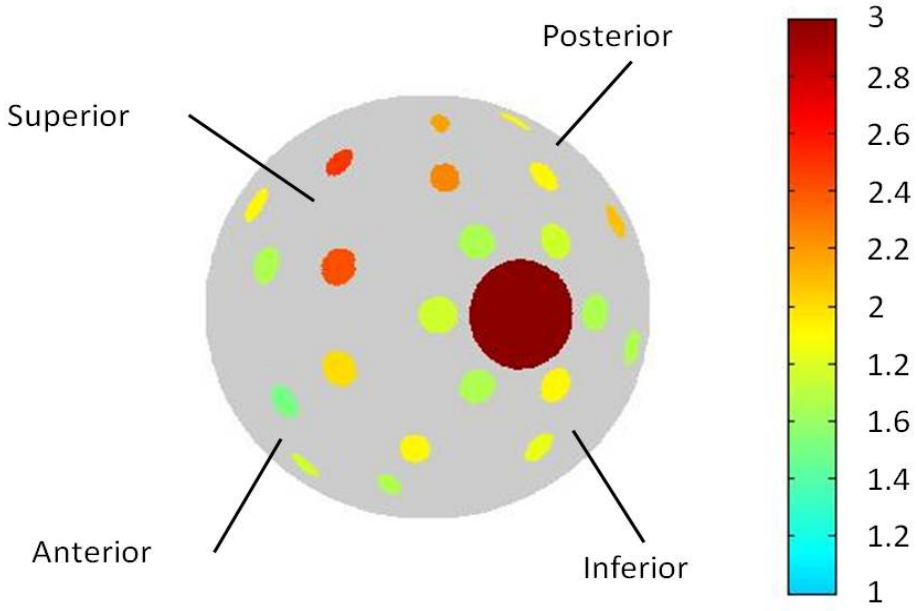

(b) Flat

Figure 5.15: The mean qualitative analysis results for the explant femoral heads.

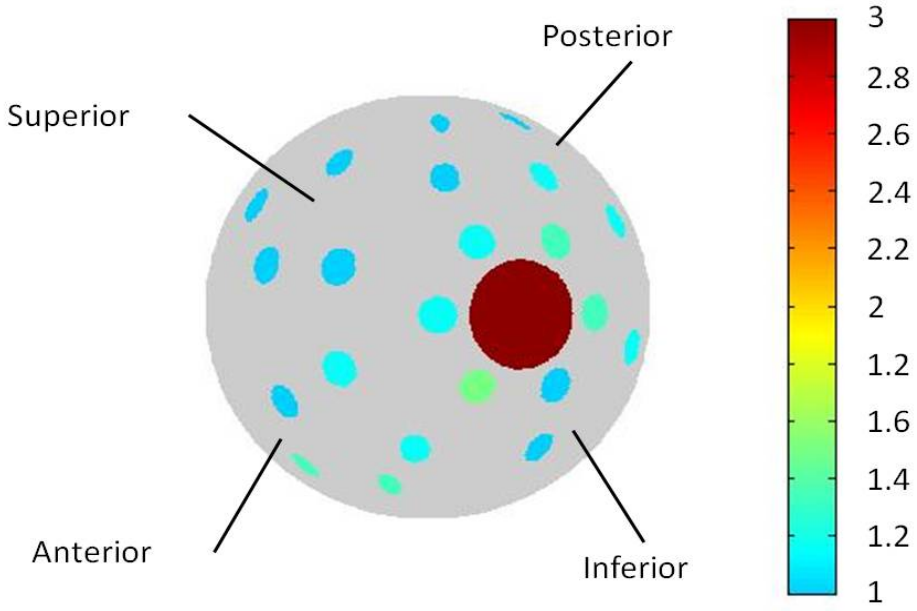

(a) Berkovich

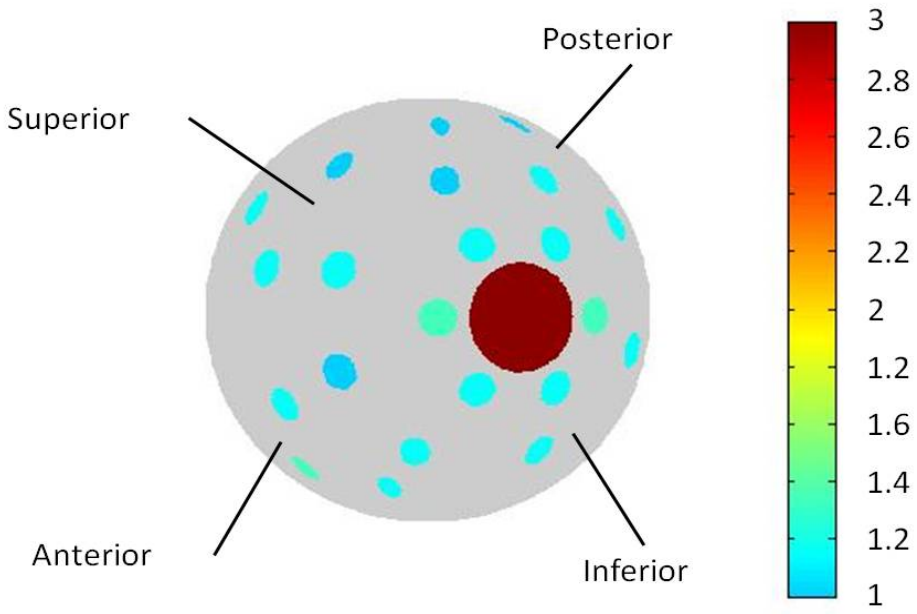

(b) Flat

Figure 5.16: The mean qualitative analysis results for the cadaveric femoral heads.

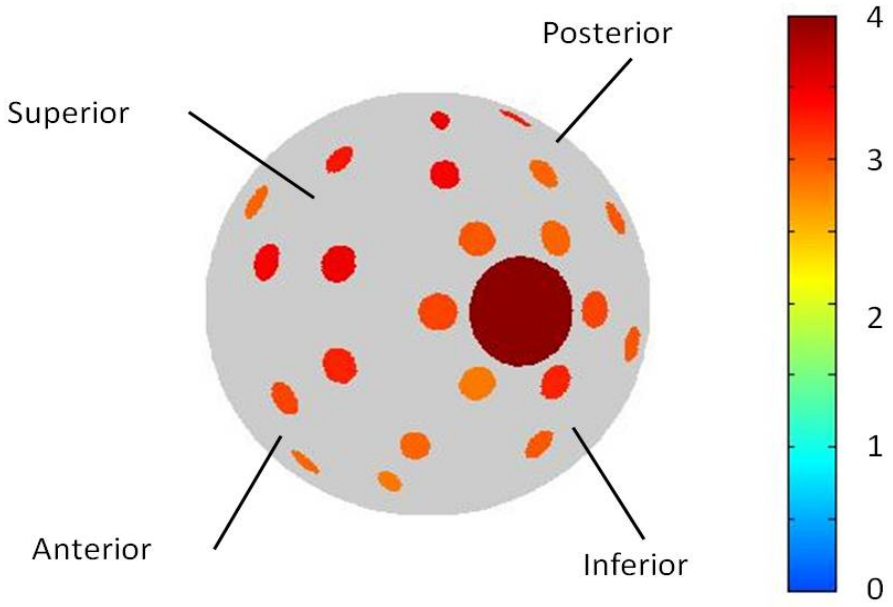

(a) Explant femoral heads

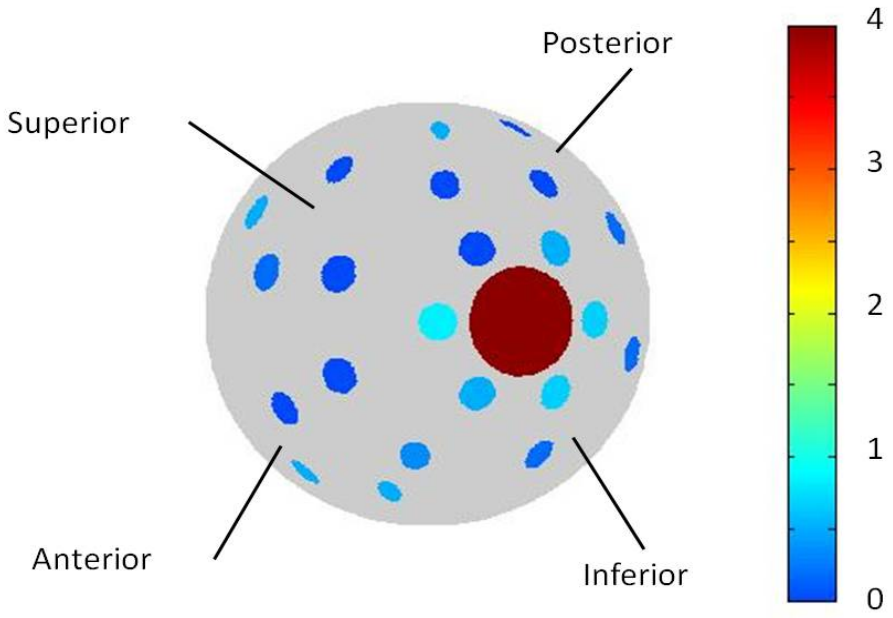

(b) Cadaveric femoral heads

Figure 5.17: The mean Outerbridge grade for each of the 22 positions on the explant and cadaveric femoral heads.

positions over the femoral head for both tip shapes. This difference between location and mechanical properties was repeated for reduced modulus and Young's modulus measurements, illustrated in Figure 5.20, Figure 5.21, Figure 5.22 and Figure 5.22, respectively. As the Er and the E were closely connected and showed the same trend, from this point on only E was reported.

It was found, when the flat punch was utilised, the cadaveric data reliably demonstrated the medial location around the fovea capitis femorus to be less stiff. This trend was not clearly displayed in the explant results or when using the Berkovich tip. The average more flexible sample for cadaveric data was located medially for both tip shapes (51.1 N/m, Berkovich, position a. and 16 N/m, flat, position e.). Similarly the smallest E was recorded in the same medial region with a value of 1.8 MPa for the Berkovich tip and 0.6 MPa for the flat punch. However, the more flexible average stiffness for degenerated explant femoral heads was found at position o for the Berkovich tip (37.8 N/m) and position t for the flat ended punch (9.4 N/m flat) and located not in a medial region but a superior and posterior region respectively.

The results for the stiffest locations for cadaveric and explant femoral heads were located in a superior area when implementing the Berkovich tip (cadaveric 324.6 N/m at location k, explants 246.7 N/m at location l). As expected, the largest average E (cadaveric 11.4 MPa, explant 8.6 MPa) was also situated in the same superior positions. Likewise the flat punch results confirmed the stiffest position to be superior at position l. for the explant tissue ($S = 124.3$ N/m E= 7.4 MPa), and for the cadaveric tissue ($S = 106.3$ N/m E= 3.6 MPa).

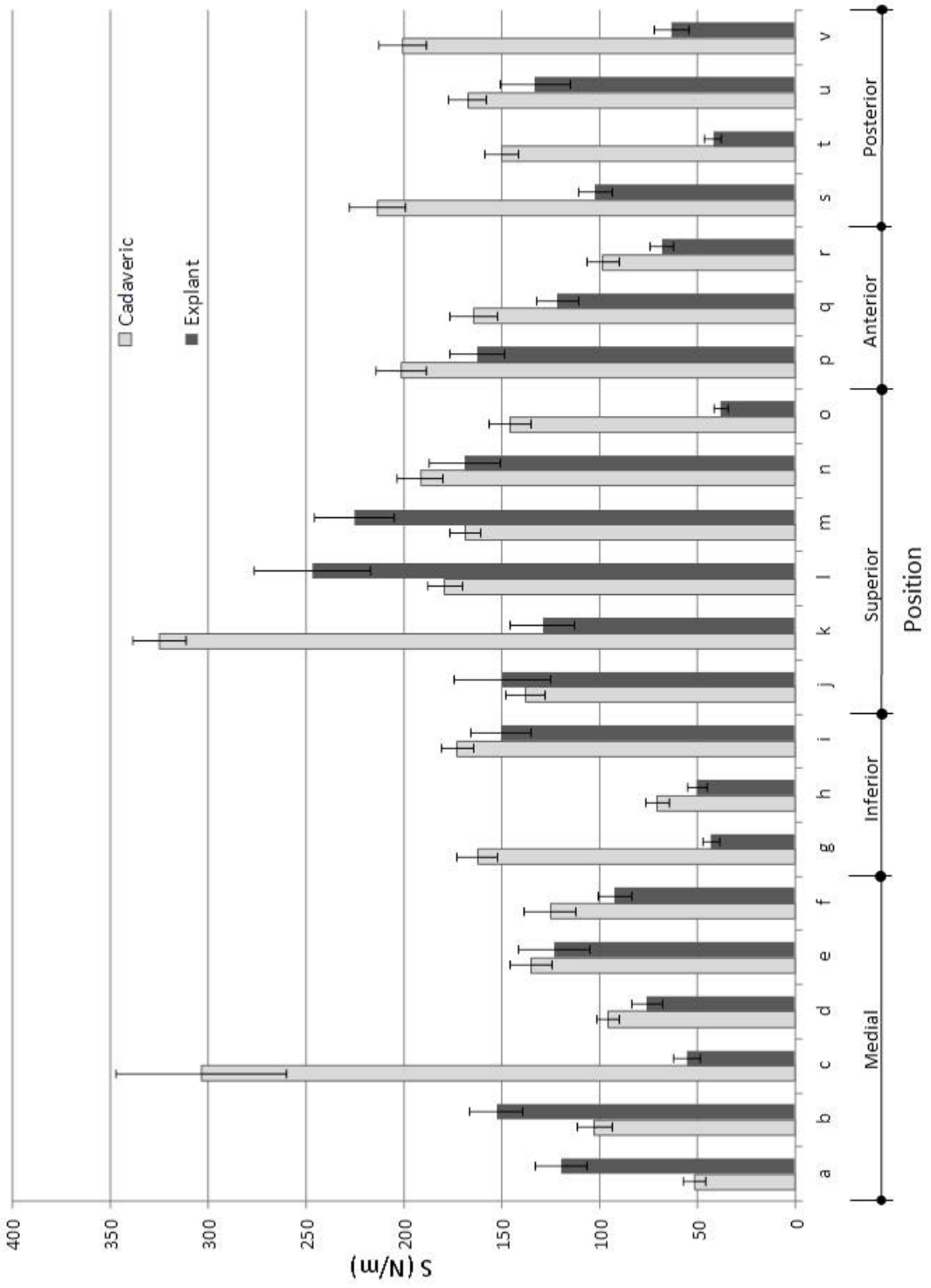

Figure 5.18: Plot of S over all 22 positions on the femoral head using the Berkovich tip.

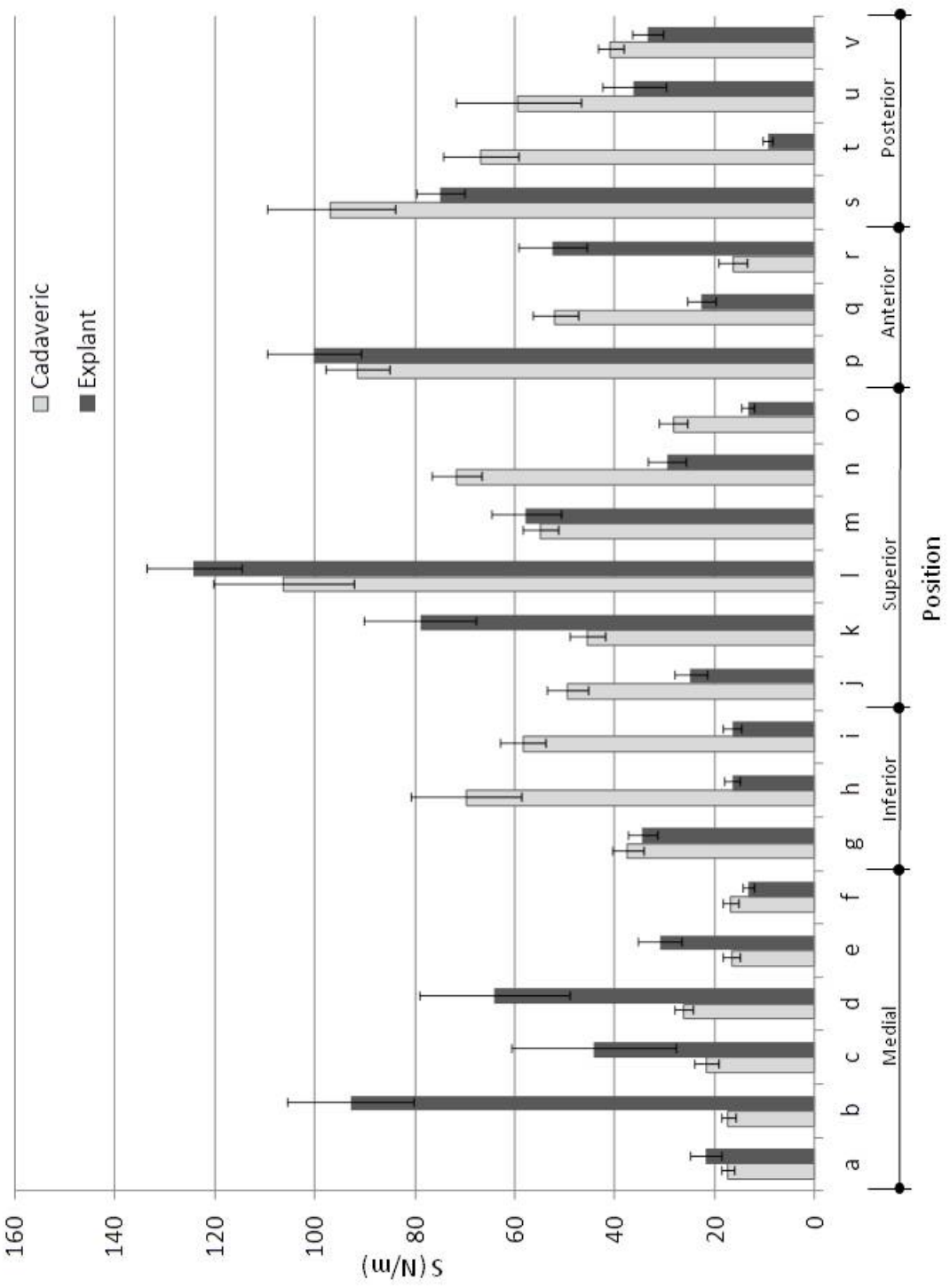

Figure 5.19: Plot of S over all 22 positions on the femoral head using the flat ended tip.

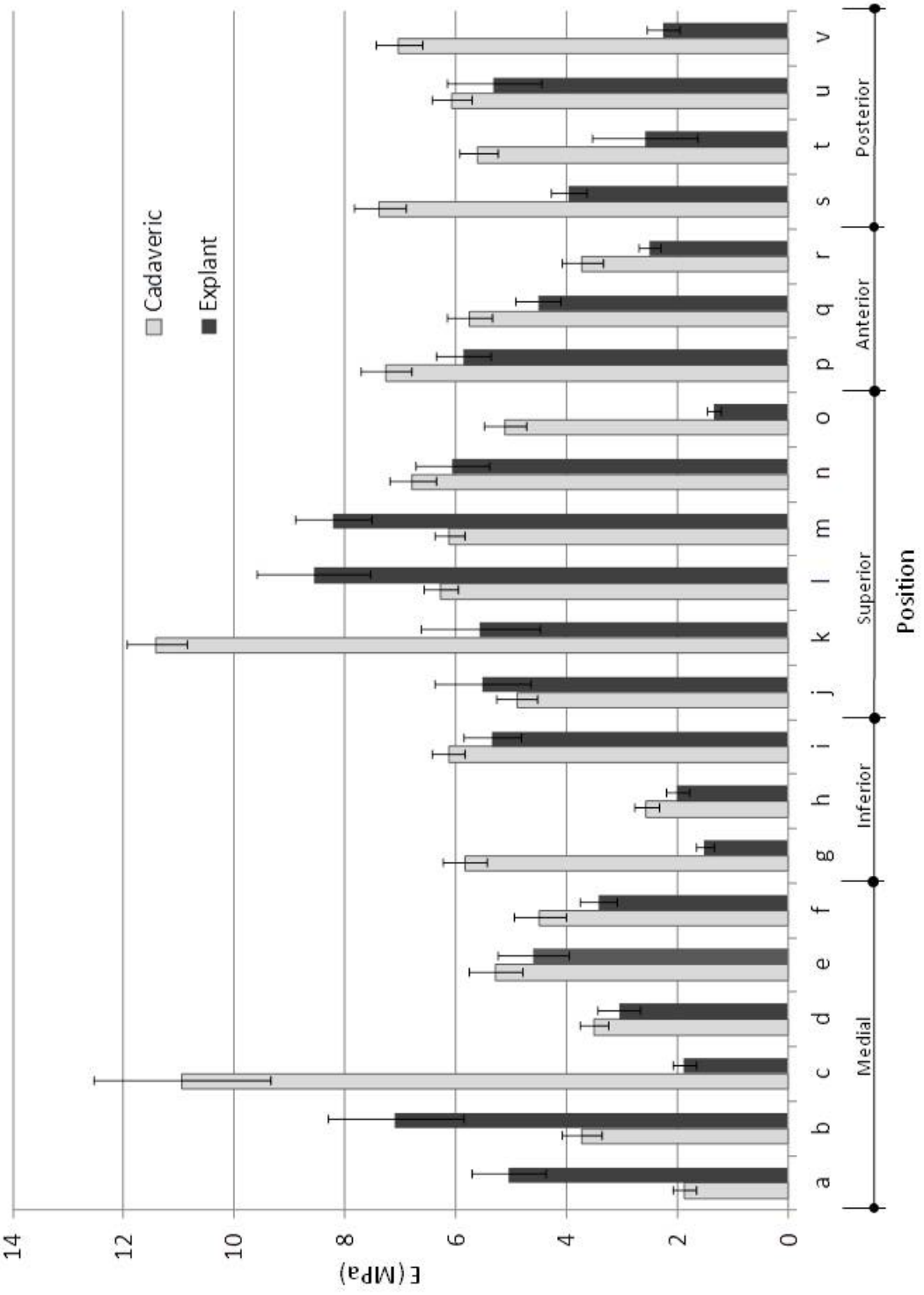

Figure 5.20: Plot of *Er* over all 22 positions on the femoral head using the Berkovich tip.

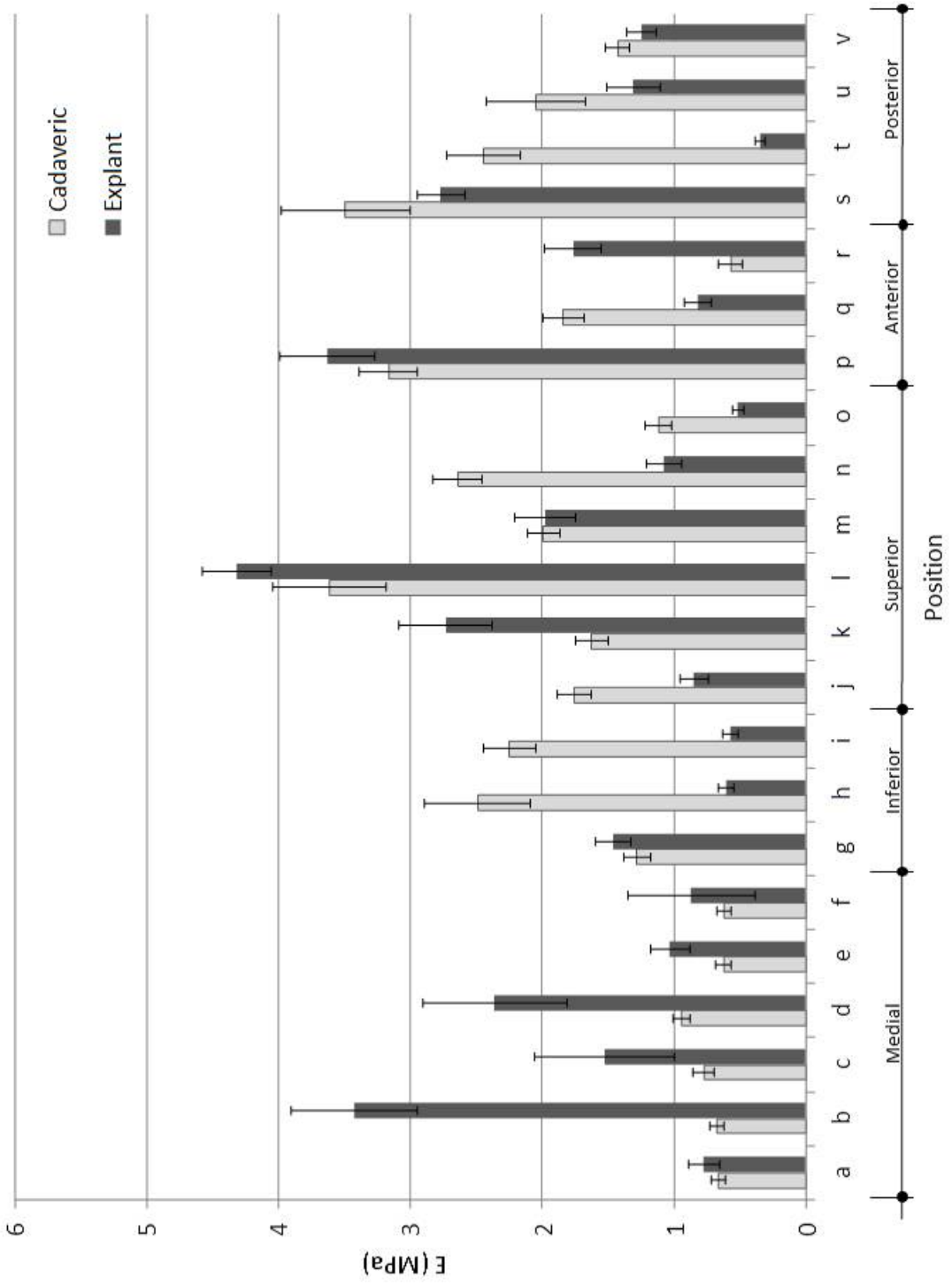

Figure 5.21: Plot of *Er* over all 22 positions on the femoral head using the flat ended tip.

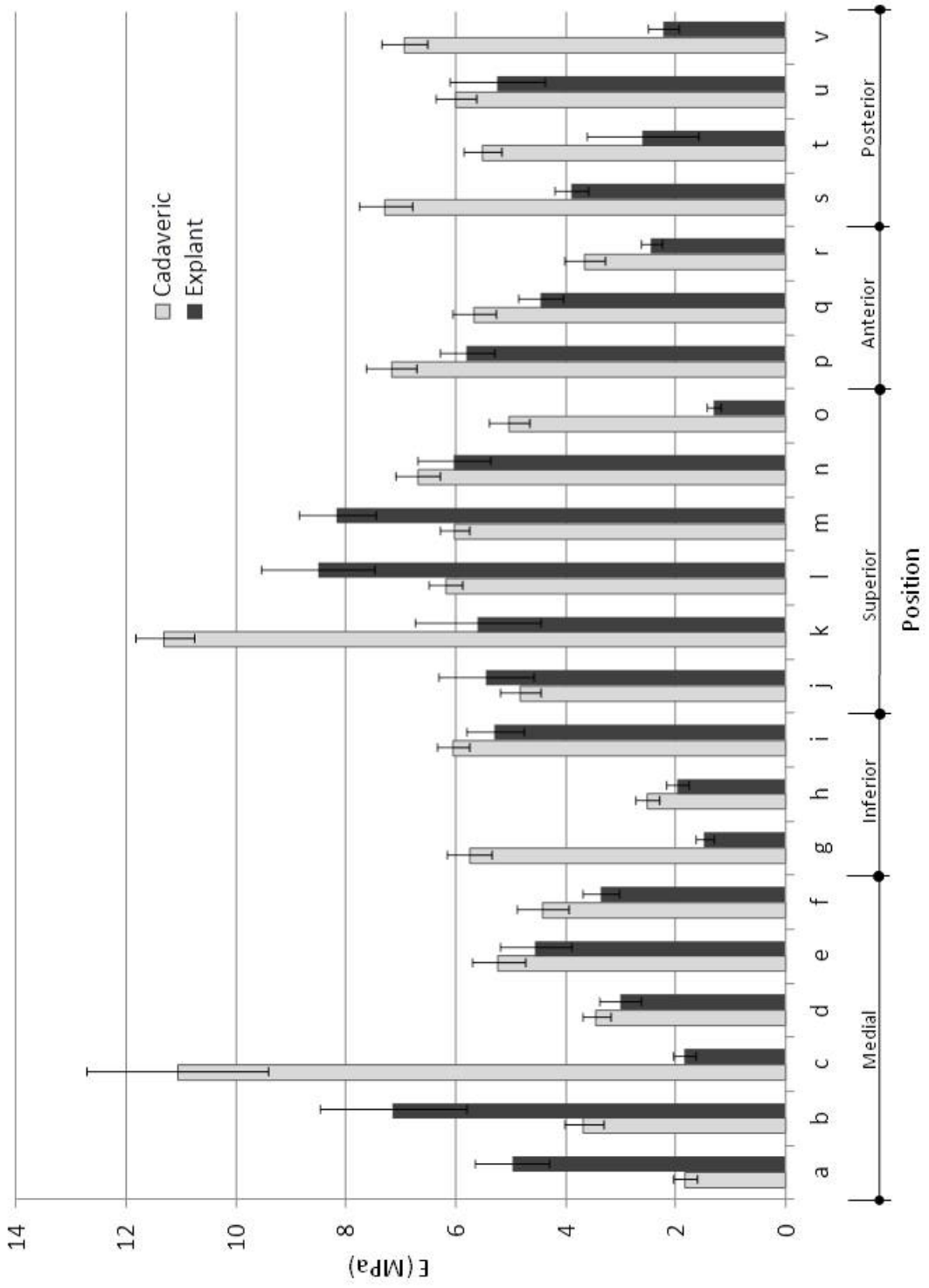

Figure 5.22: Plot of E over all 22 positions on the femoral head using the Berkovich tip.

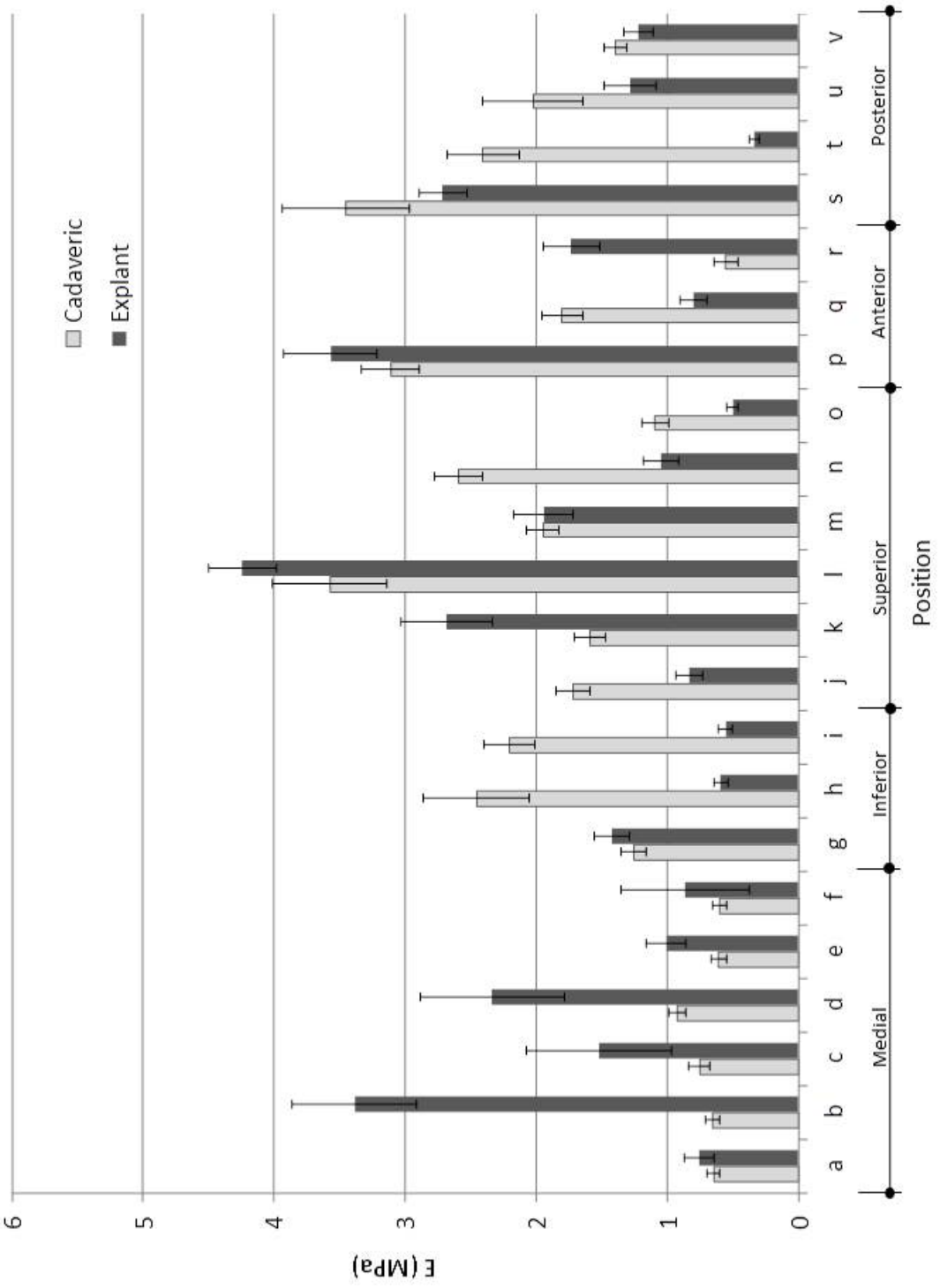

Figure 5.23: Plot of E over all 22 positions on the femoral head using the flat ended tip.

Comparisons were made between mechanical properties and Outerbridge grade on all samples (Figure 5.24, Figure 5.25). It was found that grade 4 degenerated cartilage was significantly stiffer ($p < 0.05$) than the other grades with an average S of 120.6 N/m and E of 4.79 MPa and a significant difference ($p < 0.05$) existed between the various Outerbridge grades, however no further trend was evident. In an attempt to understand the alteration in mechanical proprieties, as cartilage degenerates with osteoarthritis, the data was split into cadaveric tissue and explant tissue. The significant difference ($p < 0.05$) in mechanical properties between the Outerbridge grades continued post-split. The explant tissue gradually decreased from grade 1 to grade 3 before a considerable increase to grade 4 (Figure 5.24, Figure 5.25) but this was not seen in the cadaveric tissue results when indenting with the flat punch (Figure 5.24(b) and Figure 5.25(b)). The histological results confirmed that OA degeneration was evident in a range of samples. A typical image is demonstrated in Figure 5.26.

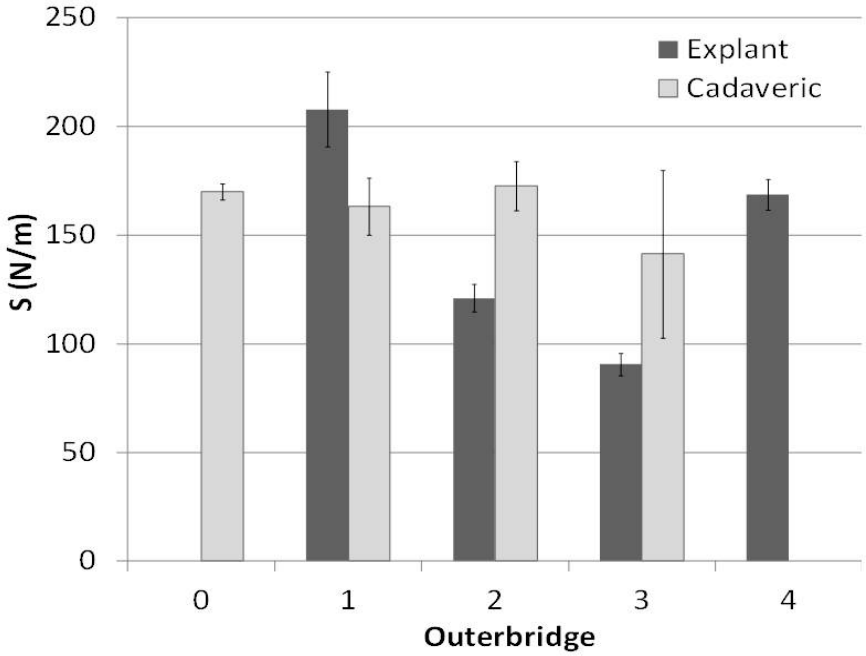

(a) Plot of S against Outerbridge grade for the Berkovich tip.

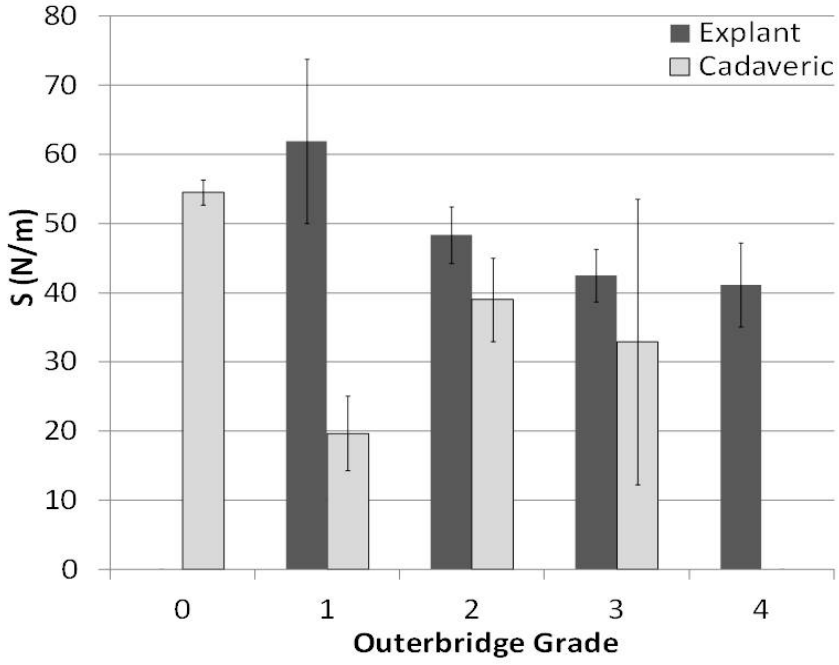

(b) Plot of S against Outerbridge grade for the flat tip.

Figure 5.24: Plots of the S comparing degeneration stage against the Outerbridge grading scale

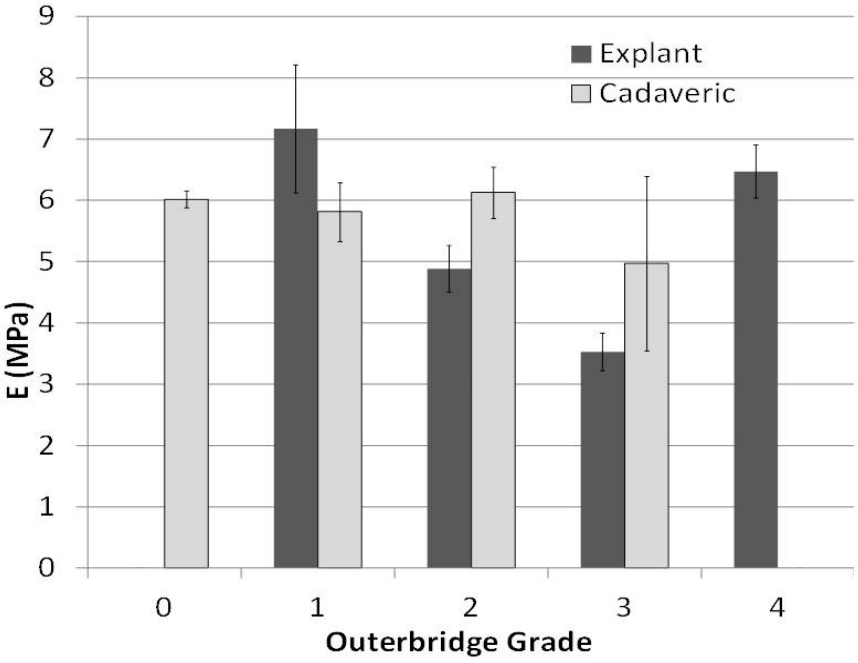

(a) Plot of E against Outerbridge grade for the Berkovich tip.

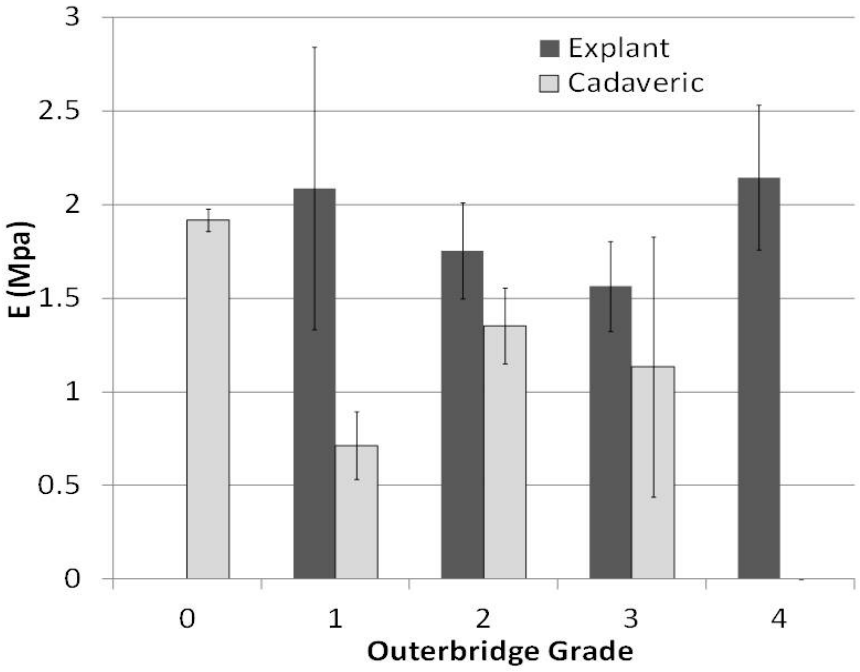

(b) Plot of E against Outerbridge grade for the flat tip.

Figure 5.25: Plots of the E comparing degeneration stage using the Outerbridge grading scale

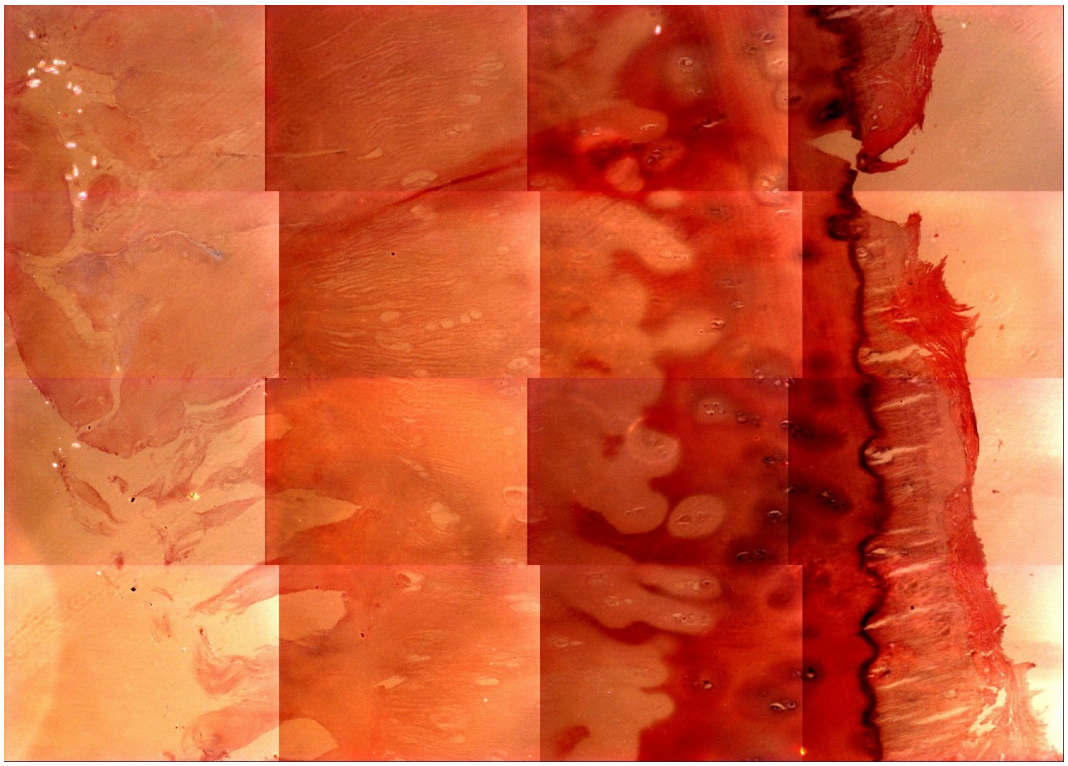

Figure 5.26: An example of a typical H and E stained histological section demonstrating osteoarthritis degeneration.

5.3.2 Experimental protocol comparisons

A comparison was made between triangular indentations with a mean S of 107.05 N/m and E of 4.1 MPa and trapezoidal indentations with a mean S of 87.5 N/m and E of 3.2 MPa. It was clear that the trapezoidal indentations with a 30 s hold were significantly ($p < 0.05$) less stiff than those without a hold period. A further comparison between the two loading conditions and sample origins identified; explant tissue showed no significant difference ($p = 0.5$) between loading conditions; the cadaveric tissue demonstrated that the triangular loading was significantly stiffer than the trapezoidal loading ($p = 0.003$). Figure 5.27 and Figure 5.28 display the stiffness results and the Young's modulus results for cadaveric tissue and explant tissue.

From the curve fit analysis of the hold period a significant difference was found for parameter a between explanted femoral heads (mean= 38.66×10^{-6}) and the cadaveric femoral heads (mean= 33.78×10^{-6}). A significant difference was also reported between the explant tissue (mean= 130.95×10^{-6}) and cadaveric tissue (mean= 84.12×10^{-6}) for parameter b. No significant difference was observed for τ_2 between the tissue origins however τ_1 was found to be significantly different for explanted femoral heads (mean= 2.39) and cadaveric femoral heads (mean= 2.02). Table 5.1 represents the data from the curve fit analysis of the hold period.

Table 5.1: Shows the mean of the parameters from the curve fit analysis of the hold period.

	Explant	Cadaveric	p
a (μN)	38.6 ±1.2	33.8 ±0.5	0.001
b (μN)	130.9 ±13.3	84.1 ±8.6	0.004
c (μN)	-78.6 ±12.5	-49.2 ±8.6	0.133
τ_1 s	2.39 ±0.1	2.01 ±0.02	0.003
τ_2 s	0.1 ±0.002	0.1 ±0.003	1

Figure 5.29(a) and Figure 5.29(b) present graphs of calculated S and E comparing the effect of tip shape. It is evident that the Berkovich tip consistently measures significantly increased ($p < 0.003$) mechanical properties, when compared to those of a flat ended punch. The Berkovich tip indicated a higher overall mean S of 147.1 N/m, and the flat punch recorded a much lower overall mean S of 50.3 N/m. The overall mean E results also reflect this trend, 5.4 MPa and 1.8 MPa respectively. This trend is continued even when the data was split to compare cadaveric tissue with explant tissue.

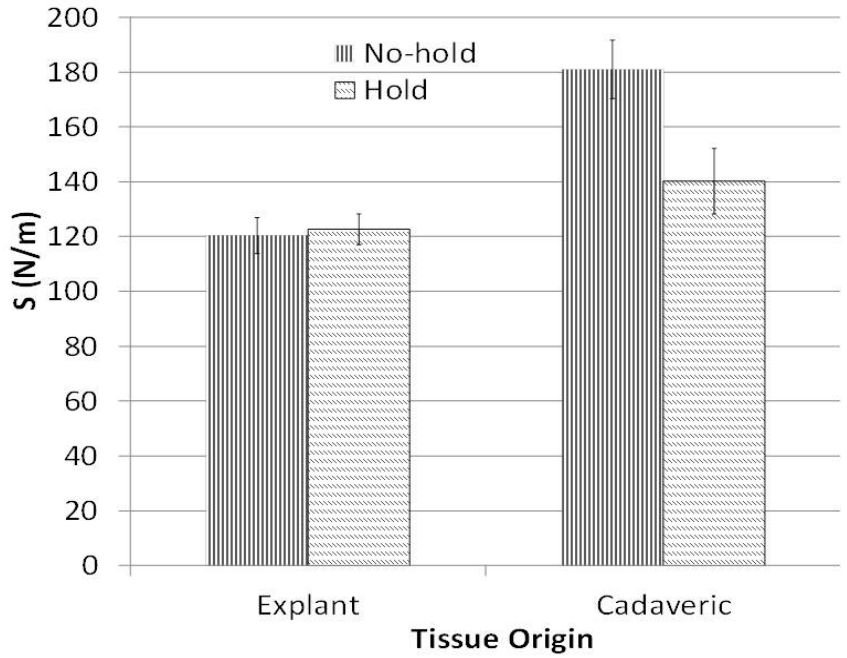

(a) Berkovich tip

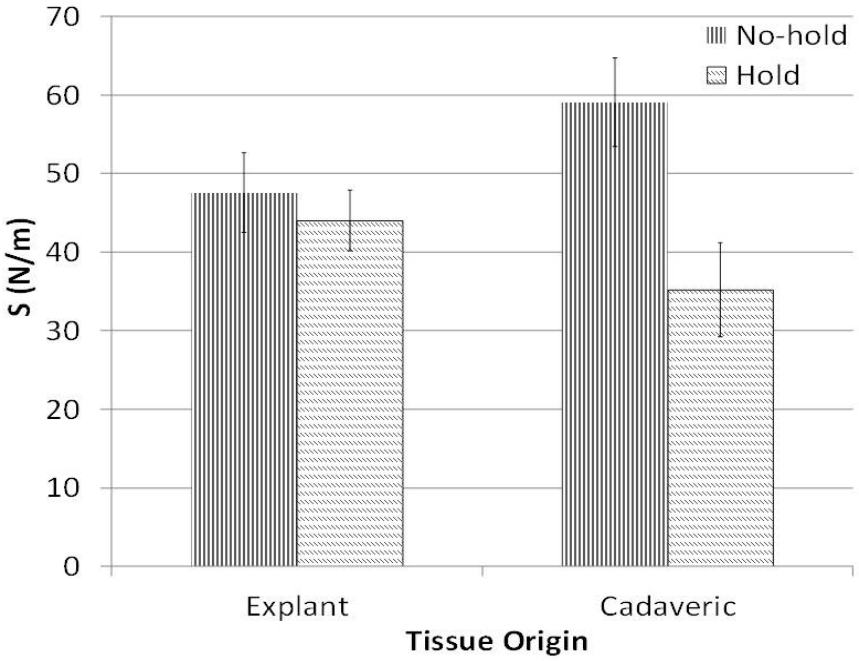

(b) Flat punch.

Figure 5.27: Plots of the S against loading pattern for the Berkovich tip and Flat punch

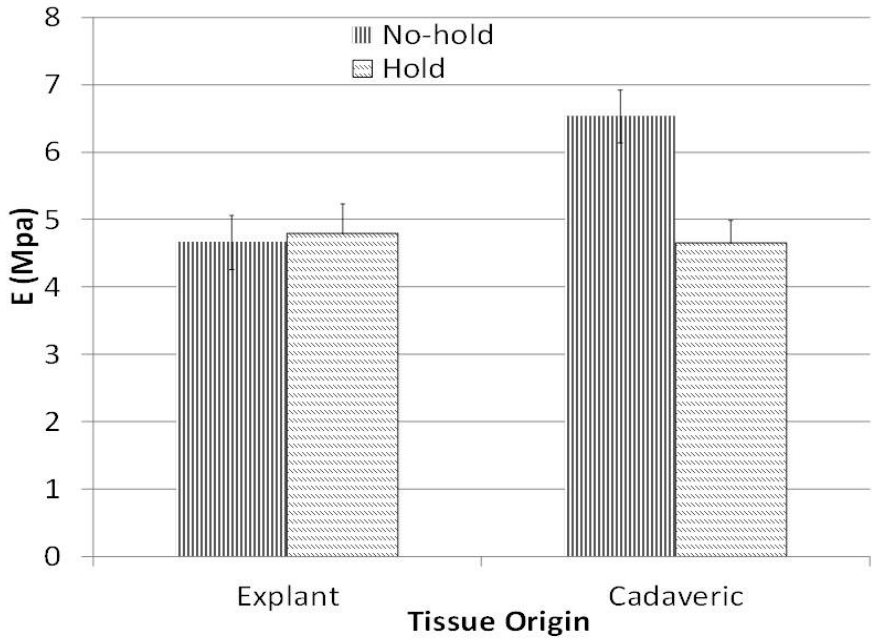

(a) Berkovich tip

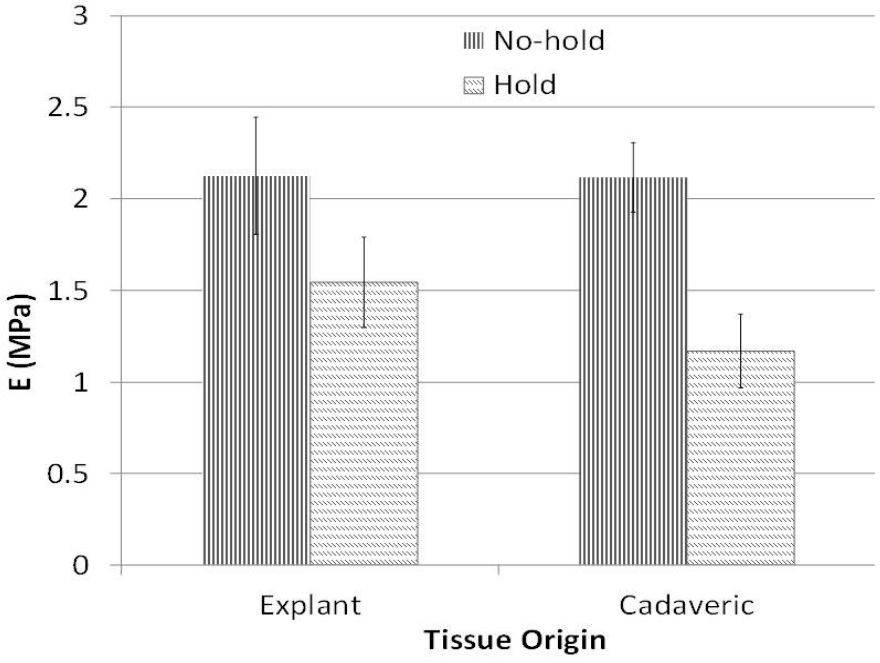

(b) Flat punch

Figure 5.28: Plots of the E against loading pattern for the Berkovich tip and Flat punch

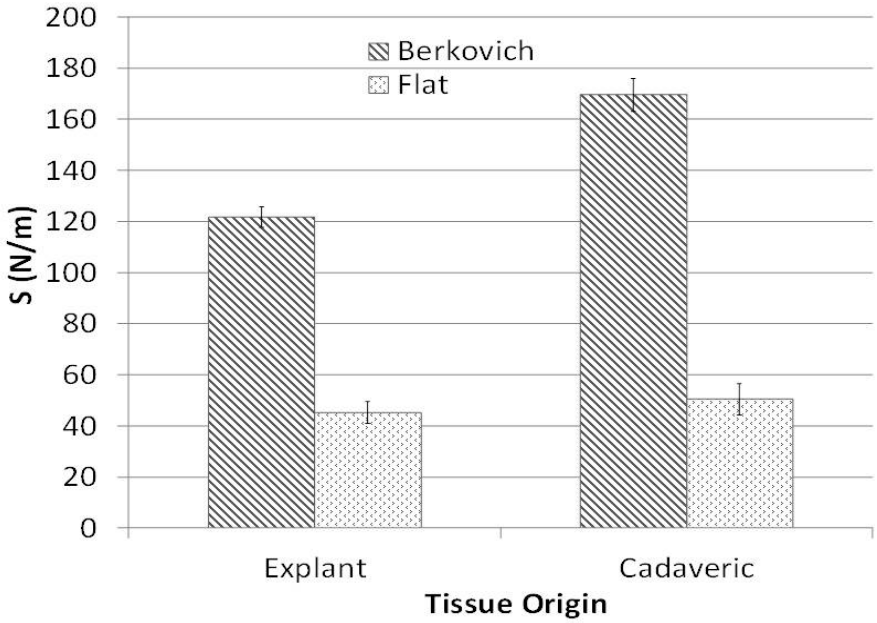

(a) Plots of the S comparing tip shape.

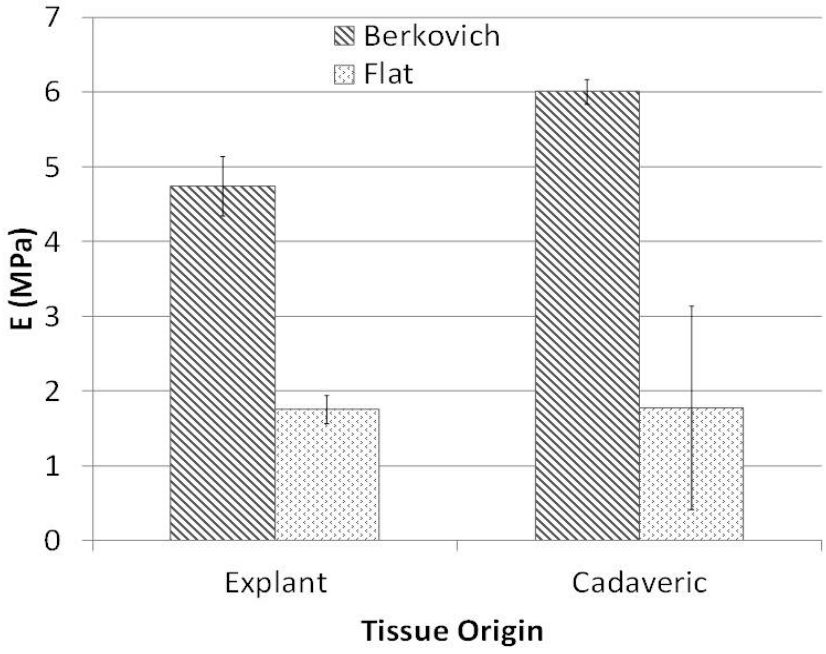

(b) Plots of the E comparing tip shape.

Figure 5.29: Plots of the S and E comparing the Berkovich tip and Flat punch

5.4 Discussion

Nanoindentation experiments on human, surgically explanted, femoral heads and age matched, cadaveric femoral heads were performed to investigate the relationship between mechanical properties and osteoarthritic degeneration. Nanoindentation has been reported to be a powerful tool for investigating the mechanical properties of articular cartilage (Franke et al., 2007; Korhonen et al., 2002a), agreeing with the work in Chapter 4 on animal tissue. Very few papers have investigated nanoindentation on human AC (Bae et al., 2006; Lyyra et al., 1999; Gupta et al., 2005).

It is difficult to compare the outcomes of this study to others due to the variety of experimental factors employed, however an average contact stiffness of 97.3 N/m ($\pm$ 2.04), and an average Young's Modulus of 3.6 MPa ($\pm$ 0.09) obtained in this study are comparable to the literature (Table 2.2).

One of the main findings of this study was that the medial positions surrounding the fovea capitis femoris for the healthy cadaveric tissue was significantly less stiff than the other anatomical areas. It was assumed, as a higher mechanical score was evident in the medial region of the cadaveric femoral heads, that this location showed the first sign of mechanical degeneration. High correlation between the mechanical grading scale (1-3) and the Outerbridge grading scale was discovered which implies that grade "2" on the mechanical scale represents OA degeneration. Further confirmation of this is seen as some cadaveric femoral heads only had healthy grade "1" cartilage, where some showed type "2" cartilage around the fovea capitis femoris and all explant femoral heads showed signs of type "2" cartilage, suggesting that OA degeneration is represented by type "2". The medial region was not the worst affected by OA in the surgically removed femoral heads;

the superior posterior region showed greatest degeneration. This suggests the hypotheses that:

1. osteoarthritis initiates around the fovea capitis femoris
2. once the superior-posterior area of a femoral head is infected it degenerates at a greater rate than other locations on the femoral head.

5.4.1 Mapping of the mechanical properties

The stiffest AC is found in a superior location for both cadaveric and explanted tissue (matching with the most severely degenerated area) corresponding to the predicted dominant loading direction by FE models (Harris et al., 2012). This could indicate that the increased mechanical properties in the superior and posterior locations are due to an adaption to contact load from normal walking and other daily activities. However literature has identified that numerical studies could not reliably calculate the true magnitude of contact stress at definite positions in the hip joint (Abraham et al., 2013) therefore, for confirmation, further research is required to identify precise loading during gait .

The results from the cadaveric tissue suggest the area around the fovea capitis femoris (medial location) is significantly less stiff implying this region has not adapted to higher contact stresses. The highly variable results found between anatomical positions are not uncommon, even numerical simulations, when based on subject-specific bone and cartilage geometries, identified a large variability in contact stress and subjects (Harris et al., 2012; Henak et al., 2011). Differences in bone cartilage geometry will strongly affect the variation in loading patterns and how the cartilage adapts to loads. The variation in loading pattern can explain the diversity of results over the femoral heads. However, despite the variation in results the cadaveric AC around the fovea capitis femoris is noticeably less stiff

in the flat punch results.This expected variation was why such high numbers of indents were performed.

The qualitative results in Figure 5.15 and Figure 5.16 give an enhanced visualisation and comparison of the different positions across the femoral head. This illustrates that, on average, the worst affected area of OA in the explanted hips is located in the superior-posterior area corresponding to Figure 5.17 (Outerbridge grading of cartilage). The regions of severe OA match well with those predicted from numerical simulation to have higher contact stress (Harris et al., 2012). The cadaveric tissue indicates the superior-posterior position to be stiffer, nevertheless this region in the explant tissue is affected to a greater degree by OA. The qualitative cadaveric data shows no indication of osteoarthritis in the superior-posterior region, conversely this is the worst affected area indicated for the explanted femoral heads which agrees with the Outerbridge grading of the tissue. This potentially suggests that once OA has initiated in the superior-posterior region, AC degenerates more aggressively than at other locations.

While the cadaveric femoral heads showed no indications of end stage OA, the qualitative results in Figure 5.16 imply the medial positions, close to the fovea capitis femoris or in the anterior area at the edge of the joint, did demonstrate symptoms of degenerate mechanical properties. This is evidenced by a number of samples attaching to the indenter tip; these samples are not mechanically viable for analysis hence implying that degeneration has begun.

Adhesive behaviour demonstrated in other studies is significantly different to that seen in this experiment. Adhesion between tip and surface on loading is an attraction force and was evident on the loading curve described in Crockett et al. (2005). The adhesion highlighted in the current experiments focussed on the unloading of

nanoindenter tip not the loading which differs from previous studies (Ebenstein and Wahl, 2006; Crockett et al., 2005). A reported pull-off adhesion upon unloading results in a slightly negative load which affects the mechanical properties' calculations and adhesion of this nature is predictable for a viscoelastic material such as cartilage (Wahl et al., 2006; Ebenstein and Wahl, 2006; Ebenstein et al., 2004). However the adherence described in this chapter was significantly different to the pull-off adhesion as the sample remained attached to the tip once fully unloaded. This was unexpected as it was not evident on macroscopic healthy cartilage (Outerbridge grade 0) implying adhesion to this extent is caused by OA degeneration. An increased contact area resulting from rapid stress relaxation may contribute to this phenomenon. Additionally a change in surface proteins may also result in increased adhesion. More work is required to elucidate the exact mechanisms behind this adhesion.

It is proposed that the medial area close to the fovea capitis femoris is the location OA originates. As this tissue was found to be less stiff, it may make this location more vulnerable and susceptible to OA. However, as predicted by numerical studies, this location may have less contact stresses so degeneration is potentially not as rapid as in the superior-posterior location due to less load. A reduction in the mechanical viability around the fovea capitus femoris may increase contact stresses superiorly, progressing OA in this region. Finite element modelling studies are required to confirm this hypothesis.

Previous studies on OA have concentrated predominantly on cartilage degradation by loss of extracellular matrix and deterioration of chondrocytes, however a soft tissue is regularly found on AC (Shibakawa et al., 2003). Over 90% of total knee anthroplasty explants have pannus-like tissue characterisations (Nakata and Bullough, 1986) showing prevalence on OA cartilage. The soft tissue found on

OA cartilage has been described as: granulation tissue, reparative fibrocartilage, reparative tissue and pannus. Immunohistochemistry studies established that OA pannus-like tissue is either devoid of collagen (Barley et al., 2010) or has similar levels of collagen type II fibres to underlying AC but the organisation and orientation are very different (Yuan et al., 2004). Well-integrated pannus-like tissue demonstrated a collagen fibre pattern expected to be found in early OA (Barley et al., 2010). According to one study on OA joints, pannus-like tissue is found at a central location and at the edges of joints (Yuan et al., 2004) which links with the qualitative data collected in this study. The anatomical positions for the cadaveric femoral heads that on average illustrated higher numbers of samples which remained attached to the indenter tips, were located centrally (medial locations around fovea capitis femoris) and at the margins of the hip (anterior locations): thus indicating a prevalence of pannus in these areas. These findings may suggest that the samples attached to the tip have a pannus-like tissue present on the cartilage. The tissue appears to attach more often to the Berkovich tip than the flat ended punch and this may be due to the more open angle creating a larger area for tissue adhesion.

Pannus-like tissue has been reported to have a large volume of proteoglycans (Barley et al., 2010) that attract a larger volume of interstitial fluid in comparison to healthy AC, potentially creating a very soft, sticky tissue. It is presumed that the altered collagen fibre orientation will not support and maintain tissue to the same extent as healthy AC due to its inability to constrain the proteoglycan swelling from fluid intake. This strengthens the arguement that a pannus-like tissue is responsible for articular specimens attaching to the nanoindenter probe. The histology results could clearly identify healthy and OA cartilage, but further clarification of detail such as identifying pannus-like tissue was unable to be confirmed due to insufficient staining and imaging methods.

The mechanically unviable samples (attached to the tip, qualitative grade "2") varied in response; some samples only adhered to the tip for a short distance after indentation while others adhered for a large distance severely deforming the surface. The diversity in quantity of integrated tissue is a potential reason for the variety of attachment response. The aggrecan distribution adjusts as the tissue becomes more interspersed into the AC cartilage. Incompletely-integrated pannus-like tissue displays a granular appearance compared to well-integrated tissue which demonstrates a more homogenous form (Barley et al., 2010). The gradual development of pannus-like tissue on cartilage can explain the variance in sample attachment to the tip during mechanical testing (demonstrated in the electronic appendix).

The majority of studies are based on animal tissue rather than human tissue. This study is the first time cartilage has been reported to attach to a nanoindenter tip, therefore was unexpected. Using this technique minimal studies have involved human tissue and as far as the author has identified no comparisons of OA femoral heads have occurred. Franke et al. (2007) and Ebenstein and Pruitt (2006) did investigate repair cartilage but from porcine and ovine sources. These studies reported that repair cartilage was mechanically inferior when compared to healthy cartilage. Repair cartilage was less stiff, had significantly lower resistance to penetration and less creep than the control cartilage (Ebenstein and Pruitt, 2006). No suggestion was made that these samples attached to the tip and histological analysis of the repair cartilage reported no evidence of a pannus-like tissue in these samples. The lack of compositional similarity between the repair cartilage (Ebenstein and Pruitt, 2006) and the pannus-like tissue (Yuan et al., 2004) potentially clarifies the lack of attachment found in these studies compared to our study.

Despite the prevalence of pannus-like tissue on OA joints, its composition and lack of stability seem to foster little scientific interest as substantiated by the limited number of journal articles in this area. The findings presented here suggest pannus-like tissue is a biological biomarker for early OA in human tissue that can be identified by increased adhesion to a nanoindenter tip. The field of osteoarthritis should investigate the appearance of pannus-like tissue on OA joints in more detail.

While Bae et al. (2006) investigated the sensitivity of indentation testing on human cadaveric knee joints, they did not report the indications of pannus-like tissue, however their results did indicate a general decrease in indentation stiffness progressing from healthy AC to mild osteoarthritic AC. The results from the surgically removed femoral heads concur with Bae et al. (2006) as a decrease in material properties are evident between Outerbridge grades 1 to 3. The cadaveric analysis also demonstrates that healthy cartilage at grade 0 has higher results for S and E than those at grade 3 degenerated cartilage, Figure 5.24. An AFM indentation study also identified a significant gradual decrease in mechanical properties between Outerbridge grades 0 to 3. Stolz et al. (2009) reported an average microstiffness in the order of 1 MPa which is smaller than our results however the flat punch (with a surface are of 0.69 μm) indentions were similar, in the order of 1 to 2 MPA. It should be highlighted that although Stolz et al. (2009) were able to identify average stiffnesses for grades 0-3 their technique was based on AFM cantilevers which are not able to produce quantitative results, only qualitative. For improved future comparisons of material properties, our indention method is superior.

There are indications from our results that as cartilage degenerates the mechanical properties decrease, however with grade 4 degenerated cartilage a significant increase is evident. Neither the study by Stolz et al. (2009) nor the study by Bae et al. (2006) investigated severe OA. It is expected that this increase in S and E are due to the effects of the subchondral bone. With such severe degeneration, the cartilage thickness is radically reduced and the hardness of the subchondral bone affects the nanoindention results by increasing both S and E.

Bae et al. (2006) and Stolz et al. (2009) demonstrated a decrease in mechanical properties of AC with increasing OA degeneration hence this trend was expected for the cadaveric and explant femoral heads. The cadaveric femoral heads did not show the predicted clear trend of gradual decrease in mechanical properties with degeneration of OA. When all samples, cadaveric or explanted, were compared, the decreasing trend of the mechanical properties with OA degeneration, suggested in previous studies (Bae et al., 2006; Stolz et al., 2009) and found in the explant results, was not visible (Figure 5.24 and Figure 5.25). While natural biological variation may contribute due to the large variation between the 396 samples taken from 18 donors, the researcher's ability to grade tissue may also be a contributing factor. Multiple experienced clinicians (Bae et al., 2006; Stolz et al., 2009) grading the tissue, may reduce this variance. Improving the quality of cartilage specimen grouping may improve the clarity of a decreasing trend when AC degeneration occurs. This opinion is reinforced as, on average, cartilage from cadaveric healthier tissue has an increased S and E when compared to the clinically diagnosed osteoarthritic explant tissue.

5.4.2 Experimental Protocol Comparisons

Due to the wide assortment of protocols and analysis techniques described in section 2.4.4 two loading patterns were investigated, a triangular loading pattern and a trapezoidal loading pattern with a 30 s dwell. It was hypothesised that an indent with a 30 s dwell would have lower S and E measurements than those indents without a hold period. Overall this hypothesis was correct and was clearly evidenced by the cadaveric tissue results, Figure 5.27 and Figure 5.28. This corresponded to the previous work on the bovine patella in Chapter 4 and the work by Han et al. (2011) who found the effective indentation modulus to decrease from 0.11 MPa to 0.06 MPa over a 600 s hold period illustrating cartilage has a time-dependent response. The force at the start of the dwell, on average, was greater than that force recorded at the end of the 30 s hold, confirming the hypothesis.

The osteoarthritic explanted hips did not show a significant difference between triangular and trapezoidal loading patterns which opposes the research hypothesis, the results from the healthier cadaveric hip and other studies (Han et al., 2011; Li et al., 2006). The degenerated collagen fibres in the OA tissue may no longer support the proteoglycans and interstitial fluid so the time-dependent effect would decrease. When analysing the hold segment, on average, for the explant tissue the initial force was significantly higher than the force recorded after 30 s; this contradicts the S and E results for the explant trapezoidal loading pattern. This knowledge, in addition to the visual inspection of the force-displacement curves during experimentation (Figure 5.30), demonstrate that in a multitude of trapezoidal loading indents of OA cartilage after a 30 s dwell, the tissue has relaxed to the extent that it was causing adhesion on the tip resulting in a "negative" force (as demonstrated in Figure 5.31). Upon unloading, force increased not decreased.

The tissue had relaxed to the extent that an unloading curve, when analysed for S and E, produced no value thus explaining the lack of contrast in mechanical properties between indents with a dwell, and without a dwell, for surgically explanted femoral heads. Further analysis of the dwell period supported this theory as the five parameter viscoelastic curves demonstrated an appropriate fit to the data, suggesting stress relaxation occurred during the dwell phase for both cadaveric and explant tissue.

The analysis of the dwell period demonstrated that the parameter a was smaller than that measured for parameter b, and τ_1 was greater than τ_2, for both tissue origins, indicating that slow mechanics are more active than fast mechanics in the stress relaxation of AC. It may be assumed that the fast mechanics are more affected by the collagen fibrils as their relaxation times has been shown to be an order of magnitude smaller than bulk tissue (Shen et al., 2011). The slow mechanics were assumed to represent the osmotic swelling pressure associated with the fluid flow through the solid matrix as previous studies (Ebenstein et al., 2004; Lu et al., 2004; Garcia and Cortas, 2007; Li et al., 2006) have demonstrated that this intrinsic viscoelastic response mainly contributes to the creep relaxation of AC. Li et al. (2005) agreed as they demonstrated stress relaxation in axial compression to be mainly influenced by the osmotic pressure and minimally influenced by the collagen fibres viscoelasticity. Significant differences were found in our results between explant tissue and cadaveric tissue for parameters a and b and the time constant τ_1 but not for the time constant τ_2 emphasising that the slow mechanics (fluid flow) have greater influence in the time-dependent relaxation of AC than the fast mechanics.

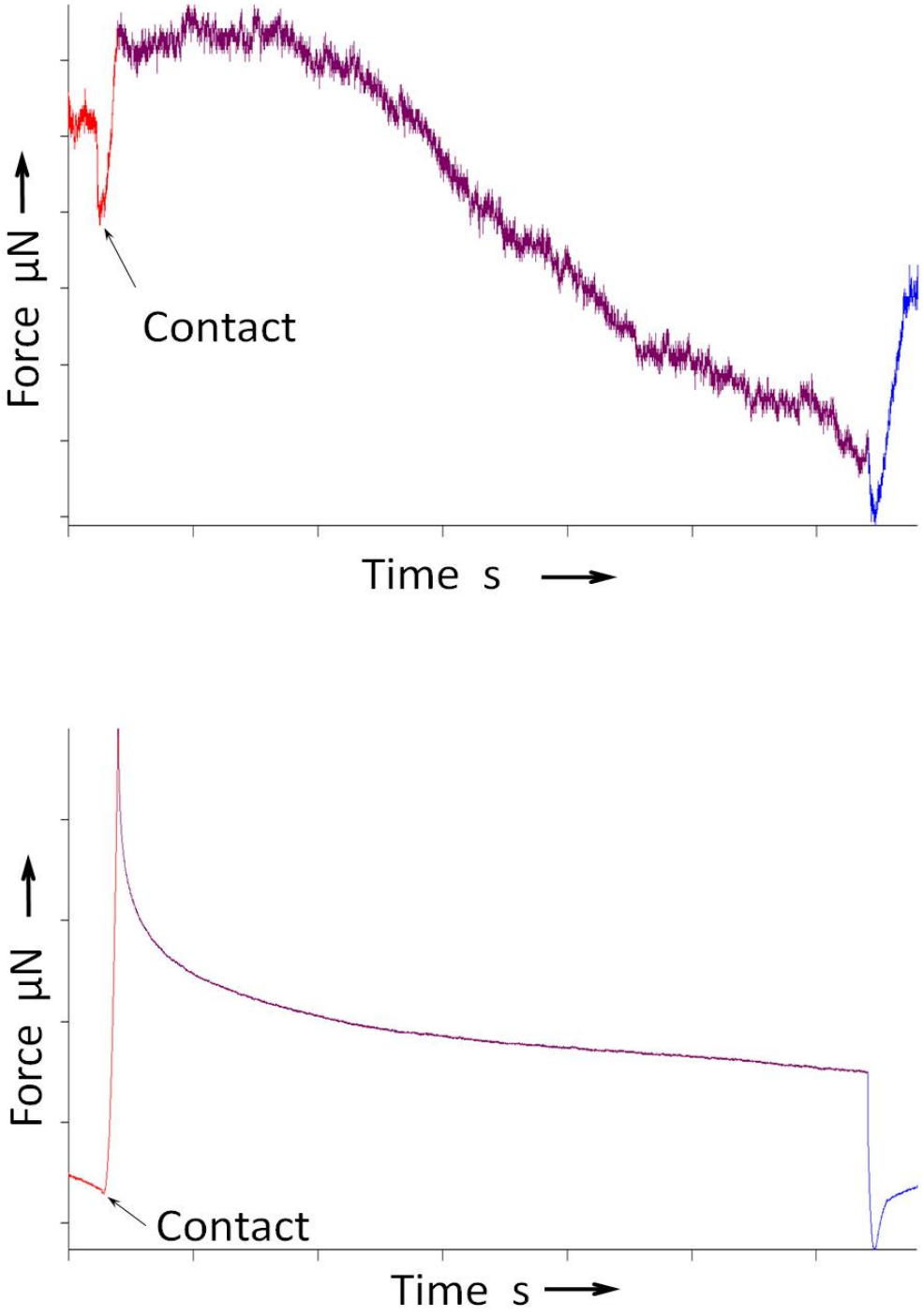

Figure 5.30: demonstrates the reduction of load over a 30 second hold (red indicates loading, purple dwell and blue unloading).

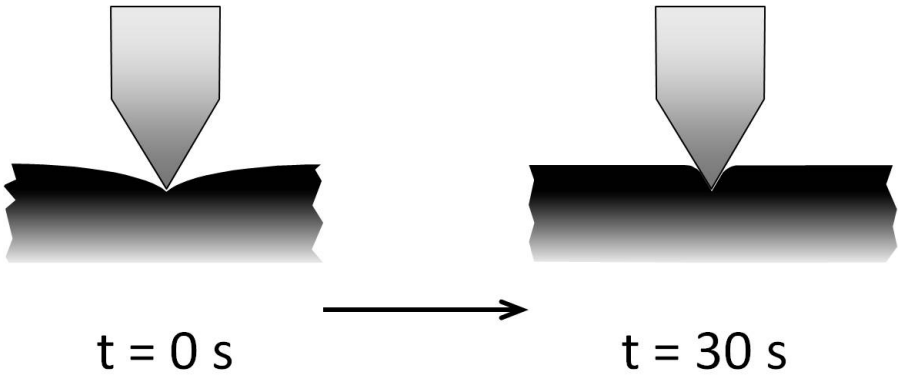

Figure 5.31: Diagram on the sample relaxing during the 30 s dwell.

Tip selection is of great import as it has been described that tip geometry can significantly affect the results of indentation experiments on a range of materials, especially cartilage (Simha et al., 2007; Bae et al., 2006). Our study agreed that there is a significant difference between Berkovich tip geometry and a flat ended punch when calculating contact stiffness and Young's modulus of AC. Both explant and cadaveric samples illustrated that the Berkovich tip measures significantly greater values for S and E than the flat ended punch. A significant difference between the a and b parameters and the time constant τ_1 was evident between the Berkovich tip and the flat punch when analysing the dwell period. The flat punch displayed lower values for a, b and τ_1. The unique flat punch consistently demonstrated smaller values for experimental parameters, potentially indicating that the smaller, constant tip geometry had greater sensitivity with the ability to record finer detail, than a traditional Berkovich tip. This was expected and was the reason the flat ended punch was chosen as it had the advantage of a smaller, known contact area which theoretically reduces the error when calculating E. It is possible that the flat punch acted more like a conical indenter, as the tip is only 0.69 μm square, but it was presumed this would not significantly change the results as a conical geometry acts like a punch geometry in the initial unloading of materials (Doerner and Nix, 1986). Pharr et al. (1992)

demonstrated that as a conical indenter tip is fully unloaded the contact radius remains reasonably constant until the sample no longer conforms to indenter geometry so the initial unloading for a conical indenter is therefore similar to that seen for the initial unloading of a punch with the same radius. The results indicated that the unique flat punch (whether it acts as a punch or a cone) produced smaller, potentially finer detail of the local mechanical properties of AC when compared with the Berkovich tip which produced higher results that presumably measured the bulk tissue. Despite the finer resolution of the tip, no bimodality of stiffness was evident, as shown by AFM tips (Loparic et al., 2010).

5.4.3 Limitations

The main limitation for this study was the incorrect assumptions for analysis of the mechanical properties of AC which are discussed in section 4.3.1. As a consequence of the inability to fully unload some of the tissue samples (sample attaching to the tip) the mechanical properties could not be measured from all samples. Qualitative analysis was performed and was considered satisfactory for comparisons of all samples.

The determination of the OA grade of cartilage was considered as a limitation. Whilst histological grading systems such as the OARSI exist, the resources available prohibited the inclusion of detailed histological grading; future work should include further histological assessment alongside mechanical testing.

5.5 Conclusion

The results from the nanoindentation mechanical testing of fresh frozen human femoral heads have shown the following.

The S and E decrease as OA degeneration increases which is consistent with the results of Stolz et al. (2009) and Bae et al. (2006). Outerbridge grade 4 degenerated cartilage is potentially too thin to only measure the mechanical response of the AC: the underlying bone influences the mechanical properties hence an increased S and E.

The position of the stiffest cartilage was found in a superior location corresponding to the location of greatest contact stress found in finite element and discrete element analysis studies (Harris et al., 2012; Abraham et al., 2013), suggesting AC has adapted to increased stress. The stiffer cartilage is presumed to absorb and resist the loads in the joint better. The position of the more flexible cartilage was found in a medial region around the fovea capitis femoris, again complementing the location of lowest contact stress found in numerical studies (Harris et al., 2012; Abraham et al., 2013). A lack in consistent trend between individual locations is not uncommon because of the natural biological variation in hip geometry and the variation in movement between individuals.

The nanoindentation of human AC showed that potential degenerated tissue can attach to the nanoindenter tip: this extreme adhesion was not evidenced in the previous chapter or other similar published data on animal AC (Franke et al., 2007; Ebenstein and Pruitt, 2006). This is a significant finding as many studies including Bae et al. (2006); Korhonen et al. (2002a); Franke et al. (2007); Ebenstein and Pruitt (2006) suggest that nanoindentation has great potential

to become a device to identify early OA. However, our results suggest indenting may damage a significant proportion of human AC potentially aggravating OA further, nevertheless the qualitative data from the AC mechanical response matched well with physiological Outerbridge grading of AC degeneration. This highlights the importance of testing on human tissue rather than on animal tissue.

The qualitative analysis demonstrated that OA degeneration is more severe at a superior posterior position however there is potential that OA originates at a medial location around the fovea capitis femoris. This is believed as the healthier cadaveric femoral heads illustrated the increased attachment of AC to the nanoindenter tips in the medial region which may be caused by a pannus-like tissue. The appearance of a pannus-like tissue, which attaches to a nanoindenter tip upon unloading, has the potential to be identified as a biomarker for initial OA degeneration of articular cartilage on femoral heads. Early identification may reduce the cost of OA to the NHS and improve the quality of life for individuals: if caught earlier the damage may be reversible or appropriate exercises may be employed to prevent further degeneration moving to the superior posterior location where it is apparent the greatest contact stresses are located.

Chapter 6

Comparison of Thiel

6.1 Introduction

New surgical techniques and implants for OA treatment are constantly being developed and tested. Laboratory evaluation by *in vitro* testing is essential before clinical trials of new procedures. The gold standard *in vitro* experiments use fresh frozen human samples as they provide good physiological and biomechanical conditions however, fresh human tissue is often difficult to procure as there is a limited supply and cost can be high. Postmortem storage is an important issue as human tissue can easily become contaminated and deteriorate rapidly. These issues commonly result in chemical fixation of human specimes for *in vitro* experiments.

In the past, the most common chemical fixation method of human tissue was formalin (Jaung et al., 2011). This technique quickly prevents bacteria and non-bacterial degeneration and preserves the histological structure of the tissue (Viidik and Lewin, 1966) but it has shown increased intra and inter fibular crosslinking, altering the mechanical properties of the tissue. One study on formalin fixed spinal specimens reported the tissue had lost its viscoelastic material behaviour

as it had become much stiffer (Wilke et al., 1998). Thiel fixation was developed in 1992 and is becoming increasingly popular for storage of biological tissue. This method has been reported to keep a more natural consistency to the tissue due to the realistic colouring and joint mobility maintained and furthermore improves safety with its virucidal and disinfectant capacity (Thiel, 1992; Wilke et al., 2011; Stefan et al., 2010; Fessel et al., 2011).

The effect of Thiel preservation on the mechanical properties of soft tissue has created conflict between studies. Histological analysis (Benkhadra et al., 2009) and biomechanical cadaveric testing (Holzle et al., 2012; Wolff et al., 2008) of Thiel embalmed tissues has shown to be similar to that of fresh frozen specimens, contrasting studies on bone (Stefan et al., 2010), tendons (Fessel et al., 2011) and spinal motion (Wilke et al., 2011) which found Thiel embalmed specimens demonstrated different tissue mechanics to those of fresh cadaveric specimens.

6.1.1 Aims and hypothesis

Thiel fixation is inexpensive and has been suggested to be well suited to anatomical investigation and surgical training workshops. Currently biomechanical experiments using Thiel-fixed tissues have not been investigated thoroughly and only Alberty et al. (2002) have qualitatively reported the effect of Thiel hyaline cartilage of the middle ear. The author found no reference to quantitative biomechanical studies on the effects of Thiel on AC, which would be required to prove that Thiel embalmed cartilage would be adequate for training in orthopeadic scenarios. Due to this lack of information, the aim of this study was to compare the mechanical nanoindentation properties of Thiel embalmed femoral heads to the mechanical properties of fresh frozen cadaveric tissue which has already been

measured in the previous chapter. It would be expected that the Thiel embalmed AC would demonstrate decreased S and E in comparison to fresh frozen AC, which has been demonstrated in other soft tissue studies, as Thiel fixation is presumed to denature the collagen fibres (Fessel et al., 2011; Stefan et al., 2010; Benkhadra et al., 2011). Thiel-fixed AC was expected to have a similar stress relaxation behaviour to fresh frozen tissue as it was presumed the chemicals would not influence the fluid flow.

6.2 Methods

For this study an additional 3 femoral heads were harvested from Thiel embalmed cadavers. The study collaborated with the Centre of Anatomy & Human Identification at the University of Dundee who supplied the prepared Thiel embalmed cadaver femoral heads.

Two solutions were prepared prior to perfusion, a stock solution containing boric acid, ethylene glycol ammonium nitrate and potassium dissolved in almost boiling water; and a chlorine cresol solution containing ethylene glycol and 4-chlorine-3-methyl phenol. For one whole cadaver 700g of sodium sulphite and 300ml of formalin were dissolved in 14,300 ml of stock solution and 500ml of chlorine cresol solution. This solution was then gradually infused into the femoral or carotid artery (Thiel, 1992). The cadavers were donated between January and August 2011 and placed into the above solution within 3 days of death.

The femoral heads were extracted from the cadaver using the typical surgical technique as described in section 5.2.3 and 22 osteochondral plugs were removed and prepared as explained in section 5.2.4 with one deviation to that sample

preparation method. The Thiel samples were not washed for multiple hours to remove the synovial fluid (section 3.18) as this would potentially rinse the preservation chemicals from the AC, instead the surface of the Thiel samples were gently dabbed to remove the synovial fluid and any excess chemicals and following this no visible signs of synovial fluid or excess chemicals were apparent when indenting.

The nanoindentation mechanical testing procedure was identical to the cadaver and explant femoral heads described previously in section 5.2.5. Briefly, two tip geometries (Berkovich and flat punch) made 16 indents in a central 50 x 50 μm area with a triangular and trapezoidal loading pattern. 4,224 indents were performed on the Thiel embalmed femoral heads (Table 6.1). The raw data was analysed in accordance to the Oliver-Pharr method detailed in section 4.1.3.

Table 6.1: Total number of new indents indented for this study.

Position	22
Tip Geometries	2
Loading Conditions	2
Positions per Sample	16
Total indents = 22 x 2 x 2 x 16	
Total indents =	**4224**

6.3 Results

The age range of the Thiel embalmed donors was between 68 and 85 years which corresponded to the range of the fresh frozen donors. The sample size was too small to split into groups of age and gender. Benkhadra et al. (2008) demonstrated the effect of these parameters to be minimal however it was believed that

activity, diet and cause of death may affect the mechanical properties but this information was not available.

Nanoindentation experiments found Thiel embalmed AC tissue showed significantly lower S and E than the cadaveric and explant fresh frozen tissue previously reported. The Thiel embalmed tissue mean S was $68 \pm 22\ N/m$ and a mean was E $2.7 \pm 1.3\ MPa$. This was significantly ($p < 0.05$) smaller than the overall mean of the fresh frozen cartilage with a mean S of $96 \pm 1.5\ N/m$ and E of 3.57 $\pm$ $0.07\ MPa$. However the Thiel embalmed tissue properties were of the same order of magnitude as the fresh frozen tissue.

The mean contact stiffness and Young's modulus for each of the 22 sample locations over the femoral head is displayed in Figure 6.1 and Figure 6.2. Again statistical analysis found a significant difference between mechanical properties ($p < 0.05$) and positions over the femoral head for both tip geometries however no clear trend between sample location and S or E was apparent, although the medial region demonstrated lower S and E for both tip geometries.

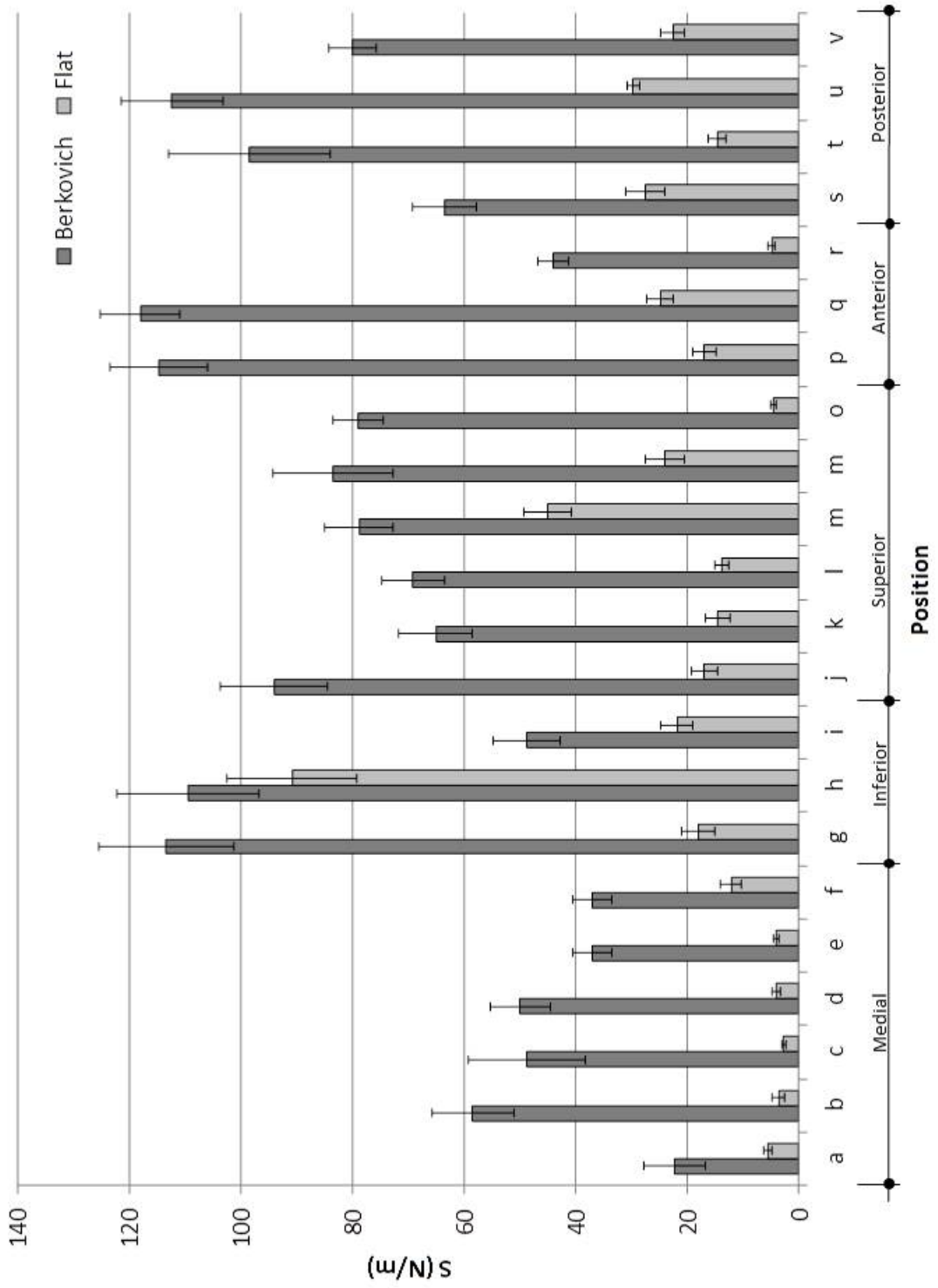

Figure 6.1: Plot of S comparing anatomical position over the femoral head for Thiel embalmed tissue.

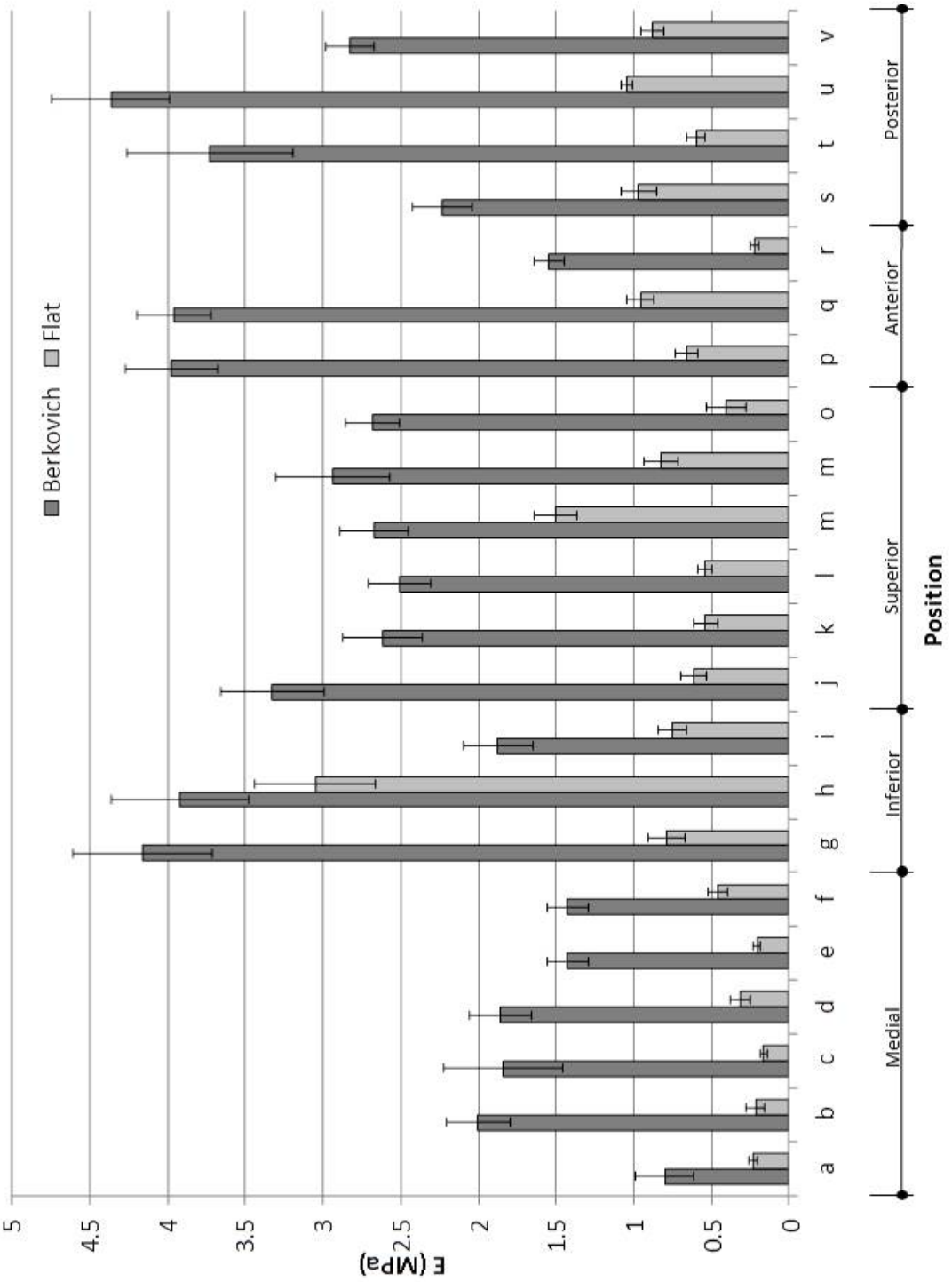

Figure 6.2: Plot of E comparing anatomical position over the femoral head for Thiel embalmed tissue.

One of the Thiel embalmed femoral heads displayed clear signs of OA: this provided the opportunity to compare the mechanical properties of healthy Thiel-fixed AC to osteoarthritic Thiel-fixed AC. Figure 6.3 and Figure 6.4 show that as AC degenerated from healthy to grade 2 Outerbridge degeneration a decrease in S and E was evident for the Thiel embalmed tissue. Grades 3 and 4 Outerbridge OA degeneration was not compared as the Thiel embalmed femoral heads did not exhibit signs of these grades. The fixed AC illustrated significantly ($p < 0.05$) lower S and E values for tissue Outerbridge grades 0 to 2 compared to fresh frozen AC.

The Berkovich tip demonstrated a significantly larger S (107.5 N/m, $p < 0.05$) and E ($4MPa$, $p < 0.05$) for the triangular loading condition compared to the trapezoidal loading condition ($S = 54.1$ N/m, $E = 2$ MPa), illustrated in Figure 6.5(a) and Figure 6.6(a). No significant effect ($p = 0.5$) was seen when using the flat punch: a mean S of 15 N/m and E of 0.4 MPa was found for triangular loading and a greater mean S of $21N/m$ and E of 1.2 MPa was found for trapezoidal loading (Figure 6.5(b) and Figure 6.6(b)). The results with the 30 s hold for the flat tip indicated a larger variation represented by the error bars.

The analysis of the hold period by fitting a curve to the section, illustrated that the Thiel fixed tissue had a similar trend to that of fresh frozen: parameter a was smaller than parameter b and τ_1 was larger than τ_2. Although a similar trend was evident, significant differences were identified between Thiel fixed tissue and fresh frozen tissue. Thiel tissue data showed parameter a to be significantly lower than the fresh frozen tissue. τ_1 was significantly higher in the Thiel tissue than the fresh frozen tissue (Table 6.2).

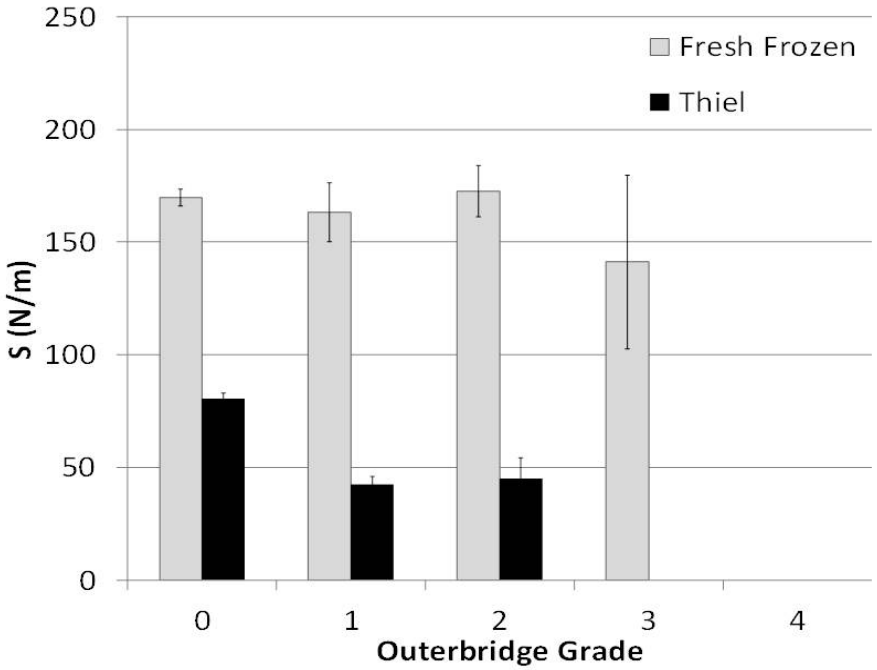

(a) Plot of S against Outerbridge grade for the Berkovich tip.

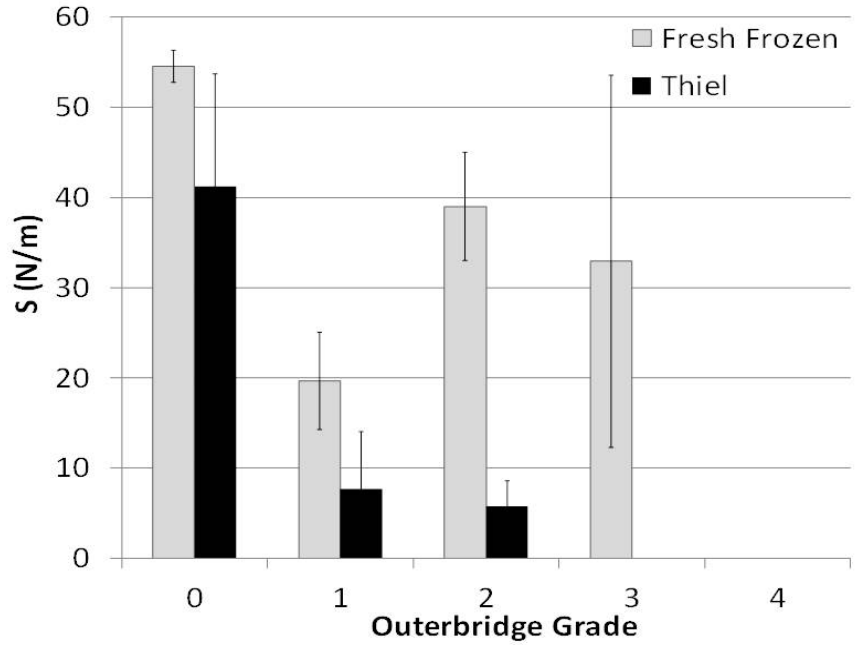

(b) Plot of S against Outerbridge grade for the flat tip.

Figure 6.3: Plots of the S comparing degeneration stage using the Outerbridge grading scale.

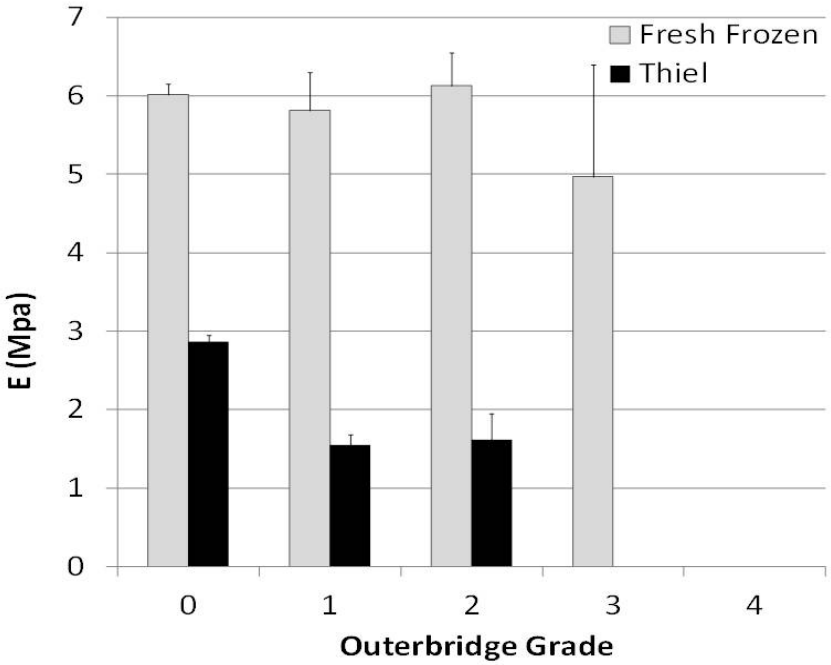

(a) Plot of E against Outerbridge grade for the Berkovich tip.

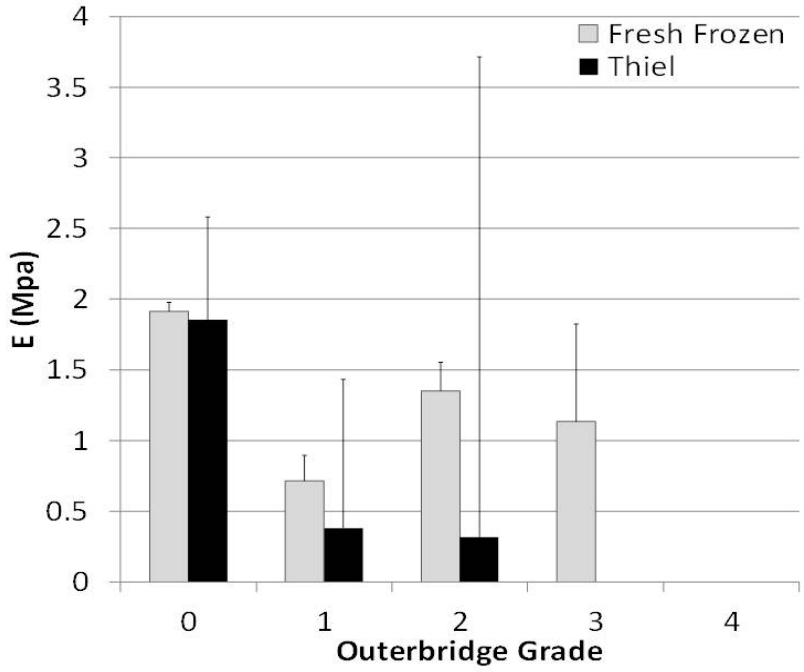

(b) Plot of E against Outerbridge grade for the flat tip.

Figure 6.4: Plots of the E comparing degeneration stage using the Outerbridge grading scale.

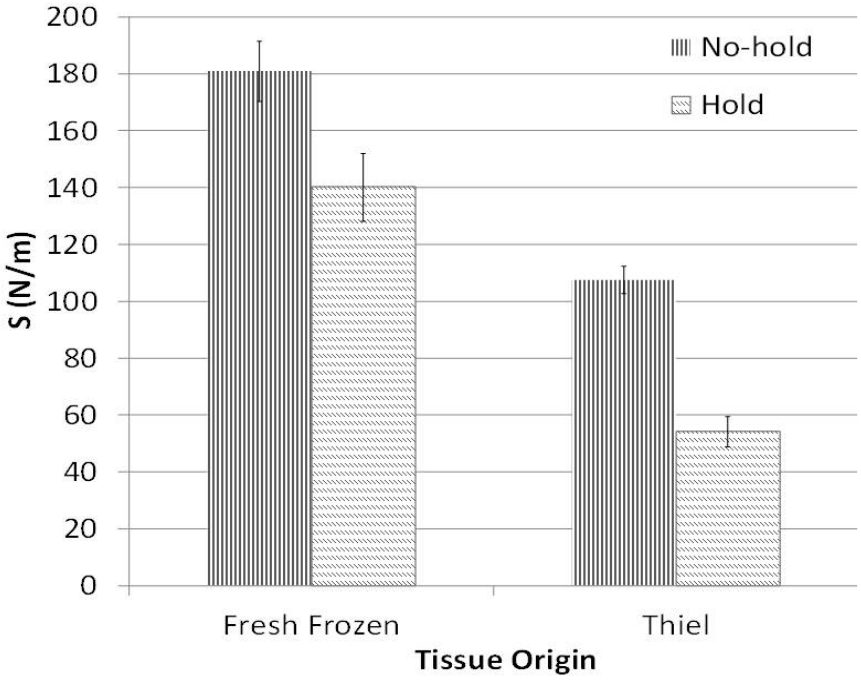

(a) Plot of S against loading pattern for the Berkovich tip.

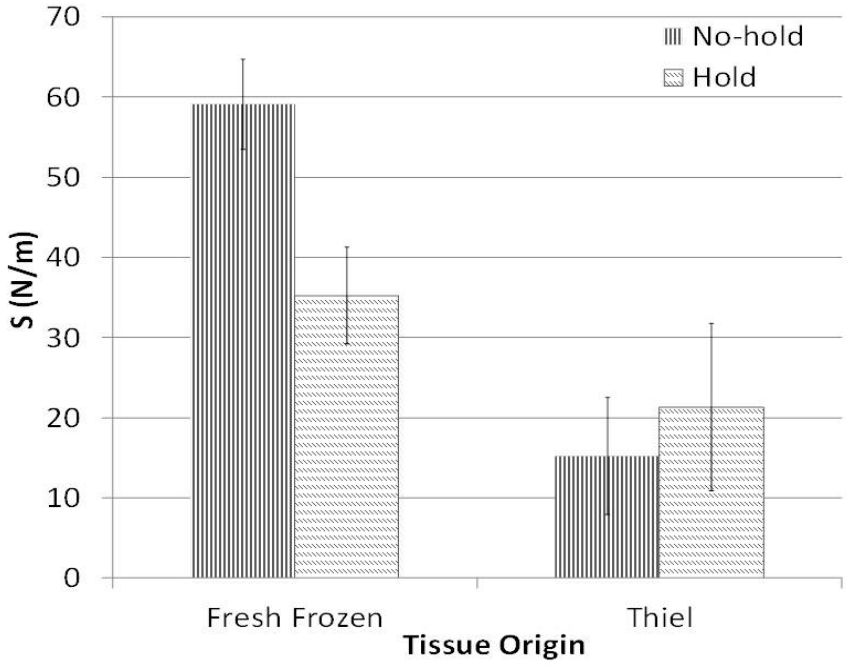

(b) Plot of S against loading pattern for the flat tip.

Figure 6.5: Plots of the S comparing degeneration stage using the Outerbridge grading scale.

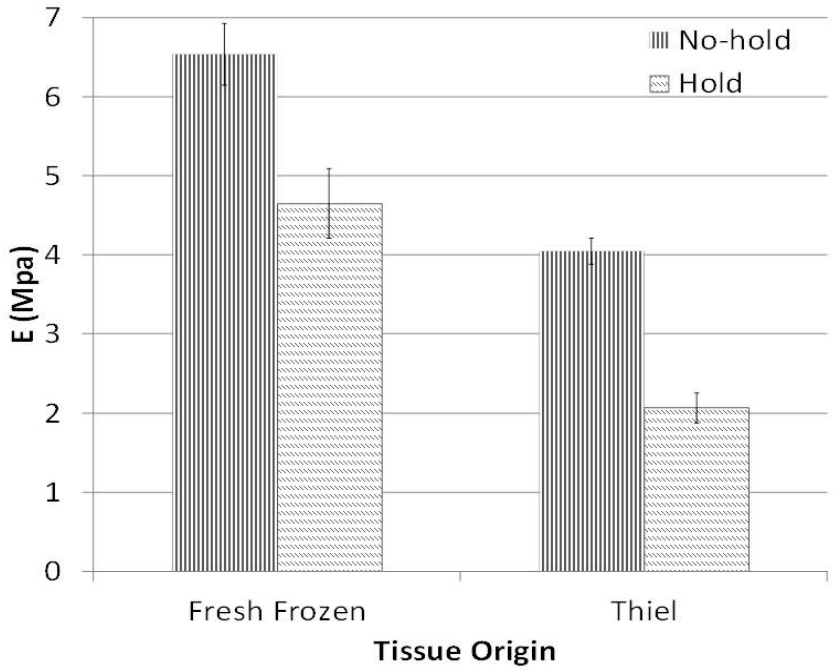

(a) Plot of E against loading pattern for the Berkovich tip.

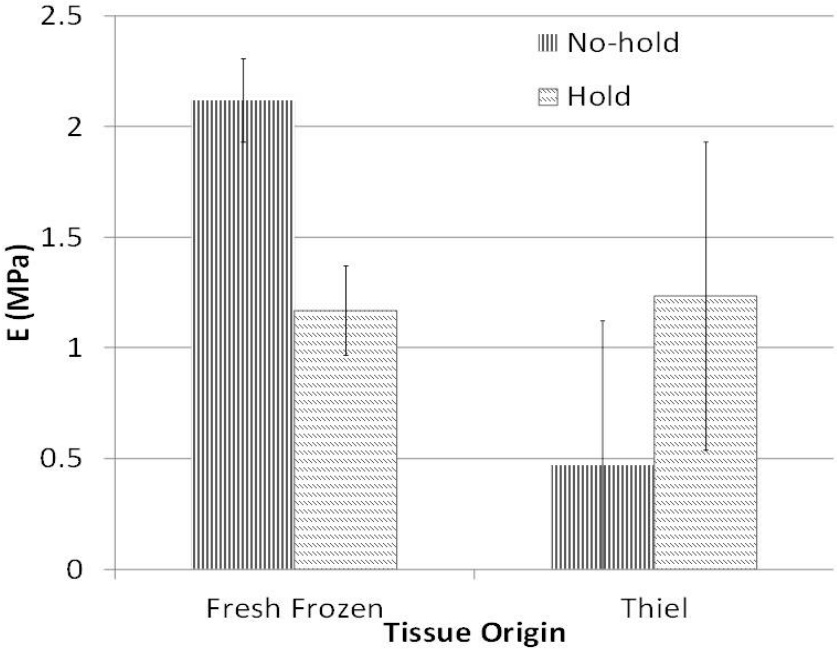

(b) Plot of E against loading pattern for the flat tip.

Figure 6.6: Plots of the E comparing degeneration stage using the Outerbridge grading scale.

Table 6.2: Shows the mean of the parameters from the curve fit analysis of the hold period.

	Thiel	Fresh Frozen	p
a (μN)	23.1 $\pm$0.9	33.8 $\pm$0.5	0.00
b (μN)	73.3 $\pm$8.6	84.1 $\pm$8.6	1
c (μN)	-50.1 $\pm$8.6	-84.1 $\pm$8.6	1
τ_1 s	2.53 $\pm$0.02	2.01 $\pm$0.02	0.00
τ_2 s	0.12 $\pm$0.003	0.1 $\pm$0.003	0.00

Figure 6.7(a) and Figure 6.7(b) present graphs comparing tip geometry and S and E. It was obvious that the Berkovich tip repeatedly measured significantly increased ($p < 0.003$) mechanical properties, when compared to those of a flat ended punch. The Thiel embalmed tissue had a mean S of 45 N/m and E of 2.08 MPa for the flat punch which was significantly lower than that of the Berkovich tip with a mean S of 90 N/m and E of 3.4 MPa.

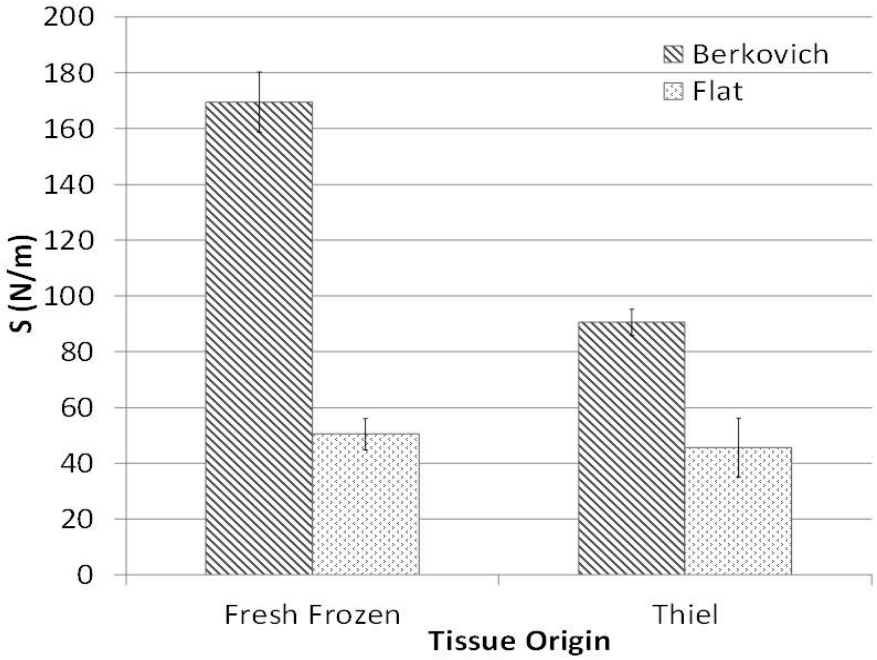

(a) Plots of the S comparing tip shape.

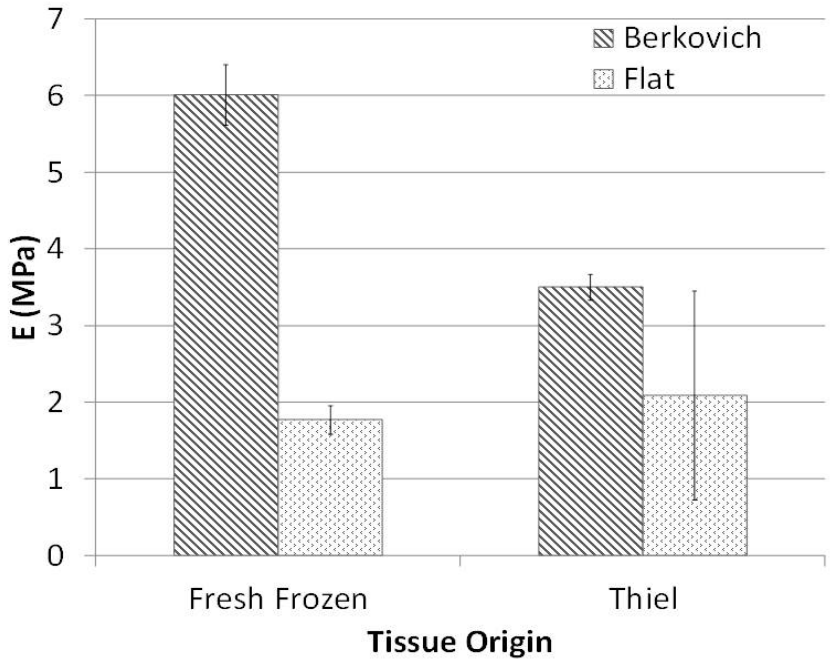

(b) Plots of the E comparing tip shape.

Figure 6.7: Plots of the S and E comparing the Berkovich tip and Flat punch.

6.4 Discussion

The results attained during this work generally compared closely with already published data (Table 2.2) however to the best of the author's knowledge the mechanical properties of Thiel-fixed AC had not been previously investigated, thus no direct comparison was possible. This study found the mechanical properties, S and E, of Thiel embalmed cadaveric AC were in the same order of magnitude as those reported for fresh frozen cadaveric AC. Overall the Thiel embalmed tissue followed a similar mechanical response to the fresh frozen AC when experimental factors were changed: mechanical properties significantly changed between position; a 30 s hold illustrated significant stress relaxation for the Berkovich tip results and the flat ended punch reported significantly smaller S and E compared to the Berkovich tip geometry. Thiel embalmed AC had a comparable mechanical reaction to the fresh frozen cadaveric AC, however Thiel-fixed AC was found to have statistically significantly lower S and E than fresh frozen AC.

Reduced S and E for Thiel fixed AC supported the hypotheisis: Thiel embalmed AC would demonstrate decreased S and E in comparison to fresh frozen AC. Thiel fixation displayed the opposite effect on the mechanical properties of AC to that of formalin fixed AC. Franke et al. (2007) investigated the effects of formalin on AC using a nanoindentation technique and discovered that formalin significantly increased the contact stiffness and reduced modulus when compared to AC in PBS. Thiel fixation did not show this trend. Thiel fixation of tendons and bone (Fessel et al., 2011; Stefan et al., 2010) also displayed lower S and E which was consistent with our results. Wilke et al. (2011) examined joint motion comparing Thiel embalming to fresh frozen joints and found that Thiel embalming demonstrated slight destabilising effects which suggested that mechanical properties have decreased. It was suspected that collagen fibres denatured due to the high

concentration of salt from the boric acid in the Thiel solution (Fessel et al., 2011; Holzle et al., 2012) . The alteration of the collagen fibrils appeared to reduce the collagen network's capability to fully confine the proteoglycans, consequently an increase in interstitial fluid may have occurred. This theory was supported by Alberty et al. (2002) who found a small increase in interstitial fluid in the cartilage of the ear which disagreed with (Thiel, 1992) who stated that Thiel embalming did not cause swelling. Our results compare with other studies on Thiel embalming of collageneous tissue (Fessel et al., 2011; Stefan et al., 2010; Wilke et al., 2011) which suggested that Thiel fixation did not reflect the mechanical properties of fresh frozen tissue.

Despite Thiel tissue indicating decreased mechanical properties, our results from femoral heads corroborate that the area of softest tissue on the femoral heads is located in a medial region, supporting the theory that the medial position around the fovea capatis ligament has lower contact stress than other locations. Thiel tissue also illustrated a decrease in mechanical properties with increasing OA degeneration agreeing with the results from Chapter 5 and the work by Stolz et al. (2009) and Bae et al. (2006): OA decreases the mechanical properties of AC. The large experimental error seen in Figure 6.3 and Figure 6.4 may be due to low numbers of tissue samples having grade 2 Outerbridge OA degeneration.

The dwell results for the flat punch are not easily understood. The triangular loading results demonstrated a lower S and E than the trapezoidal loading results. However, for the Berkovich indents and fresh frozen tissue, the trapezoidal loading results were significantly lower. The Young's modulus results for the flat ended punch indicated larger variation than the Berkovich tip. In agreement with the previous chapter, visual inspection of the force-displacement curves, during the dwell, indicated that multiple trapezoidal indents into Thiel embalmed AC

relaxed beyond the original state of the cartilage causing adhesion on the tip resulting in a lower force than at intitial contact, so force increased when unloading not decreased. This resulted in an invalid unloading curve that could not be analysed. As it was possible to fit the 5 parameters curve to the hold curve of the flat ended tip data, it was believed that the flat punch indents demonstrated a reduction in S and E after a 30 s hold however due to the extreme relaxation and inability to analysis all the hold indent unloading curves this was not seen in the flat ended tip results.

Thiel-fixed AC mechanical responses to a dwell were similar to that of fresh frozen cadaveric AC as, on average, for the analysis of the dwell section, the slow mechanical mechanisms (fluid flow) had greater effect during the hold than the fast mechanical mechanisms for both tip types. τ_1 for the Thiel-fixed tissue was significantly greater than τ_1 for the fresh frozen tissue, suggesting that Thiel embalming caused the interstitial fluid to have a greater effect on the mechanical properties. This supported the theory that Thiel-fixed tissue had a slightly greater volume of interstitial fluid than fresh frozen tissue (Alberty et al., 2002) which was potentially one of the causes for Thiel-fixed AC to have lower S and E than fresh frozen AC.

This study had one major limitation; only three femoral heads were obtained for testing. This allowed a comparison of 66 samples however two of the femoral heads were healthy and showed no signs of OA but one indicated signs of intermediate stages of OA, creating another variable within the sample size. All the femoral heads had been embalmed for over 18 months; it was found that Thiel fixation did not effect the mechanical characteristics of bone within the first 6

months of preservation. The time period of fixation may have affected the mechanical properties of AC however due to the small sample size and availability this could not be investigated.

6.5 Conclusion

In conclusion, Thiel embalming of cadaveric femoral head AC did not faithfully reflect the mechanical properties found in fresh frozen human AC. Thiel embalming significantly decreased the mechanical properties of AC, potentially because the high salt concentration denatured the collagen fibres. For these reasons, Thiel-fixed tissue cannot be recommended as a direct substitute for fresh frozen AC. The Thiel embalmed AC reacted to the loads with the same mechanical response: it was able to retain sufficient integrity to be recommended for use in preliminary experiments and surgical training, hence superior than formalin fixed tissue. However fresh frozen tissue is still the gold standard and is advisable for use in final experiments. In general, our results indicated Thiel embalmed articular cartilage showed significantly reduced contact stiffness and Young's modulus than fresh frozen articular cartilage.

Chapter 7

Discussion

7.1 General review

Articular cartilage is the soft tissue that covers the ends of bones and is designed with a smooth surface for pain free, dynamic movement and to aid load distribution. Osteoarthritis is a painful, disabling joint disease that progressively degenerates the AC surface and in time remodels the subchondral bone. AC is innervated therefore has poor regenerative capabilities. OA currently has no cure as clinical diagnostic devices do not identify early OA degeneration before permanent microarchitectural damage develops. Total joint replacement is the standard treatment for OA, a very invasive, costly treatment. Primary replacement is not always successful and in 2011, of the 80,314 hip replacements recorded by the National Joint Registry, 11% of the procedures were revision surgeries. In 2012 the number of hip replacements had risen to 89,633 following the ascending trend evident over the previous years. Osteoarthritis presents a huge financial burden to society.

Greater understanding of the mechanical properties of AC and of how OA affects these properties may assist in improving treatment prior to replacement. Identifying the alterations in mechanical properties caused by OA may provide an alternative approach for diagnosis. Indentation has been suggested as a potential device for diagnosing OA however current arthroscopic indentation devices are macroscale so do not provide the sensitivity to identify local, mechanical property changes. Nanoscale indentation has been suggested to provide the detail required to identify early osteoarthritis (Ebenstein and Pruitt, 2006; Bae et al., 2006; Korhonen et al., 2002a; Franke et al., 2007; Pollard et al., 2008).

The main purpose of this thesis was to characterise articular cartilage across the human femoral head. This study investigated osteoarthritic cartilage at a nanoscale to enhance the understanding of OA progression and to provide a basis for confirmation that nanoscale indentation has the potential to be employed as a medical device for earlier diagnosis of OA. Published studies investigating AC at nanoscale employed a variety of techniques and protocols (Jurvelin et al., 1996; Gupta et al., 2009; Julkunen et al., 2010; Loparic et al., 2010; Stolz et al., 2004, 2009; Miller and Morgan, 2009, 2010), so as AFM and nanoindentation had been highlighted as useful instruments for understanding AC, the first step of this study was to investigate these in order to provide a technique that would allow measurement of AC mechanical properties in a native environment. Chapter 3 investigated AFM but found that imaging and results were clear only in dehydrated or thin sections of tissue. As AC had already been identified to have depth-dependent mechanical properties (Huang et al., 2005), slicing the tissue into 20 μm sections required for AFM would alter the mechanical proprieties dependant on the depth of the section. Because of the extreme sample preparation

required, it was decided that current AFM techniques would not be useful to further understanding of OA or to provide a device that could identify early OA.

An instrumented nanoindenter had multiple benefits over the AFM technique: firstly, minimal sample preparation was required (no sectioning or dehydration); secondly, because of the monolithic design, direct quantitative results were acquired when calculating the mechanical properties (using AFM produced qualitative results due to cantilever rotation) and thirdly, the nanoindenter reduced drift error in comparison to AFM. Nanoindentation protocol development demonstrated that AC had a range of responses to initial contact so a defined, consistent, automatic triggering point could not be ascertained. It was concluded that automatic triggering did not provide the required fine detail necessary for accurately measuring the nanoscale mechanical properties of AC: manual identification of the surface was required, corresponding with the protocols of Miller and Morgan (2010, 2009) and Franke et al. (2007). The large range of protocols and properties available to measure when indenting AC, illustrated in Table 2.2, indicated no consistent trend between studies for best analysis, all suggested their method was superior. After consideration, it was decided to use the gradient of the unloading force-displacement curve, and to employ the Oliver-Pharr technique for analysis as it was basic and had been used as the basis for other analyses so would allow greater comparison of the data in this study with that of others.

A range in loading and unloading displacement rates have been described in other studies (ranging from 0.1 $\mu m/s$ to 130 $\mu m/s$ (Han et al., 2011; Gupta et al., 2005)); it was important to identify an appropriate loading configuration to measure the mechanical properties of AC, difficult as AC is a viscoelastic material. In Chapter 4 the effects of loading and unloading velocity on stiffness (S) and Young's modulus (E) of articular cartilage using nanoindentation were

investigated. It further examined the effect of a 30 s hold phase. 5520 indents were performed over 10 different loading configurations. The S and E results were comparable with studies by Franke et al. (2007); Simha et al. (2007); Franke et al. (2011); Kiviranta et al. (2007); Li et al. (2006); Gupta et al. (2009) suggesting that the chosen methodological protocol was appropriate for measuring these mechanical properties of AC. In accordance with our protocol, it was noted repeated indentation did not damage healthy bovine AC and preconditioning of AC was unnecessary as suggested by Miller and Morgan (2010). Approximately 10 s between indents gave the AC time to recover from indentation. Due to the time-dependent nature of AC, as expected (Lu et al., 2004; Garcia and Cortas, 2007; Li et al., 2006), after a 30 s dwell S and E had reduced: the interstitial fluid within AC had moved reducing the S and E of the tissue.

Chapter 4 results confirmed that the measured mechanical properties of healthy AC were significantly influenced by the employed loading pattern (Table 2.2). A decrease in loading displacement rate by a factor of 100 roughly halved the values of S and E. A decrease, by a factor of 100 of the unloading displacement rate, demonstrated a decrease of around 25% of the recorded S and E. As the alteration in S and E was larger when the loading rate changed, this suggested the loading history had greater effect than the unloading rate, as the loading velocity is fundamental to the fluid pressurise underneath the tip (Cheng and Cheng, 2005a). Loading and unloading at 50 $\mu m/s$ illustrated higher results of S and E suggesting that this velocity determined the apparent characteristics of AC with the tissue acting more like an incompressible material, perhaps due to fluid pressure. Loading and unloading at 0.5 $\mu m/s$ demonstrated lower S and E results suggesting that this velocity determines the intrinsic characteristics of AC: the time-dependent reaction as the fluid moves through the tissue.

Determining the most appropriate loading and unloading rates was complex as the study highlighted that AC had a hierarchal complex structure which results in a highly load and hold history dependent mechanical reaction. Stolz et al. (2004) recommended faster indentation velocities with no dwell because the frequency of normal walking and running implied loading and unloading was too rapid to allow fluid movement through the structure, hence fast velocities were appropriate. On the other hand, Najafi et al. (2010) highlighted that people spend twice as long standing than walking or running per day so to determine the creep response was more applicable. From the results of Chapter 4 this study decided that 50 $\mu m/s$ was an unnatural loading speed so a loading and unloading rate of 5 $\mu m/s$ was employed but in addition a hold of 30 s would be beneficial in furthering the understanding of the AC creep response. Two loading patterns, triangular and trapezoidal, were employed for the remaining experiments.

Mechanical testing of AC identified that AC altered between species and anatomical position (Korhonen et al., 2002b; Stolz et al., 2009; Swann and Seedhom, 1993; Athanasiou et al., 1991). Despite known differences between animal and human cartilage most nanoindentation studies focused on animal models. Minimal studies investigated the mechanical response of AC across the human knee joint (Yao and Seedhom, 1993) however, to the best of the author's knowledge, no studies had mapped the mechanical properties over the femoral head despite the prevalence of hip OA and replacement surgery.

Chapter 5 investigated both healthy and osteoarthritic femoral heads to gain knowledge of how the mechanical properties changed over the hip and investigated the OA degenerative process. OA could be graded physiologically using the Outerbridge grading system (Outerbridge, 1961) or the OARSI scale (Pritzker et al., 2006) but there was no biomechanical information to complement these scales.

As Li et al. (2007); Lu et al. (2003); Korhonen et al. (2002a); Ebenstein et al. (2004) suggested that nanoindention had the capability to be developed into a device for identifying OA it was important to investigate the OA biomechanical degeneration signature and link this with the physiological degeneration scales for future studies.

22 osteochondral plugs were removed from the same locations in each femoral head to map the topographical variation. Over 25,000 manual open loop indents, approximately 5 μm in depth, were performed on 12 explant femoral heads from hip replacement surgeries and 6 cadaveric femoral heads with no medical history of OA. Two loading patterns and two tip geometries were employed to assist cross-study comparisons and to investigate if the unique custom-made flat ended tip would provide clearer results than a traditional Berkovich tip. It was quickly discovered that occasionally the indenter tips stayed attached to the human cartilage upon unloading so manual lifting of the tip was required to separate the tip from the sample, therefore no mechanical properties could be calculated. As a result this study qualitatively analysed all the samples as well as calculating contact stiffness and Young's modulus when possible. The tissue samples were divided into three qualitative groups: mechanically viable grade 1, mechanical unviable grade 2 and endstage OA (bone) grade 3. This mechanical grading system correlated well with the Outerbridge grading scale.

The qualitative data demonstrated the worst affected area on the femoral head was located in the superior posterior region which matched the quantitative data suggesting this area had the stiffest cartilage. From the mechanically viable samples it was found that significant differences were evident between sample positions, agreeing with studies on knee joints which showed altered AC mechanical properties between positions. The stiffest cartilage was located in a superior

region and the softest in a medial location: these results were consistent with finite element models and discrete element models that simulate the superior posterior region to have the greatest contact stresses during normal day activities such as walking or stair climbing (Abraham et al., 2013; Harris et al., 2012). The increase of stiffness, matching the reported higher contact stress area, suggested the superior region had adapted to the impact (stresses) by stiffening. From the quantitative results on the cadaveric femoral head it was apparent that the softest area was in a medial location which connected to the qualitative data grading, demonstrating that OA may originate in a medial location. It was thought that, due to the decreased mechanical properties, OA was prone to initiate in the medial area. However, the most severely affected area of AC was the superior posterior region. This implied that once OA had started in the superior posterior location the OA degeneration occurred at a faster rate despite stiffer mechanical properties, probably due to the more predominantly high contact stresses in this location.

The variety of loading patterns and tip geometries investigated has enabled cross study comparison. This study greatly benefited the understanding of the effect of OA on the mechanical properties of AC over the femoral head. A simple qualitative mechanical grading system has been identified that correlates well with the current physiological grading systems, basically adhesion may be indicative of early stage OA. Importantly this project has identified that once degeneration has initiated, there is a high probability that the surface of the AC will remain attached to the tip, permanently deforming the cartilage. This has never before been identified in published studies investigating nanoindentation of AC. Repeatedly nanoindentation has been suggested to have the high potential to be used as a new medical diagnostic tool. From our test results on human tissue it was evident that nanoindentation may not be a successful tool for diagnosing OA as it

can cause permanent deformation. Nevertheless a variation on nanoindentation technique may be appropriate (section 7.1.1) This highlighted the importance of testing on human tissue instead of creating assumptions based on animal tissue. Nanoindentation can highlight the mechanical differences of local areas of AC so should be used in further investigation of osteoarthritis, however non-invasive imaging devices should be linked with this technique or non-damaging adhesive measuring devices for early diagnostic purposes.

In continuing to examine the variation of the mechanical properties of articular cartilage over the femoral head, Thiel fixation was investigated to determine if this preservation technique would be effective for use in surgical training and if it would assist in the development of new implants. Fresh frozen human tissue is the gold standard for *in vivo* testing as no chemicals have altered the mechanical properties of the tissue, however this is limited in supply, of high cost and contaminates easily with bacteria quickly degenerating its quality. Chemical fixation therefore is desired to stop contamination and degeneration and to reduce costs. Formalin fixation is known to significantly increase the mechanical properties of AC due to increased crosslinking of the collagen fibres (Wilke et al., 1998; Franke et al., 2007). The effects of Thiel fixation on cartilage were unknown.

This nanoindentation study discovered that Thiel-fixed cadaveric AC tissue has significantly lower S and E than similar fresh frozen cadaver AC tissue. These results were consistent with studies (Fessel et al., 2011; Stefan et al., 2010) which had investigated the mechanical properties of tendons and bone and discovered a decrease in mechanical properties due to collagen fibre denaturing. The collagen fibres denature due to the high salt concentration in boric acid which is a

component of Thiel embalming. Thiel-fixed tissue cannot be endorsed as a direct substitute for fresh frozen tissue, however as it retains an equivalent mechanical response to fresh frozen tissue, Thiel embalming can be recommended for use in preliminary studies and training as it is an improvement upon formalin fixation.

7.1.1 Limitations and Future Work

The foremost limitation of the work presented in this thesis is the use of the Oliver-Pharr method for analysis. This method assumed the tissue to be a smooth, homogenous, isotropic, elastic half space which does not reflect the properties of AC. The Oliver-Pharr method was a simple, adequate technique to match the intentions and purpose of this study: to aid cross study comparisons. Future improvements should adapt this method to inverse numerical methods which would provide an alternative to parameterise the tissue.

Articular cartilage has been shown to have a range of ν from 0 to 0.5 and as 0.5 was most commonly reported in nanoindentation studies this was the value assumed for ν in this study. The analyses were thus limited by the assumption of Poisson's ratio to equal 0.5. For future progress, studies would benefit from calculating Poisson's ratio for each sample to improve accuracy of analysis employing similar methods to **?**.

Another limitation of the biomechanical studies performed in this thesis, specifically chapter 5 and chapter 6, is that samples were not all mechanically viable when indenting i.e. upon unloading some samples remained attached to the indenter tip. This provided qualitative results but a lack of S and E values for this type of sample composition. Despite the lack of mechanical property measurements

the high correlation between adhesion to the tip and Outerbridge degeneration grade was substantial, suggesting this was a highly significant finding and that adhesion may be a key biomarker to the onset of OA. Future studies should not investigate arthroscopic nanoindentation devices that measure S and E as a large biological variation is evident and it has been illustrated, due to adhesion, that it is not always possible to measure the mechanical properties.

The discovery of extreme adhesion has opened up many avenues for further investigation. Efforts in developing early OA diagnostic devices should explore instruments that can measure adhesion at the nanoscale. The instrument would be required to measure the adhesion without deforming the surface which may be achieved with a spherical shaped device with less than a μm diameter or with a flat device that is larger in scale but does not move into the surface. Developers should consider the best construction material for the instrument's contact surface for providing suitable results to calculate the adhesion. The material that touches the cartilage is crucial as it may be possible to coat the device in a biodegradable layer that imports nutrients into the AC to assist reparation (as AC is innervated nutrients are important) so if deformation did occur, as the nanoindents demonstrated in this study, the cartilage would have a greater ability to recover rather than to degenerate further. Further studies are required to determine how much tissue adhesion to the device is healthy for viscoelastic AC and at what point the amount of adhesion suggests degeneration of tissue.

Another consideration is that the hip joint is encapsulated; probing the encapsulation in an attempt to identify OA can be difficult and potentially damaging. Improving non-invasive techniques may be the most appropriate line for future diagnostic device development. Non-invasive imaging techniques would need to link to the mechanical property changes which could then visualise the struc-

tural changes that in turn cause the mechanical alterations in AC. Non-invasive imaging should also be connected to increased adhesion results so that the imaging could identify the type of tissue that would attach to a nanoindenter tip and the type of tissue that would not attach to the tip. Although AFM imaging has been shown to highlight thickening of collagen in mice and other compositional changes on AC that may be due to OA, this technique would potentially still be an arthroscopic technique, causing high risk of damage to the hip capsule. AFM currently involves extreme sample preparation which means AFM is not a suitable diagnostic imaging device. In comparison to arthroscopic devices, non-invasive imaging would reduce risk, pain and recovery time to the patient therefore further imaging techniques need to be developed in order that OA can be diagnosed earlier.

The attachment of the tissue to the tip was suggestive of a pannus-like tissue, however when tested histologically, a pannus-like tissue was not identified with the methods used in this study. Despite multiple attempts at staining techniques the histological results were disappointing. A change in surface proteins or rapid stress relaxation as a result of an increased contact area may contribute to the adhesion affect. To aid further investigation and the understanding of the reasons for sample attachment to the indenter tip, a variety of histological stains and techniques should be researched. In future this information could be linked with potential, non-invasive imaging devices to identify early OA.

The angle of the femoral neck should be considered by subsequent research when investigating hip geometry. This study assumed the fovea capitis ligament to be in a medial location however the neck angle could slightly alter the anatomical positions. Precise femoral head orientation may be achieved with knowledge gained from preoperative MRI scans and x-rays and this exact ori-

entation may further explain the variation of mechanical properties between locations and better match contact stress data from finite element analysis or experimental gait analysis.

Confirmation that OA initiates in a medial location on the femoral head opens further lines of research. One option could be a long term study that recruits a large number of participants aged 30 (both female and male of a variety of activity levels), the aim of which would be to MRI each participant at least once per year until OA is clearly identified and then, after review of these MRI scans, identify where first signs of OA were indicated. A better resolution imaging device than standard MRI would need to be utilised. This kind of experiment may be unrealistic as it would be high in cost, due to the number of scans, and would be expected to extend a minimum of 25 years.

Further studies using nanoindentation, comprising of a higher number of cadaveric femoral heads incorporating a larger age range and activity level and including preoperative MRI orientation information, would help validate this study if the medial location was pinpointed as the origin of OA. Linking these experimental results with finite element analysis that models the same femoral heads, taking into account their exact shape, activity levels (average time spent walking, running, sitting, sleeping, walking stairs etc) and measured mechanical properties may be the most realistic future study to ascertain if OA initiates in a medial location. Further work into OA degeneration is vital as the earlier osteoarthritis is diagnosed the greater the possibility of reversal or the better the prospect of slowing the rate of degeneration, resulting in less pain to the patient and a reduction in surgeries and cost.

Stefan et al. (2010) investigated the effects of Thiel embalming on bone: in comparing Young's modulus to fresh frozen bone no significant differences were initially discovered, however after 6 months of immersion in Thiel fixative solution a significant decrease in Young's modulus was evident. Further investigation into whether Thiel-fixed AC is appropriate for surgical training and for testing new implants should explore how the mechanical properties alter depending on the length of time tissue is immersed in solution. Moreover, it would be interesting to attempt to reduce the salt concentration in Thiel solution and discover how this may affect the mechanical properties of articular cartilage and whether the physiological preservation was maintained.

7.1.2 Conclusion

This thesis has determined the softest AC is located in the medial location around the fovea capitis ligment and the stiffest AC is located in a superior posterior position. These results corresponded with numerical simulation studies which demonstrated the superior posterior location had the highest contact stresses suggesting the cartilage had adapted to these stresses. The qualitative results indicate that OA initiated in a medial location however the superior posterior region was worst affected, possibly due to the increased loads. Chapter 5 found that degenerated samples, on occasion, remained attached to the indenter tip, but this had not been identified in animal models. This attachment may be explained by the appearance of a pannus-like tissue found in osteoarthritic joints (Shibakawa et al., 2003; Barley et al., 2010; Yuan et al., 2004) however further histology experiments are required for confirmation. The attachment of the sample to the tip correlated well with the physiological degeneration of the cartilage according to the Outerbridge scale. The presence of this pannus-like tissue in a

medial location may be a biomarker for early osteoarthritis. However, the use of nanoindentation on degenerated AC tissue permanently deformed the tissue causing further damage therefore a non-damaging arthroscopic adhesion measuring device is an avenue worth pursing for OA diagnostics. The nanoindentation results obtained from this research suggest that osteoarthritis originates in a medial location and can be identified by the potential presence of pannus-like tissue. If this information is linked with non-invasive imaging techniques, a consequence of this study could be the eventual production of a diagnostic tool that identifies osteoarthritis early, while there is still the possibility to reverse damage or simply improve muscle strength, to reduce the load on the superior location as inevitably this will degenerate faster and cause greater pain. However, considerably more work is required before the full potential of nanoindentation and atomic force microscopy can be fully appreciated and applied.

Bibliography

Abraham, C. L., Maas, S. A., Weiss, J. A., Ellis, B. J., Peters, C. L., and Anderson, A. E. (2013). A new discrete element analysis method for predicting hip joint contact stresses. *Journal of Biomechanics*, 46(6):1121–1127.

Ainsworth, L., Budelier, K., Clinesmith, M., Fiedler, A., Landstrom, R., Leeper, B., Moeller, L., Mutch, S., O'Dell, K., Ross, J., Radhakrishnan, R., and Sluka, K. A. (2006). Transcutaneous electrical nerve stimulation (TENS) reduces chronic hyperalgesia induced by muscle inflammation. *Pain*, 120(12):182–187.

Akhter, M. P., Fan, Z., and Rho, J. Y. (2004). Bone intrinsic material properties in three inbred mouse strains. *Calcif. Tissue Int.*, 75(5):416–420.

Alberty, J., Filler, T. J., Schml, F., and Peuker, E. T. (2002). [thiel method fixed cadaver ears. a new procedure for graduate and continuing education in middle ear surgery]. *HNO*, 50(8):739–742.

Appleyard, R. C., Burkhardt, D., Ghosh, P., Read, R., Cake, M., Swain, M. V., and Murrell, G. A. C. (2003). Topographical analysis of the structural, biochemical and dynamic biomechanical properties of cartilage in an ovine model of osteoarthritis. *Osteoarthr. Cartil.*, 11(1).

Appleyard, R. C., Swain, M. V., Khanna, S., and Murrell, G. A. C. (2001). The accuracy and reliability of a novel handheld dynamic indentation probe for analysing articular cartilage. *Phys. Med. Biol.*, 46(2):541.

Ateshian, G. A. and Wang, H. (1997). Rolling resistance of articular cartilage due to interstitial fluid flow. *Proc Inst Mech Eng H*, 211(5):419–424.

Ateshian, G. A., Warden, W. H., Kim, J. J., Grelsamer, R. P., and Mow, V. C. (1997). Finite deformation biphasic material properties of bovine articular cartilage from confined compression experiments. *J Biomech*, 30(11-12):1157–1164.

Athanasiou, K., Rosenwasser, M., Buckwalter, J., Malinin, T., and Mow, V. (1991). Interspecies comparisons of insitu intrinsic mechanical-properties of distal femoral cartilage. *J. Orthop. Res.*, 9(3):330–340.

Athanasiou, K. A., Agarwal, A., and Dzida, F. J. (1994). Comparative study of the intrinsic mechanical properties of the human acetabular and femoral head cartilage. *J. Orthop. Res.*, 12(3):340–349.

Bae, W. C., Lewis, C. W., Levenston, M. E., and Sah, R. L. (2006). Indentation testing of human articular cartilage: Effects of probe tip geometry and indentation depth on intra-tissue strain. *Journal of Biomechanics*, 39(6):1039–1047.

Bae, W. C., Temple, M. M., Amiel, D., Coutts, R. D., Niederauer, G. G., and Sah, R. L. (2003). Indentation testing of human cartilage: sensitivity to articular surface degeneration. *Arthritis Rheum.*, 48(12):3382–3394.

Baker, K. and McAlindon, T. (2000). Exercise for knee osteoarthritis. *Curr Opin Rheumatol*, 12(5):456–463.

Balooch, M., Wu-Magidi, I. C., Balazs, A., Lundkvist, A. S., Marshall, S. J., Marshall, G. W., Siekhaus, W. J., and Kinney, J. H. (1998). Viscoelastic properties of demineralized human dentin measured in water with atomic force microscope (AFM)-based indentation. *J. Biomed. Mater. Res.*, 40(4):539–544.

Barbakadze, N., Enders, S., Gorb, S., and Arzt, E. (2006). Local mechanical properties of the head articulation cuticle in the beetle pachnoda marginata (coleoptera, scarabaeidae). *J. Exp. Biol.*, 209(Pt 4):722–730.

Barley, R. D. C., Adesida, A. B., Bagnall, K. M., and Jomha, N. M. (2010). Immunohistochemical characterization of reparative tissue present in human osteoarthritic tissue. *Virchows Arch*, 456(5):561–569.

Bartel, D. L., Bicknell, V. L., and Wright, T. M. (1986). The effect of conformity, thickness, and material on stresses in ultra-high molecular weight components for total joint replacement. *J Bone Joint Surg Am*, 68(7):1041–1051.

Benkhadra, M., Bouchot, A., Grard, J., Genelot, D., Trouilloud, P., Martin, L., Girard, C., Danino, A., Anderhuber, F., and Feigl, G. (2011). Flexibility of thiel's embalmed cadavers: the explanation is probably in the muscles. *Surg Radiol Anat*, 33(4):365–368.

Benkhadra, M., Faust, A., Ladoire, S., Trost, O., Trouilloud, P., Girard, C., Anderhuber, F., and Feigl, G. (2009). Comparison of fresh and thiel's embalmed cadavers according to the suitability for ultrasound-guided regional anesthesia of the cervical region. *Surg Radiol Anat*, 31(7):531–535.

Benkhadra, M., Lenfant, F., Nemetz, W., Anderhuber, F., Feigl, G., and Fasel, J. (2008). A comparison of two emergency cricothyroidotomy kits in human cadavers. *Anesth. Analg.*, 106(1):182–185.

Binnig, G., Quate, C. F., and Gerber, C. (1986). Atomic force microscope. *Phys. Rev. Lett.*, 56(9):930–933.

Biot, M. (1956). Theory of propagation of elastic waves in a fluid-saturated porous solid .1. low-frequency range. *J. Acoust. Soc. Am.*, 28(2):168–178.

Bjordal, J. M., Johnson, M. I., Lopes-Martins, R. A., Bogen, B., Chow, R., and Ljunggren, A. E. (2007). Short-term efficacy of physical interventions in osteoarthritic knee pain. a systematic review and meta-analysis of randomised placebo-controlled trials. *BMC Musculoskeletal Disorders*, 8(1):51.

Black, J., Shadle, C. A., Parsons, J. R., and Brighton, C. T. (1979). Articular cartilage preservation and storage. 22(10):1102–1108.

Blankenbaker, D. G., Ullrick, S. R., Kijowski, R., Davis, K. W., Smet, A. A. D., Shinki, K., Rio, A. M. d., and Keene, J. S. (2011). MR arthrography of the hip: Comparison of IDEAL-SPGR volume sequence to standard MR sequences in the detection and grading of cartilage lesions. *Radiology*, 261(3):863–871.

Blitzer, C. M. (1993). Arthroscopic management of septic arthritis of the hip. *Arthroscopy: The Journal of Arthroscopic & Related Surgery*, 9(4):414–416.

Boryor, A., Hohmann, A., Wunderlich, A., Geiger, M., Kilic, F., Sander, M., Sander, C., Bckers, T., and Gnter Sander, F. (2010). In-vitro results of rapid maxillary expansion on adults compared with finite element simulations. *J Biomech*, 43(7):1237–1242.

Boschetti, F., Pennati, G., Gervaso, F., Peretti, G. M., and Dubini, G. (2004). Biomechanical properties of human articular cartilage under compressive loads. *Biorheology*, 41(3-4):159–166.

Boschetti, F. and Peretti, G. M. (2008). Tensile and compressive properties of healthy and osteoarthritic human articular cartilage. *Biorheology*, 45(3-4):337–344.

Bradley, J. D., Brandt, K. D., Katz, B. P., Kalasinski, L. A., and Ryan, S. I. (1992). Treatment of knee osteoarthritis: relationship of clinical features of

joint inflammation to the response to a nonsteroidal antiinflammatory drug or pure analgesic. *J. Rheumatol.*, 19(12):1950–1954.

Brama, P. A. J., Holopainen, J., van Weeren, P. R., Firth, E. C., Helminen, H. J., and Hyttinen, M. M. (2009). Effect of loading on the organization of the collagen fibril network in juvenile equine articular cartilage. *J. Orthop. Res.*, 27(9):1226–1234.

Brandt, K. D., Doherty, M., and Lohmander, S. (2003). *Osteoarthritis*.

Briscoe, B. J., Fiori, L., and Pelillo, E. (1998). Nano-indentation of polymeric surfaces. *J. Phys. D-Appl. Phys.*, 31(19):2395–2405.

Brosseau, L., Yonge, K. A., Robinson, V., Marchand, S., Judd, M., Wells, G., and Tugwell, P. (2003). Thermotherapy for treatment of osteoarthritis. *Cochrane Database Syst Rev*, (4):CD004522.

Bruet, B., Qi, H., Boyce, M., Panas, R., Tai, K., Frick, L., and Ortiz, C. (2005). Nanoscale morphology and indentation of individual nacre tablets from the gastropod mollusc trochus niloticus. 20(09):2400–2419.

Buckwalter, J. A., Rosenberg, L. C., and Tang, L. H. (1984). The effect of link protein on proteoglycan aggregate structure. an electron microscopic study of the molecular architecture and dimensions of proteoglycan aggregates reassembled from the proteoglycan monomers and link proteins of bovine fetal epiphyseal cartilage. *J. Biol. Chem.*, 259(9):5361–5363.

Burry, H. C. (1974). Adult articular cartilage. *Proc R Soc Med*, 67(7):691.

Byrd, J. W. T. and Jones, K. S. (2004). Diagnostic accuracy of clinical assessment, magnetic resonance imaging, magnetic resonance arthrography, and intra-articular injection in hip arthroscopy patients. *Am J Sports Med*, 32(7):1668–1674.

Byrd, J. W. T. and Jones, K. S. (2010). Prospective analysis of hip arthroscopy with 10-year followup. *Clin Orthop Relat Res*, 468(3):741–746.

Cao, Y., Ma, D., and Raabe, D. (2009). The use of flat punch indentation to determine the viscoelastic properties in the time and frequency domains of a soft layer bonded to a rigid substrate. *Acta Biomater.*, 5(1):240–248.

Cao, Y., Yang, D., and Soboyejoy, W. (2005). Nanoindentation method for determining the initial contact and adhesion characteristics of soft polydimethylsiloxane. *Journal of Materials Research*, 20:2004–2011.

Carballido-Gamio, J., Bauer, J. S., Stahl, R., Lee, K.-Y., Krause, S., Link, T. M., and Majumdar, S. (2008). Inter-subject comparison of MRI knee cartilage thickness. *Med Image Anal*, 12(2):120–135.

Chen, A., Bae, W., Schinagl, R., and Sah, R. (2001). Depth- and strain-dependent mechanical and electromechanical properties of full-thickness bovine articular cartilage in confined compression. *Journal of Biomechanics*, 34(1):1–12.

Chen, A., Gupte, C., Akhtar, K., Smith, P., and Cobb, J. (2012). The global economic cost of osteoarthritis: How the UK compares. *Arthritis Rheum.*, 2012:1–6.

Chen, Q., Rho, J. Y., Fan, Z., Laulederkind, S. J. F., and Raghow, R. (2003). Congenital lack of COX-2 affects mechanical and geometric properties of bone in mice. *Calcif. Tissue Int.*, 73(4):387–392.

Cheng, L., Xia, X., Yu, W., Scriven, L. E., and Gerberich, W. W. (2000). Flat-punch indentation of viscoelastic material. *Journal of Polymer Science*, 38(1):10–22.

Cheng, Y. T. and Cheng, C. M. (2005a). General relationship between contact stiffness, contact depth, and mechanical properties for indentation in linear

viscoelastic solids using axisymmetric indenters of arbitrary profiles. *Appl. Phys. Lett.*, 87(11):3.

Cheng, Y. T. and Cheng, C. M. (2005b). Relationships between initial unloading slope, contact depth, and mechanical properties for spherical indentation in linear viscoelastic solids. *Mater. Sci. Eng. A-Struct. Mater. Prop. Microstruct. Process.*, 409(1-2):93–99.

Chia, H. N. and Hull, M. L. (2008). Compressive moduli of the human medial meniscus in the axial and radial directions at equilibrium and at a physiological strain rate. *Journal of Orthopaedic Research*, 26(7):951–956.

Clarke, I. C. (1974). Articular cartilage: a review and scanning electron microscope study. II. the territorial fibrillar architecture. *J Anat*, 118(Pt 2):261–280.

Collins, D. H. (1949). *The Pathology of Articular and Spinal Diseases*.

Collins, D. H. and McElligott, T. F. (1960). Sulphate (35SO4) uptake by chondrocytes in relation to histological changes in osteo-arthritic human articular cartilage. *Ann Rheum Dis*, 19(4):318–330.

Corcoran, S. G., Colton, R. J., Lilleodden, E. T., and Gerberich, W. W. (1997). Anomalous plastic deformation at surfaces: Nanoindentation of gold single crystals. *Phys. Rev. B*, 55(24):16057–16060.

Crockett, R., Roos, S., Rossbach, P., Dora, C., Born, W., and Troxler, H. (2005). Imaging of the surface of human and bovine articular cartilage with ESEM and AFM. *Tribol. Lett.*, 19(4):311–317.

Cuy, J. L., Mann, A. B., Livi, K. J., Teaford, M. F., and Weihs, T. P. (2002). Nanoindentation mapping of the mechanical properties of human molar tooth enamel. *Arch. Oral Biol.*, 47(4):281–291.

Deal, C. L., Schnitzer, T. J., Lipstein, E., Seibold, J. R., Stevens, R. M., Levy, M. D., Albert, D., and Renold, F. (1991). Treatment of arthritis with topical capsaicin: a double-blind trial. *Clin Ther*, 13(3):383–395.

DiSilvestro, M. R. and Suh, J.-K. F. (2001). A cross-validation of the biphasic poroviscoelastic model of articular cartilage in unconfined compression, indentation, and confined compression. *Journal of Biomechanics*, (4):519–525.

Do, S. A. and McAlindon, T. (2005). Considerations in the treatment of early osteoarthritis. *Curr Rheumatol Rep*, 7(1):29–35.

Doerner, M. and Nix, W. (1986). A method for interpreting the data from depth-sensing indentation instruments. *Journal of Materials Research*, 1(04):601–609.

Donnan, F. G. (1924). The theory of membrane equilibria. *Chem. Rev.*, 1(1):73–90.

Donnelly, E., Baker, S. P., Boskey, A. L., and van der Meulen, M. C. (2006). Effects of surface roughness and maximum load on the mechanical properties of cancellous bone measured by nanoindentation. *Journal of Biomedical Materials Research*, 77A(2):426–435.

Doube, M., Firth, E. C., Boyde, A., and Bushby, A. J. (2010). Combined nanoindentation testing and scanning electron microscopy of bone and articular calcified cartilage in an equine fracture predilection site. *Eur. Cells Mater.*, 19(3):242–251.

Ebenstein, D. M., Chapman, J. M., Li, C., Saloner, D., Rapp, J., and Pruitt, L. A. (2001). Assessing structure-property relations of diseased tissues using nanoindentation and FTIR. *MRS Proceedings*, 711.

Ebenstein, D. M., Kuo, A., Rodrigo, J. J., Reddi, A. H., Ries, M., and Pruitt, L. (2004). A nanoindentation technique for functional evaluation of cartilage repair tissue. *Journal of Materials Research*, 19(01):273–281.

Ebenstein, D. M. and Pruitt, L. A. (2006). Nanoindentation of biological materials. *Nano Today*, 1(3):26–33.

Ebenstein, D. M. and Wahl, K. J. (2006). A comparison of JKR-based methods to analyze quasi-static and dynamic indentation force curves. *Journal of Colloid and Interface Science*, 298(2):652–662.

Einhorn, T., O'Keefe, R. J., and O'Keefe, R. (2000). *Orthopaedic Basic Science 3 Foundations of Clinical Practice.* American Academy of Orthopaedic Surgeons Rittenhouse Book Distributors [Distributor], Rosemont; Kng Of Prussa.

Enders, S., Barbakadse, N., Gorb, S., and Arzt, E. (2004). Exploring biological surfaces by nanoindentation. *Journal of Materials Research*, 19(03):880–887.

Erb, R. E. (2001). Current concepts in imaging the adult hip. *Clinics in sports medicine*, 20(4):661–696.

Ettinger WH, J. (1997). A randomized trial comparing aerobic exercise and resistance exercise with a health education program in older adults with knee osteoarthritis: The fitness arthritis and seniors trial (fast). *JAMA*, 277(1):25–31.

Fan, Z., Swadener, J. G., Rho, J. Y., Roy, M. E., and Pharr, G. M. (2002). Anisotropic properties of human tibial cortical bone as measured by nanoindentation. *J. Orthop. Res.*, 20(4):806–810.

Fassbender, H. G. and Simmling-Annefeld, M. (1983). The potential aggressiveness of synovial tissue in rheumatoid arthritis. *The Journal of Pathology*, 139(3):399–406.

Felson, D. T., Lawrence, R. C., Dieppe, P. A., Hirsch, R., Helmick, C. G., Jordan, J. M., Kington, R. S., Lane, N. E., Nevitt, M. C., Zhang, Y., Sowers, M., McAlindon, T., Spector, T. D., Poole, A. R., Yanovski, S. Z., Ateshian, G., Sharma, L., Buckwalter, J. A., Brandt, K. D., and Fries, J. F. (2000). Osteoarthritis: New insights. part 1: The disease and its risk factors. *Ann Intern Med*, 133(8):635–646.

Felson, D. T. and Zhang, Y. (1998). An update on the epidemiology of knee and hip osteoarthritis with a view to prevention. *Arthritis & Rheumatism*, 41(8):1343–1355.

Feng, G. and Ngan, A. H. W. (2002). Effects of creep and thermal drift on modulus measurement using depth-sensing indentation. *Journal of Materials Research*, 17(03):660–668.

Fessel, G., Frey, K., Schweizer, A., Calcagni, M., Ullrich, O., and Snedeker, J. G. (2011). Suitability of thiel embalmed tendons for biomechanical investigation. *Ann. Anat.*, 193(3):237–241.

Fischer-Cripps, A. C. (2004). *Nanoindentation*. Springer.

Fong, H., Sarikaya, M., White, S. N., and Snead, M. L. (2000). Nano-mechanical properties profiles across dentin-enamel junction of human incisor teeth. *Materials Science and Engineering: C*, 7(2):119–128.

Foster, N. E., Thomas, E., Barlas, P., Hill, J. C., Young, J., Mason, E., and Hay, E. M. (2007). Acupuncture as an adjunct to exercise based physiotherapy for osteoarthritis of the knee: randomised controlled trial. *BMJ*, 335(7617):436.

Frank, E. and Grodzinsky, A. (1987). Cartilage electromechanics .2. a continuum model of cartilage electrokinetics and correlation with experiments. *J. Biomech.*, 20(6):629–639.

Franke, O., Durst, K., Maier, V., Gken, M., Birkholz, T., Schneider, H., Hennig, F., and Gelse, K. (2007). Mechanical properties of hyaline and repair cartilage studied by nanoindentation. *Acta Biomaterialia*, 3(6):873–881.

Franke, O., Goeken, M., and Hodge, A. M. (2008). The nanoindentation of soft tissue: Current and developing approaches. *JOM*, 60(6):49–53.

Franke, O., Goeken, M., Meyers, M. A., Durst, K., and Hodge, A. M. (2011). Dynamic nanoindentation of articular porcine cartilage. *Mater. Sci. Eng. C-Mater. Biol. Appl.*, 31(4):789–795.

Froimson, M., A, R., and V.C., M. (1989). Patellar cartilage mechanical properties vary with site and biochemical composition. *Trans Orthop Res Soc*, 14(6):150.

Froimson, M. I., Ratcliffe, A., Gardner, T. R., and Mow, V. C. (1997). Differences in patellofemoral joint cartilage material properties and their significance to the etiology of cartilage surface fibrillation. *Osteoarthr. Cartil.*, 5(6):377–386.

Gao, H., Ji, B., Jger, I. L., Arzt, E., and Fratzl, P. (2003). Materials become insensitive to flaws at nanoscale: Lessons from nature. *PNAS*, 100(10):5597–5600.

Garcia, J. J., Altiero, N. J., and Haut, R. C. (1998). An approach for the stress analysis of transversely isotropic biphasic cartilage under impact load. *J. Biomech. Eng.-Trans. ASME*, 120(5):608–613.

Garcia, J. J. and Cortas, D. H. (2007). A biphasic viscohyperelastic fibril-reinforced model for articular cartilage: Formulation and comparison with experimental data. *Journal of Biomechanics*, 40(8):1737–1744.

Gelse, K., Mahle, C., Franke, O., Park, J., Jehle, M., Durst, K., Goken, M., Hennig, F., Mark, K. V. D., and Schneider, H. (2008). Cell-based resurfac-

ing of large cartilage defects: Long-term evaluation of grafts from autologous transgene-activated periosteal cells in a porcine model of osteoarthritis. *Arthritis and Rheumatism*, 58(2):475–488.

Ghadially, F. N. (1983). *Fine Structure of Synovial Joints: A Text and Atlas of the Ultrastructure of Normal and Pathological Articular Tissues*. Butterworths.

Gold, S. L., Burge, A. J., and Potter, H. G. (2012). MRI of hip cartilage: joint morphology, structure, and composition. *Clin. Orthop. Relat. Res.*, 470(12):3321–331.

Guo, X. E. and Goldstein, S. A. (2000). Vertebral trabecular bone microscopic tissue elastic modulus and hardness do not change in ovariectomized rats. *J. Orthop. Res.*, 18(2):333–336.

Gupta, H. S., Schratter, S., Tesch, W., Roschger, P., Berzlanovich, A., Schoeberl, T., Klaushofer, K., and Fratzl, P. (2005). Two different correlations between nanoindentation modulus and mineral content in the bone-cartilage interface. *J. Struct. Biol.*, 149(2):138–148.

Gupta, S., Lin, J., Ashby, P., and Pruitt, L. (2009). A fiber reinforced poroelastic model of nanoindentation of porcine costal cartilage: A combined experimental and finite element approach. *Journal of the Mechanical Behavior of Biomedical Materials*, 2(4):326–338.

Guterl, C. C., Hung, C. T., and Ateshian, G. A. (2010). Electrostatic and non-electrostatic contributions of proteoglycans to the compressive equilibrium modulus of bovine articular cartilage. *J Biomech*, 43(7):1343–1350.

Han, L., Frank, E. H., Greene, J. J., Lee, H.-Y., Hung, H.-H. K., Grodzinsky, A. J., and Ortiz, C. (2011). Time-dependent nanomechanics of cartilage. 100(7):1846–1854.

Haque, F. (2003). Application of nanoindentation development of biomedical to materials. *Surface Engineering*, 19(4):255–268.

Hardya, P. A., Newmark, R., Liu, Y. M., Meier, D., Norris, S., Piraino, D. W., and Shah, A. (2000). The influence of the resolution and contrast on measuring the articular cartilage volume in magnetic resonance images. *Magnetic Resonance Imaging*, 18(8):965–972.

Harris, M. D., Anderson, A. E., Henak, C. R., Ellis, B. J., Peters, C. L., and Weiss, J. A. (2012). Finite element prediction of cartilage contact stresses in normal human hips. 30(7):1133–1139.

Hasler, E. M., Herzog, W., Wu, J. Z., Muller, W., and Wyss, U. (1999). Articular cartilage biomechanics: Theoretical models, material properties, and biosynthetic response. *Crit. Rev. Biomed. Eng.*, 27(6):415–488.

Hassenkam, T., Fantner, G. E., Cutroni, J. A., Weaver, J. C., Morse, D. E., and Hansma, P. K. (2004). High-resolution AFM imaging of intact and fractured trabecular bone. *Bone*, 35(1):4–10.

Hayes, W. and Bodine, A. (1978). Flow-independent viscoelastic properties of articular cartilage matrix. *Journal of Biomechanics*, 11(89):407–419.

Henak, C. R., Ellis, B. J., Harris, M. D., Anderson, A. E., Peters, C. L., and Weiss, J. A. (2011). Role of the acetabular labrum in load support across the hip joint. *J Biomech*, 44(12):2201–2206.

Hertz, H., Jones, D. E., and Schott, G. A. (1896). *Miscellaneous papers*. London: Macmillan, New York, Macmillan and co.

Hoffler, C. E., Moore, K. E., Kozloff, K., Zysset, P. K., Brown, M. B., and Goldstein, S. A. (2000). Heterogeneity of bone lamellar-level elastic moduli. *Bone*, 26(6):603–609.

Holzle, F., Franz, E.-P., Lehmbrock, J., Weihe, S., Teistra, C., Deppe, H., and Wolff, K.-D. (2012). Thiel embalming technique: a valuable method for teaching oral surgery and implantology. *Clin Implant Dent Relat Res*, 14(1):121–126.

Horak, Z., Kubovy, P., Stupka, M., and Horakova, J. (2011). Biomechanical factors influencing the beginning and development of osteoarthritis in the hip joint. *Wien Med Wochenschr*, 161(19-20):486–492.

Huang, C. Y., Mow, V. C., and Ateshian, G. A. (2001). The role of flow-independent viscoelasticity in the biphasic tensile and compressive responses of articular cartilage. *J Biomech Eng*, 123(5):410–417.

Huang, C.-Y., Stankiewicz, A., Ateshian, G. A., and Mow, V. C. (2005). Anisotropy, inhomogeneity, and tensional, compression nonlinearity of human glenohumeral cartilage in finite deformation. *Journal of Biomechanics*, 38(4):799–809.

Huber, N., Nix, W. D., and Gao, H. (2002). Identification of elastic-plastic material parameters from pyramidal indentation of thin films. *Proc. R. Soc. London Ser. A-Math. Phys. Eng. Sci.*, 458(2023):1593–1620.

Hung, C. T., Mauck, R. L., Wang, C. C.-B., Lima, E. G., and Ateshian, G. A. (2004). A paradigm for functional tissue engineering of articular cartilage via applied physiologic deformational loading. *Annals of Biomedical Engineering*, 32(1):35–49.

Hyttinen, M. M., Holopainen, J., Ren van Weeren, P., Firth, E. C., Helminen, H. J., and Brama, P. A. J. (2009). Changes in collagen fibril network organization and proteoglycan distribution in equine articular cartilage during maturation and growth. *Journal of Anatomy*, 215(5):584–591.

Jamsa, T., Rho, J.-Y., Fan, Z., MacKay, C. A., Marks, Sandy C, J., and Tuukkanen, J. (2002). Mechanical properties in long bones of rat osteopetrotic mutations. *J Biomech*, 35(2):161–165.

Jaung, R., Cook, P., and Blyth, P. (2011). A comparison of embalming fluids for use in surgical workshops. *Clin Anat*, 24(3):155–161.

Jazrawi, L. M., Alaia, M. J., Chang, G., FitzGerald, E. F., and Recht, M. P. (2011). Advances in magnetic resonance imaging of articular cartilage. *J Am Acad Orthop Surg*, 19(7):420–429.

Joshi, M. D., Suh, J.-K., Marui, T., and Woo, S. L.-Y. (1995). Interspecies variation of compressive biomechanical properties of the meniscus. *Journal of Biomedical Materials Research*, 29(7):823–828.

Julkunen, P., Halmesmaki, E. P., Iivarinen, J., Rieppo, L., Narhi, T., Marjanen, J., Rieppo, J., Arokoski, J., Brama, P. A., Jurvelin, J. S., and Helminen, H. J. (2010). Effects of growth and exercise on composition, structural maturation and appearance of osteoarthritis in articular cartilage of hamsters. *J. Anat.*, 217:262–274.

Julkunen, P., Korhonen, R. K., Herzog, W., and Jurvelin, J. S. (2008). Uncertainties in indentation testing of articular cartilage: A fibril-reinforced poroviscoelastic study. *Medical Engineering & Physics*, 30(4):506–515.

Junqueira, L. C. U., Bignolas, G., and Brentani, R. R. (1979). Picrosirius staining plus polarization microscopy, a specific method for collagen detection in tissue sections. *Histochem J*, 11(4):447–455.

Jurvelin, J., Kiviranta, I., Smnen, A. M., Tammi, M., and Helminen, H. J. (1990). Indentation stiffness of young canine knee articular cartilage–influence of strenuous joint loading. *J Biomech*, 23(12):1239–1246.

Jurvelin, J. S., Mller, D. J., Wong, M., Studer, D., Engel, A., and Hunziker, E. B. (1996). Surface and subsurface morphology of bovine humeral articular cartilage as assessed by atomic force and transmission electron microscopy. *J. Struct. Biol.*, 117(1):45–54.

Kaufman, J. D. and Klapperich, C. M. (2009). Surface detection errors cause overestimation of the modulus in nanoindentation on soft materials. *J Mech Behav Biomed Mater*, 2(4):312–317.

Keenan, K. E., Besier, T. F., Pauly, J. M., Han, E., Rosenberg, J., Smith, R. L., Delp, S. L., Beaupre, G. S., and Gold, G. E. (2011). Prediction of glycosaminoglycan content in human cartilage by age, t1? and t2 MRI. *Osteoarthritis Cartilage*, 19(2):171–179.

Kempson, G., Freeman, M., and Swanson, S. (1971a). Determination of a creep modulus for articular cartilage from indentation tests on human femoral head. *J. Biomech.*, 4(4):239–&.

Kempson, G., Swanson, S., Spivey, C., and Freeman, M. (1971b). Patterns of cartilage stiffness on normal and degenerate human femoral heads. *J. Biomech.*, 4(6):597–&.

Kempson, G. E., Freeman, M. a. R., and Swanson, S. a. V. (1968). Tensile properties of articular cartilage. *Nature*, 220(5172):1127–1128.

Kinney, J. H., Marshall, S. J., and Marshall, G. W. (2003). The mechanical properties of human dentin: A critical review and re-evaluation of the dental literature. *Crit. Rev. Oral Biol. Med.*, 14(1):13–29.

Kiviranta, P., Rieppo, J., Korhonen, R. K., Julkunen, P., Tyrs, J., and Jurvelin, J. S. (2006). Collagen network primarily controls poisson's ratio of bovine articular cartilage in compression. *J. Orthop. Res.*, 24(4):690–699.

Kiviranta, P., Toyras, J., Nieminen, M. T., Laasanen, M. S., Saarakkala, S., Nieminen, H. J., Nissi, M. J., and Jurvelin, J. S. (2007). Comparison of novel clinically applicable methodology for sensitive diagnostics of cartilage degeneration. *Eur. Cells Mater.*, 13:46–55.

Kleemann, R., Krocker, D., Cedraro, A., Tuischer, J., and Duda, G. (2005). Altered cartilage mechanics and histology in knee osteoarthritis: relation to clinical assessment (ICRS grade). *Osteoarthritis and Cartilage*, 13(11):958–963.

Koff, M. F. and Potter, H. G. (2009). Noncontrast MR techniques and imaging of cartilage. *Radiologic Clinics of North America*, 47(3):495–504.

Korhonen, R., Wong, M., Arokoski, J., Lindgren, R., Helminen, H., Hunziker, E., and Jurvelin, J. (2002a). Importance of the superficial tissue layer for the indentation stiffness of articular cartilage. *Medical Engineering & Physics*, 24(2):99–108.

Korhonen, R. K., Laasanen, M. S., Toyras, J., Rieppo, J., Hirvonen, J., Helminen, H. J., and Jurvelin, J. S. (2002b). Comparison of the equilibrium response of articular cartilage in unconfined compression, confined compression and indentation. *J. Biomech.*, 35(7):903–909.

Kotlarz, H., Gunnarsson, C. L., Fang, H., and Rizzo, J. A. (2009). Insurer and out-of-pocket costs of osteoarthritis in the US: evidence from national survey data. *Arthritis Rheum.*, 60(12):3546–3553.

Kumar, M. V. R. and Narasimhan, R. (2004). Analysis of spherical indentation of linear viscoelastic materials. *Curr. Sci.*, 87(8):1088–1095.

Laasanen, M. S., Saarakkala, S., Tayraos, J., Hirvonen, J., Rieppo, J., Korhonen, R. K., and Jurvelin, J. S. (2003a). Ultrasound indentation of bovine knee articular cartilage in situ. *J Biomech*, 36(9):1259–1267.

Laasanen, M. S., Tyrs, J., Korhonen, R. K., Rieppo, J., Saarakkala, S., Nieminen, M. T., Hirvonen, J., and Jurvelin, J. S. (2003b). Biomechanical properties of knee articular cartilage. *Biorheology*, 40(1-3):133–140.

Larsson, P. and Carlsson, S. (1998). On microindentation of viscoelastic polymers. *Polymer Testing*, 17(1):49–75.

Lee, H.-i., Pietrasik, J., Sheiko, S. S., and Matyjaszewski, K. (2010). Stimuli-responsive molecular brushes. *Progress in Polymer Science*, 35(12):24–44.

Lewis, N. T., Hussain, M. A., and Mao, J. J. (2008). Investigation of nano-mechanical properties of annulus fibrosus using atomic force microscopy. *Micron*, 39(7):1008–1019.

Li, C., Pruitt, L. A., and King, K. B. (2006). Nanoindentation differentiates tissue-scale functional properties of native articular cartilage. *J. Biomed. Mater. Res. Part A*, 78A(4):729–738.

Li, L. P., Herzog, W., Korhonen, R. K., and Jurvelin, J. S. (2005). The role of viscoelasticity of collagen fibers in articular cartilage: axial tension versus compression. *Med. Eng. Phys.*, 27(1):51–57.

Li, X., An, Y. H., Wu, Y.-D., Song, Y. C., Chao, Y. J., and Chien, C.-H. (2007). Microindentation test for assessing the mechanical properties of cartilaginous tissues. *J. Biomed. Mater. Res. Part B Appl. Biomater.*, 80(1):25–31.

Liu, K., VanLandingham, M. R., and Ovaert, T. C. (2009). Mechanical characterization of soft viscoelastic gels via indentation and optimization-based inverse

finite element analysis. *Journal of the Mechanical Behavior of Biomedical Materials*, 2(4):355–363.

Loparic, M., Wirz, D., Daniels, A., Raiteri, R., VanLandingham, M. R., Guex, G., Martin, I., Aebi, U., and Stolz, M. (2010). Micro- and nanomechanical analysis of articular cartilage by indentation-type atomic force microscopy: Validation with a gel-microfiber composite. *Biophysical Journal*, 98(11):2731–2740.

Loubet, J. L., Oliver, W. C., and Lucas, B. N. (2000). Measurement of the loss tangent of low-density polyethylene with a nanoindentation technique. *Journal of Materials Research*, 15(05):1195–1198.

Lu, H., Wang, B., Ma, J., Huang, G., and Viswanathan, H. (2003). Measurement of creep compliance of solid polymers by nanoindentation. *Mechanics of Time-Dependent Materials*, 7(3-4):189–207.

Lu, X. L., Miller, C., Chen, F. H., Guo, X. E., and Mow, V. C. (2007). The generalized triphasic correspondence principle for simultaneous determination of the mechanical properties and proteoglycan content of articular cartilage by indentation. *Journal of Biomechanics*, 40(11):2434–2441.

Lu, X. L., Sun, D. D. N., Guo, X. E., Chen, F. H., Lai, W. M., and Mow, V. C. (2004). Indentation determined mechanoelectrochemical properties and fixed charge density of articular cartilage. *Annals of Biomedical Engineering*, 32(3):370–379.

Lu, X. L., Wan, L. Q., Guo, X. E., and Mow, V. C. (2010). A linearized formulation of triphasic mixture theory for articular cartilage, and its application to indentation analysis. *J Biomech*, 43(4):673–679.

Lundkvist, A., Lilleodden, E., Siekhaus, W., Kinney, J., Pruitt, L., and Balooch, M. (1996). Viscoelastic properties of healthy human artery measured in saline solution by AFM-Based indentation technique. 436:353.

Lyyra, T., Jurvelin, J., Pitknen, P., Vtinen, U., and Kiviranta, I. (1995). Indentation instrument for the measurement of cartilage stiffness under arthroscopic control. *Medical Engineering & Physics*, 17(5):395–399.

Lyyra, T., Kiviranta, I., Vaatainen, U., Helminen, H. J., and Jurvelin, J. S. (1999). In vivo characterization of indentation stiffness of articular cartilage in the normal human knee. *J. Biomed. Mater. Res.*, 48(4):482–487.

Macchi, V., Munari, P. F., Brizzi, E., Parenti, A., and De Caro, R. Workshop in clinical anatomy for residents in gynecology and obstetrics. *Clin Anat*, 16(5):440–447.

Macirowski, T., Tepic, S., and Mann, R. W. (1994). Cartilage stresses in the human hip joint. *J Biomech Eng*, 116(1):10–18.

Mak, A. (1986). The apparent viscoelastic behavior of articular-cartilage - the contributions from the intrinsic matrix viscoelasticity and interstitial fluid-flows. *J. Biomech. Eng.-Trans. ASME*, 108(2):123–130.

Mak, A., Lai, W., and Mow, V. (1987). Biphasic indentation of articular-cartilage .1. theoretical-analysis. *J. Biomech.*, 20(7):703–714.

Mankin, H. J., Dorfman, H., Lippiello, L., and Zarins, A. (1971). Biochemical and metabolic abnormalities in articular cartilage from osteo-arthritic human hips. II. correlation of morphology with biochemical and metabolic data. *J Bone Joint Surg Am*, 53(3):523–537.

Manninen, P., Riihimaki, H., Heliovaara, M., and Makela, P. (1996). Overweight, gender and knee osteoarthritis. *Int. J. Obes. Relat. Metab. Disord.*, 20(6):595–597.

Maroudas, A. I. (1976). Balance between swelling pressure and collagen tension in normal and degenerate cartilage. *Nature*, 260(5554):808–809.

Marshall, G W, J., Balooch, M., Gallagher, R. R., Gansky, S. A., and Marshall, S. J. (2001). Mechanical properties of the dentinoenamel junction: AFM studies of nanohardness, elastic modulus, and fracture. *J. Biomed. Mater. Res.*, 54(1):87–95.

Mayes, R. W., Mason, R. M., and Griffin, D. C. (1973). The composition of cartilage proteoglycans. an investigation using high-and low-ionic-strength extraction procedures. *Biochem J*, 131(3):541–553.

Mazzuca, S. A., Brandt, K. D., Katz, B. P., Hanna, M. P., and Melfi, C. A. (1999). Reduced utilization and cost of primary care clinic visits resulting from self-care education for patients with osteoarthritis of the knee. *Arthritis and Rheumatism*, 42(6):1267–1273.

McCarthy, M. C., Ranzinger, M. R., Nolan, D. J., Lambert, C. S., and Castillo, M. H. (2002). Accuracy of cricothyroidotomy performed in canine and human cadaver models during surgical skills training. *J. Am. Coll. Surg.*, 195(5):627–629.

Messier, S. P., Loeser, R. F., Miller, G. D., Morgan, T. M., Rejeski, W. J., Sevick, M. A., Ettinger, Walter H, J., Pahor, M., and Williamson, J. D. (2004). Exercise and dietary weight loss in overweight and obese older adults with knee osteoarthritis: the arthritis, diet, and activity promotion trial. *Arthritis Rheum.*, 50(5):1501–1510.

Miller, G. J. and Morgan, E. F. (2009). *Use of Nanoindentation to Determine Biphasic Material Properties of Articular Cartilage.* Amer Soc Mechanical Engineers, New York.

Miller, G. J. and Morgan, E. F. (2010). Use of microindentation to characterize the mechanical properties of articular cartilage: comparison of biphasic material properties across length scales. *Osteoarthritis Cartilage*, 18(8):1051–1057.

Milsom, J. W., Bhm, B., Decanini, C., and Fazio, V. W. (1994). Laparoscopic oncologic proctosigmoidectomy with low colorectal anastomosis in a cadaver model. *Surg Endosc*, 8(9):1117–1123.

Mintz, D. N., Hooper, T., Connell, D., Buly, R., Padgett, D. E., and Potter, H. G. (2005). Magnetic resonance imaging of the hip: Detection of labral and chondral abnormalities using noncontrast imaging. *Arthroscopy: The Journal of Arthroscopic & Related Surgery*, 21(4):385–393.

Morris, V. J., Kirby, A. R., and Gunning, A. P. (1999). Using atomic force microscopy to probe food biopolymer functionality. *Scanning*, 21(5):287–292.

Mow and Huiskes (1982). *Biomechanics, principles and applications: selected proceedings of the 3rd General Meeting of the European Society of Biomechanics, Nijmegen, The Netherlands, 21-23 January 1982.* M. Nijhoff.

Mow, V., Ateshian, G., Lai, W., and Gu, W. (1998). Effects of fixed charges on the stress relaxation behavior of hydrated soft tissues in a confined compression problem. *International Journal of Solids and Structures*, 35(35):4945–4962.

Mow, V., Gibbs, M., Lai, W., Zhu, W., and Athanasiou, K. (1989). Biphasic indentation of articular-cartilage .2. a numerical algorithm and an experimental-study. *J. Biomech.*, 22(8-9):853–861.

Mow, V., Kuei, S., Lai, W., and Armstrong, C. (1980). Biphasic creep and stress-relaxation of articular-cartilage in compression - theory and experiments. *J. Biomech. Eng.-Trans. ASME*, 102(1):73–84.

Mow, V. C. and Huiskers, R. (2005). *Basic Orthopaedic Biomechanics and Mechano-Biology*.

Moyer, J. T., Abraham, A. C., and Haut Donahue, T. L. (2012). Nanoindentation of human meniscal surfaces. *J Biomech*, 45(13):2230–2235.

Najafi, B., Crews, R. T., and Wrobel, J. S. (2010). Importance of time spent standing for those at risk of diabetic foot ulceration. *Dia Care*, 33(11):2448–2450.

Nakata, K. and Bullough, P. G. (1986). The injury and repair of human articular cartilage: a morphological study of 192 cases of coxarthrosis. *Nippon Seikeigeka Gakkai Zasshi*, 60(7):763–775.

Narhi, T., Siitonen, U., Lehto, L. J., Hyttinen, M. M., Arokoski, J. P. A., Brama, P. A., Jurvelin, J. S., Helminen, H. J., and Julkunen, P. (2011). Minor influence of lifelong voluntary exercise on composition, structure, and incidence of osteoarthritis in tibial articular cartilage of mice compared with major effects caused by growth, maturation, and aging. *Connect. Tissue Res.*, 52(5):380–392.

Natzli, H. P., Wyss, T. F., Stoecklin, C. H., Schmid, M. R., Treiber, K., and Hodler, J. (2002). The contour of the femoral head-neck junction as a predictor for the risk of anterior impingement. *J Bone Joint Surg Br*, 84(4):556–560.

Newey, D., Wilkins, M. A., and Pollock, H. M. (1982). An ultra-low-load penetration hardness tester. *J. Phys. E: Sci. Instrum.*, 15(1):119.

Ng, L., Grodzinsky, A. J., Patwari, P., Sandy, J., Plaas, A., and Ortiz, C. (2003). Individual cartilage aggrecan macromolecules and their constituent

glycosaminoglycans visualized via atomic force microscopy. *J. Struct. Biol.*, 143(3):242–257.

Ngan, A., Wang, H., Tang, B., and Sze, K. (2005). Correcting power-law viscoelastic effects in elastic modulus measurement using depth-sensing indentation. *International Journal of Solids and Structures*, 42(56):1831–1846.

Nix, W. D. and Gao, H. J. (1998). Indentation size effects in crystalline materials: A law for strain gradient plasticity. *J. Mech. Phys. Solids*, 46(3):411–425.

Nordin, M. (2001). *Basic biomechanics of the musculoskeletal system*. Lippincott Williams & Wilkins, Philadelphia [etc.].

Ohman, C., Dall'Ara, E., Baleani, M., Van Sint Jan, S., and Viceconti, M. (2008). The effects of embalming using a 4% formalin solution on the compressive mechanical properties of human cortical bone. *Clin Biomech (Bristol, Avon)*, 23(10):1294–1298.

Oliver, W. and Pharr, G. (1992). An improved technique for determining hardness and elastic-modulus using load and displacement sensing indentation experiments. *J. Mater. Res.*, 7(6):1564–1583.

Oliver, W. C. and Pharr, G. M. (2004). Measurement of hardness and elastic modulus by instrumented indentation: Advances in understanding and refinements to methodology. *J. Mater. Res.*, 19(1):3–20.

Outerbridge, R. E. (1961). The etiology of chondromalacia patellae. *J Bone Joint Surg Br*, 43-B:752–757.

Oyen, M. L. and Cook, R. R. (2009). A practical guide for analysis of nanoindentation data. *J. Mech. Behav. Biomed. Mater.*, 2(4):396–407.

Park, S., Costa, K. D., and Ateshian, G. A. (2004). Microscale frictional response of bovine articular cartilage from atomic force microscopy. *Journal of Biomechanics*, 37(11):1679–1687.

Pearle, A. D., Warren, R. F., and Rodeo, S. A. (2005). Basic science of articular cartilage and osteoarthritis. *Clin Sports Med*, 24(1):1–12.

Perlau, R., Frank, C., and Fick, G. (1995). The effect of elastic bandages on human knee proprioception in the uninjured population. *Am J Sports Med*, 23(2):251–255.

Peuker, E. T., Werkmeister, R., Pera, F., Joos, U., and Filler, T. J. (2001). [surgical procedures in mouth, jaw and facial surgery in thiel embalmed body donors]. *Mund Kiefer Gesichtschir*, 5(2):141–143.

Pham, T. (2004). Laterally elevated wedged insoles in the treatment of medial knee osteoarthritis a two-year prospective randomized controlled study. *Osteoarthritis and Cartilage*, 12(1):46–55.

Pharr, G., Oliver, W., and Brotzen, F. (1992). On the generality of the relationship among contact stiffness, contact area, and elastic modulus during indentation. *Journal of Materials Research*, 7(03):613–617.

Pollard, T. C. B., Gwilym, S. E., and Carr, A. J. (2008). The assessment of early osteoarthritis. *J Bone Joint Surg Br*, 90(4):411–421.

Pritzker, K., Gay, S., Jimenez, S., Ostergaard, K., Pelletier, J.-P., Revell, P., Salter, D., and van den Berg, W. (2006). Osteoarthritis cartilage histopathology: grading and staging. *Osteoarthritis and Cartilage*, 14(1):13–29.

Pritzker, K. P. (1977). Aging and degeneration in the lumbar intervertebral disc. *Orthop. Clin. North Am.*, 8(1):66–77.

Raynauld, J.-P., Buckland-Wright, C., Ward, R., Choquette, D., Haraoui, B., Martel-Pelletier, J., Uthman, I., Khy, V., Tremblay, J.-L., Bertrand, C., and Pelletier, J.-P. (2003). Safety and efficacy of long-term intraarticular steroid injections in osteoarthritis of the knee: a randomized, double-blind, placebo-controlled trial. *Arthritis Rheum.*, 48(2):370–377.

Reginster, J.-Y., Bruyere, O., and Henrotin, Y. (2003). New perspectives in the management of osteoarthritis. structure modification: facts or fantasy? *J Rheumatol Suppl*, 67:14–20.

Rho, J. Y., Roy, M E, n., Tsui, T. Y., and Pharr, G. M. (1999a). Elastic properties of microstructural components of human bone tissue as measured by nanoindentation. *J. Biomed. Mater. Res.*, 45(1):48–54.

Rho, J. Y., Zioupos, P., Currey, J. D., and Pharr, G. M. (1999b). Variations in the individual thick lamellar properties within osteons by nanoindentation. *Bone*, 25(3):295–300.

Rho, J. Y., Zioupos, P., Currey, J. D., and Pharr, G. M. (2002). Microstructural elasticity and regional heterogeneity in human femoral bone of various ages examined by nano-indentation. *J Biomech*, 35(2):189–198.

Roschger, P., Gupta, H., Berzlanovich, A., Ittner, G., Dempster, D., Fratzl, P., Cosman, F., Parisien, M., Lindsay, R., Nieves, J., and Klaushofer, K. (2003). Constant mineralization density distribution in cancellous human bone. *Bone*, 32(3):316–323.

Roy, M. E., Rho, J.-Y., Tsui, T. Y., Evans, N. D., and Pharr, G. M. (1999). Mechanical and morphological variation of the human lumbar vertebral cortical and trabecular bone. *Journal of Biomedical Materials Research*, 44(2):191–197.

Sadro, C. (2000). Current concepts in magnetic resonance imaging of the adult hip and pelvis. *Seminars in Roentgenology*, 35(3):231–248.

Saha, R. and Nix, W. D. (2002). Effects of the substrate on the determination of thin film mechanical properties by nanoindentation. *Acta Mater.*, 50(1):23–38.

Said, S., Mall, J., Peter, F., and Mller, J. M. (1999). Laparoscopic aortofemoral bypass grafting: human cadaveric and initial clinical experiences. *J. Vasc. Surg.*, 29(4):639–648.

Schinagl, R. M., Gurskis, D., Chen, A. C., and Sah, R. L. (1997). Depth-dependent confined compression modulus of full-thickness bovine articular cartilage. *J. Orthop. Res.*, 15(4):499–506.

Serafini-Fracassini, A. and Smith, J. W. (1974). *The structure and biochemistry of cartilage*. Churchill Livingstone, Edinburgh.

Setton, L., Mow, V., Muller, F., Pita, J., and Howell, D. (1994). Mechanical-properties of canine articular-cartilage are significantly altered following transection of the anterior cruciate ligament. *J. Orthop. Res.*, 12(4):451–463.

Setton, L. A., Zhu, W., and Mow, V. C. (1993). The biphasic poroviscoelastic behavior of articular cartilage: Role of the surface zone in governing the compressive behavior. *Journal of Biomechanics*, 26(45):581–592.

Shen, Z. L., Kahn, H., Ballarini, R., and Eppell, S. J. (2011). Viscoelastic properties of isolated collagen fibrils. *Biophys J*, 100(12):3008–3015.

Shepherd, D. E. T. and Seedhom, B. B. (1997). A technique for measuring the compressive modulus of articular cartilage under physiological loading rates with preliminary results. *Proceedings of the Institution of Mechanical Engineers, Part H: Journal of Engineering in Medicine*, 211(2):155–165.

Shibakawa, A., Aoki, H., Masuko-Hongo, K., Kato, T., Tanaka, M., Nishioka, K., and Nakamura, H. (2003). Presence of pannus-like tissue on osteoarthritic cartilage and its histological character. *Osteoarthr. Cartil.*, 11(2):133–140.

Silva, M. J., Brodt, M. D., Fan, Z., and Rho, J.-Y. (2004). Nanoindentation and whole-bone bending estimates of material properties in bones from the senescence accelerated mouse SAMP6. *J Biomech*, 37(11):1639–1646.

Simha, N. K., Jin, H., Hall, M. L., Chiravarambath, S., and Lewis, J. L. (2007). Effect of indenter size on elastic modulus of cartilage measured by indentation. 129(5):767–775.

Simon, S. R., Radin, E. L., Paul, I. L., and Rose, R. M. (1972). The response of joints to impact loading part II in vivo behavior of subchondral bone. *Journal of Biomechanics*, 5(3):267–272.

Smalley, W. E., Griffin, M. R., Fought, R. L., and Ray, W. A. (1996). Excess costs from gastrointestinal disease associated with nonsteroidal anti-inflammatory drugs. *J Gen Intern Med*, 11(8):461–469.

Sneddon, I. N. (1965). The relation between load and penetration in the axisymmetric boussinesq problem for a punch of arbitrary profile. *International Journal of Engineering Science*, 3(1):47–57.

Soltz, M. A. and Ateshian, G. A. (1998). Experimental verification and theoretical prediction of cartilage interstitial fluid pressurization at an impermeable contact interface in confined compression. *J Biomech*, 31(10):927–934.

Soltz, M. A. and Ateshian, G. A. (2000). Interstitial fluid pressurization during confined compression cyclical loading of articular cartilage. *Ann Biomed Eng*, 28(2):150–159.

Stefan, U., Michael, B., and Werner, S. (2010). Effects of three different preservation methods on the mechanical properties of human and bovine cortical bone. *Bone*, 47(6):1048–1053.

Stoller, D. W. (2007). *Magnetic Resonance Imaging in Orthopaedics and Sports Medicine. 2Bde.* Lippincott Williams & Wilkins.

Stolz, M., Gottardi, R., Raiteri, R., Miot, S., Martin, I., Imer, R., Staufer, U., Raducanu, A., Daggelin, M., Baschong, W., Daniels, A. U., Friederich, N. F., Aszodi, A., and Aebi, U. (2009). Early detection of aging cartilage and osteoarthritis in mice and patient samples using atomic force microscopy. *Nat Nanotechnol*, 4(3):186–192.

Stolz, M., Raiteri, R., Daniels, A. U., VanLandingham, M. R., Baschong, W., and Aebi, U. (2004). Dynamic elastic modulus of porcine articular cartilage determined at two different levels of tissue organization by indentation-type atomic force microscopy. *Biophys. J.*, 86(5):3269–3283.

Supe, A., Dalvi, A., Prabhu, R., Kantharia, C., and Bhuiyan, P. (2005). Cadaver as a model for laparoscopic training. *Indian J Gastroenterol*, 24(3):111–113.

Swann, A. C. and Seedhom, B. B. (1993). The stiffness of normal articular cartilage and the predominant acting stress levels: implications for the aetiology of osteoarthrosis. *Br. J. Rheumatol.*, 32(1):16–25.

Sweigart, M. A., Zhu, C. F., Burt, D. M., deHoll, P. D., Agrawal, C. M., Clanton, T. O., and Athanasiou, K. A. (2004). Intraspecies and interspecies comparison of the compressive properties of the medial meniscus. *Annals of Biomedical Engineering*, 32(11):1569–1579.

T L Willett, R. W. (2005). Artefacts in the mechanical characterization of porcine articular cartilage due to freezing. *Journal of engineering in medicine*, 219(1):23–29.

Tamayo, J. and Garcia, R. (1998). Relationship between phase shift and energy dissipation in tapping-mode scanning force microscopy. *Applied Physics Letters*, 73(20):2926–2928.

Taylor, S. D., Tsiridis, E., Ingham, E., Jin, Z., Fisher, J., and Williams, S. (2012). Comparison of human and animal femoral head chondral properties and geometries. *Proceedings of the Institution of Mechanical Engineers, Part H: Journal of Engineering in Medicine*, 226(1):55–62.

Tesch, W., Eidelman, N., Roschger, P., Goldenberg, F., Klaushofer, K., and Fratzl, P. (2001). Graded microstructure and mechanical properties of human crown dentin. *Calcif. Tissue Int.*, 69(3):147–157.

Thiel, W. (1992). [the preservation of the whole corpse with natural color]. *Ann Anat*, 174(3):185–195.

Thomas Byrd, J. (2002). Hip arthroscopy in the supine position. *Operative Techniques in Sports Medicine*, 10(4):184–195.

Thurner, P. J. (2009). Atomic force microscopy and indentation force measurement of bone. *WIREs Nanomed Nanobiotechnol*, 1(6):624–649.

Tomkoria, S., Patel, R. V., and Mao, J. J. (2004). Heterogeneous nanomechanical properties of superficial and zonal regions of articular cartilage of the rabbit proximal radius condyle by atomic force microscopy. *Med Eng Phys*, 26(10):815–822.

Turner, C. H., Rho, J., Takano, Y., Tsui, T. Y., and Pharr, G. M. (1999). The elastic properties of trabecular and cortical bone tissues are similar: re-

sults from two microscopic measurement techniques. *Journal of Biomechanics*, 32(4):437–441.

Urabe, I., Nakajima, S., Sano, H., and Tagami, J. (2000). Physical properties of the dentin-enamel junction region. *Am J Dent*, 13(3):129–135.

VanLandingham, M. (2003). Review of instrumented indentation. *Journal of Research of the National Institute of Standards and Technology*, 108(4):249.

VanLandingham, M. R., Villarrubia, J. S., Guthrie, W. F., and Meyers, G. F. (2001). Nanoindentation of polymers: An overview. *Macromol. Symp.*, 167(1):15–43.

Viidik, A. and Lewin, T. (1966). Changes in tensile strength characteristics and histology of rabbit ligaments induced by different modes of postmortal storage. *Acta Orthopaedica*, 37(2):141–155.

Wahl, K., Asif, S., Greenwood, J., and Johnson, K. (2006). Oscillating adhesive contacts between micron-scale tips and compliant polymers. *Journal of Colloid and Interface Science*, 296(1):178–188.

Wan, L. Q., Miller, C., Guo, X. E., and Mow, V. C. (2004). Fixed electrical charges and mobile ions affect the measurable mechano-electrochemical properties of charged-hydrated biological tissues: the articular cartilage paradigm. *Mech Chem Biosyst*, 1(1):81–99.

Wang, X. M., Cui, F. Z., Ge, J., Zhang, Y., and Ma, C. (2002). Variation of nanomechanical properties of bone by gene mutation in the zebrafish. *Biomaterials*, 23(23):4557–4563.

Wen, C.-Y., Wu, C.-B., Tang, B., Wang, T., Yan, C.-H., Lu, W., Pan, H., Hu, Y., and Chiu, K.-Y. (2012). Collagen fibril stiffening in osteoarthritic cartilage of

human beings revealed byatomic force microscopy. *Osteoarthritis and Cartilage*, 20(8):916–922.

Wilke, H.-J., Jungkunz, B., Wenger, K., and Claes, L. E. (1998). Spinal segment range of motion as a function of in vitro test conditions: Effects of exposure period, accumulated cycles, angular-deformation rate, and moisture condition. 251(1):15–19.

Wilke, H.-J., Werner, K., Hussler, K., Reinehr, M., and Backers, T. M. (2011). Thiel-fixation preserves the non-linear load-deformation characteristic of spinal motion segments, but increases their flexibility. *J Mech Behav Biomed Mater*, 4(8):2133–2137.

Williamson, A. K., Chen, A. C., and Sah, R. L. (2001). Compressive properties and functional composition relationships of developing bovine articular cartilage. *Journal of Orthopaedic Research*, 19(6):1113–1121.

Wilson, W., van Donkelaar, C. C., van Rietbergen, B., Ito, K., and Huiskes, R. (2004). Stresses in the local collagen network of articular cartilage: a poroviscoelastic fibril-reinforced finite element study. *J. Biomech.*, 37(3):357–366.

Wilusz, R. E., Zauscher, S., and Guilak, F. (2013). Micromechanical mapping of early osteoarthritic changes in the pericellular matrix of human articular cartilage. *Osteoarthritis and Cartilage*.

Wolff, K.-D., Kesting, M., Mcke, T., Rau, A., and Hlzle, F. (2008). Thiel embalming technique: A valuable method for microvascular exercise and teaching of flap raising. *Microsurgery*, 28(4):273–278.

Wong, M., Wuethrich, P., Eggli, P., and Hunziker, E. (1996). Zone-specific cell biosynthetic activity in mature bovine articular cartilage: a new method using

confocal microscopic stereology and quantitative autoradiography. *J. Orthop. Res.*, 14(3):424–432.

Woolf, A. D. and Pfleger, B. (2003). Burden of major musculoskeletal conditions. *Bulletin of the World Health Organization*, 81(9):646–656.

X L Lu, V. C. M. (2009). Proteoglycans and mechanical behavior of condylar cartilage. *Journal of dental research*, 88(3):244–8.

Yao, J. Q. and Seedhom, B. B. (1993). Mechanical conditioning of articular cartilage to prevalent stresses. *Br. J. Rheumatol.*, 32(11):956–965.

Yasuda, k. (1987). The mechanics of treatment of the osteoarthritic knee with a wedged insole.

Yavuz, U., Skc, S., Albayrak, A., and ztrk, K. (2012). Efficacy comparisons of the intraarticular steroidal agents in the patients with knee osteoarthritis. *Rheumatol Int*, 32(11):3391–3396.

Yuan, G.-H., Tanaka, M., Masuko-Hongo, K., Shibakawa, A., Kato, T., Nishioka, K., and Nakamura, H. (2004). Characterization of cells from pannus-like tissue over articular cartilage of advanced osteoarthritis. *Osteoarthritis and Cartilage*, 12(1):38–45.

Yuan, Y. and Verma, R. (2006). Measuring microelastic properties of stratum corneum. *Colloids Surf B Biointerfaces*, (1):6–12.

Zhang, W., Moskowitz, R., Nuki, G., Abramson, S., Altman, R., Arden, N., Bierma-Zeinstra, S., Brandt, K., Croft, P., Doherty, M., Dougados, M., Hochberg, M., Hunter, D., Kwoh, K., Lohmander, L., and Tugwell, P. (2007). OARSI recommendations for the management of hip and knee osteoarthritis, part i: Critical appraisal of existing treatment guidelines and systematic review of current research evidence. *Osteoarthritis and Cartilage*, 15(9):981–1000.

Zhang, W., Moskowitz, R., Nuki, G., Abramson, S., Altman, R., Arden, N., Bierma-Zeinstra, S., Brandt, K., Croft, P., Doherty, M., Dougados, M., Hochberg, M., Hunter, D., Kwoh, K., Lohmander, L., and Tugwell, P. (2008a). OARSI recommendations for the management of hip and knee osteoarthritis, part II: OARSI evidence-based, expert consensus guidelines. *Osteoarthritis and Cartilage*, 16(2):137–162.

Zhang, W., Robertson, J., Jones, A. C., Dieppe, P. A., and Doherty, M. (2008b). The placebo effect and its determinants in osteoarthritis: meta-analysis of randomised controlled trials. *Ann. Rheum. Dis.*, 67(12):1716–1723.

Zysset, P. K., Guo, X. E., Hoffler, C. E., Moore, K. E., and Goldstein, S. A. (1999). Elastic modulus and hardness of cortical and trabecular bone lamellae measured by nanoindentation in the human femur. *J Biomech*, 32(10):1005–1012.